Digitally Driven Microfabrication of 3D Multilayer Embedded Electronic Systems

By

Thomas James Wasley

Doctoral thesis submitted in partial fulfilment of the requirements of the award of Doctor of Philosophy of Loughborough University

July 2016

Abstract

The integration of multiple digitally driven processes is seen as the solution to many of the current limitations arising from standalone Additive Manufacturing (AM) techniques. A technique has been developed to digitally fabricate fully functioning electronics using a unique combination of AM technologies. This has been achieved by interleaving bottom-up Stereolithography (SL) with Direct Writing (DW) of conductor materials alongside mid-process development (optimising the substrate surface quality), dispensing of interconnects, component placement and thermal curing stages. The resulting process enables the low-temperature production of bespoke three-dimensional, fully packaged and assembled multi-layer embedded electronic circuitry.

Two different Digital Light Processing (DLP) Stereolithography systems were developed applying different projection orientations to fabricate electronic substrates by selective photopolymerisation. The bottom up projection orientation produced higher quality more planar surfaces and demonstrated both a theoretical and practical feature resolution of 110 µm. A top down projection method was also developed however a uniform exposure of UV light and planar substrate surface of high quality could not be achieved. The most advantageous combination of three post processing techniques to optimise the substrate surface quality for subsequent conductor deposition was determined and defined as a mid-processing procedure. These techniques included ultrasonic agitation in solvent, thermal baking and additional ultraviolet exposure. SEM and surface analysis showed that a sequence including ultrasonic agitation in D-Limonene with additional UV exposure was optimal.

DW of a silver conductive epoxy was used to print conductors on the photopolymer surface using a Musashi dispensing system that applies a pneumatic pressure to a loaded syringe mounted on a 3-axis print head and is controlled through CAD generated machine code. The dispensing behaviour of two isotropic conductive adhesives was characterised through three different nozzle sizes for the production of conductor traces as small as 170 µm wide and 40 µm high. Additionally, the high resolution dispensing of a viscous isotropic conductive adhesive (ICA) also led to a novel deposition approach for producing three dimensional, z-axis connections in the form of high freestanding pillars with an aspect ratio of 3.68 (height of 2mm and diameter of 550µm). Three conductive adhesive curing regimes were applied to printed samples to determine the effect of curing temperature and time on the resulting material resistivity. A temperature of 80 °C for 3 hours resulted in the lowest resistivity while displaying no substrate degradation.

Compatibility with surface mount technology enabled components including resistors, capacitors and chip packages to be placed directly onto the silver adhesive contact pads before low-temperature thermal curing and embedding within additional layers of photopolymer. Packaging of components as small as 0603 surface mount devices (SMDs) was demonstrated via this process. After embedding of the circuitry in a thick layer of photopolymer using the bottom up Stereolithography apparatus, analysis of the adhesive strength at the boundary between the base substrate and embedding layer was conducted showing that loads up to 1500 N could be applied perpendicular to the embedding plane. A high degree of planarization was also found during evaluation of the embedding stage that resulted in an excellent surface finish on which to deposit subsequent layers. This complete procedure could be repeated numerous times to fabricate multilayer electronic devices.

This hybrid process was also adapted to conduct flip-chip packaging of bare die with 195 μm wide bond pads. The SL/DW process combination was used to create conductive trenches in the substrate surface that were filled with isotropic conductive adhesive (ICA) to create conductive pathways. Additional experimentation with the dispensing parameters led to consistent 150 μm ICA bumps at a 457 μm pitch. A flip-chip bonding force of 0.08 N resulted in a contact resistance of 2.3 Ω at a standoff height of ~80 μm. Flip-chips with greater standoff heights of 160 μm were also successfully underfilled with liquid photopolymer using the SL embedding technique, while the same process on chips with 80 μm standoff height was unsuccessful.

Finally the approaches were combined to fabricate single, double and triple layer circuit demonstrators; pyramid shaped electronic packages with internal multilayer electronics; fully packaged and underfilled flip-chip bare die and; a microfluidic device facilitating UV catalysis. This new paradigm in manufacturing supports rapid iterative product development and mass customisation of electronics for a specific application and, allows the generation of more dimensionally complex products with increased functionality.

Table of Contents

Acknowledgements

Firstly I would like to thank my supervisor Robert Kay for providing me with unwavering support and guidance throughout the past three years. Without his positivity and enthusiasm for this subject matter I would not have progressed this far. The confidence he has placed in me to both conduct and present this research has helped me grow personally and professionally.

I would also like to thank the Additive Manufacturing Research Group and all those associated with it for the opportunities it has provided me throughout my time at Loughborough. This includes academic and research staff as well as my fellow students and technicians, all of whom have made the past three years more enjoyable.

A number of technicians have been generous enough to provide me with a huge amount of time and resource during my research, most notably David Thompson, John Webster and Jagpal Singh. I would like to convey my thanks not only to those mentioned but all the technicians who have contributed to my work.

In addition, I would like to express my gratitude to academic collaborators based at Heriot Watt University, Edinburgh; The University of Sheffield and The University of Warwick for the opportunity to work alongside them on the multifaceted EPSRC 'IAMP – Integration of Advanced Manufacturing Processes' project, from which I have gained a wealth of knowledge and experience.

I would like to thank my family, in particular my parents whose constant support is a source of huge confidence and motivation for me. They have never doubted my ability, despite my occasional misgivings, and for that I will be forever grateful.

Finally and most importantly, I would like to thank my wonderful girlfriend Danielle. The past three years have been tough, however her commitment and belief in me has never wavered and I truly cannot describe in words how much that means to me. Without her I would not be where I am today.

Publications

Journal Papers

- *Hybrid additive manufacturing of 3D electronic systems.* **Wasley, T.J., Li, J., Kay, R.W., Ta, D., Shephard, J., Stringer, J., Smith, P., Esenturk, E. and Connaughton, C.** Journal of Micromechanics and Microengineering 26.10 (2016): 105005

- *Miniaturised embedded electronic systems via hybrid additive manufacturing.* **Wasley, T.J., Li, J., Kay, R.W., Ta, D., Shephard, J., Stringer, J., Smith, P., Esenturk, E. and Connaughton, C.** Rapid Prototyping Journal, ISSN: 1355-2546. (final preparation)

- *Integration of additive manufacturing and inkjet printed electronics: a potential route to parts with embedded multifunctionality.* **Stringer, J., Althagathi T.M., Christopher, C.W., Shephard, J.D., Esenturk, E., Connaughton, C., Wasley, T.J., Li, J., Kay, R.W. and Smith, P.J.** Manufacturing Review 3 (2016): 12

- *Nanosecond laser textured superhydrophobic metallic surfaces and their chemical sensing applications.* **Ta, D., Dunn, A., Shephard, J., Wasley, T.J., Li, J., Kay, R.W., Stringer, J., Smith, P., Esenturk, E. and Connaughton, C.** Applied Surface Science 357 (2016): 248-254

- *Laser textured superhydrophobic surfaces and their applications for homogeneous spot deposition.* **Ta, D., Dunn, A., Shephard, J., Wasley, T.J., Li, J., Kay, R.W., Stringer, J., Smith, P., Esenturk, E. and Connaughton, C.** Applied Surface Science 365 (2016): 153-159

- *Laser textured surface gradients.* **Ta, D., Dunn, A., Shephard, J., Wasley, T.J., Li, J., Kay, R.W., Stringer, J., Smith, P., Esenturk, E. and Connaughton, C.** Applied Surface Science 371 (2016): 583-589

- *Dynamically controlled deposition of colloidal nanoparticles suspension in evaporating drops using laser radiation.* **Ta, D., Dunn, A., Shephard, J., Wasley, T.J., Li, J., Kay, R.W., Stringer, J., Smith, P., Esenturk, E. and Connaughton, C.** Soft Matter 12(20) (2016): 4530-4536

Conference Publications

- *Enabling Rapid Production and Mass Customisation of Electronics Using Digitally Driven Hybrid Additive Manufacturing Techniques.* **Wasley, T.J., Li, J., Kay, R.W., Ta, D., Shephard, J., Stringer, J., Smith, P., Esenturk, E. and Connaughton, C.** Electronic Components and Technology Conference (ECTC), 2016 IEEE 66th. IEEE, 2016.

- *Additive Manufacturing of High Resolution Embedded Electronic Systems.* **Wasley, T.J., Li, J., Kay, R.W., Ta, D., Shephard, J., Stringer, J., Smith, P., Esenturk, E. and Connaughton, C.** Proceedings of the 27th Solid Freeform Fabrication Symposium, Austin, TX, 2016.

- *Generation of Superhydrophobic Surfaces and Wettability Gradients on Metallic Substrates by Nanosecond Laser Irradiation.* **Ta, D., Dunn, A., Shephard, J., Wasley, T.J., Li, J., Kay, R.W., Stringer, J., Smith, P., Esenturk, E. and Connaughton, C.** ICALEO 2015, Atlanta, USA.

Poster Presentations

- *Hybrid Additive Manufacturing of 3D Electronic Circuits.* **Wasley, T., Li, J. and Kay, R.** IeMRC 9th Annual Conference 2014, Loughborough, UK. (2nd prize)

- *3D Printing of Ceramic Packaging for Harsh Environments.* **Wasley, T., Mirgkizoudi, M., Campos Zatarain, A., Flynn, D. and Kay, R.** iMAPS UK 'Heat of the Matter' Conference 2014, Oxford, UK.

Acronyms

μSL	Micro-Stereolithography
2D	Two Dimensional
3D	Three Dimensional
3D-IMA	Three Dimensional Interdigitated Micro-battery Architectures
ADDIMID	Additive 3D Moulded Interconnect Device
ADM	Absorbing Dye Material
AM	Additive Manufacturing
ASTM	American Society for Testing and Materials
CAD	Computer Aided Design
CLIP	Continuous Liquid Interface Production
CNC	Computer Numerical Control
CO_2	Carbon Dioxide
DCA	Direct Chip Attach
DLP	Digital Light Processing
DMD	Digital Micro Mirror Device
DPSS	Diode-Pumped Solid State
DSC	Differential Scanning Calorimetry
DSP	Differential Scanning Photocalorimetry
DW	Direct Writing
EMM	Electrochemical Micro-Machining
EPSRC	Engineering and Physical Sciences Research Council
eSLA	Embedding Stereolithography

EUV	Extreme Ultraviolet
FC	Flip Chip
FDM	Fused Deposition Modelling
FILM	Functional Integrated Layered Manufacturing
FR-4	Flame Retardant
GUI	Graphical User Interface
HALT	Highly Accelerated Life Test
i3DP	Inkjet 3D Printing
IAMP	Integration of Advanced Manufacturing Processes
IC	Integrated Circuit
ICA	Isotropic Conductive Adhesive
ID	Inner Diameter
IPA	Isopropyl Alcohol
IR	Infra-Red
ISO	International Organisation for Standardisation
JEDEC	Joint Electron Device Engineering Council
LCD	Liquid Crystal Display
LED	Light Emitting Diode
LFP	$LiFePO_4$
LTO	$Li_4Ti_5O_{12}$
MAM	Multifunctional Monomer
MEMS	Micro-Electromechanical Systems
MID	Molded Interconnect Device

MIP-SL	Mask Image Projection based Stereolithography
MMSL	Multi Material Stereolithography
MSOP	Mini Small Outline Package
MuCAD	Musashi Computer Aided Design
Nd:YAG	Neodymium-doped Yttrium Aluminium Garnet
Nd:YVO$_4$	Neodymium-doped Yttrium Orthovanadate
PAA	Poly(acrylic acid)
PCB	Printed Circuit Board
PCOB	Flip Chip on Board
PDMS	Polydimethylsiloxane
PSP	Print-Stick-Peel
QD-LED	Quantum Dot Light Emitting Diode
RoHS	Restriction of Hazardous Substances
S$_a$	Arithmetical Mean Height of Surface
SAC	Tin, Silver and Copper
SEM	Scanning Electron Microscope
SL	Stereolithography
SLA	Stereolithography Apparatus
SLM	Selective Laser Melting
SLS	Selective Laser Sintering
SMD	Surface Mount Device
SOIC	Small Outline Integrated Circuit
S$_p$	Maximum Height of Peaks

S_q Root Mean Square Height of Surface

STL   Standard Triangle Language

S_v Maximum Depth of Valleys

S_z Average Height of Surface

Ti:Sapphire   Titanium Sapphire

TSSOP   Thin Shrink Small Outline Package

UBM   Under Bump Metallisation

UC   Ultrasonic Consolidation

UV   Ultraviolet

WEEE   Waste Electrical and Electronic Equipment

WXGA   Wide Extended Graphics Array

List of Figures

List of Tables

1 Introduction

1.1 Research Motivation

There are three motivating factors that promote the need for research and development into the integration of Additive Manufacturing (AM) processes:

- The multi-material, versatile production capability of hybrid Additive Manufacturing systems.
- High resolution geometrically complex electronic packaging.
- Overcoming limitations of traditional electronics manufacturing.

Each of these are described in the following sections.

1.1.1 Hybrid Additive Manufacturing Systems

AM technologies are being widely publicised and promoted as the future of manufacturing [1] because of their direct digital fabrication capability. This refers to their ability to produce even the most complex geometries from a CAD file. This paves the way for significant research to be conducted into the technology, with market growth trending from US$3.8 billion in 2014 to an expected value of US$16.2 billion by 2018 [2]. To-date a vast majority of research has been conducted on the use of individual AM processes that are limited in their range of materials, processing speed and resolution. The ability to integrate multiple processes, combining advantageous characteristics and material capabilities provides a significantly larger range of applications [3].

The integration of two different digitally driven manufacturing processes has been successfully demonstrated by a collaborative research project between Stratasys and Optomec Inc. The wing of an unmanned aerial vehicle was produced using the Stratasys' AM Fused Deposition Modelling process before an Optomec Aerosol Jet Direct Write (DW) system printed an antenna, conformal sensor and circuitry on its surface [4]. Similarly, separate research at The University of Texas at El Paso has combined Stereolithography (SL) and DW technologies to produce 3D structural electronics [5]. The use of these technologies enables the creation of conductors printed on free form structures and lighter weight mechanical components that are much easier to maintain and repair in the field. This intuitive concept could provide benefits for a range of industries including medical devices, automotive and aerospace.

The microelectronics industry in particular has much to gain from additive manufacturing technologies, with its potential to revolutionise the way electronic equipment is made and packaged. Arguably the most valuable characteristic of AM for electronics manufacturing is its direct digital

fabrication capability, eliminating the need for templates and moulds and creating a highly flexible design and production method for bespoke electronics. Its development involves a range of considerations to allow integration including the eradication of contamination between processes as well as a number of high value applications, creating an alternative to traditional electronic manufacturing methods.

Since the expiry of a number of several significant patents alongside the development of DLP technology, Stereolithography technology has become more accessible and resulted in the development of custom machines, some of which have resulted in small crowd funded business start-ups. Guides have also been written and published online providing instruction on how to build a system including information regarding a variety of exposure methods, structural elements and, control software and firmware [6][7][8].

1.1.2 High Resolution Geometrically Complex Packaging

The capability to directly write and mount electronics into a complex package provides the opportunity to create bespoke electronics direct from a digital design to suit a specific application. This would consist of a photopolymer encapsulation matrix that would take the form of the final structure, for example, a fully fabricated digital watch.

Sensing systems in a wide variety of industries would benefit from this manufacturing approach. The production of microfluidics for flow chemistry would promote in situ measurement and feedback from a device produced in one single manufacturing process, reducing cost, time and production complexity. In addition, the ever increasing variety of available material pastes enables the production of electrodes within the 3D printed substrate for devices such as particle counters and pH sensors. This internal sensing technology could also be applied to mechanical testing of prototype parts in industries such as motor racing. New design iterations could be rapidly fabricated with internal strain gauges, connected to a data recorder and aerodynamically tested in a wind tunnel with the force data captured. These sensing systems can be freely distributed through the structure with the build orientation varied to capture data in different planes. In addition, this concept could also facilitate the development of wireless performance analysis in real time and be further applied to the health and fitness industry for remote activity monitoring.

Significant improvements in the printing resolution and materials for direct write technologies, particularly material dispensing, has led to micro scale fully printed functional electronics. With further process development these methods could be integrated with a complex additive manufacturing packaging method. Quantum dot light-emitting diodes have been created using a

multiple material extrusion-based 3D printing approach [9]. Five different material layers were deposited on top of one another within an encapsulating matrix to produce the components shown in Figure 1.1.
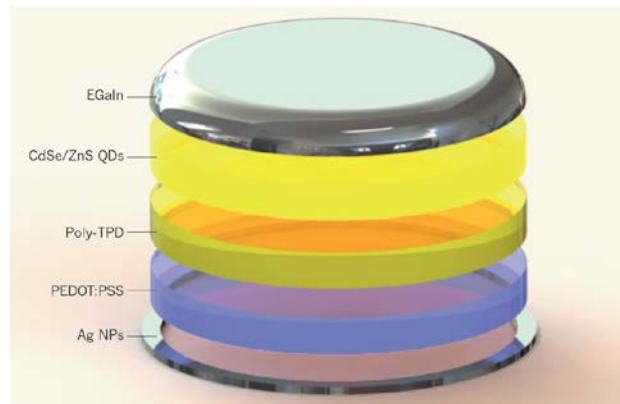
Figure 1.1.   Fully 3D-printed quantum-dot-based light-emitting diodes (QD-LEDs) [10]

In addition, Figure 1.2 shows research conducted on the high resolution printing of $Li_4Ti_5O_{12}$ (LTO) anode, and $LiFePO_4$ (LFP) cathode materials through a 30 μm nozzle for the production of rechargeable 3D interdigitated micro-battery architectures (3D-IMA) [11].
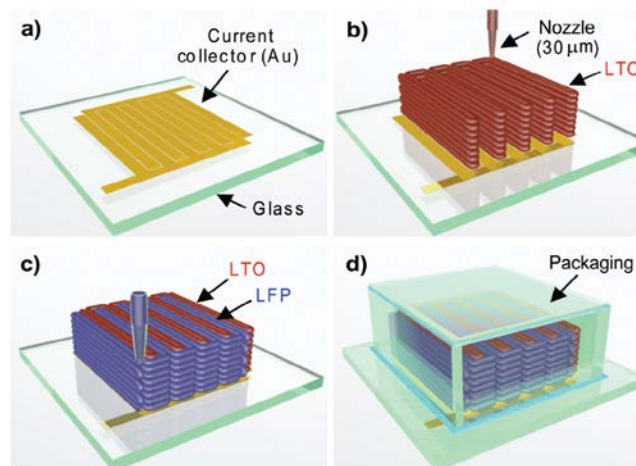
Figure 1.2.   Illustration of 3D-IMA fabricated on a) gold current collector by printing b) LTO c) LFP inks followed by sintering and d) packaging [11]

Fully printed components could soon be integrated with hybrid additive manufacturing processes and surface mount assembly thereby increasing the printed proportion of the circuit.

1.1.3   Overcoming Limitations of Traditional Electronics Manufacturing

The first printed circuit board was created in 1936 by Paul Eisler and comprised three main elements, a dielectric substrate, interconnects and components [12]. Following advancements in PCB technology, double sided and eventually multi-layer boards were produced to accommodate the increasing density and complexity of electrical circuitry. Fabrication of the circuit involves mask exposure, a number of chemical development stages to remove unwanted photoresist and copper

before solder paste can be stencil or screen printed, components positioned and solder paste reflowed to adhere it to the substrate surface.

These traditional processes demonstrate two major limitations that could be overcome using AM techniques. Firstly, the template-driven nature of the process, characterised by the need for a mask for photoresist exposure and a stencil for accurate solder paste deposition would benefit from the direct digital fabrication capability of AM, completely eliminating the template requirement. Secondly, the achievable geometric complexity of traditionally manufactured substrates can be improved through the high resolution nature of the Stereolithography process, provided by a laser or digital light projection (DLP) source.

The DW dispensing process facilitates the use of the aforementioned benefits of Stereolithography using isotropic conductive adhesives (ICA) to create the conductors in the form of traces, novel z-axis through-layer connections and surface mount device (SMD) interconnects. This reduces the number of manufacturing stages and allows surface mount assembly (SMA) directly onto the deposited ICA before thermal curing. In their current state, combined SL/DW processes are limited in their resolution, with trace widths of 250 µm achieved with an undisclosed gap, compared to 100 µm tracks with a gap of 100 µm recommended for traditional copper etching processes to ensure efficient solvent circulation and prevent damage to narrow features. In addition silver filled ICAs present a significantly higher resistivity than copper tracks and bulk silver, $\sim5\times10^{-3}$ Ω.cm [13] compared to 1.68x10^{-6} Ω.cm [14] and 1.59x10^{-6} Ω.cm [15] respectively, making them unsuitable at this time for high frequency electronics.

Despite lower resolution and higher material resistivity, the investigation of hybrid additive manufacturing systems for the production of packaged electronics is beneficial. The geometric advantages of Stereolithography can be exploited to fabricate highly complex packages unachievable in the same time scale using traditional manufacturing techniques. In addition to geometric complexity, functional structures can also be produced, designed for example, to analyse different chemical flow reactions or conduct chemical spectroscopy. Figure 1.3 outlines the differences between traditional PCB manufacturing methods and the newly proposed hybrid additive manufacturing technique, highlighting a reduction in the number of processing steps, eliminating the fabrication of templates and template suppliers which can add days to production. By comparison, the AM approach inclusive of the design process, can produce single customised circuits in between 6 and 8 hours and is fully driven by digital input from the user.

	Traditional	Additive
Substrate production and patterning	Laminate substrate with copper	Create CAD model of desired part
	Photoresist coating	Process, load and initiate in SL system
	Create photomask	Pause SL procedure and mid-process
	Photolithography	
Conductive track development	Photoresist development	Deposit ICA conductors
	Etching	
Packaging	Produce stencil or screen template	Surface mount assembly
	Screen or stencil printing solder paste	Embed
	Surface mount assembly	
	Reflow solder	

Figure 1.3. Comparison between traditional and additive manufacturing of PCBs

With abundant research funding in additive manufacturing, the further development of improved material properties and process resolution would result in narrowing the gap between traditional electronics manufacturing capabilities and integrated AM technologies. This has been demonstrated through Figure 1.4 which introduces a proposed Additive manufacturing approach to the fabrication of multilayer embedded electronic systems.
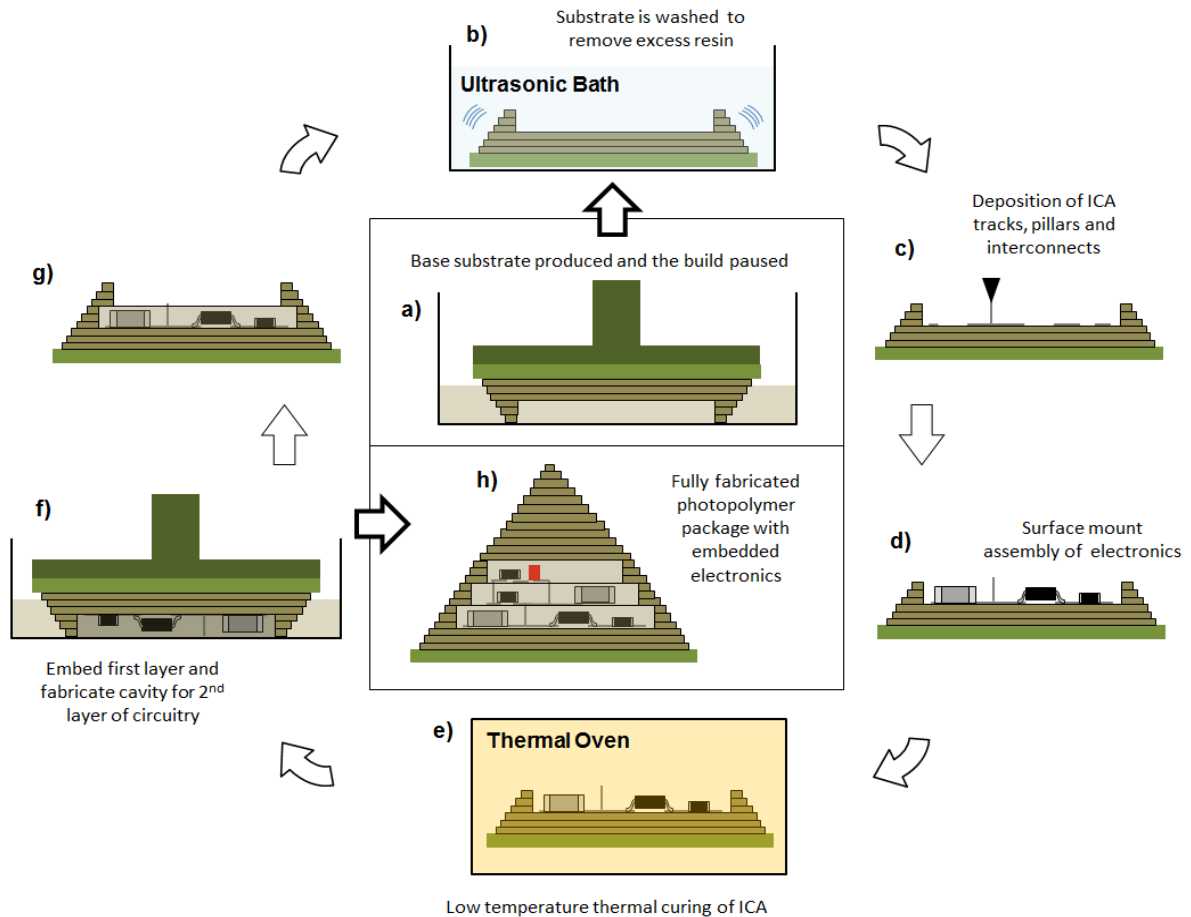
Figure 1.4.   Proposed hybrid additive manufacturing process flow

This process includes substrate production via Stereolithography, a mid-processing stage involving cleaning and the complete crosslinking of the photopolymer surface, deposition of isotropic conductive adhesive conductors, surface mount electronics assembly and thermal curing.

Due to the required investment in manufacturing infrastructure this process would never replace a high throughput mass manufacturing operation however, it would lend itself to low volume production of bespoke electronic systems in industries with the requirement for rapid design iteration and condition monitoring.

1.2   Research Intentions

1.2.1   Aims and Objectives

This PhD thesis examines the potential to integrate DLP based Stereolithography with Direct Write technology allowing fully functioning embedded circuits to be created on multiple layers. This required a number of objectives:

- To develop bespoke Stereolithography apparatus with an ultraviolet DLP light source.

- To define the optimal combination of Stereolithography and photoresist processing techniques to prepare a photopolymer substrate for direct writing.

- To determine the optimal curing regime of low temperature curable conductive epoxies.

- To characterise the compatibility between direct write conductive materials and liquid photo curable resins.

- To develop a z-axis via fabrication method to facilitate multi-layered electronics manufacturing.

- To miniaturise the fabrication process for application in electronics packaging.

1.2.2 Research Novelty

The combination of laser-based Stereolithography and direct write technology has been used previously to produce embedded electronics. However, these processes require intricate processing capabilities to embed the electronic components with channels to contain the direct written conductive materials and, trenches in which through-hole components are placed with their pins facing upward for interconnection. These limitations have facilitated the need to approach the additive manufacturing of functional electronics from a different perspective by:

- Using the Stereolithography process with a DLP projection based dynamic mask to produce a substrate and embed circuitry.

- Designing a 'mid-processing' procedure by evaluating substrate development techniques and solvents to optimise the surface quality of the photopolymer.

- Dispensing conductive adhesives directly onto the substrate surface to simultaneously produce conductive tracks, interconnects and z-axis connections.

- Positioning surface mount components and using a low temperature curing process to cure the adhesive thereby fixing the components to the substrate in one thermal baking process.

- Improving processing capabilities to allow the technique to be minimised for application in electronic packaging and chemical sensing.

- Using the hybrid Additive Manufacturing (AM) technique to flip chip package bare die.

The integration of Digital Light Processing (DLP) based Stereolithography and Direct Write technology to create a manufacturing line, facilitating the creation of fully functioning, packaged electronic circuits from a digital model makes this PhD research direction unique. The combination of DLP Stereolithography, mid processing and dispensing systems with surface mount component assembly and thermal curing provides the multi material, multi process functionality required to produce high quality, high density printed electronics.

1.3 Integration of Advanced Manufacturing Processes

The Stereolithography system created through this research has been incorporated into a wider project entitled 'Direct Digital Fabrication: Integration of Advanced Manufacturing Processes (IAMP)' and funded by the Engineering and Physical Sciences Research Council (EPSRC) under grants EP/L017431/1, EP/L017350/1, EP/L016907/1 and EP/L017415/1. This allowed further process integration with jetting systems, laser based ink curing and laser surface texturing processes. This multidisciplinary project has four academic partners (Loughborough University, Heriot-Watt University, Sheffield University and The University of Warwick) and four industrial partners (Xaar, SPI, M-Solv and Renishaw) that cover a range of research expertise and industrial applications. The vision of this project is to fabricate multilayer circuits embedded within a 3D geometry as graphically depicted in Figure 1.5.
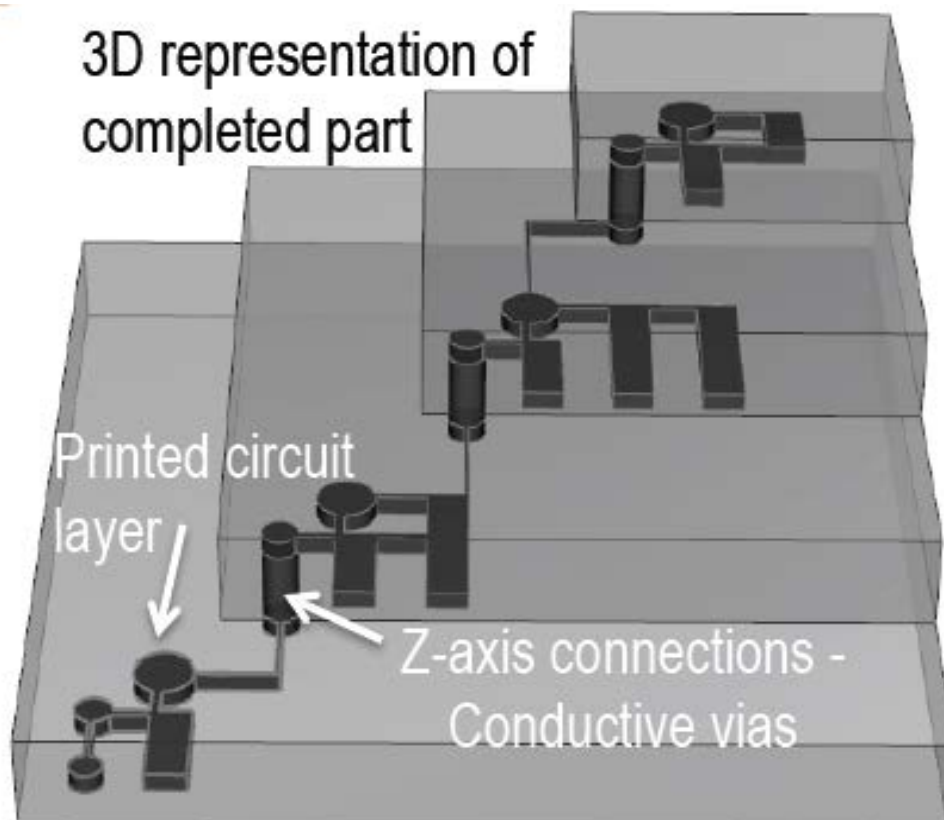
Figure 1.5.   Representation of a 3D printed multilayer electronic circuit

The Stereolithography system developed through the PhD research was also used in the IAMP project, the only differences being the ink jetting of conductive tracks and the laser textured surface used to control the ink rheology and droplet behaviour. Figure 1.6 displays in red, the areas of overlap between this thesis and the IAMP project.
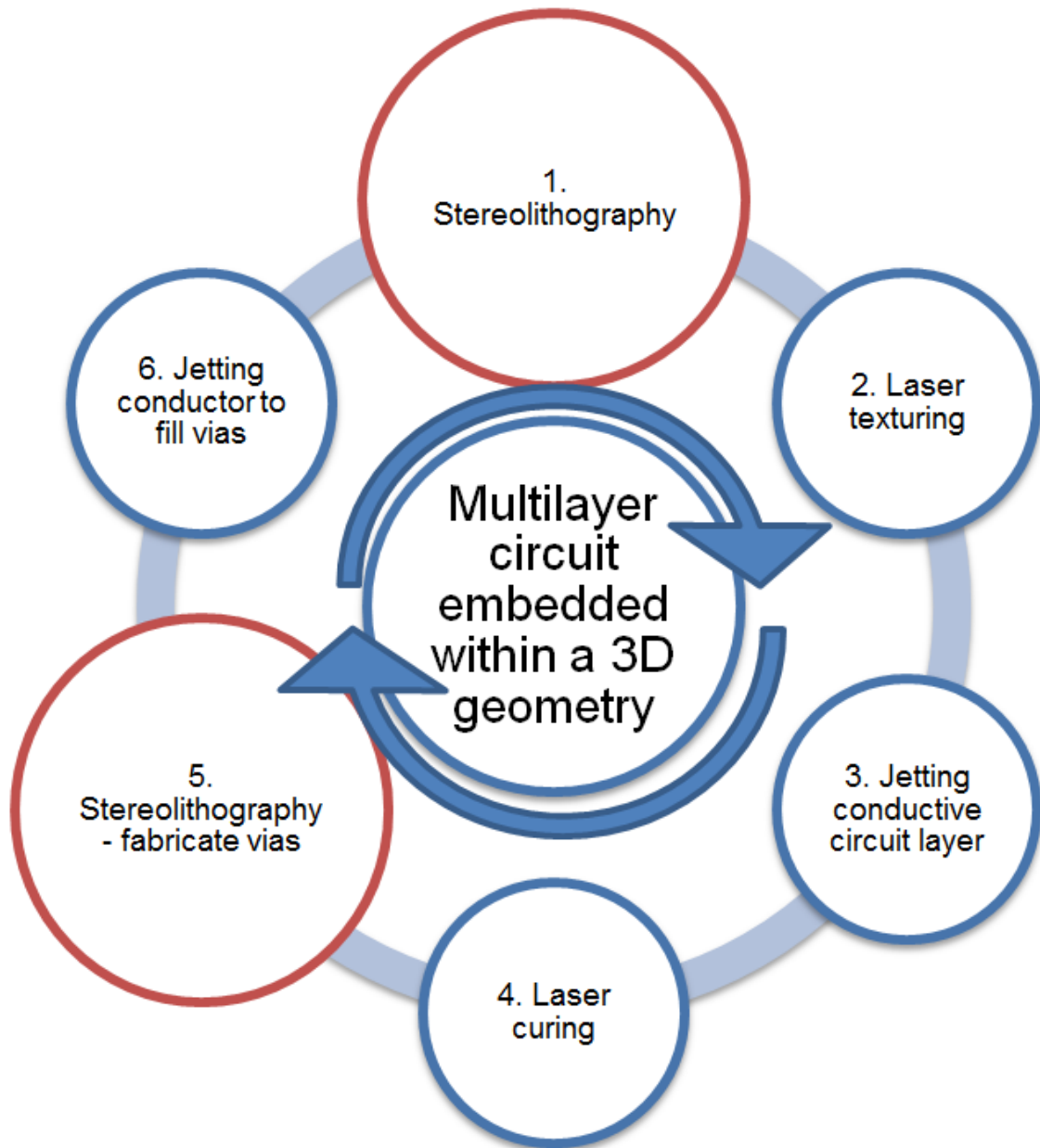
Figure 1.6.　　　IAMP project structure

1.3.1　Plan of Development and Thesis Structure

The thesis has been broken down into individual chapters, the aims of which have been detailed in Figure 1.7. A step-by-step approach to this research revealed four main stages starting with background research and determination of novelty, continuing with the development of three individual processes that were combined, characterised, tested and applied.

STAGE 1

Chapter 1: Introduction

Chapter 2: Background

Additive Manufacturing, Stereolithography, Direct Write Technology, Process Integration and Embedded Electronics

STAGE 2

Chapter 3: Multilayer Photopolymer Substrate Fabrication

Aim: Develop a bespoke high resolution Stereolithography system for electronic substrate production and electronics packaging

Chapter 4: Substrate Mid Process Development

Aim: Investigate and amalgamate a combination of Stereolithography and electronic photoresist post processing steps to improve substrate surface quality

Chapter 5: Fabrication of Electronic Circuitry

Aim: Determine the optimal dispensing parameters, curing regime and materials to produce high resolution conductive traces, z-axis connections and interconnects using isotropic conductive adhesives

STAGE 3

Chapter 6: Process Integration and Electronic Packaging

Aim 1: Characterise the relationship between the photopolymer package, conductive adhesive and surface mount electronic components

Aim 2: Conduct flip-chip packaging using this hybrid AM technique

Chapter 7: Demonstrators

Aim 1: Produce a 3D geometrically complex multilayer electronic device

Aim 2: Design and develop a microfludic device for UV catalysis

STAGE 4

Chapter 8: Conclusions

Chapter 9: Future Recommendations

Figure 1.7.   Thesis Structure

Stage 1 comprised background research that has been summarised in chapter 2, detailing relevant available literature to provide a comprehensive overview of Printed Circuit Board (PCB) production, Additive Manufacturing, the Stereolithography process, Direct Write technologies, conductive materials, printed electronics and embedding of electronics. This review provides direction within this study and an indication of the novelty of the approach being undertaken during the course of this research.

Stage 2 is reported in the principal characterisation chapters, each of which detail one of the three development steps that facilitate the integration of two different Additive Manufacturing processes. Chapter 3 details the development and evaluation of a bespoke Stereolithography system designed to build electronic substrates and embed electronics within a liquid photopolymer. Chapter 4 presents a combination of Stereolithography and photoresist post processing steps designed to optimise the substrate surface during transition between Stereolithography and direct write technologies. Finally, chapter 5 investigates the optimal dispensing parameters for three different conductors, curing regime and conductive material choice as well as introducing a novel z-axis fabrication method.

Stage 3 concerned the integration of the processes detailed in stage 2. In chapter 6 the packaging process including surface mount electronics compatibility is explained and the relationship between substrate and conductive material is quantified. In addition the use of this hybrid process to conduct flip-chip (FC) packaging is presented before the evolution of feasibility, geometrically complex and applied demonstrators are presented and discussed in chapter 7.

Finally, this research is concluded and future recommended work identified in stage 4, chapters 8 and 9.

2 Review of Additive Manufacturing Processes for Electronics Fabrication

A review of available literature was conducted providing an overview of topics relating to the fabrication of electronics, both traditional Printed Circuit Board production processes and Additive Manufacturing technologies. An overview of PCB manufacturing technology is presented including an introduction to conventional processes, their achievable resolution and its limitations. In addition, an overview of additive manufacturing is presented, focusing specifically on stereolithography and material dispensing processes and their compatible materials. Finally, the concept of AM process integration for the fabrication of electronic systems is discussed and examples given from previous work. This section will comprise advantages and disadvantages of a number of differing hybrid processes and evaluate the potential of the technology for use in embedding of electronics and electronic packaging.

2.1 Electronics Manufacturing

Electronic circuits typically consist of four main elements:

- **Printed Circuit Boards** contain the routing and connection sites to allow various electronic components to communicate between one another.
- **Integrated circuits (ICs)** are semiconducting devices containing a high density of transistors. ICs usually conduct some form of processing such as amplification, memory or signal processing.
- **Discrete components** are an electronic device with just one circuit element, such as a resistor, capacitor, transistor, etc.
- **Microelectromechanical Systems (MEMS)** conduct some form of sensing or actuation. Examples include CCD camera chips, accelerometers, etc.

Surface mount assembly is the method by which all these various components (ICs, discrete devices, MEMS) are positioned on and bonded to the PCB via mechanical and electrical connections. The overall packaged device forms the final electronic system. The electronics manufacturing industry is driven by size reduction and increased complexity; a trend in the production of integrated circuits has been described and predicted using Moore's Law [16].

2.1.1   PCB Manufacturing

Printed circuit boards consist of an insulating material, patterned with a network of conductive tracks designed to connect a number of different electronic components together such as integrated circuits, discrete components and microelectromechanical systems such as sensors and actuators.

Printed circuit substrates have to meet a number of requirements, most notably high electrical insulation. Both rigid and flexible substrates can be produced depending on the application. One of the most commonly used rigid substrates is FR-4, a flame retardant glass fibre epoxy composite laminated with copper foil and capable of producing single and multilayer circuit boards. Flexible substrates can take the form of sheets of polyimide, acrylic, epoxy and fluoropolymer based materials to name just a few. These materials can then be metallised via cladding, commonly with a thin layer of copper [17][18].

The first stage in PCB production is the application of a photoresist to a copper coated substrate. There are two types of photoresist, positive and negative [19]. When exposed to ultraviolet light, these photoresists behave in one of two ways: if positive, the areas exposed to the light become soluble during the development procedure and can typically produce minimum feature sizes of 0.5µm [20]; if negative, the exposed area becomes insoluble to the developer and 2µm features are achievable [21]. Lamination is the simplest form of coating whereby a sheet of photoresist, normally between 25 and 35 µm thick [22] can be applied to the copper surface of the substrate by the application of heat and pressure.

Once deposited, a photomask is used to pattern the photoresist in a process called photolithography. This firstly involves generating a physical mask which can be used in conjunction with an ultraviolet light source. The mask which can be printed on a polymer film or glass plate, is placed over the photoresist before it is exposed to the UV light. The resolution of the photolithography process is determined by a collection of parameters including the specified resolution of the photoresist, its thickness, exposure method and type of photomask used.

Developing refers to the process by which the soluble photoresist is removed. This exposes the copper that will be etched away during the next stage of manufacture and protects the track geometry from the etchant. Positive and negative photoresist materials require different developers, both aqueous and organic based and have different resistance to wet chemicals used during the etching process, with negative resists showing a greater resistance [20].

The final process in the production of copper tracks is the removal of excess copper. Areas left exposed after development are removed by chemical etchants. Immersion etching is most common

for low volume production and is conducted by submerging the board in a solution such as ferric chloride. Commercially, spray etching distributes the etchant over the boards using nozzles with the capability to adjust flow rate, spray pattern and temperature to control the rate of reaction [23]. Some PCB manufacturers quote resolution capabilities of 35 μm track width at 40 μm spacing [24]. The dimensions of these tracks are conventionally decided by the required electrical properties of the circuit and dictated by the thickness of the copper, with higher thicknesses resulting in wider tracks [25]. Tight process control is required to prevent the occurrence of undercutting, where the copper protected by the resist is isotropically etched, resulting in an overhanging feature causing open circuits between adjacent tracks.

Conventional manufacturing processes have the capability to produce double sided and multilayer electronic circuits by laminating alternating layers of copper and insulator for example, Fujitsu quote the capability to produce up to 72 layers in a single PCB [26]. This allows the production of very high density PCBs with through layer connections created by drilling and either filling or electroplating the partial, buried or through hole vias measuring between 100 μm and 150 μm in diameter once electroplated to create a conductive connection between separate layers [27].

2.1.2 Surface Mount Assembly

The consumer requirements for smaller, faster, more functional and portable electronic devices have driven the industry to continually strive for higher density boards with finer pitch component connections. Surface-mount assembly (SMA) is a method in which the components are mounted or placed directly onto the surface of PCBs. Presently SMA is the most common packaging method for producing complex electronic circuits due to its low cost, high throughput and high density capability with current pick and place systems capable of mounting 1000's of devices per hour.

Soldering is the primary technique by which components are joined to printed circuit boards. Solder paste is a suspension of solder alloy particles in a printing medium containing a flux. Solder paste can be made from any solder alloy. Traditionally the most frequently used alloy composition was eutectic tin-lead. However the Restriction of Hazardous Substances (RoHS) directive and the Waste Electrical and Electronic Equipment (WEEE) directive from European legislation have restricted the use of lead in many electronic packaging applications. Lead-free solder paste can be made up of many formulations however tin-silver-copper is the most common [28].

Solder paste is applied to the etched copper pads on the PCB typically by stencil printing. Stencil printing for electronic packaging is a process by which a viscous material (isotropic conductive adhesive or solder paste) is deposited through the aperture openings of a stencil onto the bond pads

on a substrate. This template driven process allows rapid deposition of solder in a high volume production line [29][30]. Stencil printing of 90μm pitch interconnects through 20 μm orifices have been achieved [31]. These deposits had diameters of ~50 μm and a height of ~15 μm due to material slumping. These dimensions are more suited to chip scale packaging [32]. Components are then placed onto the wet solder paste over the corresponding pads. Reflow soldering bonds the components to the pads by melting the solder alloy powder causing it to coalesce together. The solder alloy is the only permanent part of the metallurgical bond left from the solder paste after reflow. The flux vehicle contains flux, solvents and binders. Flux removes oxidation from the surfaces to be soldered; it seals out air thus preventing further oxidation and improves wetting characteristics of the liquid solder. The binders and solvents function to evenly disperse the solder powder throughout the paste, maintain paste consistency during printing, clean the surface to be soldered to and hold the component in place during reflow [33].

Reflow usually occurs over a number of highly controlled stages of heating to prevent damage to components and activate constituents of the solder paste material. Electrically conductive adhesives typically also applied through a stencil can be used as a low temperature alternative to solder. Instead of reflowing like solder paste the epoxy heavily loaded with conductive flakes or particles is cured. As the material cures it draws the conductive particles into contact creating a mechanical and electrical connection [34].

Packaged integrated circuits and MEMS devices, specifically Small Outline Integrated Circuits (SOICs), are commonly surface mounted onto PCBs and have replaced Dual Inline Packages (DIP) which were compatible with through-hole component technology. Small Outline Packages (SOPs) represent one branch of integrated circuits which has been further categorised into Plastic Small Outline Packages (PSOPs), Thin Small Outline Packages (TSOPs) and Thin Shrink Small Outline Packages (TSSOPs), all of which have small dimensional differences relevant to specific applications [35][36] with the main objective being a reduction in device footprint, pad size and pitch with the smallest devices demonstrating pin pitches of 650 μm, reduced from DIP package pitches of 2.5 mm.

Discrete components are available in sizes from 2512 to 01005, referring to the imperial dimension of the packaged two terminal resistors, 250 mil x 120 mil (~6.3 mm x 3.2 mm) to 10 mil x 5 mil (~0.4 mm x 0.2 mm). These components demonstrate a higher density of components and connections than through hole devices and require less processing, can be assembled faster and demonstrate better mechanical performance [37].

2.1.3 Flip-chip packaging

Flip-chip packaging is a further evolution of surface mount assembly where, rather than a pre-packaged component being assembled, the bare microchip known as a die is attached face down onto a substrate. The chip is connected by means of conductive bumps such as solder paste placed onto the chip bond pads. Flip-chip packaging is also commonly referred to as Direct Chip Attach (DCA) since the chip is directly attached to the substrate. The flip-chip device is either attached to a wafer, circuit board or carrier. Flip-chip devices are predominantly semiconductor chips but, components such as passive microwave filters, optical detector arrays, optoelectronic emissive devices and MEMs devices can also be found in direct chip attach format. A number of advantages can be realised by directly attaching an electronic device to the substrate:

- Higher input/output density can be achieved through closer bond pads and use of the full chip area.

- Weight and size reduction from the loss of the electronic package.

- Lower profile making the device thinner.

- Less production materials making the product cheaper to manufacture and more environmentally friendly.

- Reduced and repeatable signal inductance due to the much shorter interconnect length, a key factor in high-speed communication and switching devices.

- Decrease of noise within the chip due to reduction of the power to ground inductance [38].

Flip-chip packaging is traditionally conducted onto an interposer board where redistribution traces are used to increase the pitch of interconnects from as small as 50 μm [32], making it suitable for combination with lower resolution surface mount assembly processes. With resolution improvements in PCB manufacture flip-chip bare die can now be mounted directly onto a PCB. It is achieved by aligning solder bumped conductive pads on the underside of the chip with a matrix of distribution traces on the package [39]. An insulating epoxy is then used to encapsulate the IC and more securely attach it to the PCB. This isolates the chip from the external environment and distributes heat evenly across the whole package. An electrically insulating underfill material can also be used to fill the gap between the chip and package or PCB. This material is designed for two purposes: protecting the chip and joints from mechanical stresses and, enhancing the performance of the package [40][41]..

2.1.4 Summary of Electronics Manufacturing

Current electronics manufacturing processes are capable of producing highly complex circuitry with total production automation. These techniques however have a vast number of limitations, most

notably, the geometric freedom afforded to these processes is severely limited. In addition, an abundance of highly hazardous chemicals are required for processing and a significant amount of energy is required to conduct a number of the separate practices discussed during section 2.1. Additive manufacturing offers solutions to many of these disadvantages by providing a versatile, template free alternative to conventional electronics manufacturing methods. With further process and material development, AM could demonstrate great benefits when compared to the alternative traditional methods.

2.2 Additive Manufacturing

Additive Manufacturing is defined as the process of joining materials to make objects from 3D model data, usually layer upon layer, as opposed to subtractive manufacturing technologies [42]. Another term commonly used to refer to Additive Manufacturing is '3D Printing'. However, this expression from a technical point of view only refers to those processes where thin layers of material are layered or deposited via a nozzle or orifice, and does not encompass those processes that have a material bed or vat that is selectively sintered, melted or cured [43]. To the general public the term '3D printing' has however become synonymous with Additive Manufacturing and therefore the terms are commonly viewed as interchangeable. All additive manufacturing processes follow the same basic steps to produce the final model as shown in Figure 2.1.
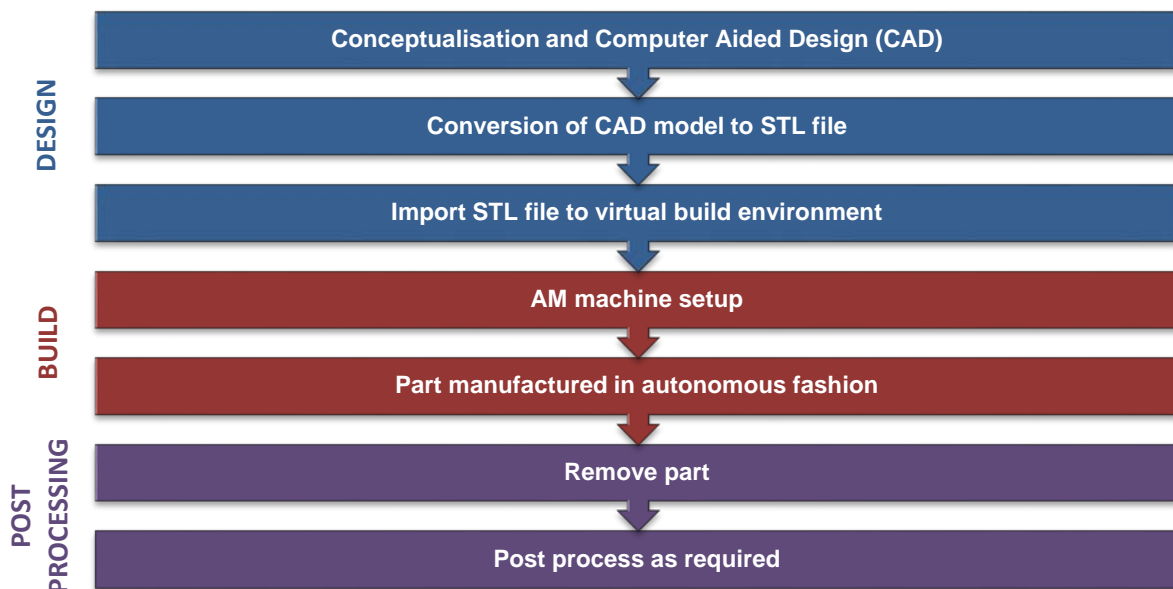
Figure 2.1.   Additive Manufacturing processing steps

The specific terminology representing each additive manufacturing technique can be confusing as identical or very similar methods may be referred to by different process names. In some instances machine suppliers have trademarked a process name or given the same manufacturing process a different name depending on its application or the material it can process. The American Society for

Testing and Materials (ASTM) F42 standard categorises the various AM processes into seven key process families [42]. This enables the processes to be easily grouped into a specific category depending on what manufacturing approach the machine uses. These 7 ASTM categories defined in Table 2.1 each have their own advantages and disadvantages making them suitable for different applications.

Table 2.1. Description of 7 ASTM Standards [42][44][45][46]

ASTM Standard	Process Summary	Materials
Material Extrusion	• Material extruded through a nozzle. • 3D geometries can be fabricated by the deposition of consecutive material layers in the z-axis. • Examples include Fused Filament Fabrication (FFF) and Fused Deposition Modelling (FDM).	Thermoplastic polymers, pastes, waxes, chocolate
Vat Photo-polymerisation	• Photosensitive resin selectively cured by exposure to a light source. • Capable of producing high resolution, accurate parts with good surface finish. • Stereolithography is one process example.	Acrylate, epoxy, vinyl ether based photosensitive resins
Powder Bed Fusion	• Layers of powder are selectively fused together by a heat source, commonly a laser or electron beam. • Common processes include Selective Laser Sintering (SLS) for polymer processing, Selective Laser Melting (SLM) and Binder Sintering for metals.	Thermoplastic polymers, metals, ceramics, composites
Material Jetting	• Material droplets selectively ejected from a print head, similar to ink jet printing. • Droplets ejected by either piezoelectric or drop-on-demand (most common in industry) actuation. • Potential for multi material printing using multiple print heads. • Objet and Projet are examples of material jetting systems.	Polymers, wax, conductors
Binder Jetting	• Layers of powder are selectively bonded together by a jetted adhesive. • The 'green' part is then infiltrated with other materials to improve its properties. • Capable of printing in colour. • Examples include Z-corp and ExOne processes.	Polymers, metals, ceramics
Sheet Lamination	• Sheet material is fed into the build area where it is bonded to the previous layer. • A cross section is then cut out using a blade or laser, building up the part one layer at a time. • For example, sheet metal can be bonded using Ultrasonic Consolidation (UC), creating a solid state weld between metal foils.	Sheets of paper, polymer, metal and 'green state' ceramic
Direct Energy Deposition	• Uses a focused heat source to melt a feedstock material as it is deposited to produce a 3D geometry. • Feedstock takes the form of wire, with 100% capture efficiency, or powder, which does not. • Laser Engineered Net Shaping (LENS) is one example.	Metals (titanium alloys, aluminium alloys and copper alloys)

2.3 Stereolithography

Stereolithography, as with any additive technique, starts with a CAD model, which is converted into an STL file, imported into processing software and sliced into cross sectional layers with a thickness determined by the user. These cross-sections are then individually processed by the machine which selectively cures an individual layer of photosensitive resin by exposing it to an ultraviolet light source. The process is then repeated layer-by-layer to produce a fully fabricated, solid part. Stereolithography is based around the principle of photolithography used in traditional electronics manufacturing to transfer a pattern from a photomask onto a light sensitive photoresist. The liquid photopolymer in stereolithography is basically a negative tone resist whereby sections exposed to light are cross-linked to form a solid material. After manufacture, the part is removed from the vat containing the resin and cleaned to remove any uncured material. The support structures are then removed and finally, the part is post-processed using a UV oven to ensure the material is completely cross-linked [47].
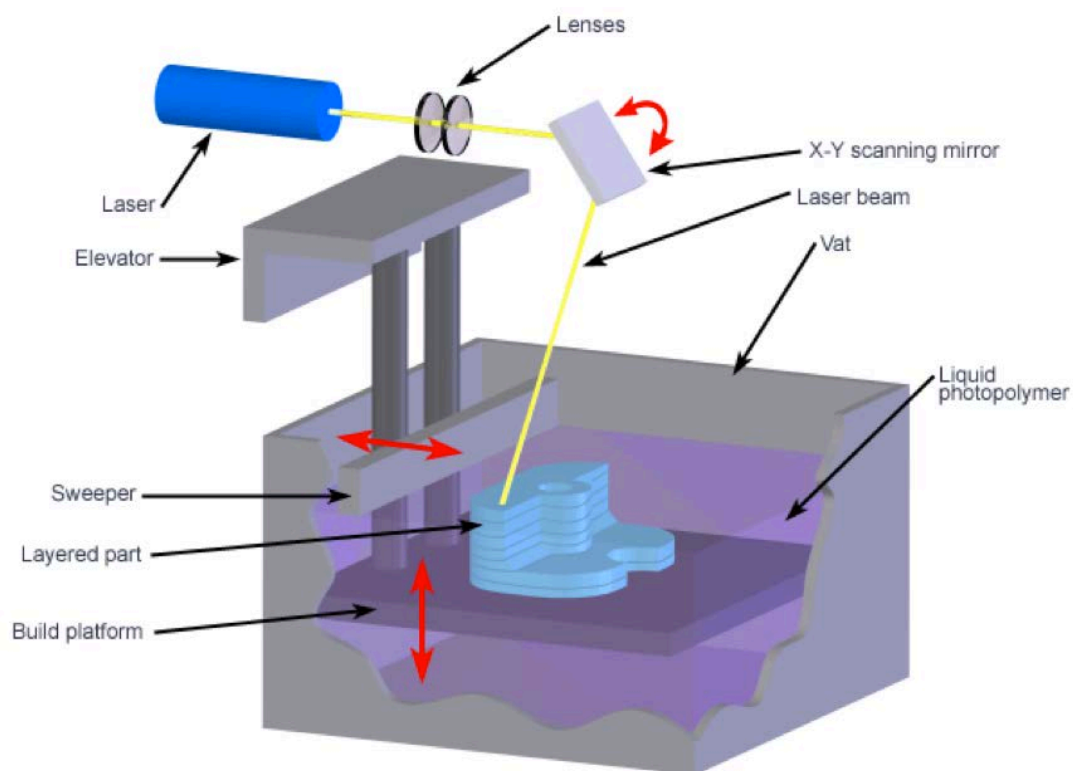
Figure 2.2.   Stereolithography apparatus [48]

Figure 2.2 shows the generic layout of a laser point source, top-down Stereolithography system. In this example, a laser is focused through a lens array and onto a mirror controlled by a galvanometer enabling the precise x-y translation of the laser on the surface of the resin. The laser cures the resin onto the build platform whose z-axis position is altered by an elevator or linear actuator. It is also

the resolution of movement of this elevator that determines the minimum achievable layer thickness of the part.

Micro-Stereolithography (μSL) is a variant of the Stereolithography process which aims to build higher resolution parts, but with the trade-off of smaller sized objects. There have been a collection of μSL machines built by various research groups using differing light sources and dynamic masks, the details and results of which are shown in Table 2.2.

Table 2.2.   Performance of Mask Projection micro-Stereolithography systems realised by other research groups derived from [49]

Mask	Light Source	Resolution	Component Size	Speed	Publication
LCD	Laser: 515 nm	5 x 5 x 5 μm	1.3 x 1.3 x 10 mm^3	Not reported	[50]
SLM	Laser 351.1 nm	5 μm lateral resolution	Not reported	60 s exposure time per 50 μm layer	[51][52][53] [54]
LCD	Broadband visible light	2 μm lateral resolution	Not reported	10 μm layers at 1 layer/min	[55][56]
DMD	Lamp (visible)	5 x 5 x 5 μm	6 x 8 x 15 mm^3	1 mm/h	[57][58]
DMD	Lamp (UV)	10 x 10 x 10 μm	10.24 x 7.68 x 20 mm^3	673 layers at 5 μm layer thickness in 3h	[59]
DMD	Lamp (UV)	20 μm lateral resolution	Not reported	Not reported	[60]

Stereolithography setups can differ from the example shown in Figure 2.2 above in terms of light exposure method and orientation, types of materials and recoating technique all of which will be reviewed later in this section. Combinations of the machine setups are presented in the process tree in Figure 2.3.
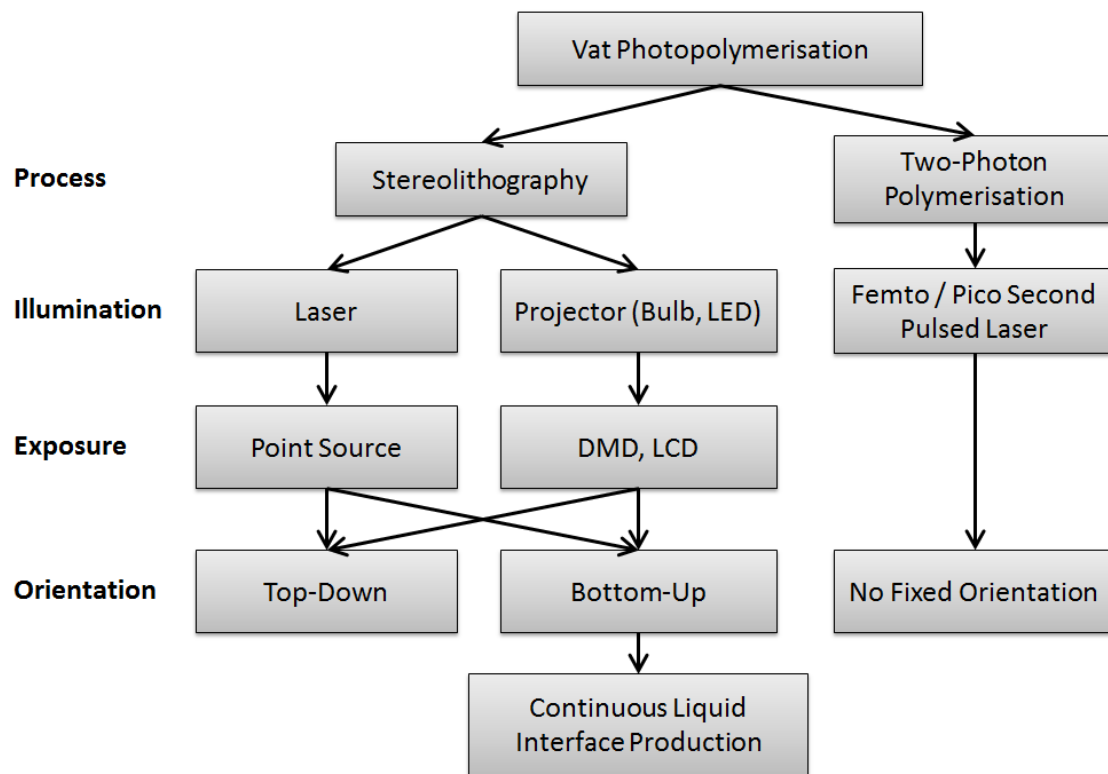
Figure 2.3.   Vat photopolymerisation process tree

2.3.1   Exposure Method

There are two main methods of exposure in a Stereolithography system, point source and light projection. Point source refers to the use of a laser spot to initiate curing of the photopolymers. Galvo mirrors are used to control the laser position, selectively scanning the surface of the resin. Projection exposure uses Digital Light Processing (DLP) or Liquid Crystal Display (LCD) technology as a dynamic mask to expose consecutive layers of resin to consecutive cross sectional images of the design.

An assortment of beams can be used in a laser based system all of which have differing spot sizes, the sole property that has an influence on the resolution of the system. Argon-Ion lasers have been used to create gearwheels with diameters ranging from 500-700 μm achieving a layer thickness of 50 μm and lateral resolution as low as 20 μm. Neumeister *et al.* developed their own setup using a Nd:YAG laser with a wavelength of 355 nm. This resulted in a focal radius of approximately 7 μm, theoretically creating a minimum feature resolution of the same value [61].

Projection exposure was first achieved using Liquid Crystal Displays (LCDs) as live motion masks for Stereolithography. Exposure mask images were created from the cross-sectional data of the 3D structure designed in CAD software. The light source used by Gohki *et al.* [62] was a UV spot source which was adapted by a direct beam uniform illumination unit to expose a larger area with a uniform

light intensity. When transmitted through an LCD display, the pixel size determined the resolution of the process in much the same way as DLP however, the LCD demonstrated issues achieving a high light intensity.

The development of Digital Micro Mirror Device (DMD) technology provided a new method for projection exposure in Stereolithography. The DMD consists of an array of individual micro mirrors that can be selectively controlled and orientated to display chosen images. Each mirror on the device is responsible for one pixel [49]. This projection method has been shown to produce parts with high contrast and resolution. There are however a number of potential failure mechanisms, mirrors breaking as a result of handling, hinges breaking over time, lifetime limitations caused by high working temperatures and due to intense UV light exposure [63]. The integration of a DMD with a laser source and tailored optics has been proven to produce resolutions of approximately 10 μm [64]. This particular example is also designed to conduct scanning projection stereolithography, a process whereby multiple exposures occur on a single layer and 'knit' together to create a larger image, this allows a high resolution exposure method such as this to be applied to a larger 5 cm^2 area.

The light source used for DLP projection through a DMD can have a significant impact on the properties of the resulting part and the efficiency of the curing process. SLA resins have specific wavelengths of light at which they are designed to optimally cure, determined by the photo initiator. With different light sources producing light of varying wavelengths, resins and sources can be matched to produce the optimal cure in the shortest time. Mercury lamps typically emit a high intensity of light between 350 nm and 450 nm which can be tailored with the addition of a filter. Once channelled through a lens array and occasionally, a high density optical fibre [65], it can be selectively exposed to the surface of the resin with the mask provided by a DMD. Lamps however tend to produce a wide range of wavelengths not all of which will cure the resin whereas LED's produce a light source with a very narrow band of wavelengths and therefore have the potential to create a much more efficient light source for curing photosensitive resin at a constant speed.

2.3.2   Build Orientation

Stereolithography systems can be set up in one of two orientations, known as bottom-up or top-down. This denotes the position of the exposure mechanism and the direction from which the vat is exposed.

Top-down systems are most commonly found in commercial systems and have the light source mounted above the vat with light being directed down onto the resin surface. The biggest challenge in top-down Stereolithography is recoating as levelling mechanisms require smooth movement

capability with accurate height control. Processes without levelling systems often result in inaccurate or domed surfaces caused by the surface tension of the resin [66]. A full vat of resin is also required for this process as well as a perforated build platform, both of which ensure that the resin can flow over the top surface of the part to create a new, uncured, layer ready for exposure. There are also additional features of top-down technology that require monitoring to ensure parts are accurately fabricated, these include both the resin level at rest and also how much material has been displaced once the build platform has been submerged.

Bottom-up systems have the light source mounted beneath the vat and directed onto its base. In this situation the build platform is placed one layer thickness away from the transparent base of the vat and curing of the resin takes place upside down, before the build platform is raised and the next layer cured [67]. The multi-material Stereolithography setup shown in Figure 2.4 was developed by Zhou *et al.* [67] based on a bottom-up mask-image-projection (MIP-SL) method. This process relies upon the inclusion of an oxygen inhibition layer to control the termination of resin curing once exposure has finished.
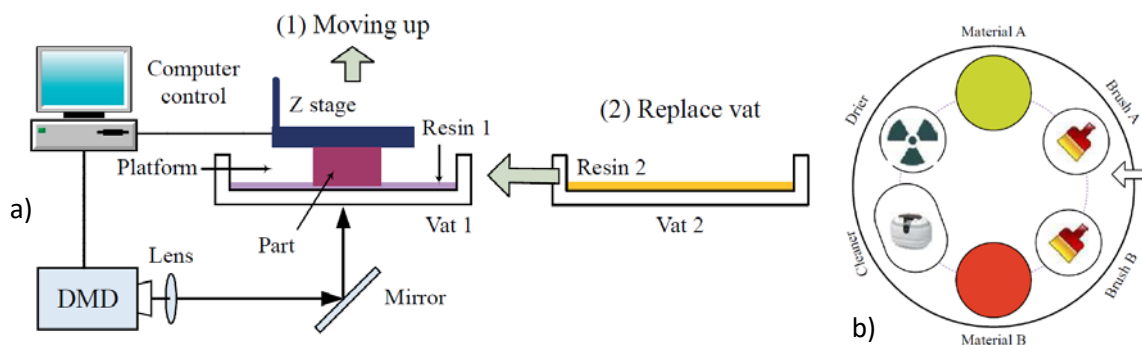
Figure 2.4.   MIP-SL process a) setup and b) vat arrangement

The bottom-up DLP process presents a number of advantages over alternative systems. Firstly, no recoating method is required, the layer thickness and planeness is determined by the distance between the part and the bottom surface of the vat and, the surface finish of that face. Secondly, the build platform can be solid as perforations are not required for the flow of the liquid photopolymer. Finally, a minimal quantity of resin is required to produce parts as only the very bottom of the vat needs to be filled. The nature of the final removal of the part also allows it to drain naturally as it rises above the surface of the resin. One disadvantage of the process is caused by diffraction of the light as it passes through the transparent base of the vat, which can limit the process resolution [68].

2.3.3 Liquid Photopolymers

The basic composition of materials used in Stereolithography is important as it ensures that the material becomes fully cured when exposed to the light source. These materials are comprised of three elements: photoinitiators, liquid monomers and inhibitors all of which play specific roles in the accurate curing of the resin, with the end goal to link small molecules (monomers) to form larger molecules (polymers).

The photopolymerisation process in Stereolithography also has three main stages: initiation, propagation and termination, referring to the beginning, middle and end of the reaction. Once irradiated the polymerisation process begins and can be sped up with higher exposure doses [69]. Although common photoinitiators are designed to react to UV light at 365 nm, broadband photoinitiators can result in photopolymerisation using visible light sources up to 500 nm wavelength, as well as curing industrial microelectronic formulations that are opaque to UV light [70].

Low powered UV lasers can be used to initiate the photopolymerisation process due to it being an efficient exothermic process. UV radiation of certain frequencies causes the creation of free radicals which subsequently react with monomers to initiate a chain reaction [71]. The Van der Waals forces between monomers change to covalent bonds, resulting in an observed change of material state.

Once exposure ceases, the inhibitor prevents any further bonding to ensure that only the exposed area of resin reacts to form a solid substrate [72]. Without the inhibitor, the Stereolithography process would lose accuracy, as the resin outside the exposure boundaries would continue to cure indefinitely.

There are three classifications of modern photopolymers: acrylate, epoxy and vinyl ether based materials, however the former two are the most commonly used. Acrylates were the first resins developed for the Stereolithography process. The greatest influence on the polymerisation of acrylate based photopolymers is the UV exposure time when free radicals are initiated. Thermal curing has little effect as the reaction is inhibited by oxygen in the surrounding material. Such materials are also very susceptible to shrinkage and produce weak and inaccurate parts [73].

Epoxy resins show improved performance over acrylates with minimal swelling, decreased yet linear shrinkage and the ability to produce highly accurate Stereolithography parts [74]. One disadvantage of epoxy resins is their propensity to continue curing over time in a process known as 'dark reaction' [75]. Epoxies also possess suitable viscosity and have a low shrinkage enabling them to be used in higher resolution micro-Stereolithography processes [53].

Comparisons of physical properties of acrylate and epoxy resin for Stereolithography determined that epoxy resins show the same linear shrinkage as acrylates however, due to the slower curing speed of epoxies, lower shrinkage stresses and therefore better part accuracy are observed [76]. Tensile testing was performed on samples exposed to UV light for 10-250 seconds, conducted as relaxation tests, showing that acrylate based photopolymers reach their peak tensile strength at 60 seconds exposure to an UV light intensity of 100 mJ/cm^2 whereas, it takes in excess of 240 seconds of exposure to 144 mJ/cm^2 for the epoxy based material to display the same properties, finally reaching a maximum Young's Modulus of 19 MPa in contrast to 15 MPa achieved by the acrylate material. Previous research has observed that the tensile strength of epoxy based photopolymers continues to increase for up to two hours post exposure [73].

In a laser based stereolithography system the laser power and layer thickness both significantly impact the shape stability [77]. Shape distortion can result from inconsistent energy absorption of the photopolymer by different laser and post process curing exposure times. Further experimentation on acrylic based photopolymer resins show that higher shrinkage was observed using the shadow Moiré method as a result of heat treatment than UV post curing, however considerable shrinkages were generated by both post-treatment processes [78].

Stresses in thin films causing substrate distortion during microelectronics manufacturing can be determined using the Stoney Equation [79] however this has never been used to measure stress in SL fabricated substrates. Instead, blind hole drilling has been used to aid in the calculation of residual stresses caused by the Stereolithography process. The hole relaxes the stresses in a certain area of the model and a strain gauge can be used to quantify the relaxation. The stresses caused by build parameters including hatching spacing and curing depth as well as thermal and ultraviolet post-processing treatments were assessed and their effects were found to be negligible, holding steady at approximately 6.5% of the ultimate tensile stress [80].

Further analysis of curing behaviours of acrylate-based resins were conducted by Fuh *et al.* [81] who used a combination of differential scanning calorimetry (DSC) and Raman spectrum analysis to characterise photopolymerisation on a micro scale. On a single scan profile, Raman spectrum analysis showed a degree of curing value before post cure of 70% to 75%, however 120 seconds of ultraviolet post curing increased the degree of curing to approximately 92%. DSC measurements were taken to determine the curing percentage after different exposure doses, demonstrating a slow initial reaction with only 7% after 2 seconds, before a significant increase to 48% after 4 seconds and then a slowing of the reaction indicated by a linear increase in curing percentage to 92% over the subsequent 8 seconds.

The effect of thermal curing versus ultraviolet curing of photopolymers has also been assessed using DSC and differential scanning photo-calorimetry (DSP). DSP is the same as DSC however it measures the heat in a reaction induced by UV light rather than from heating the sample directly. Once a reaction has been initiated by UV light, heat cannot be used to re-initiate a reaction however, further exposure to UV light will continue the polymerisation of material [82]. In contrast, light cannot be used to initiate a reaction already started by heat therefore exhibiting no correlation between the two initiation methods in this process. Due to the differing energy levels released by the initiation methods, different curing percentages are also achieved by each method.

Stereolithographic resins possess certain characteristics that are advantageous for their use in the integration with direct writing technology. Lopes *et al.* considered the dielectric nature, ability to withstand high temperatures and viscosity of the resins when selecting those most suitable for the research [83]. This investigation was designed to find cured resins able to endure the high post-processing temperatures produced by the laser system when curing the conductive ink tracks and also to make the cleaning phase easier during fabrication. Eventually, DSM Somos® ProtoTherm™ 12120 resin [84] was selected as it has a high heat deflection temperature of 126.2 °C and viscosity of 0.550 Pa-s at 30 °C, which is relatively low for a SLA photosensitive resin. This resin has been used frequently during the research into the integration of multiple additive manufacturing processes that involve Stereolithography [85].

As mentioned previously, resin viscosity is of vital importance in process integration with top-down SL exposure orientation as deep dip recoating is largely relied upon as a recoating method. Low viscosity reduces the height of the apparent dome on the build surface by lowering the surface tension. The addition of Diethyl Fumarate (DEF) has been used to reduce resin viscosity where increased concentration of DEF correlated with decreasing elastic modulus and fracture strength. This is a result of the partial inhibition of crosslinking by DEF, weakening the structure [86]. Resin viscosity can be lowered via the addition of suitable thinners such as propoxylated neopentyl glycol diacrylate (PNGD) [87] to produce a range of solutions with specific ratios of resin to PNGD, from 100% to 50%, all of which can be cured, but may display slightly differing material properties. These formulations altered the viscosities as shown in Figure 2.5.
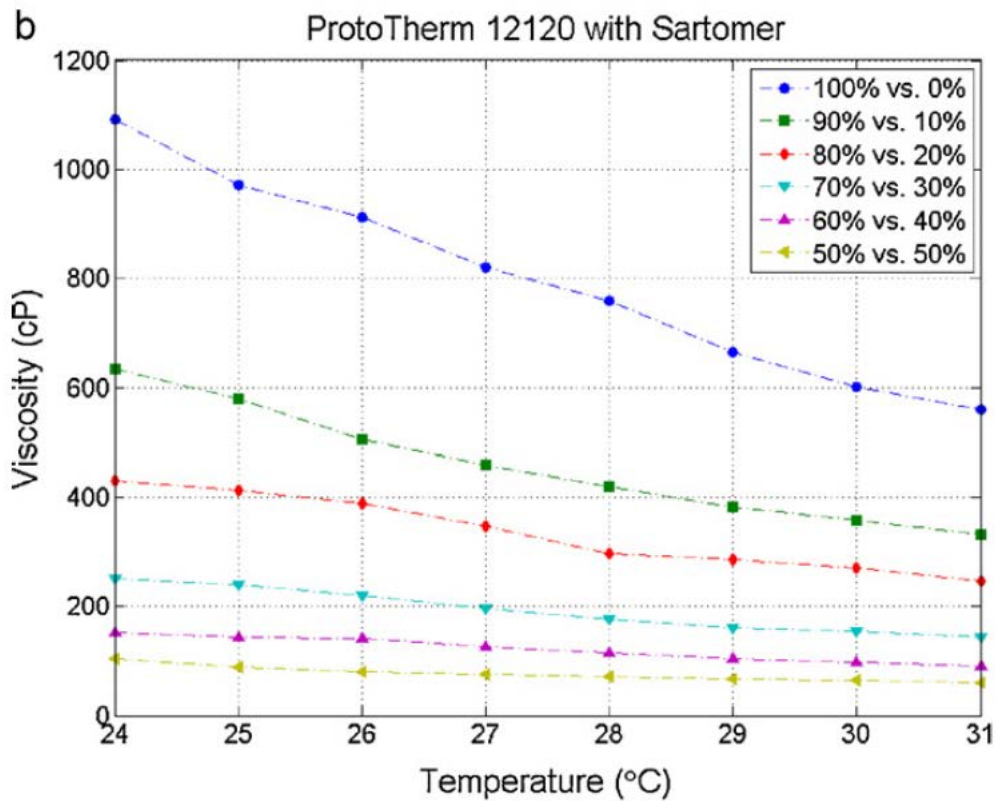
Figure 2.5.   Viscosity variation of diluted resin according to the concentration of diluent and solution
temperature [87]

Resins with a ratio of 1:1 resin to PNGD were used to fabricate multi-material chess pieces which all showed dimensional errors in the fabricated parts [88]. This error is caused by shrinkage and distortion and has a significant effect on the dimensional accuracy of parts created using Stereolithography. By measuring the amount of shrinkage this was then compensated for in the build process. Dilution with a low viscosity multifunctional monomer (MAM) and an absorbing dye material (ADM) has also been investigated with the long term goal of maintaining feature resolution while reducing the settling time of the resin and reducing optical penetration depth. The highest process resolution was achieved with a dilution of 50% MAM and 0.5% ADM however [89], the lateral resolution can be adjusted between 7 µm and 80 µm by varying the MAM and ADM content.

Research into the development of new materials for use in harsh conditions is desired by the aerospace industry and for down-hole oil drilling. Due to the ability of ceramics to withstand high pressure, work has been carried out to suspend ceramic powder in SLA resin which when cured acts as a binding agent for the ceramic material before it is then heat treated, a process involving both de-binding and sintering. The creation of a ceramic based resin requires the balancing of two opposing properties, ensuring that the quantity of ceramic powder added doesn't affect bonding between layers of cured resin whilst guaranteeing that the sintering process occurs correctly and

ensuring that the resin can still flow freely to create suitably thin layers for SLA processing [90]. The alternative to a ceramic doped resin is a high viscosity ceramic paste that doesn't require a vat and is spread using a blade. The advantage of this technique over the resin based alternative is speed. The paste does not require any settling time as the sweeping blade is completely responsible for the creation of each layer. The sweeping process allows the concentration of ceramic to be higher, therefore creating a more suitable material for the de-binding and sintering processes [91]. This high loading does reduce shrinkage, commonly approximately 10%, but values as high as 30% have been recorded in SL processing of ceramics. However the resolution is limited due to loaded particles scattering the light used during UV exposure [92]. Additive Manufacturing of ceramic parts allows testing to be carried out before parts are made by more expensive means and in greater quantities. It also allows very complex designs to be fabricated which would otherwise be impossible to produce.

2.3.4 Recoating

A level and ripple free resin surface must be achieved between curing cycles and this can be achieved using a variety of both proven and experimental methods. The method of recoating has proven to have a significant effect on the quality and accuracy of parts produced using Stereolithography and studies have been completed to determine the most efficient recoating method for different applications of the technology [66]. Commercial systems commonly use a recoating blade and change in elevation for recoating. Conventionally there are four steps to recoating using a blade: the build surface is fully immersed in the resin, one layer thickness below the surface; the blade then moves across the part removing all excess resin and leaving exactly one layer on top of the part; the platform moves down again and adds a layer of resin; it is allowed to settle before levelling and exposure [93]. Inaccuracies in the blade height can have consequences on the final part dimensions as the dimensional error is multiplied by the number of build layers.

There are many parameters affecting the recoating of resin into a uniform layer of the correct thickness due to properties of the resin and the forces acting on the blade and the resin during the sweeping process. On solid substrates the controlling parameter on layer thickness is the distance between the substrate and the blade. Solid-liquid substrates, for example, parts with entrapped volumes have a more complicated recoating process. They require the control of more process parameters including scraping velocity where a balance between force and free flow and, the depth of the trapped volume is necessary. Larger volumes require a greater blade velocity [93].

A variety of recoating concepts include XYZ Gantry, Selective Sweeping, Spray gun, Telescopic Blade and Rotating Blade have been developed [47]. The XYZ gantry system allows greater freedom of

movement of the blade as it is mounted to a system capable of multi-axis movement, allowing it to move around obstructions while the selective sweeping method uses changeable blades. The choice of blades is dependent on the quantity and position of the insert on each surface, allowing them to be avoided. Telescopic blades also create a versatile recoating system as the same blade can be shortened and lengthened. The rotating blade system resembles a conventional milling process, once the build surface has been dipped into the resin and left to settle, the rotating blade makes a pass over the surface, removing any excess resin. Finally, the spray gun method recoats the build surface by spraying an atomized layer of resin onto the build surface. This technique is capable of five axis control including rotation in x and y axes to allow coating of surfaces with diagonal or curved orientation [47].

Due to its relative simplicity 'deep dip' recoating has proven to be the most popular method used in research into process integration. This is because any sweeping blade, which is conventionally used in commercial systems, could make contact with an embedded component or structure protruding from the top surface of the part. The 'deep dip' coating method involves lowering the build platform to allow a new layer of resin to flow on top of the previously cured layer and waiting for the resin to settle as flat as possible. It is this waiting period, often called the 'z-wait interval' which has to occur for every layer, usually lasting between 6 and 10 minutes [94] depending on resin viscosity and can significantly increase build time when compared to other recoating methods. One solution to reduce z-wait time and therefore overall build time is to use a less viscous resin. This would reduce the time required for the resin to level. The advantages and disadvantages of low viscosity resins have been discussed in Section 2.3.3.

Blade recoating provides many advantages, the most important of which pertains to the uniformity of SLA layer thicknesses. The deep dip coating method described above creates a slightly domed top surface on the part once recoating has taken place, this occurs due to the dome effect that forms on the surface as a result of the surface tension of the resin, much in the same way a water droplet holds its shape. The introduction of a blade, allows more precise surface levelling to take place. A Zephyr™ blade in particular, which pumps resin from a reservoir in the blade during sweeping, can create layers as small as 100 μm due to a better control of the doming effect [95].

A 'bottom-up' Stereolithography projection orientation demonstrates a number of advantages pertaining to the recoating process. The recoating process is a function of the platform movement, raising the model from the build plane before lowering and positioning one unit of layer thickness above the build plane. No additional mechanism is required to level the layer where instead, the quality of the top surface is determined by the surface quality of the vat base.

2.3.5   Resin Level Monitoring

Recoating can ensure that uniform layers are produced each and every time, one on top of the other. It is however important in 'top-down' exposure based Stereolithography that the level of the resin is always the same height above the build surface, ensuring that layers are a consistent thickness. This process of monitoring and making the required alteration to the resin level has been carried out using a number of different techniques.

Inamdar *et al.* [95] manually checked the resin level on the build surface using a wet film coating thickness gauge. This was also demonstrated by Sandoval *et al* [96] and was combined with the multi pump levelling system of their bespoke Multi-Material Stereolithography (MMSL) machine consisting of a sensing head coupled to a floatation device and laser displacement sensor. The resin level could be accurately measured and the level raised or lowered dependant on the given reading. This was particularly necessary in this case due to multiple materials being utilised thereby requiring the need for regular movement between separate material vats due to differing material characteristics. Laser displacement sensors have also been used by Kruth and Renap [93] to monitor the height of the build surface as well as the layer of resin on that surface. This enables accurate measurement of the layer thickness using a reference and current measurement.

2.3.6   Stereolithography Post Processing

Once the model has been manufactured, post processing is required to make the part fit for use in one of a variety of applications. This can include removing any excess resin, removing any support structures and ensuring that the part is fully cured.

When the 'green' part emerges from the machine, support structures are removed. These structures ensure that any overhanging geometries over a pre-determined angle are printed as designed and do not sink into the liquid resin during manufacture. A sharp implement is often used for this, most commonly a chisel or scraping tool, taking care not to damage the part itself. The quantity and position of support structures can be significantly affected by the build orientation, making removal easier and improving overall part quality.

Due to its characteristics, excess liquid resin cannot be successfully removed with water and therefore a different rinsing medium is required. Suitable solvents are used to remove any uncured resin and are applied by rinsing, immersion or via washing in an ultrasonic bath. The removal of excess resin prevents it curing naturally on the part creating geometric defects and avoids leaving a sticky surface finish. This choice of application is largely based on the part geometry as ultrasonic agitation can remove resin from microscopic features by means of cavitation [97][98].

The removal of resin and cleaning of the part requires a solvent that reduces the viscosity of the resin, making it easier to remove from the part. There are a number of solvents that are commonly used to clean SL parts: Isopropanol, Methanol and Acetone, all of which have low viscosities to allow them to flow down narrow channels that can be achieved in the Stereolithography process. Dependant on the type of resin, different solvents may be chosen however some may cause degradation, cracking and swelling of parts. After exposure to solvents the part requires drying. A high pressure air feed can be used to dry the remaining solvent effectively.

Finally, the cleaned 'green' part is placed in an ultraviolet oven to ensure the part is fully cured. It is essential that all excess resin has been removed by this stage or it will end up being cured on the part. Parts are positioned on a turntable to be irradiated equally for a set period of time by 365 nm tube lighting in an ultraviolet oven. Larger parts require longer curing time within the oven to ensure sufficient UV light has penetrated the full part [81].

2.3.7   Stereolithography Applications

Stereolithography has applications in a number of industry sectors such as medical, aerospace, electronics and motorsport, largely due to its capability to produce very accurate parts with a high resolution. There are also a number of material properties that can be tuned through the use of different resin additives. They include thermal properties, dielectric constant, colour, etc. For example ceramic powders can produce materials better suited for electronics or high temperature based applications and elastomer based materials can be added to give the part a rubbery feel [72].

Additive manufacturing has been applied to the production of functional testing of Formula 1 racing car parts. Due to the high volume production of bespoke parts in Formula 1, the ability to rapidly make and alter prototypes as well as test them aerodynamically and through a variety of other mechanical tests, sweeping design changes can be made iteratively and in real time. Previously, test pieces were made using traditional time consuming cutting and deposition methods with materials such as carbon fibre, epoxy board and metal. In 2012 the Lotus Manufacturing team used Stereolithography to produce 14,000 parts for aerodynamic testing, directly from highly accurate CAD designs, to reduce both cycle time and cost. This resulted in a reduction in the average lap time by approximately one second from the beginning to the end of the season. Through the evolution of materials and their properties, additively manufactured parts can now be created directly for use on the racing cars themselves [99]. The future development of additive manufacturing in Formula 1 has been focused on material development to allow 'under the hood' testing with parts able to withstand the extreme conditions during racing, facilitated by the development of ceramic SL formulations described in Section 2.3.3.

The developments of multiple material SLA models increases the number of potential applications for prototyping and producing demonstration models [95]. With a wide variety of resins, models can be customised to suit requirements. For example, medical demonstration models could be created in a variety of colours. Stereolithography has been demonstrated to have various applications within medical engineering. Materials called hydrogels have been developed that, when cured, display properties, both mechanical and structural, that compare very closely to those of an extracellular matrix [100], a structural element present in living organisms. It has also been used to mass produce customised tooling for the manufacture of hearing aids. In this approach a mould is taken of the patients ear, reverse engineered using a laser scanning system to create a CAD model from which a negative mould can be fabricated using Stereolithography [68].

Finally, additive manufacturing technology also exhibits benefits for the rapid production of tooling and masters. Many mass manufacturing techniques require tooling to be made in a specific size and shape, costing anywhere from £10,000 up to £1 million and taking a significant amount of time to produce. Additive manufacturing allows rapid production of tooling at a fraction of the cost but with the trade-off of lower durability and longevity. The technology does however provide a more economically viable method of tooling production while allowing easier creation of custom, one-off tools.

2.3.8   Multi-Material Stereolithography

Additive Manufacturing processes are usually limited to using one material class to create a three dimensional model. Naturally, as the technology improves, processes will expand to facilitate fabrication from multiple materials allowing the production of devices with greater functionality. Inamdar *et al.* [95] used a rotating vat arrangement to create SLA parts using a laser source, top-down build orientation and multiple resins, generating the potential to have multifunctional models with a variety of advantageous properties. The resulting fully automated, MMSL system [101] provided further potential for the combination of multiple AM processes. There are however some issues with the process, primarily the likelihood of contamination between vats of material. With movement in any system there is also the potential for misalignment of the part, which could again cause inaccuracies in the finished product. Zhou *et al.* [67] have developed a similar arrangement using a DMD-based dynamic mask to enable bottom-up production.

2.3.9   Two-Photon Stereolithography

This variant of Stereolithography is conducted in a volume of material whereby the curing of the material occurs through moving the focal point of a femtosecond near infrared laser. This results in the transmission of the light through the material with polymerisation confined to the focal volume

[102]. This process requires the absorption of two photons of light to enable the transition of electrons from a low to high energy level. Generally a Titanium:Sapphire laser is used due to its generation of super high power pulses.

A variety of engineering materials including ceramics and metals can be created by loading resins with fillers to produce 'green' parts which can then be post processed. Two photon photopolymerisation provides several advantages over standard laser based processing, especially in the semiconductor industry which conventionally requires high resolution and small feature sizes [103]. Feature sizes of 1.7 µm have been produced in SU-8 photolithographic resin. Developments have been made to improve horizontal resolution by reducing the spot size of the laser source, reduce the need for fine focusing of light by using image projection and improve transverse resolution whereby layers are polymerised within the medium rather than on the surface using two photon polymerisation [104].

2.3.10 Continuous Liquid Interface Production

The stereolithography process has evolved past layer based manufacturing and its procedural characteristics have been developed to create continuous liquid interface production (CLIP). This has resulted in fabrication times 25 to 100 times faster than convention, reaching speeds of up to 500 mm/hour [105]. These speeds are achieved as the cure time is no longer determined by the layer thickness but instead the rate of production is controlled by the resin viscosity and the rate at which the resin cures.

The CLIP process has been outlined in Figure 2.6 and is a variant of bottom-up projection Stereolithography. The digital model is processed to create a video file of the continuous cross section of the model from bottom to top. Once the build process is initiated, the video file is projected onto the base of the vat and the build platform is continuously moved away from the base as polymerisation occurs.
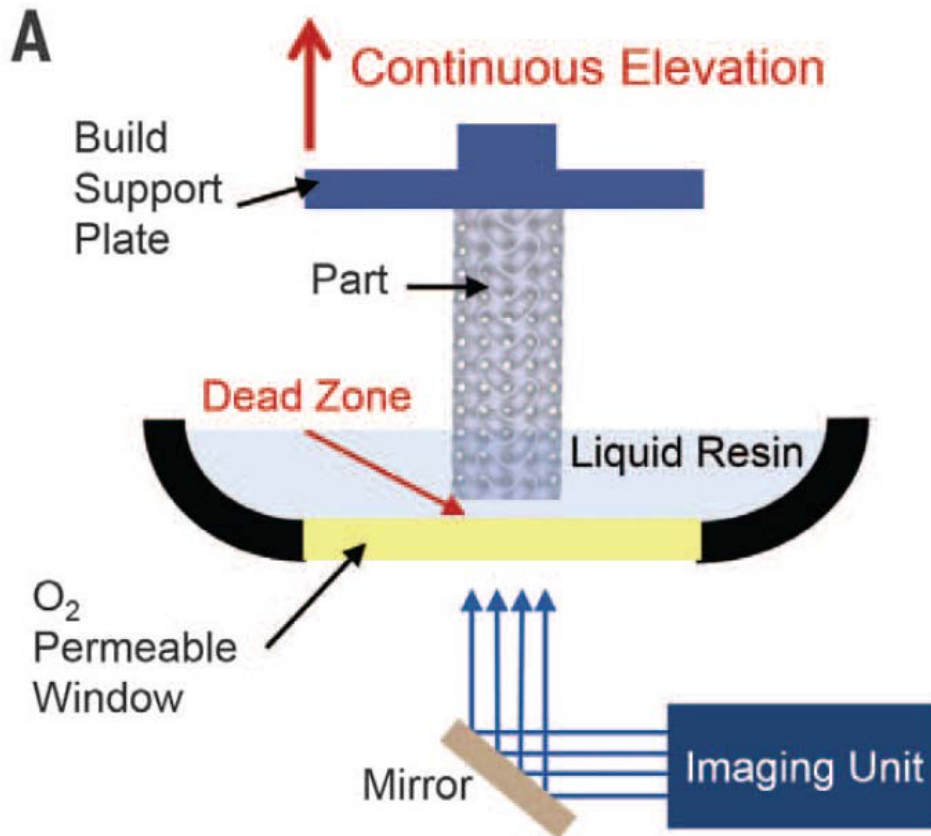
Figure 2.6.   Schematic of CLIP Technology [105]

Uninterrupted polymerisation was achieved using a UV transparent, chemically inert, oxygen permeable window made of an amorphous fluoropolymer, inhibiting curing of the resin between the window and the fabricated part [106][107]. An optimum dead zone thickness of between 20 μm and 30 μm has been identified to ensure no adhesion between the base of the vat and the part while minimising the diffraction of projected light. This layer-less process eliminates the stair stepping effect demonstrated by all additive manufacturing processes however, struggles to cure large surface areas as the liquid photopolymer cannot replace itself to ensure continuous curing.

2.4   Direct Writing Technology

Direct Writing has been defined by Lewis and Gratson [108] as 'fabrication methods that employ a computer-controlled translation stage that moves a pattern-generating device, for example, an ink deposition nozzle or laser writing optics, to create materials with controlled architecture and composition.' This tends to be with functional materials, hence its frequent application in the deposition of conductive materials.

A vast number of processes are covered by the umbrella of DW [109] that can generally be categorised into material jetting, material dispensing and aerosol jetting. There is some

disagreement surrounding the definition of direct writing technology as an additive manufacturing process. Material jetting and dispensing both possess the capability to fabricate 3D geometries in a layer-by-layer fashion however, the layer thickness of material deposited by Aerosol Jetting limits its three dimensional potential. Direct writing processes are designed for the production of thin features and not three dimensional geometries. That said, dispensing in particular has the potential to be applied to 3D fabrication.

Material jetting refers to the selective deposition of droplets of material from a print head in close proximity to the substrate surface. Due to the actuation methods required to jet the material, certain rheological properties are necessary. In particular, a viscosity and surface tension that allows the material to be jetted through a small orifice while maintaining a uniform droplet once ejected from the print head. These required characteristics can also cause problems with the droplets' interaction with the substrate including issues with wetting and adhesion of droplets. Conductive traces approximately 30-40 μm in width and down to 100 nm thick have been produced. [110][111]. The nanoparticle silver based ink produced a resistivity approximately twice that of bulk silver at 3 μΩ.cm.

Aerosol Jetting technology combines an aerosolised stream of ink and a sheath gas to direct the materials towards the substrate surface in a continuous torrent. The sheath gas stream focuses the aerosol jet creating line widths only a fraction of the size of the nozzle. Specified track widths of ~50 μm can be realized with material improvements and process characterisation resulting in 10 μm wide tracks [112]. Small changes in the specified 2 mm to 3 mm print gap do not have a significant effect on the trace width making it ideal for uneven topographies achieved without encountering issues common with other direct writing processes [113]. This technology also facilitates use in printing on conformal substrates in 3D when attached to a five axis Computer Numerical Control (CNC) system [4]. Inks with a viscosity in the range of 1-1000 cP, higher than those compatible with material jetting and, commonly metal, polymer or adhesive based, can be atomised and directed at the substrate in a steady particle stream. This includes the capability to jet conductive traces from nanoparticle inks including gold and silver as well as biocompatible materials, silicones and photopolymers. The machine consists of two critical modular parts, one for atomizing the material, creating a dense aerosol of droplets, and the other for directing and depositing that material [114]. The droplets are deposited in a stream measuring between 1 μm and 5 μm in diameter, travelling at approximately 50-80 m/s, with a density approaching 10 million droplets per cubic millimetre [115] and the print head positioned approximately 2-5 mm from the substrate [116]. The stream diameter is achieved as any drops larger than 5 μm will drop back into the ink due to the force of gravity. A

flow of gas then forces the aerosol through the print head, compressing and focusing the particle stream. The substrate material and angle at which the jetting occurs determine its wetting properties and can require surface texturing in particular cases to improve wetting and prevent free flow of the jetted ink. Aerosol jetting has also been applied to selectively deposit photopolymers before being polymerised [117]. This process has demonstrated the capability to produce 5.3 μm line widths.

Dispensing refers more closely to the extrusion of higher viscosity materials onto a substrate [118][108] typically using mechanically or pneumatically driven pressure. These materials typically possess a paste-like property which improves their wetting characteristics when compared to inks, but still allows an uninterrupted flow through the deposition nozzle. Dispensing has been proven to produce features as small as 1 μm [11], a capability which is controlled through differing sizes of nozzle, material properties and pressure. The movement of the dispensing head has been achieved through its combination with a multi axis machine head, capable of, at the very least, moving in x and y axes and in some cases, in 5 axes allowing material to be dispensed on surfaces with increased topological complexity.

Analysis has been conducted on the effect of dispensing head velocity on the contact angle, track height and track width whilst dispensing pressure, nozzle diameter and temperature remain constant [119]. Although the height of the tracks remained consistent at approximately 200 μm, the dispensed track was very wide measuring 1200 μm at 800 mm/min velocity and decreasing linearly to 800 μm at 1600 mm/min. These tracks however are too large to be considered for use in MEMS and potential use in microscale packaging applications.

Fully functional microscale devices and micro-electro-mechanical systems have been completely fabricated through direct write technologies. 3D micro batteries have been created using a material dispensing technology capable of producing features as small as 1 μm [11]. A collection of 30 μm cylindrical nozzles were used to dispense the material on a glass substrate in a high aspect ratio.

Much of the research surrounding the integration of direct write systems focus on the use of the commercially available nScrypt Smart Pump 100 [120] which is capable of dispensing lines with a width of 25 microns, ideal for the deposition of conductive tracks on a micrometre scale to create functional circuitry. The system also allows creation of complex circuit designs and allows tracks to be printed in three dimensions. Stereolithography parts have been placed and aligned in the dispensing system before tracks are printed and recovered with cured resin [83].

There are other commercially available dispensing systems which have been used to write conductive ink tracks, one such example is the 2405 Ultra Dispensing System by EFD Inc. Medina *et al.* [121][122] dispensed sliver based conductive ink, CI-1002 by ECM, selected due to its low cost, low curing temperature and low resistivity. A variety of dispensing tips and pressures were tested to determine the most suitable combination to create a minimal track width, the best results were achieved by a 60 µm tip at 4 psi, creating a line approximately 0.4 mm wide. Tracks that wide would make this equipment unsuitable for much of the research being conducted as track width helps to determine the overall size of the fabricated object and would therefore hinder minimisation of the footprint of the circuit.

Kong *et al.* have used micro scale, multiple material dispensing capability to print quantum-dot-based LEDs (QD-LEDs) printing an array of LEDs in a 2 mm x 2 mm x 2 mm cube [9]. All parts of this cube have been 3D printed using the extrusion process including the emission of semiconducting inorganic nanoparticles, elastomeric matrix, organic polymers, solid and liquid metal leads and transparent encapsulation material. Their research proved that functional electronic structures can be completely fabricated using DW technologies.

2.4.1   Conductor Materials

There are a vast range of materials to complement DW processes that take the form of a base fluid, solvent or epoxy, filled with a specified weight of particles to create a paste or ink which solidifies through a phase change induced by a change in temperature, solvent evaporation or gelation [118]. Materials include polymer melts, colloidal gels, waxes, dilute colloidal fluids and highly shear thinning colloidal suspensions. The two most commonly dispensed conductive materials within the context of this research are conductive inks/pastes and Isotropic Conductive Adhesives (ICAs).

Conductive adhesives differ from inks in their designed application, printing characteristics and curing regimes. They achieve conductivity through a combination of two mechanisms: 1) during the thermal curing process the resin part of the epoxy formulation shrinks, causing increased contact between particles or flakes of the filler material; and 2) evaporation of lubricants which reduces the distance between particles further, subsequently reducing the contact resistance [123].

ICAs are typically designed to be screen printed onto circuit boards to adhere components to their conductive pads and as such, tend to be more viscous and traditionally thermally cured. Direct writing in these materials could prove hugely beneficial as it would eliminate the need for an additional deposition process to facilitate surface mount assembly and can be conducted directly from a digital design. Although stencil and screen printing is quicker than the direct writing approach,

it does require the manufacturing of bespoke tooling for each new pattern. There is however very little research to-date conducted into the integration of conductive epoxies with a Stereolithography substrate fabrication process.

Niese *et al.* [119] conducted experimentation on laser curing of conductive epoxies in an attempt to improve resistivity when compared to thermal curing regimes. Epoxy performance after thermal curing could not be improved through the use of laser sintering without damage to the epoxy on and adjacent to the travel path. At higher laser powers, the substrate material was also degraded. A sample showing no damage was produced at a power of 0.7 W on the pulsed solid state (Nd:YVO$_4$) laser system with wavelength of 355 μm. An average resistance of 0.43 Ω was measured on a 20 mm trace, approximately 160% higher than the average resistance measured from identical samples after oven curing. The trace also demonstrated a lower adhesive strength during simple scratch tests versus the oven cured sample.

Much research has been conducted in the field of conductive inks. These inks are particle based and contain metal flakes or particles, most commonly, of gold, silver and copper [124]. Due to the high price of gold and issues with copper particle oxidation, silver is the most commonly used conductor material. Although silver does also oxidise, silver oxides have much better conductive properties than copper oxides [125]. On a nanoscale, silver has also proven to be more easily dispersed in a solvent than gold, maintaining a stable suspension for more than a year [126]. These ink or paste materials usually achieve their optimum conductivity through temperature-based phase change. Sintering is specifically used for nanoparticle inks and is achieved through exposure of the material to a thermal oven, a laser or a flash lamp. Nanoparticles can be sintered at much lower temperatures than their microscale alternatives and result in the fusion of particles in the paste or ink to form a conductive connection. Micro-particle filled inks achieve conductivity through a curing process whereby the reaction of an epoxy or other adhesive resin draws the micro-particles into contact, but does not result in a metallurgical bond. If the ink's curing temperature is too high it could cause secondary damage to the substrate.

The rheology of inks is also incredibly important in the determination of their suitability for use in particular applications and to be dispensed using particular methods. They must demonstrate shear thinning, ensuring they flow through the nozzle yet behave in a predictable fashion when they make contact with the substrate ensuring they don't slump and, adhere suitably to the substrate [11]. Advantageous rheological properties are achieved by removing oversize powder particles above certain diameters using a centrifuge before it is mixed with the solvent to minimise the clogging of nozzles.

Silver nanoparticle inks have been developed specifically for dispensing. Lewis *et al.* [127] have developed a recipe for synthesising amphiphilic silver micro particles as shown in Figure 2.7. In addition, the multi-material extrusion Voxel8 system has been produced that prints Polylactic Acid (PLA) substrates and conductors using this conductive ink and a 250 µm nozzle [128].
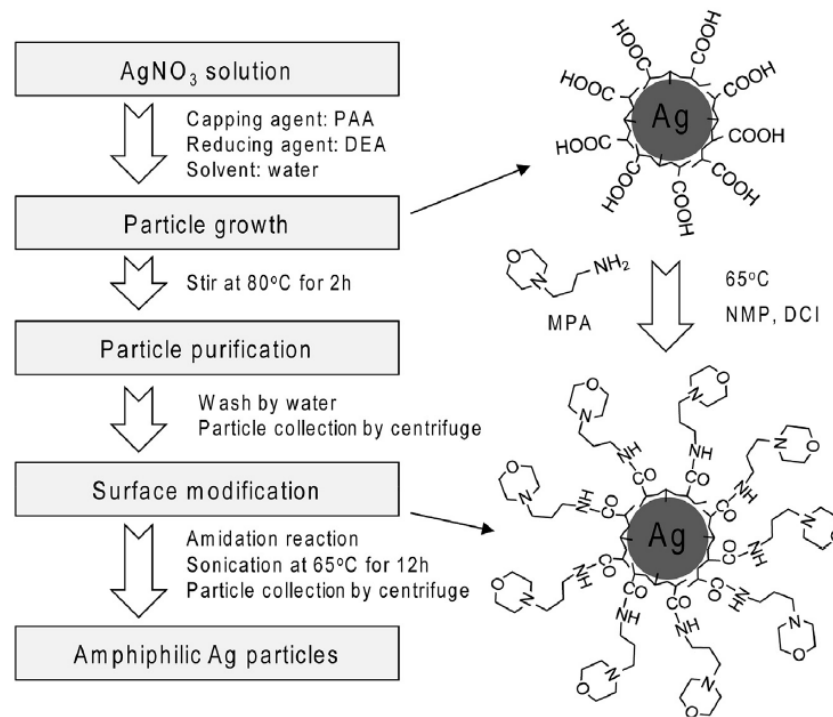
Figure 2.7.   Flow diagram and schematic illustration of PAA (Poly(acrylic acid))-capped Ag microparticle synthesis and surface modification by amidation reaction using MPA [127]

Using aerosol jetting technology a 27.5 wt% silver in 1:1 water:IPA by volume ink was created and deposited in 36 µm wide and 1.2 µm thick tracks. A 6 wt% ink in ethanol has also achieved a resistivity as low as 3.9 µΩcm. Further aerosol jetting of conductive materials has shown track widths as low as 10 µm with smooth profiles, clean edges and even thickness [115].

Lopes *et al.* [85] tested the properties of various conductive inks on a number of potential substrates to determine the best candidate for the direct writing of the functional circuitry, the results of which are presented in Table 2.3. In this research, E1660 silver conductive ink produced the lowest average resistance at 3.039×10^{-1} Ω along a 1 inch track length across all non-traditional photopolymer substrates. Frequency and high voltages were not considered in this study and therefore, the conclusions of this study are only valid for low-voltage and low frequency / direct current devices. Navarrete *et al.* [129] experimented further with the frequency factor in the conductive media, firstly by proving that it directly affects the capacitance, inductance and resistance of the circuit

which in turn, impedes changes in voltages and currents, and secondly, by testing this theory on four candidates for suitable conductive inks (E1660, E1440, PTF-10A and CI-1001).

Table 2.3.   Average and standard deviation of measured resistance, inductance and capacitance values derived from [129]

Test Sample	Average Resistance (Ω)	Resistance Standard Deviation	Average Capacitance (F)	Capacitance Standard Deviation	Average Inductance (H)	Inductance Standard Deviation
PCB	2.117×10^{-1}	1.127×10^{-2}	6.750×10^{-6}	1.215×10^{-6}	3.978×10^{-3}	9.869×10^{-4}
E1660	3.039×10^{-1}	7.944×10^{-3}	3.375×10^{-6}	1.130×10^{-6}	7.775×10^{-3}	1.242×10^{-3}
E1440	6.094×10^{-1}	1.462×10^{-1}	1.253×10^{-6}	5.397×10^{-7}	2.165×10^{-2}	8.552×10^{-3}
PTF-10A	8.475×10^{-1}	1.221×10^{-1}	5.611×10^{-7}	7.465×10^{-8}	4.609×10^{-2}	1.768×10^{-2}
CI-1001	1.513	8.382×10^{-2}	2.203×10^{-7}	1.371×10^{-8}	1.595×10^{-1}	1.887×10^{-2}

Values taken during this study on the four inks were compared to a copper track on a conventional PCB and again, E1660 was proven to be the most suitable as its parasitic values most closely resembled those of the PCB, suggesting that radiation of electromagnetic waves will be effected least by the impedance values of this ink. The average resistance of E1660 was 43% or ~0.1 Ω greater than the PCB however this demonstrates good performance as the next highest performer was E1440 with an average resistance 180% higher than the PCB.

Further work was also conducted to determine the effect of the volume of ink on its resistivity on different substrates. Again, the same five silver based inks as shown above were used with a variety of viscosities, cure temperatures and cure times [83], which, when assessed alongside the volume resistivity, also determined that E1660 was the best ink for this application. Finally, experimentation also showed that curing the conductive ink for 80 °C for 16 hours increases the conductivity and reduces the resistivity of the ink traces, increasing the temperature and time from this point will increase the resistance. It was also shown that embedded traces displayed a higher resistance than those open to the air but not significant enough to discount the idea of embedding conductive traces. This is most likely the result of stresses in the substrate material acting on the conductive trace, cleaving the conductive particles apart and reducing therefore conductivity.

Alongside ink curing parameters, differing methods were also investigated and their varying effects on the post curing properties of the conductive traces and substrate were analysed. As the curing process relies on heat to evaporate the silver particles' transport medium, the most commonly used method is through an oven, however the potential for selective laser curing has been examined with

the determination that the process would be faster, capable of more localised curing, reducing the exposure of the entire part to high heat and allowing all processing to take place in one machine [130]. The laser curing concept relies upon the energy source providing enough energy to evaporate the particle loaded solvent and enough residual heat to fuse the remaining particles together to create a dense conductive trace [131].

As the particle size decreases the required curing temperature also decreases [132]. This characteristic is a mechanism of the surface area to volume ratio, making it suitable for deposition on materials with a lower temperature resistance. The electrical properties of nanoparticle silver inks are also impacted by their curing regimes [133]. It has been suggested that an incremental temperature curing regime may result in the highest conductivity despite near bulk resistivity values achieved at only 150 °C. Reduced sintering temperatures in gold nanoparticles have also been demonstrated for use with temperature sensitive substrates [134].

Experimentation with a range of different lasers on a variety of micro and nanoparticle inks has been previously conducted. Maekawa *et al.* [135] used a variety of laser sources to determine the effect of wavelengths between 488 nm and 1064 nm on the sintering of silver nanoparticles. They discovered that, as the laser power increased, the resistivity of the sintered silver decreased and that, diode lasers and Argon Ion lasers produced sintered silver with resistivity values 310% and 500% that of bulk silver. Experiments using a Diode-Pumped Solid State (DPSS) laser have also been conducted at 532 nm by Kim *et al.* [136] to cure a silver based conductive ink and proved that oven curing is a longer process than laser curing to achieve a comparable resistivity. Silver inks were also successfully cured by Fu *et al.* [137] using repeated irradiations of a 532 nm Nd:YAG laser and finally, Shang *et al.* tested various traversing speeds to determine a relationship between this parameter and resistivity. The quality of laser curing, using different beam intensities of a CO_2 laser, on silver based ink was studied using a laser assisted direct write method. These varying investigations have determined that the curing process tends to be more efficient and effective with increased laser power and that energy absorption of the silver ink can be influenced by the wavelength of the source. It is only the materials that limit the effectiveness of the process, for example, laser power has to be restricted to prevent damage to the substrate [138].

Lopes *et al.* [83] examined the effect of laser curing on the properties of Ercon E1660 ink, previously proven to be most suitable for oven curing. Four different scan locations were used for the study, 'on ink' whereby the laser is focused on the centre of the channel and three other positions where the laser is positioned 190 μm ('on edge'), 445 μm ('SL substrate 1') and 570 μm ('SL substrate 2')

from the centre of the ink trace, the last two of which are positioned solely on the substrate. The track resistance corresponding to the laser position and number of passes is detailed in Figure 2.8.
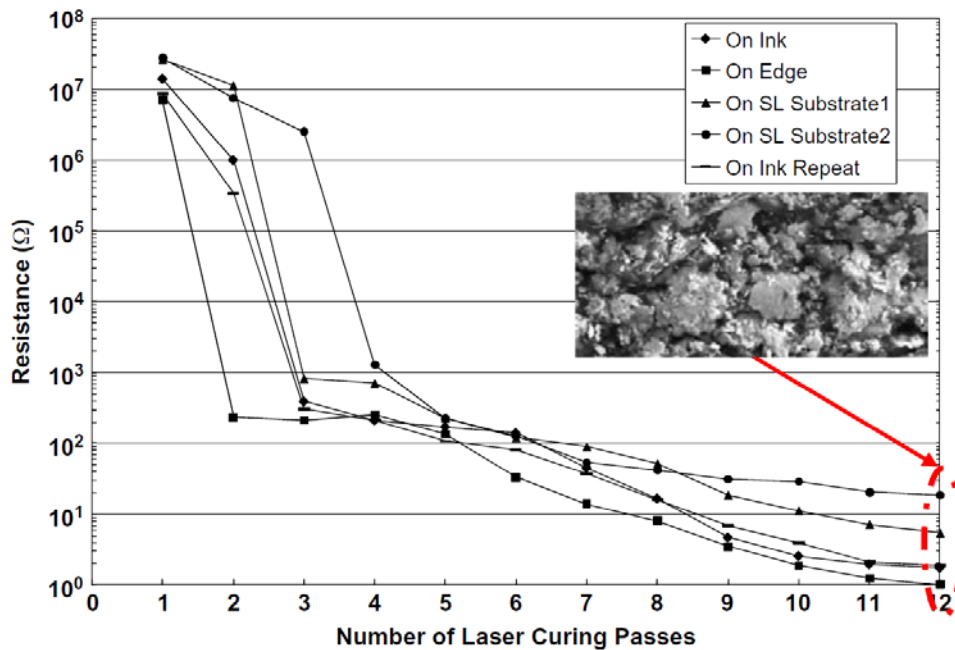
Figure 2.8.   Effect of Laser Curing Method on Trace Resistance [83]

The results show that all laser curing paths lowered trace resistance with the 'on edge' position producing tracks with the least resistance and, both SL substrate positions result in trace resistances that are approximately 10 times higher, explained by the vastly reduced energy transfer between the laser and the ink in the latter curing paths. The reduction of resistance occurs in two distinct stages: firstly a sharp drop caused by evaporation of the solvent pulling the particles into contact, shortly followed by a longer period of gradual reduction as the silver particles begin to fuse together, reducing porosity in the tracks.

Further work was conducted by Lopes *et al.* [130] to determine the effects of a wider variety of different laser scanning patterns as well as scanning speed. The previously tested 'on ink' and 'on edge' locations were compared to the newly added 'on both edges' and 'adjacent' positions, the first of which simply mirrored the 'on edge' location by introducing another laser and the latter, by widening the two lasers whereby the innermost point of the beam diameter formed a tangent with the edge of the ink trace. The new scan paths were also tested at two different speeds, 'faster' and 'fastest', with approximate scanning speeds of 1925 µm/s and 13500 µm/s respectively. Both scan patterns produced comparatively similar results both from observations and quantifiable data however, the 'fastest' scan speed resulted in a trace resistance approximately 20 times higher than the 'faster' value. In addition, from an observational perspective, no charring was present on the

substrate at the 'fastest' speed, but did at lower speeds. Due to the higher trace resistance associated with a higher scan speed, and substrate charring associated with 'on edge' and 'on substrate' scan patterns, the most suitable laser curing method was determined to be a slower speed, approximately 480 μm/s, 'on ink' whereby a similar resistance is achieved without any damage to the substrate. This speed is very slow and would not translate well to a production environment without the use of multiple lasers.

Laser curing has been proven to be more effective than oven curing alone, however, the final part of Lopes *et al.* research in Figure 2.9 shows that oven curing after laser curing can further reduce the resistivity of the conductive traces [130].
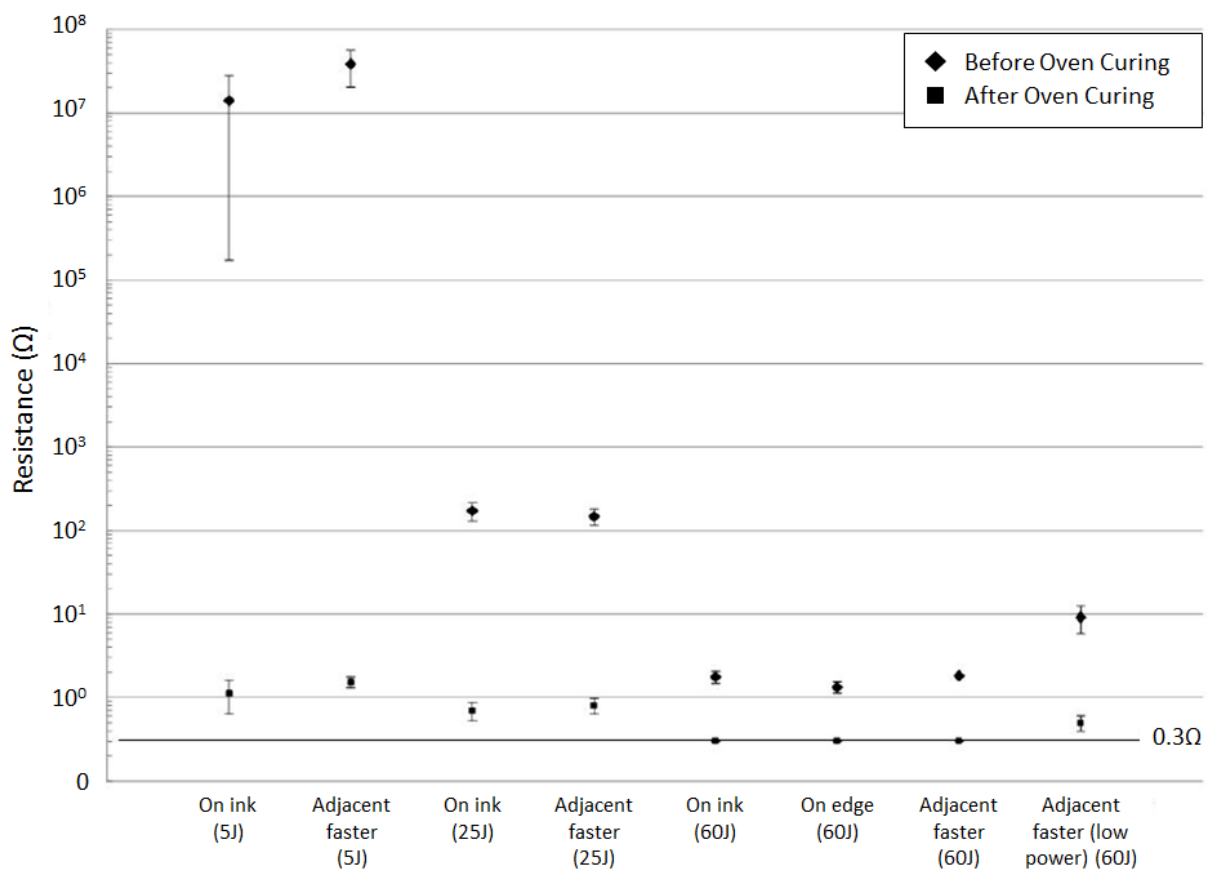
Figure 2.9.   Effect of oven curing on trace resistance of different laser cured ink traces [130]

Electrical sintering was first tested on ink-jet printed tracks on a temperature sensitive photo paper [139], resulting in increase in conductivity by more than five orders of magnitude. The term 'ohmic' curing was introduced by Roberson *et al.* [140] who used 'ohmic' heating as a means to decrease the resistivity of conductive traces. This mechanism is achieved by passing an electrical current through the material causing rapid uniform heating. Both micro and nanoparticle inks were cured in seconds through this method when compared to traditional oven curing which nominally takes an hour or

longer. In this experiment current density and time were varied producing resistivites 36% lower than thermally cured samples in micro-particle inks. The 'ohmic' curing process in this research was however a secondary curing process as all inks had already been thermally dried to a state just prior to the occurrence of particle sintering, allowing the sintering effect of the ohmic heating to be evaluated. The lowest resistivities produced were five times and three times that of bulk silver for micro-particle and nano-particle inks, respectively. Ohmic curing presents a method of improving the resistivities of conductive tracks in materials incapable of resisting high temperatures for long periods of time. This process has been demonstrated in both 2D and 3D structures, with a matrix of prefabricated channels created, filled with conductive ink and a combination of thermal and ohmic curing used to cure the ink even in embedded channels [141]. This process shows significant benefits as in situ curing can occur provided there is a conductive connection to the volume of ink.

2.4.2 Direct Write Applications

Printed electronics is a very advantageous alternative to conventional electronics fabrication techniques due to its lower cost and flexibility [142]. Considered a very important milestone within printed electronics, the ability to fabricate low resistance electrodes in a high aspect ratio, spanning three dimensions, has many real-world applications. These include flexible displays and antennas, a significant improvement on current screen and inkjet printing methods [143]. In addition, some direct write processes, particularly dispensing and aerosol jetting in combination with conductive materials, have proven their capability to create PCB-like conductors and interconnects, producing functional electronic devices.

Improvements in DW process resolution has improved the process versatility facilitating the production of micro batteries weighing approximately 100 micrograms, 0.1% of the weight of those currently available, each costing less than a penny. This revolution could create a new age of microsystems, one such potential application being in the creation of tiny flying drones dubbed as RoboBees [144].

Aerosol jetting provides an array of applications and provides the potential for a significant reduction in the footprint of many personal electronic devices. Manufacturers of handheld mobile devices in particular are implementing new 3D packaging ideas [114]. This technology has also been employed to create 30 μm wide conductive traces along the staircase sidewall of staggered multi-chip die stacks using silver based nanoparticle ink, demonstrating the three dimensional capability of the technology to produce finer pitches and reduced size of the final module [115]. Aerosol jetting has also been proven in its use to create electronic devices, in both a single layer of a single material and multiple layers of multiple materials, with conductive lines crossing over one another with layers

of dielectric material between them to maintain electrical isolation. The three dimensional capability is further demonstrated in the use of Aerosol jetting to print a sensor, antenna and power distribution circuit on the wing of an Unmanned Aerial Vehicle [4].

The capability of DW technology to produce stretchable and flexible microelectrodes in three dimensional spaces presents a variety of potential applications. This enabled silver nanoparticle inks to be printed on curvilinear surfaces creating electrically small antennas [145]. These devices support the ever increasing demand for compact devices that still maintain their full functionality; this is especially difficult when applied to antennas due to the inherent limitations in system range, gain, bandwidth and efficiency associated with their reduction in size.

In addition to printed electronics, research into the antimicrobial properties of amphiphilic silver particles is also being conducted. Hybrids of particles between 1 nm and 2 nm in size can adhere to polar solvents to create eco-friendly antimicrobial coatings. Glass slides coated with these particles demonstrated a 98% reduction in bacterial growth [146].

2.5 Process Integration

The potential to integrate many different Additive Manufacturing technologies would allow vast improvements in manufacturing of electronics, especially in unique applications where bespoke parts are required. A number of different approaches to both substrate fabrication and printing of conductors have been developed and are summarised in Table 2.4.

Table 2.4.　　Previous research conducted into integrated AM processes

Substrate Fabrication (material)	Conductor Fabrication	Min. Conductor Width (μm)	Min. Conductor Resistivity	Publication/s
PolyJet (photopolymer)	Dispensing (silver ink)	400	Not available	[147][148]
Ultrasonic Consolidation (metals/alloys)	Dispensing (silver ink)	350	Not available	[109]
Stereolithography (photopolymer)	Dispensing (silver ink)	250	Not available	[129][83][85][94][121]
Fused Deposition Modelling (ULTEM 9085)	Aerosol Jetting (silver ink)	30	11.8×10^{-6} Ω.cm	[149][4]

Selective Laser Sintering (nylon)	Aerosol Jetting (silver ink)	n/a	0.004-0.080 Ω.cm	[150]
Selective Laser Sintering (nylon)	Dispensing (silver paste)	3175	0.001 Ω.cm	[150]

With the exception of the Aerosol jetting process, all others show high conductive trace widths restricting the resolution of the hybrid manufacturing process, despite the proven resolution capability of material dispensing in Section 2.4. Navarrete *et al.* demonstrated a reduction in the overall size of the circuit, embedded components within the final part and enhanced protection from the external environment, all alongside greater strength and reliability [129].

2.5.1 Additive Manufacturing Hybridisation

Design considerations for hybrid additive manufacturing and direct write processes were presented by Perez and Williams [147] who evaluated component embedding methods, a variety of potential direct write technologies and materials, all for integration with the PolyJet™ manufacturing process. These considerations were then adapted for use with additional additive manufacturing substrate fabrication processes.

There are three processes that have been considered for the creation of electronic substrates, Selective Laser Sintering (SLS), Stereolithography (SLA) and Ultrasonic Consolidation (UC) which, when integrated with a Direct Write technology, can be used to print passive or active components. Robinson *et al.* [109] explained the use of Ultrasonic Consolidation and Direct Write technologies to create compact, complex, multifunctional structures for small satellites. Similarities between the use of Ultrasonic Consolidation and Stereolithography are apparent in their use to embed the conductive inks within the substrate however they have different base materials in polymers and metals. A primitive version of process and material integration for electronic circuitry was demonstrated by Periard *et al.* [151] who created simple timer and flashlight circuits on a table top Fab@Home machine by embedding conductive ink and components into a 2-part epoxy material. Although the result was not as accurate as would be achievable through the use of alternate processes and machines, it provided a sound demonstration of the potential of the technology.

An integrated PolyJet™ printing process has been designed to overcome a number of perceived difficulties identified in additive manufacturing process integration including the inability to treat the surface between processes resulting in low surface quality, degradation of the polymer matrix

caused by the conductive ink sintering process and, structural weaknesses caused by prolonged pauses in the printing process [148]. PolyJet™ printing has been utilized for the production of an encapsulation matrix for printed sensors created by aerosol jetting. Strain sensors were jetted onto polytetrafluoroethylene or perfluoroalkoxy alkane films, transferred to a substrate via a 'print-stick-peel' (PSP) method before encapsulation by PolyJet™. This method, shown in Figure 2.10, has removed the requirement for channels to print into; a common method in hybrid processing and a continuous manufacturing procedure for smart structures was proposed.
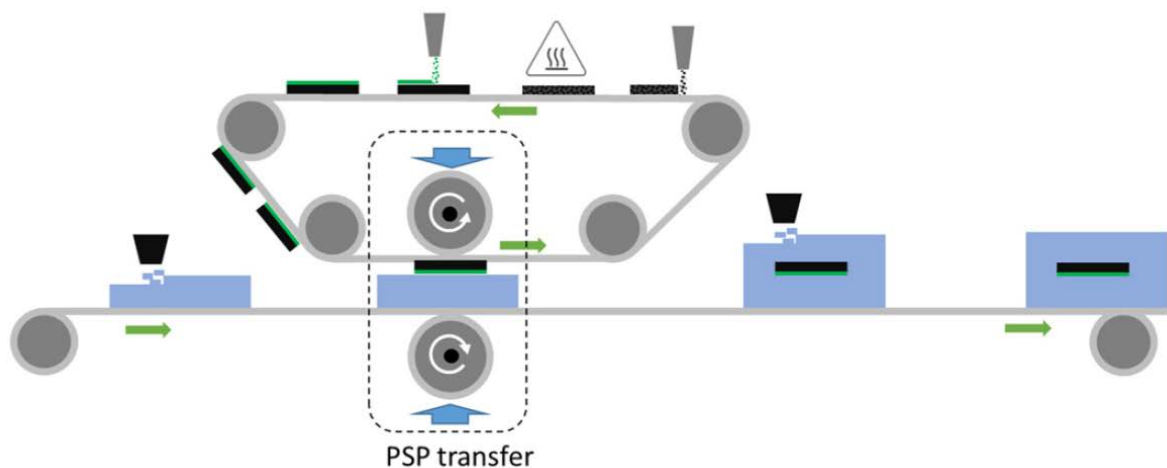
Figure 2.10.   Schematic of the PSP-enabled continuous manufacturing for smart structures [148]

The significant limitation of this PSP-based printing method is its ability to only produce 2D devices. Interconnections in the z-axis cannot be fabricated and therefore, although this process may address some limitation of hybrid processing, it does not provide an alternative method for multi-layered electronics at this stage of development.

Additive Manufacturing processes have previously been combined with Aerosol Jetting technology under a project entitled '3D Additive Manufacturing of Electrical and Electronic Applications' funded by the US Federal Ministry of Electronics and Technology. Powder bed processes were used to create a substrate on which conductive tracks were deposited, however, due to the porous and uneven nature of the substrate, the behaviour of the ink was significantly affected [115].

2.5.2   Stereolithography and Direct Write Integration

The most commonly hybridised additive manufacturing process with direct write technology is laser-based, top-down Stereolithography. Process and scheduling planning has been carried out in previous work to develop a multi-material Stereolithography system [152]. This enabled modelling of the fabrication process and determination of the steps required to optimise this process, from

material changeover to the mid-build cleaning procedures. A set of rules for optimisation and an algorithm to determine if a material changeover was required were also written.

The use of Stereolithography in the creation of an electronic substrate for embedding functional components and circuitry was proposed by Kataria and Rosen [153] in 2001. This method would eliminate secondary assembly steps saving time and reducing cost of production. The additive technology also provides a much higher geometric freedom than conventional methods. These ideals were further developed by Palmer *et al.* who proposed that Stereolithography and direct write additive manufacturing technologies could be integrated to create both the substrate and conductive tracks required for the circuit to function. A junction box was created by direct writing conductive material into fabricated channels to replace the manual wiring process. This wiring was then encapsulated by a single layer of resin [154].

The benefits of Stereolithography combined with these solutions do make it incredibly advantageous. Justifications include a variety of material options which offer slightly differing material properties, high quality surface finish, dimensional accuracy and the ability to implant foreign materials. Also, SLA provides easy access to the build chamber for picking and placing parts manually and the process provides a significant amount of flexibility to be stopped and restarted mid-build [155]. Stereolithography would however not normally be considered ideal for integration with another process, primarily because of its potential for contamination between processes, where cross contamination can affect the performance and characteristics of the final part. Any excess resin remaining on the part can cause problems with layer thickness of subsequent layers as well as issues with the adhesion of conductive ink to the substrate. Concerns can be prevented through the use of various post processing techniques including washing in solvent and oven curing to reduce the chances of contamination.

A number of hybrid machines have been developed combining laser-based Stereolithography with direct write technologies. Lopes *et al.* [83] combined Stereolithography and direct print technologies to aid in the innovative fabrication of 3D electronics. Their work involved a large amount of user interference from transferring the part between processes as well as cleaning and preparing the part before each new stage can begin. These processes can be automated to create a system that can run independently of the user. A micro-dispensing tool was used to deposit conductive material in tracks fabricated during the Stereolithography process. This successful hybrid machine allowed the development of a fabrication process cycle for 3D electronic structures that includes processes such as cleaning, positioning and uncured resin removal. The model undergoes this repeatable cycle until the whole part has been completely manufactured, layer by layer. In addition the performance of a

variety of silver particulate based conductive inks were compared to one another with respect to viscosity, volume resistivity, cure temperature and cure time and their properties examined after curing of the ink traces by laser irradiation.

Figure 2.11 shows two and three-dimensional models of a simple 555-based timer circuit created to test the functionality of the integrated processes, both of which performed as expected, with frequency of the embedded LED blinking changing with temperature as intended.
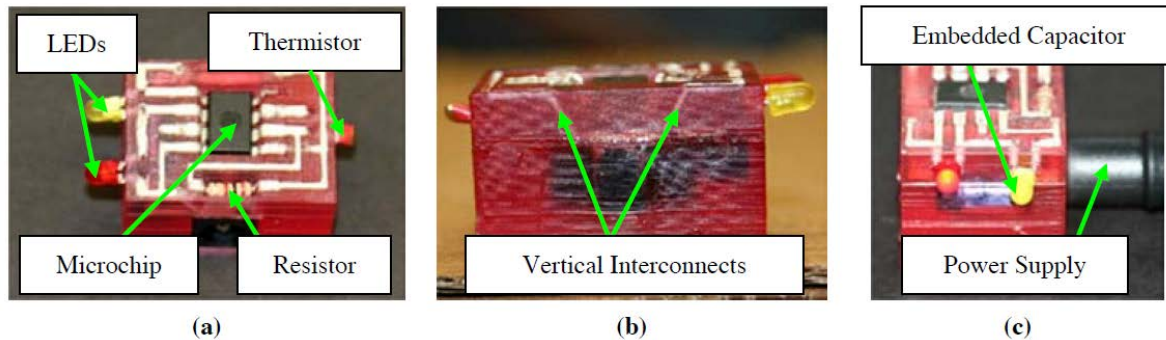
Figure 2.11.   a) 3D 555 timer circuit; b) vertical interconnects; c) working 3D circuit [83]

Key features of the process were also evaluated, including, design freedom, channels for conductive ink traces, cleaning of receptacles and accurate conductive ink dispensing.

Medina *et al.* [121] also developed a hybrid machine that offered enormous potential to create hybrid manufactured electromechanical devices. The aim was to use additive processes that produce more compact and reliable solutions, as opposed to subtractive processes and conventional methods that can take longer, be more wasteful and significantly more expensive. Work was also on going to fully automate the process. Low viscosity resin prevented the need to sweep and reduced cleaning time prior to direct writing of the conductive inks as well as being able to withstand higher temperature that it will be exposed to during the curing of the conductive ink.

This machine employed a start and stop process to allow both Stereolithography and direct write technologies to be used simultaneously to create functional products. Medina *et al.* [122] used integrated technology to build an alarm clock with embedded electronics for a camera. During this process issues with integrating multiple additive manufacturing procedures were examined including the continuous cleaning and curing processes as well as part positioning and relocation onto new build platforms, all of which are required during process changeover between Stereolithography and direct write technologies. A fiducial was created in the substrate to allow alignment on the build platform to be made, if automated, this alignment would require a form of image recognition system. These efforts provided a platform for the automation of an integrated Stereolithography and direct

write manufacturing process for 3D electronic structures. Medina *et al.* [122] created the concept of a Functional Integrated Layered Manufacturing (FILM) environment whereby a 'tool box' of various types of hardware, software and materials can be combined to create a highly versatile manufacturing environment, this is however just a theoretical development.

Further research has been carried out to determine how and when integrated systems such as that created by Medina *et al.* [121] would be most effective when compared to traditional methods. In 2006 Lopes *et al.* [85] assessed the ability of a hybrid system to develop electronic systems for unique applications where arbitrary form was required with initial effort focused on embedding parametrically sensitive systems into a Stereolithography substrate. These systems could not be produced using traditional PCB technology. Embedding components using this technique ensures they are protected for external influences such as weather conditions, however this does bring about the issue of high power circuits overheating due to the lack of available cooling within the substrate [85].

This was the first system to demonstrate an embedding process and the inclusion of vertical conductors through the substrate material. There were however limitations to this process. Multiple processes are required to create just a single layer of circuitry. Apart from both substrate manufacturing and ink dispensing, conductive adhesives would be required to mount components and an additional exposure process to embed components within their individual cavities. Embedding still requires proximity to the surface of the geometry, limiting the design freedom.

An alternative laser based Stereolithography technique has also been developed, presenting a modular assembly arrangement in which components can be placed. In addition, due to the low temperature resistance of photopolymer resins, conductive glue was used to make electrical connections between component modules [156]. This method is limited by its incompatibility with surface mount electronics, a result of its reliance on through-hole component pins. For this reason electronics can only be reduced to the size of the smallest available through hole component.

Figure 2.12 presents the results of a study to compare average resistivities of various inks on a variety of different substrates to determine which was most suitable for the creation of electrical interconnects between components.
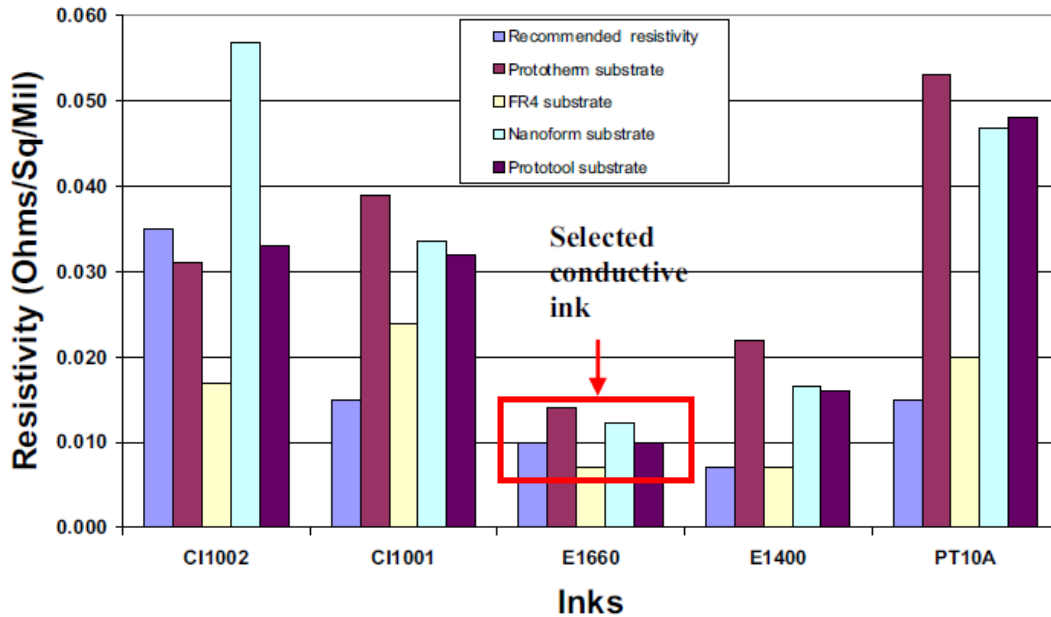
Figure 2.12.   Comparison of average resistivity of various inks on different substrates [85]

This experimentation determined that conductive inks cured on a traditional FR-4 board displayed a resistivity approximately half that of the nearest resin.

One particular issue with integration of Stereolithography with another process is the integrity of the substrate with particular attention paid to the plane on which the direct writing of tracks has taken place. The adhesion between the substrates cured either side of the dispensing process gets weaker as the substrate goes through the thermal cycling process required to cure the conductive ink traces. Delamination was shown to increase in both length and width as the number of thermal cycles increases [94].

Palmer *et al.* [94] conducted research based on encapsulating dimensional interconnects in the form of large trapezoid wedges 12.7 mm x 2.03 mm x 1.52 mm in dimension. An approach for the manufacturing of multi-functional, low cost modules is presented through the integration of Stereolithography and direct write technologies. This involved interrupting the build sequence to insert components and dispense conductive ink traces to create an electrical distribution network. Registration fixtures were also used to align the part when moved between processes to allow components to be manually inserted between process cycles. To embed these manually inserted components, the conventional blade recoating method needed to be disabled and 'deep dip' coating was used until there was adequate clearance between the path of the recoating blade and the component. This significantly slowed the manufacturing process as the levelling time required for each deep dipped layer was 10 minutes. As yet, there are no solutions to this problem however Geving and Ebert-Uphoff [157] presented possible solutions to these recoating issues by identifying

the potential of a liquid curtain recoating device or spray bar to improve the consistency of the layer thickness across the whole surface of the part whilst passing seamlessly over any obstructing elements.

An embedding stereolithography (eSLA) concept was introduced by Niese *et al.* [119] and combines additive and electrical manufacturing methods to produce functional circuitry. The stereolithography process itself is proposed as an encapsulation method for lead frame assemblies and printed circuit board assemblies. Cavities are created in which components can be positioned upside down before a conductive adhesive can be dispensed in two and a half dimensions from a 200 μm nozzle and sintered. Smaller nozzles also lead to agglomeration of the material within the nozzle itself. The recoating mechanism presents one of two limitations in this process as components cannot protrude from the cavity without interfering with the sweeper system. The second disadvantage is the filling of fabricated cavities with liquid photopolymer resulting in the necessary addition of a vacuum pumping process to remove the resin before components are positioned. It is also suggested that once positioned the component cavities will be refilled however a bulk curing method is not proposed, resulting in active components sitting in the liquid photopolymer until such time as it cures by exposure to environmental UV radiation.

The act of doping a photopolymer with a coated catalytic material has recently been introduced as a method for producing conductive structures within a stereolithography substrate, using stereolithography to produce Molded Interconnect Devices (MID) in the process shown in Figure 2.13, combining electrical and mechanical functionality with integrated circuits in a single fabrication procedure [158].
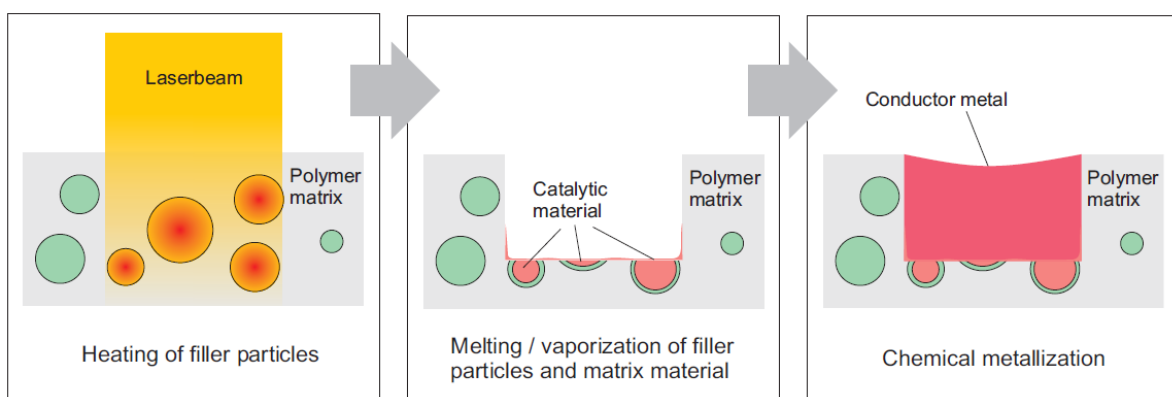
Figure 2.13.   ADDIMID material concept and basic mechanism of laser activation [159]

The ADDIMID process relies on a photopolymer substrate, exposed to a pulsed ns-IR-laser to reveal the electrical functionality of the device. On absorption of the laser radiation the metal doping particles heat the polymer and activate the surface of the part, developing catalytic nucleation sites

of the exposed metal [159]. Copper is then deposited by chemical metallisation into the pre-fabricated channels. Track widths of 300 μm were produced, a similar width to conductive epoxy tracks dispensed through a 200 μm nozzle however, the chemically metalized copper tracks are only 6-8 μm high and at 10 mm in length have a resistance of 0.14 Ω to 0.16 Ω, demonstrating a much lower resistivity than silver inks and epoxies currently being direct written onto stereolithography substrates.

At the University of Texas in El Paso, Wicker and MacDonald [155] have developed a multi-material Stereolithography machine which has been integrated with material dispensing. Using rotating material vats to include different resins based on poly ethylene glycol based hydrogen scaffolds and an nScrypt Micro Dispensing System attached to a three axis movement mechanism to lay down conductive tracks as thin as 25 microns on the dielectric substrate. Using CAD software, models of the build process can be developed with the geometry of the tracks included and demonstrated by creating channels where the material will be dispensed in the direct writing process. The software also provides much more design freedom as conductive traces can be built in any orientation. This process also includes embedded components and as such, demonstrated the ability to pause the SL process mid-build, automatically clean and cure the partially built substrate. During this particular study, the machines were not directly integrated; the part was instead moved manually from the multi-material Stereolithography system to a system previously developed by Lopes *et al.* [83] to complete the direct writing of the conductive tracks.

There are advantages and disadvantages of integrated additive methods and traditional methods of manufacturing functional circuits. A comparison of resistance and capacitance of a thermistor, 1 kΩ resistor and capacitor in a 555 timer circuit built on both an Additive manufactured substrate and a conventional breadboard was carried out for a variety of different temperatures which alter the resistance of the thermistor [85]. None of the measured data from either circuit shows greater than a 1% difference which is well within allowable differences for the components. Any slight deviation between measurements of the two circuits is more than likely explained by component variation as opposed to differences between the two fabrication methods.

Following on from the manufacturing of customised circuits on a small scale, research has also been directed towards mass production using the Stereolithography process. This was carried out using multi-beam scanning techniques and based on the 'IH process' [160] previously developed and as such, has been named the 'Mass-IH process' [161]. Having been verified experimentally, this process presents a number of advantages including its simplicity, easy miniaturisation of the system, uniform resolution and accuracy across the entire build, high aspect ratio and low cost.

2.6 Embedded Electronics

A broad variety of manufacturing methods, both additive and conventional, can be used to embed components within a substrate to create more compact circuits with greater functionality and dexterity. Pique *et al.* [162] used a combination of laser micromachining and laser direct write technologies to embed functional components within a pre-existing substrate. A trench is micro machined into the substrate before the insert is positioned, covered with a polyimide resin and then a polyimide sheet, which is pressed onto the resin to encapsulate the component. Finally holes are drilled in the polyimide sheet to expose the conductive vias before conductive paste is added and cured to create interconnects. Although this process creates reductions in circuit weight and volume, it does contain subtractive manufacturing methods that cause some material to be wasted. Using additive processes to shape the substrate would cause this material to be saved, create cost reductions and introduce potential new substrate materials.

In 2001 Katari and Rosen [153] began building around functional inserts and embedding components into resin based substrates created using stereolithography. A number of different approaches to component insertion have been used and common issues that have been encountered multiple times were assessed. Firstly, fixing can be achieved by creating cavities for components to slot into before being encapsulated in resin. This also requires interconnects to be dispensed to allow these inserts to connect to the circuit in the required configuration. Two different configurations were presented, both horizontal and vertical fixtures, determined by the orientation of the component. Once inserted, components can be encapsulated whilst ensuring that they maintain their functionality. Appropriate tolerances for both cylindrical and rectangular inserts have been investigated for clearance, transition and interference fits. Issues with these clearances would arise when using inserts with abnormal shapes, if a component is wider at the bottom than top, there would not be enough clearance at the top of the cavity to position the insert. Other identified problems include laser shadowing, support structures and recoating and therefore, the build process was changed to reduce the visibility of these problems. Periard *et al.* [151] used the same concept to create small embedded circuits in the form of a cube shaped timer circuit and a small flashlight using a publically available Fab@Home printer. This printer was used in combination with silver conductive ink to produce the parts however, due to the limitations of the printer and behaviour of the ink, electrical contact may be broken if connecting vias are not cured within approximately ten minutes of one another.

Following the introduction to the concept of embedded components Cham *et al.* [163] presented process planning considerations to be used in the design of the proposed model. This planning

process is based on the use of Boolean operations to subtract material, in the same shape and size as the components being embedded to allow the insert to be positioned correctly and fixed in place. The operations used within the algorithm created by Cham *et al.* include, addition, subtraction, intersection and exclusive or, all of which are used to mathematically model the substrate around the insert. During this study additive and subtractive methods of shaping were used to create a customised substrate for component insertion. Issues accredited to this approach can be minimised or eradicated through using Stereolithography as the primary manufacturing process.

The fabrication of functional assemblies not only encompasses embedding circuitry, but also producing moving joints in one build process. The precision in the Stereolithography process was demonstrated by Laurentis and Mavroidis [164] in its use to develop a full robotic hand in one build with embedded circuitry. This hand is therefore fully functional as soon as manufacturing has been completed as joints conventionally requiring assembly including ball and socket, revolute and spherical joints can all be created during the one step. In addition components and circuitry were embedded into the robotic hand and a variety of process steps and considerations were determined.

Firstly, Laurentis and Mavroidis [164] established a list of challenges of inserting components that are non-specific to the manufacturing technique. These included the components' reaction to the substrate, tolerances on embedded components, and use of support structures, build orientation and where to place the inserts. Secondly, key points were identified for embedding inserts during the Stereolithography build process, a list that is also inclusive of the non-specific challenges above. Other steps comprise of preventing trapped volumes, appropriate component selection, preparation of sensitive inserts and location of correct insertion layer.

Components are not only limited to being inserted flat into a substrate but can also be positioned off axis on substrate such as that in Figure 2.14. DeNava *et al.* [165] used additive techniques to create a bespoke substrate with trenches for the inserts to be situated both on the top faces and side faces of the substrate. Routing of interconnects has also developed from two dimensional, traditional methods, to two and a half and three dimensional routing through a substrate using additive manufacturing technologies. Two and a half dimensional modelling has been applied to create under-arch tunnel routing to avoid vias intersecting and short circuiting, creating conductive routes in the z-axis as well as x and y.
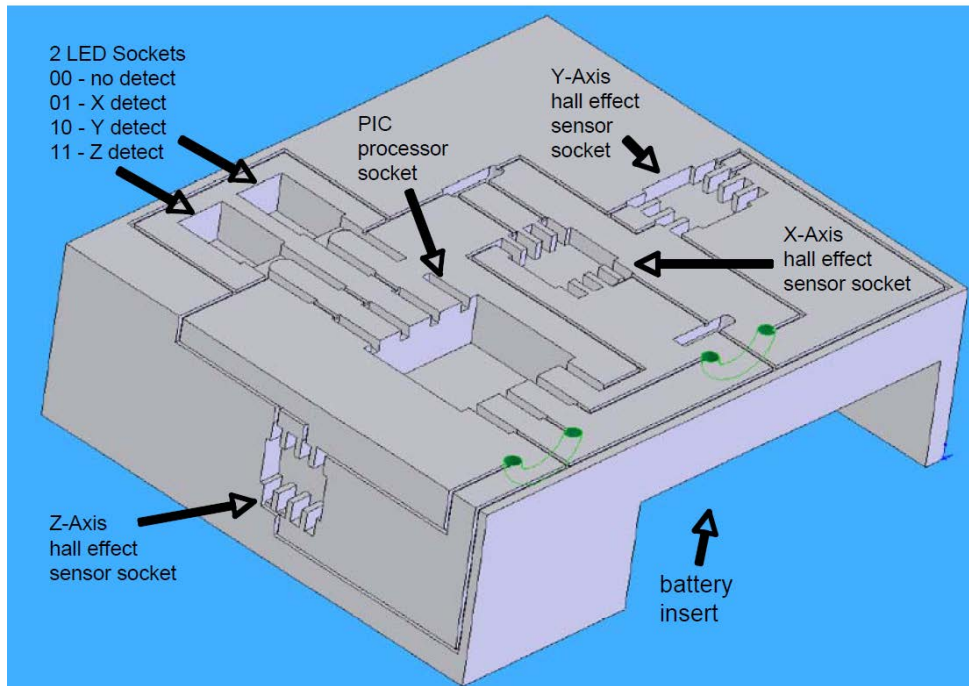
Figure 2.14.   Schematic of trenches for component embedding [165]

Further work at the University of Texas at El Paso has demonstrated the placement and embedding of components in individual cavities, prefabricated in the surface of the substrate. In addition locations were also produced below the circuit plane where power supplies and larger inserts can be fitted after complete fabrication of the sample. Although these embedding processes have proven the capability to embed components, all encapsulation has occurred close to the surface of the substrate, limiting the ability of this process to fabricate multiple adjacent layers of stacked circuitry.

Alongside encapsulation, press and snap fits are utilised with each component being inserted upwards through one via and down through a second before excess material is removed. This creates a snap fit for the pins whereby a chip can be press fitted into place [129].

2.7   Summary

Additive manufacturing technology has been shown to possess great potential for the direct digital fabrication of electronic devices with liquid photopolymers demonstrating good dielectric properties. To this point integrated stereolithography substrate fabrication techniques have had limited flexibility, restricting the potential of this technology to conduct electronic packaging. DLP stereolithography offers increased process versatility, greater control and, with a suitable light source and optics, greater process resolution. This process shows some similarities to conventional photoresist exposure however, the direct digital fabrication capability removes the need for templates and masks.

A number of limitations of current research in AM of electronics have been identified including the inability to create geometrically complex packaging with internal multilayer electronics. Evidence has been presented that shows the deposition of conductive materials in channels on the surface and the majority of through-hole components have been embedded in surface trenches. Conductive vias have all been fabricated by creating subsurface channels and pumping them full of conductive ink before sintering by laser or electrical methods. To completely fill the via would require multiple cycles due to the loss of volume by solvent evaporation due to heat exposure and therefore, this process is inefficient and may not be achievable on a smaller scale.

There is little background examining the use of isotropic conductive adhesives for use in combination with additively manufactured substrates. Conductive inks, most requiring higher temperature sintering/curing (>100 °C) have commonly been integrated with stereolithography based photopolymers however, these materials are not directly compatible with surface mount technology, hence the reliance on through-hole components. In addition, the viscoelastic and rheological properties of ICAs eradicate the need for surface features to control their behaviour and, can help eliminate the appearance of damage on the substrate as a result of high temperatures created by the laser. The research that will be presented during this thesis aims to align with previous work with the objective to reduce both conductor widths to less than 200 μm and produce a track resistivity lower than other integrated Stereolithography and material dispensing fabrication processes detailed in Table 2.4. Additionally, adding the increased production capability of multiple embedded layers of circuitry separates this proposed process apart from previous hybrid Stereolithography and Direct Write systems.

Finally, the consumer requirements for smaller, faster, more functional and portable electronic devices continues to pressure the industry into focusing on the miniaturisation of available technology. Studies introduced covering both micro-stereolithography and micro-dispensing demonstrate the potential for a further reduction in scale of electronics produced using AM however, research to date has been based around the feasibility of additively manufacturing electronics by combining multiple processes and there is no literature describing small scale packaging using these hybrid AM technologies.

3 Multilayer Photopolymer Substrate Fabrication

Conventional electronic substrates exhibit a number of important material properties that make them well suited to their application as a dielectric insulator. Stereolithography was identified from a plethora of Additive Manufacturing techniques as a viable alternative for the development of electronic substrates as epoxy and acrylate resin materials have demonstrated a number of beneficial characteristics including dielectric constants of 3 and 2.7 and loss tangents of between 0.1 and 0.5 [166][167], compared to a dielectric constant of 4.2 and loss tangent of 0.023 [168] demonstrated by a common FR4 board. A higher dielectric constant is considered detrimental to an electronic substrate as it demonstrates the increased capability of a material to hold electric charge therefore reducing the transmission speed of conductors. Additionally, the loss tangent quantifies the capability of the material to dissipate electromagnetic energy, but only relates to higher frequency electronics [169]. Unfortunately, photopolymer materials demonstrate a higher coefficient of thermal expansion of at least $7.1 \times 10^{-5} \, K^{-1}$ [170] compared to $1.4 \times 10^{-5} \, K^{-1}$ in the x-axis, $1.2 \times 10^{-5} \, K^{-1}$ in the y-axis and $7 \times 10^{-5} \, K^{-1}$ in the z axis for FR4 board [171].

There are two DLP Stereolithography orientations, top-down and bottom-up, both of which are capable of fabricating electronics substrates. These methods have been explained fully in the review of the Stereolithography process and present their own advantages and disadvantages for use in embedding conductive tracks and components, the details of which can be found in Section 2.3.2. During this research apparatus has been developed to facilitate the implementation of both methods, allowing testing to determine their suitability for the production of multilayer electronics with embedded circuitry.

There are two specific applications of Stereolithography within the context of this research. Firstly, a substrate needs to be created on which conductors can be dispensed, surface mount devices placed and the conductive epoxy cured. A number of characteristics are required of the substrates to facilitate integration. A high quality, planar surface is necessary to ensure successful dispensing of conductive material; stresses on the substrate must be minimal; resolution of the exposure mechanism must be high; and the substrate must be able to withstand the temperatures required to thermally cure the isotropic conductive adhesive used in the dispensing process.

The second stage involves packaging the electronic circuitry. After surface mount assembly and epoxy curing, the part can be aligned and submerged for a second time into the liquid photopolymer. Additional photopolymer material can then be cured over the conductors, embedding components and z-axis interconnects and, subsequently providing a high quality surface onto which subsequent

layers of electronics can be printed. Both comparable Stereolithography build orientations present their own advantages with regard to embedding. These different layering methods will be discussed in Chapter 6. The SL process overview is outlined in Figure 3.1.
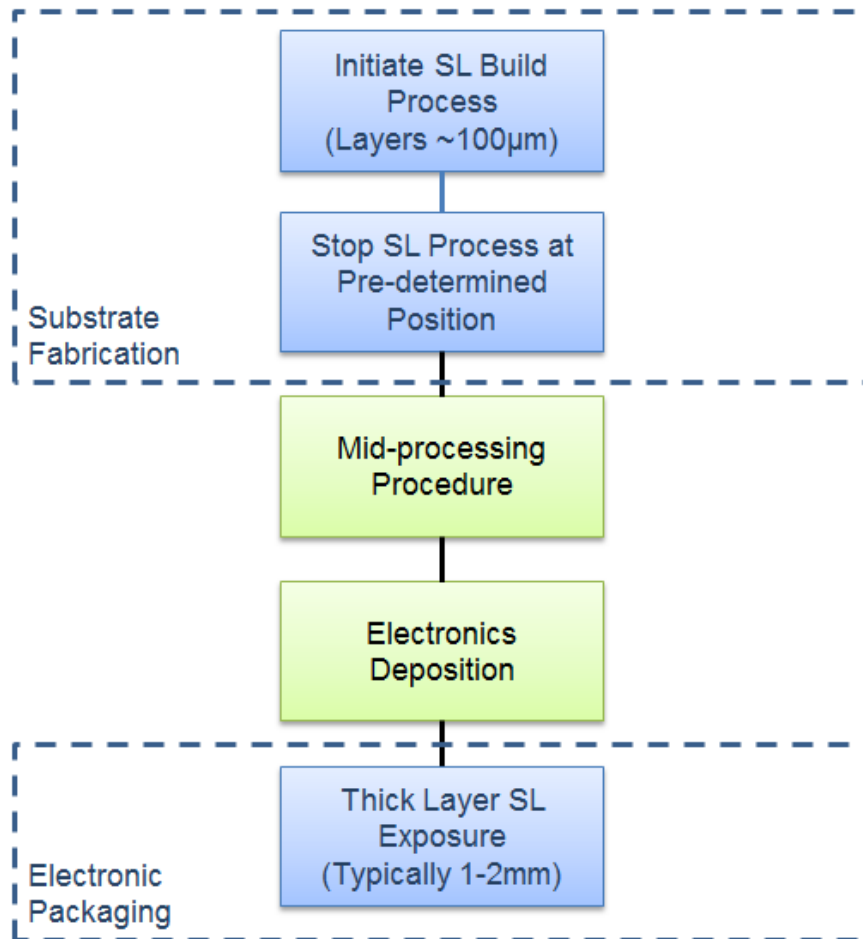
Figure 3.1.   Flow Diagram highlighting use of SL process

This Stereolithography process was controlled by Creation Workshop open source software and an Arduino Mega microprocessor with Marlin firmware providing increased flexibility to the user. The software allowed a wide variety of printing parameters to be programmed including layer thickness, z-axis movement speed and exposure time in addition to a manual control interface with influence over the build platform movement and play/pause/stop controls.

This chapter describes the design and development of a bespoke top-down DLP SL apparatus and both advantages and disadvantages of this process. The process of integrating a UV light source into a DLP projector and the subsequent testing of the system is documented, including intensity mapping and surface profile analysis of fabricated specimens. An alternate bottom-up projection orientation will also be presented, characterised in the same way as its predecessor and analysed for its suitability for application in electronic substrate fabrication. The surface quality of parts produced

using both projection orientations will be compared before the capability of the more advantageous setup is scrutinised further to determine process resolution in x, y and z axes.

3.1 Top-down DLP SLA Substrate Production

Stereolithography utilising a top-down projection orientation facilitates the fabrication of three-dimensional parts layer-by-layer, by projecting images of cross sectional layers of the design sequentially onto a build platform, a schematic of the apparatus is shown in Figure 3.2 [172].
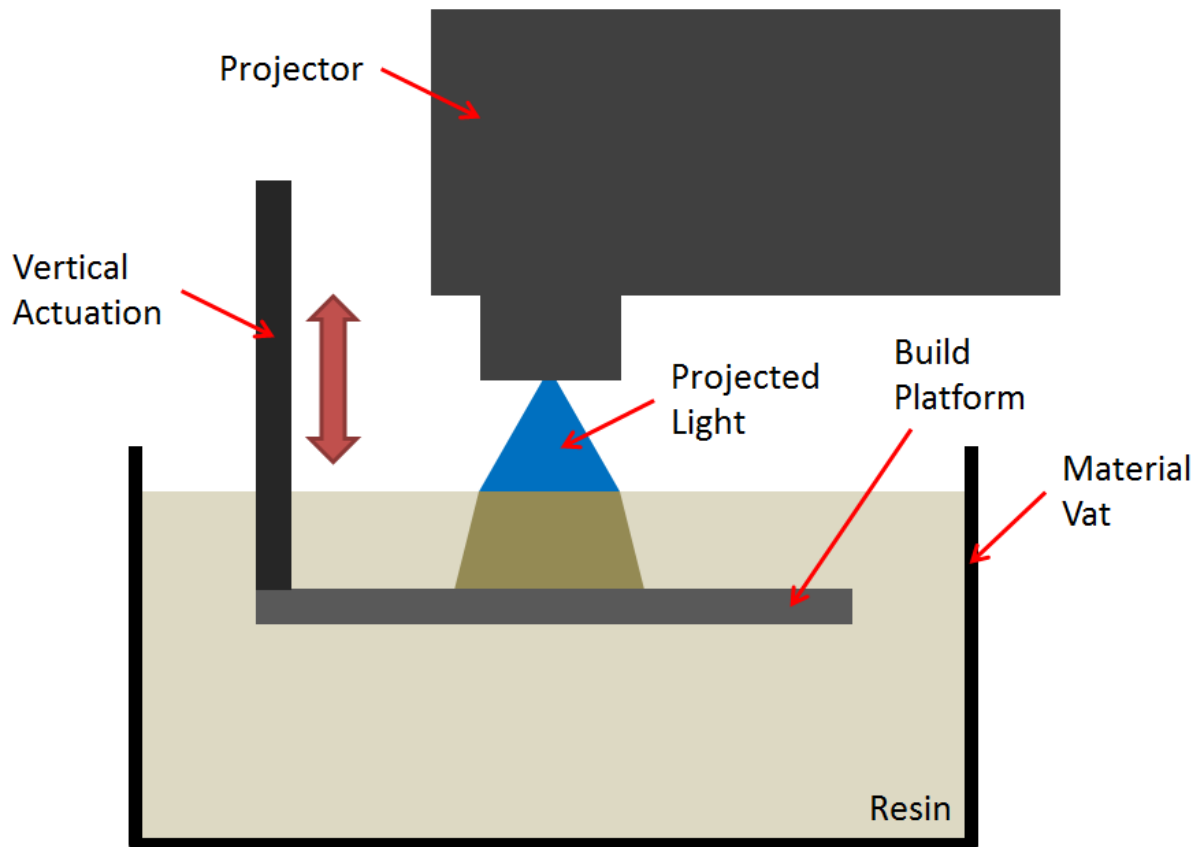
Figure 3.2.   Top-down Stereolithography apparatus setup

The recoating mechanism traditionally used in this orientation is a blade however, embedded components could cause obstructions to this mechanism. A bespoke, top-down Stereolithography system was designed and developed with a deep dip recoating method whereby a new layer is added through submersion in the photopolymer. This orientation demonstrates the most suitable method for embedding electronics as no inversion of the substrate is required.

3.1.1 Design of a Top-down DLP Stereolithography System

A number of essential features were specified for inclusion in the design of a top-down Stereolithography machine as highlighted in Table 3.1 to aid in the fabrication of multi-layered embedded electronics.

Table 3.1.   Features specified for inclusion in the top-down SL system

Feature	Explanation
DLP exposure	• Faster build times laser based processes [67] • Lower cost as compared to laser spot exposure • Resolution determined by image quality of projector • Versatile control through open source software
LED light source	• Narrow band wavelength light source emitted, tailored to the sensitivity of the photopolymer [173]
Z-axis projector movement	• Projection distance and build area size can be adjusted • Resolution of the projected image can be optimised by changing projection distance and lens focus
80mm x 80mm build platform	• Substrate sizes will start at 50 mm x 50 mm with eventual reduction to a maximum of 20 mm x 20 mm • Minimises vat size, reducing required material volume
Fixed X and Y axes	• Eliminates alignment errors to enable highly repeatable platform positioning • Ensures that subsequent layers are built directly on top of the previous layer with no unwanted offset.
Deep dip recoating method	• Prevents obstruction of recoating systems by embedded components but increases build time [94] • Reduces complexity of the SL system
Micrometre Z-axis Resolution	• Motor capable of a 1/16 step = 0.625 μm z-axis resolution [174] • Greater process control and accuracy over large distances • Minimises stair stepping effect
Optical Table	• Provides vibrational damping • Versatile build platform, allowing changes in system position • Aids integration with other processes • Structural materials and fasteners will also be standardised to make the system easily adaptable.
Stainless steel submerged parts	• Any parts of the system that are to be exposed to the resin are to be made from stainless steel to prevent any reactions with the photopolymer.

3.1.2 Design Iteration Process

The Stereolithography system design process involved a number of iterations to ensure the correct functionality from the machine. This not only focused on ease of access to major components but also ensured the accuracy of the setup was optimised before the machine was built. This design process was conducted in Siemens NX7.5 computer aided design software, allowing accurate dimensions for all components to be determined. Two developmental iterations and the final design with changes made to the method of vertical movement actuation, fixture to the optical table and build platform design are displayed and labelled in Figure 3.3(a)-(c).
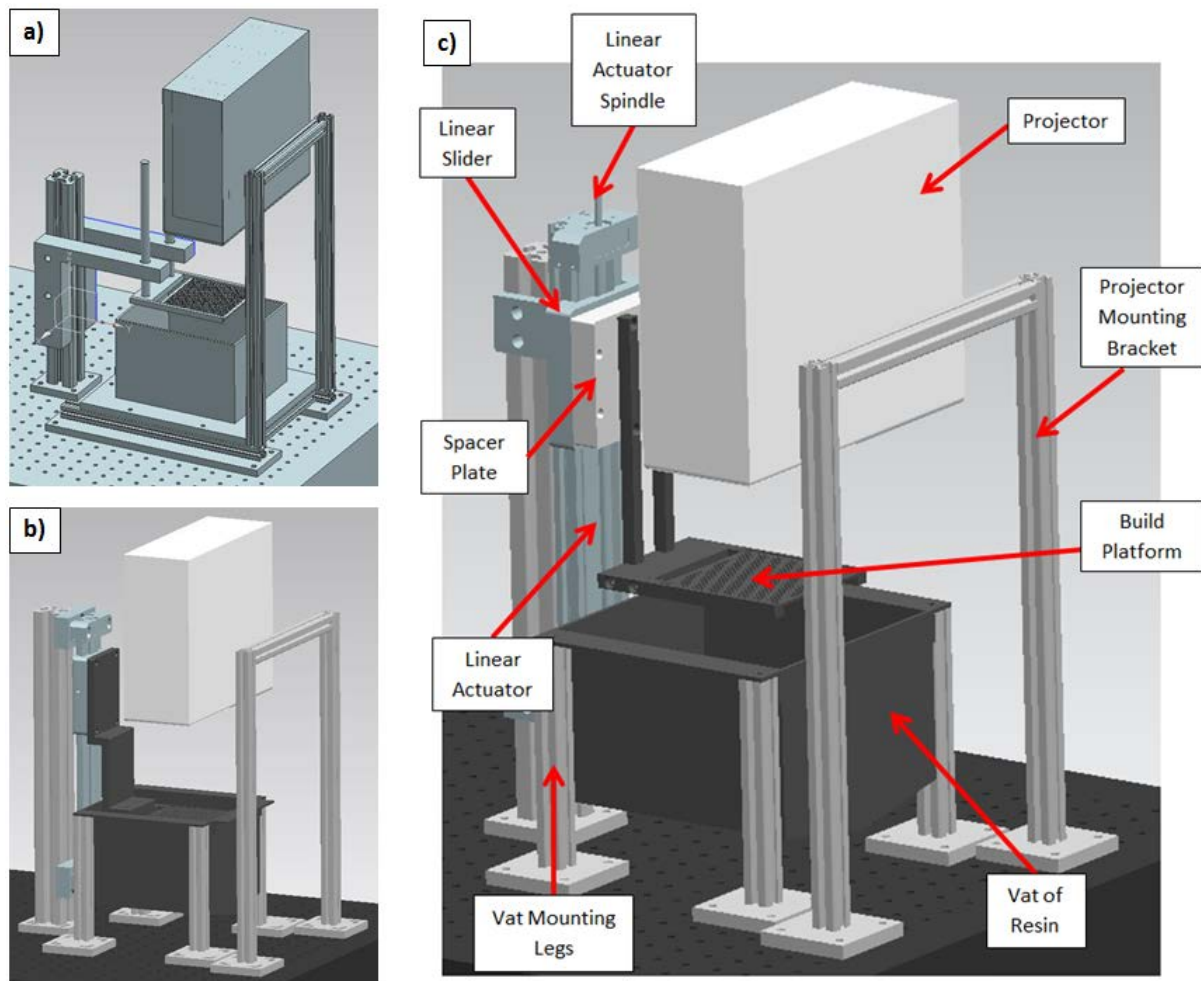
Figure 3.3.   a) First, b) second and c) final design Iterations

The design in Figure 3.3(c) meets the specification developed in Table 3.1 and the resultant system is shown in Figure 3.4. The standardised supporting elements and mounts can be located anywhere in 25 mm increments on the optical table and, with the use of dedicated fasteners, can be fixed to one another in a variety of orientations and configurations. The vat sits level on four supports and has been designed with an angled base and drain hole to facilitate removal of the liquid photopolymer and cleaning of the system. The projector has its own designated mount allowing z-axis movement

to centre the projected image onto the platform. The motor controlled linear actuator also provides highly accurate movement of the build platform in the z-axis. Finally all submerged elements have been fabricated from stainless steel to avoid an adverse reaction with the photopolymer. The build platform has also been perforated to aid the flow of resin over the part during deep dip recoating.
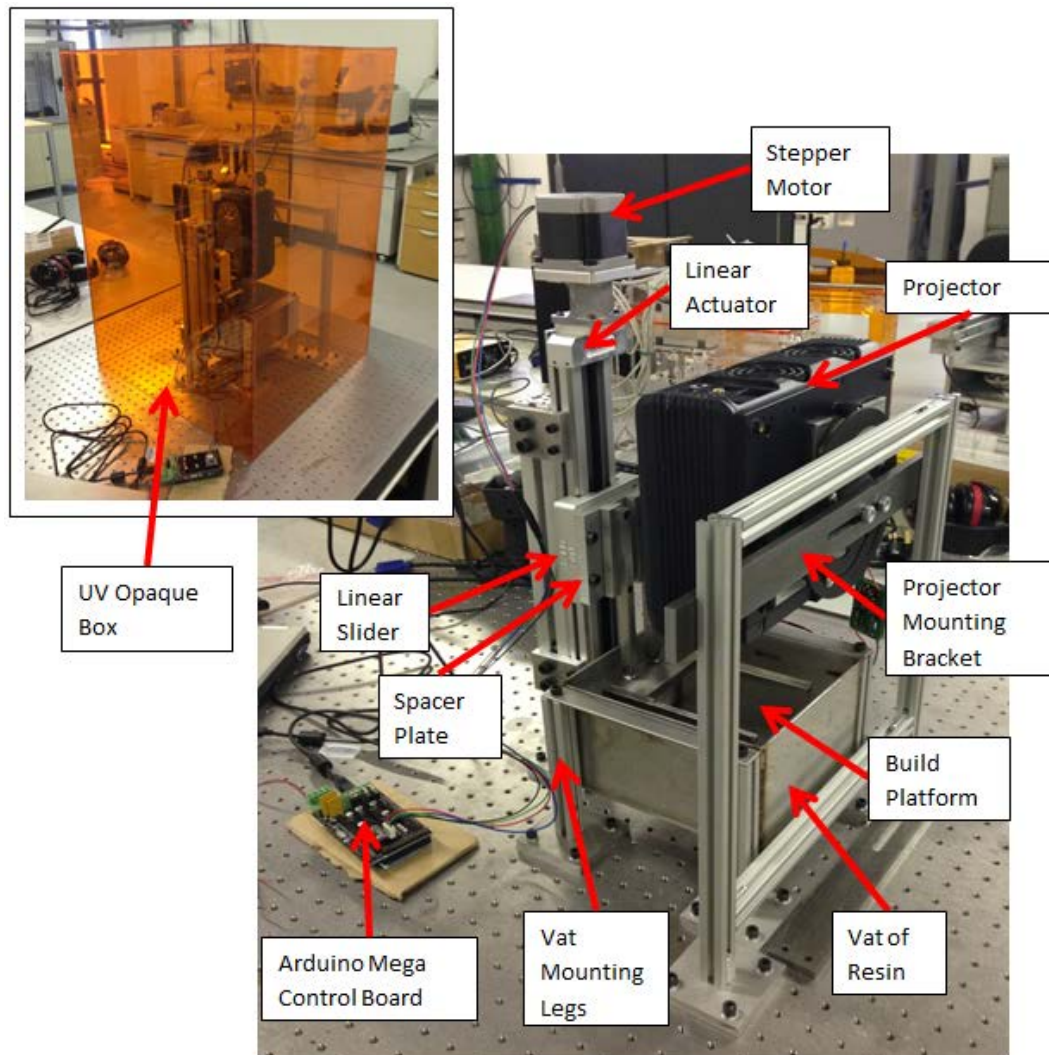
Figure 3.4.   Functional top-down system produced to the final iteration design

The final addition to this system is an amber coloured, UV opaque acrylic cover (inset in Figure 3.4). This prevents the liquid photopolymer from reacting to external sources of ultraviolet radiation and also to protect the machine operator from exposure to UV radiation.

3.1.3   DLP UV Projection Development

For the purpose of ultraviolet projection, a mounting system was designed to project 365 nm light into the light gate of the projector, allowing the use of the DMD as a dynamic mask for the selective exposure of the photopolymer. This could facilitate the use of commercially available epoxy resins such as 3D Systems Accura® 60, designed for laser-based exposure mechanisms which demonstrate

greater stability and better mechanical properties than their acrylate-based equivalents, a further description of which can be found in Section 2.3.3. The advantages of this UV material and exposure combination led to an investigation of the feasibility of DLP and UV LED integration.

The chosen method of projection and light source can have a significant bearing on the resolution of the system. Using DLP technology in conjunction with ultraviolet LEDs should theoretically produce a highly accurate part as it will provide a narrow spectrum light source that can be tailored to the curing wavelength of the resin. This ensures that the resin cures at a single speed as opposed to different rates resulting from exposure to multiple wavelengths therefore reducing residual stresses in the cured photopolymer, a phenomenon discussed further in Section 3.1.5. The chosen source is an array of LEDs with individual lenses which creates a single coherent front of light converging to give the appearance of a single source. Figure 3.5 shows the optical setup alongside intensity measurement points labelled A-D. The LED mount displayed allows the light source (point A) to be mounted in a light box with a polished aluminium interior in an attempt to reflect as much light as possible through the lens array. The LED is then directed towards a plano-convex lens (point B), designed with a high UV transmittance to ensure an accurate refractive index of the lens is known. The projection lenses however are not designed specifically for use with UV light and would demonstrate a different refractive index than with white light. This could result in aberration and therefore difficulty creating an image with sharp focus. The light is then focused onto an optical fibre (point C) which is then fed into the light gate of the projector bypassing the colour wheel (point D).
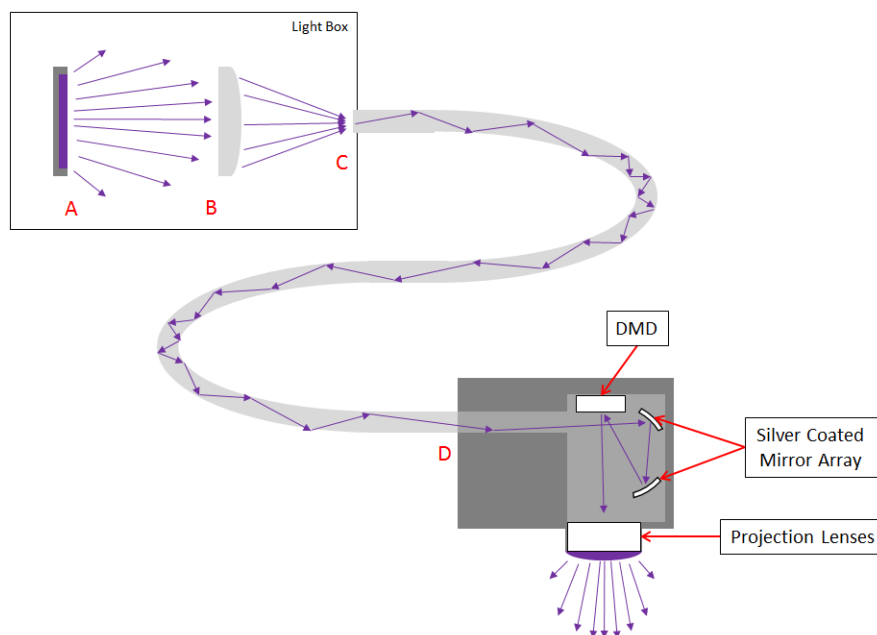
Figure 3.5.   Setup of UV LED, converging lens and optical fibre light source

In order to specify a suitable lens (for position B) for this application, a trade-off had to be made between the available space, which is restricted by the size of the light box, and the spot size once focused, which needs to be larger than the entrance to the optical fibre. Figure 3.6 diagrammatically depicts the variables which determine focal length.
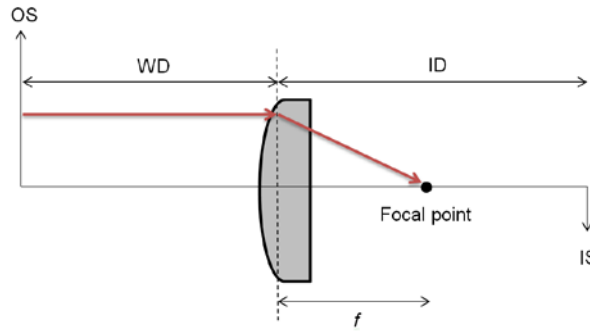
Figure 3.6.   LED lens array

Focal lengths (*f*) of potential lenses, the object size (OS) and required image size (IS) were substituted into Equation 1 [175] to calculate a working distance (WD):

$$OS = \frac{WDxIS}{f} \qquad (1)$$

After which the working distance and focal length are entered into Equation 2 [175] to determine the image distance (ID):

$$\frac{1}{WD} + \frac{1}{ID} = \frac{1}{f} \qquad (2)$$

As summarised in Table 3.2 the lens was positioned 20 mm from the entrance to the optical fibre and the LED a further 60 mm from the lens creating a spot of light with a diameter of 5 mm entering the optical fibre.

Table 3.2.   Dimensions used and determined for lens specification and development

	Dimension (mm)	Source
Object Size (OS)	20	Measured LED size
Focal Length (*f*)	15	Edmund Optics [176]
Image Size (IS)	5	Diameter of fibre entrance
Working Distance (WD)	60	Calculated using Equation 1
Image Distance (ID)	20	Calculated using Equation 2

This provides the greatest luminosity through the fibre, theoretically creating a higher intensity source in the light gate and resulting in the fastest curing process.

Initially, to ensure that the DLP projector still functions after the removal of the colour wheel and default light source, a white light source was shone through the light gate to produce a simple pattern as shown in Figure 3.7. This confirmed that the projector could be correctly positioned without exposing the user to UV radiation while the system was being set-up. The UV light source was then subsequently positioned within the projector.
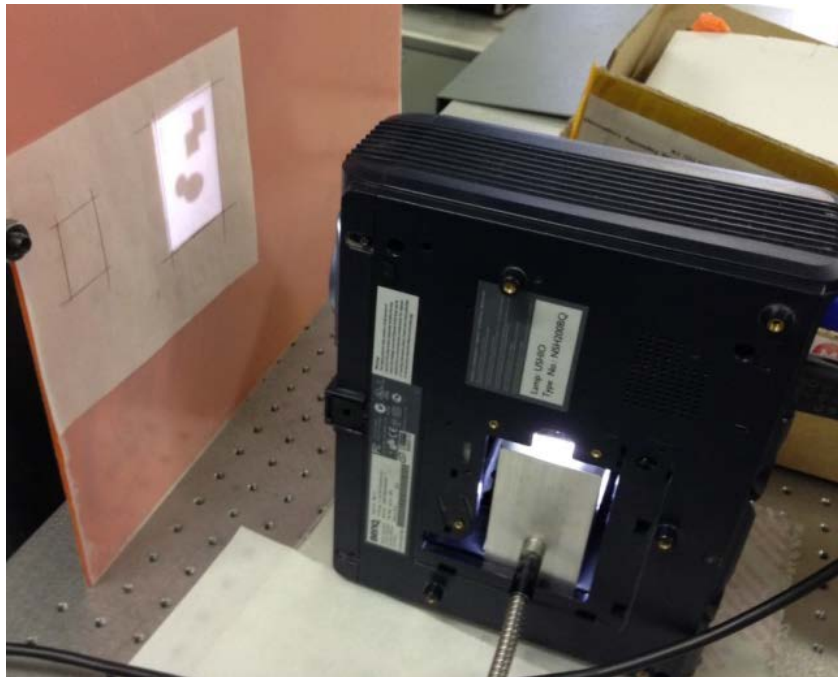
Figure 3.7.   Experiment to determine projection distance

A custom block was manufactured to allow the white light to be focused directly into the light gate using a mirror. By dividing the image size by pixel size, the projection size of each pixel and therefore the minimum possible feature size can be calculated using Equation 3. This calculated value can then be tested through experimentation.

$$Pixel\ Size = Projector\ Resolution \div Projection\ Area \qquad (3)$$

This projection mechanism has the capability to expose parts with a working area down to 40 mm x 30 mm and with a minimum pixel size of 50 µm. Using the existing projector lens system further reductions in resolution are not possible since the focal length is designed for projecting images over a larger area. A change in the lens system would however enable further reductions. The light source was then changed to a 20 Watt 365-370 nm LED, as shown in Figure 3.8, for intensity testing to determine the capability of this bespoke system to cure a liquid photopolymer.

Figure 3.8.   Projected UV image from DLP projector

The projection distance and focal length were minimised to produce the smallest possible focused image on a piece of blank paper. The projection area was then traced and measured, finally allowing the theoretical resolution to be calculated alongside the discovery of the required projection distance of 125 mm, the shortest projection distance at which an image can be focused.

3.1.4   Ultraviolet Projection Characterisation

This process is designed to expose photopolymers to 365 nm light, the same wavelength at which commercial resins for laser-based SL systems are sensitive. A critical exposure energy of 7.6 mJ/cm^2 is required to initiate curing of the 365 nm sensitive 3D Systems Accura® 60 liquid photopolymer [170]. This can be calculated and compared to measurements of intensity taken from an ultraviolet light meter through the application of the conversion calculation shown in Equation 4 [177].

$$Energy\left(\frac{mJ}{cm^2}\right) = Intensity\left(\frac{mW}{cm^2}\right) \times Time(s) \qquad (4)$$

This critical exposure energy is therefore defined as a result of exposure to a given intensity or power density of light for a specified period of time.

To assess the suitability and characteristics of the 365-370 nm LED, its intensity distribution was mapped. An 80 mm x 60 mm grid was created and split into 12 equal 20 mm x 20 mm sections to correspond with the 800 x 600 pixel resolution of the projector. Using an International Light IL1400A UV light meter sensitive between 280 nm and 410 nm wavelengths, the intensity was then measured at the centre of each grid square to determine the light distribution of both the UV LED and the UV LED in combination with the DLP projector. This data can then be interpreted and a percentage drop

in light intensity can be shown across the source as well as a comparison made between primary and secondary sources, helping determine the projector's effect on the light distribution. Measurements were also taken at various points through the lens array to determine any intensity losses.

The intensity was first measured at 120 mW/cm^2 at a distance 5mm from the light source. This was the closest point at which measurement could be taken as the UV light detector is offset 5 mm from the surface of the probe. A sample of the 365 nm sensitive resin was also positioned underneath the light source at this distance to validate curing by this LED array at its highest intensity.

Initial testing of UV intensity variation from the LED array showed some drop off towards the edges of the illuminated grid as shown in Figure 3.9. These values were taken at a 125 mm distance from the LED array, chosen as this was previously determined as the optimal projection distance for the DLP projector. Maximum and minimum intensity values were measured at 1610 µW/cm^2 and 1110 µW/cm^2.
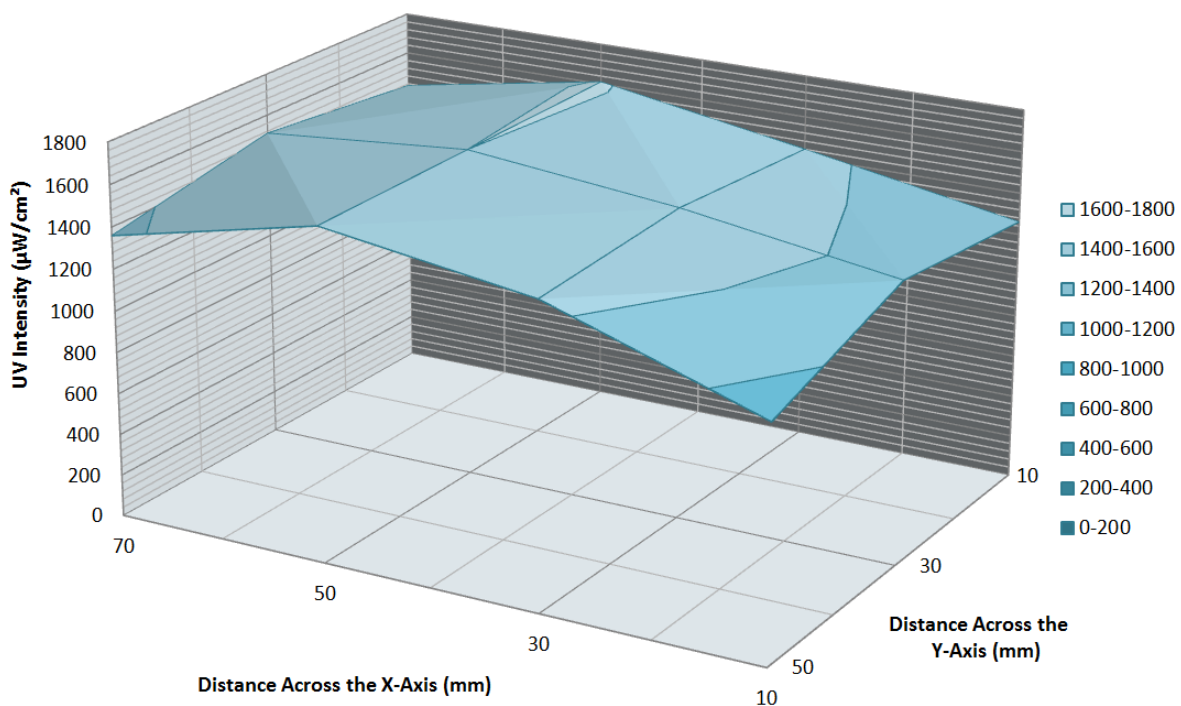
Figure 3.9.   Ultraviolet light intensity distribution at 125 mm from primary 365 nm LED source

The LED behaviour could be characterised by the inverse square law as shown in Figure 3.10 whereby the strength of the field or intensity of the light is inversely proportional to the square of the distance to the source (Equation 5) [178]. Therefore, the further the light travels, the lower its intensity. In addition, the light is projected at a 120° angle from each LED, 60° either side of the centre point and therefore not all emitted light will hit the surface of the light meter. Finally, a Gaussian distribution of light could also result in the observed characteristics, resulting in an initially

slow increase in light distribution before it eventually becomes proportional to the distance from the source [179]. These three mechanisms all provide a possible individual or combined explanation for both the loss of intensity due to increased distance from the source and, the lower intensity observed at the extremities of the sample area, a value as high as 0.5 mW/cm^2 between specific areas.
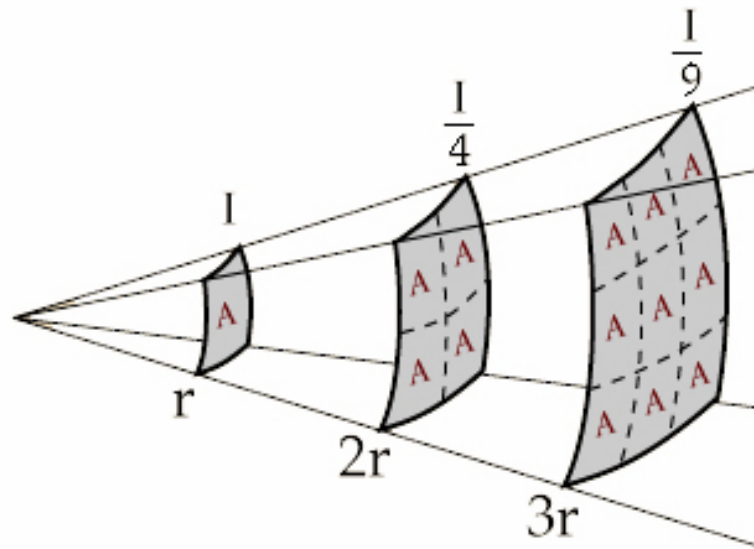
Figure 3.10.   The Inverse Square Law for Light [178]

$$Illumination = \frac{Intensity}{Distance^2} \qquad (5)$$

The intensity of light was measured at 120 mW/cm^2 at 5 mm distance from the LED source. Figure 3.11 shows the percentage of light intensity remaining after moving the UV intensity meter 120 mm further from the source. At a distance of 24r, the inverse square law predicts an intensity of 0.208 mW/cm^2 at 120 mm, lower than was actually measured from the source and therefore, the use of an array of single point sources appears to reduce the dissipative effect resulting from increasing distance. An approximate 99% intensity loss was measured whether it be due to a lack of collimation of the light, scattered emission from the source or the inverse square law. Despite this loss, there is still a high enough intensity providing the energy to cure the photopolymer at 125 mm distance over a 10 second exposure period, validated through simple exposure of a 5 mm droplet of resin on a microscope slide, all of which was polymerised.
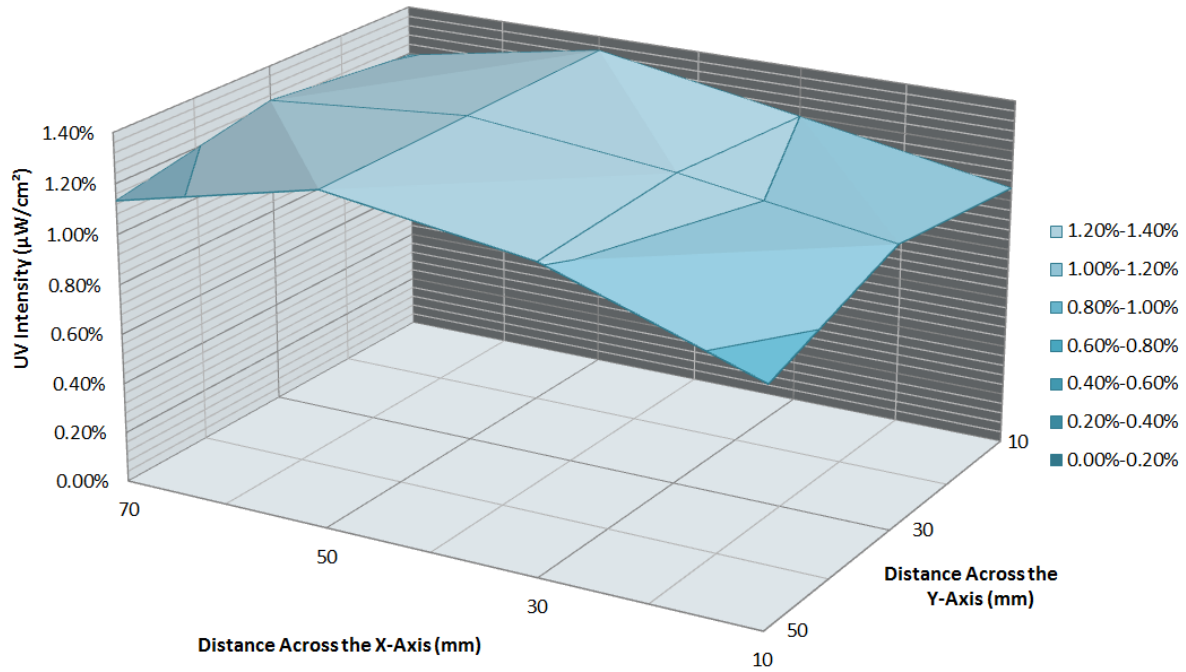
Figure 3.11.   Percentage of the UV intensity at 5mm distance remaining when the distance is increased to 125 mm

Due to the distance and number of surfaces through which the light needs to pass, losses of intensity are inevitable. After characterisation of the light source, the success of its integration into the DLP projection setup was assessed. Initially, off the face of the LED array at point A in Figure 3.5 the intensity was measured at 120 mW/cm^2, reducing to 8 mW/cm^2 at point B just before the converging lens and 3.6 mW/cm^2 at the entrance to the optical fibre at point C. It further reduced to 2 mW/cm^2 at point D as it exits the optical fibre and enters the light gate of the projector. This value entering the light gate is still 25% greater than that measured at 125 mm from the LED array due to the design of the light box and arrangement of lenses to collect and focus the light. This was achieved despite the light having travelled more than twice the distance.

The relationship between distance travelled and light intensity is additionally supported by the results from the fibre optic. Projection of light from the fibre optic source shows significant losses across the projection area, showing that the DLP projector and its internal optical configuration absorbs light between the primary source and the projection lens.

Finally, the distribution was measured through the DLP projector yielding significant losses in intensity across the projection area, most noticeably at the extremes of the image. The maximum value measured at the centre of the grid was 17.6 μW/cm^2, a loss of more than 99% of the light intensity entering the projector through the optical fibre. This was accounted for by the discovery that the light gate itself was a mirror coated in highly UV absorbent silver [180], the absorbance

spectra of which is shown in Figure 3.12, created to filter out ultraviolet light and selected as they are cheap and reflect visible light very efficiently. Lenses were also coated in UV absorbent filtering material.
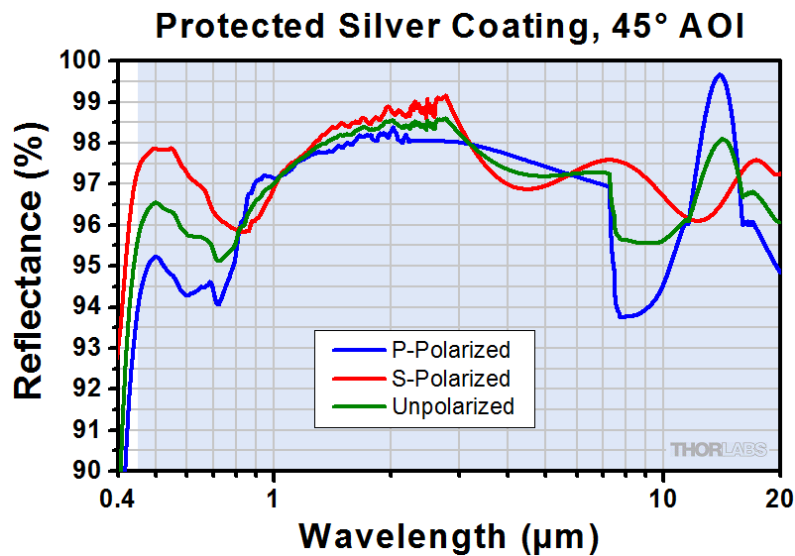
Figure 3.12.   UV-visible absorbance spectra of silver thin films [181]

Figure 3.13 also shows an elevated intensity drop off at the edges of the illuminated grid, demonstrating a significantly increased loss (90%) between the centre and extremities of the projected light when compared to the LED alone (30%). This can again be accounted for by the three mechanisms discussed previously in addition to the absorbance by UV filtering elements, compounding this loss.
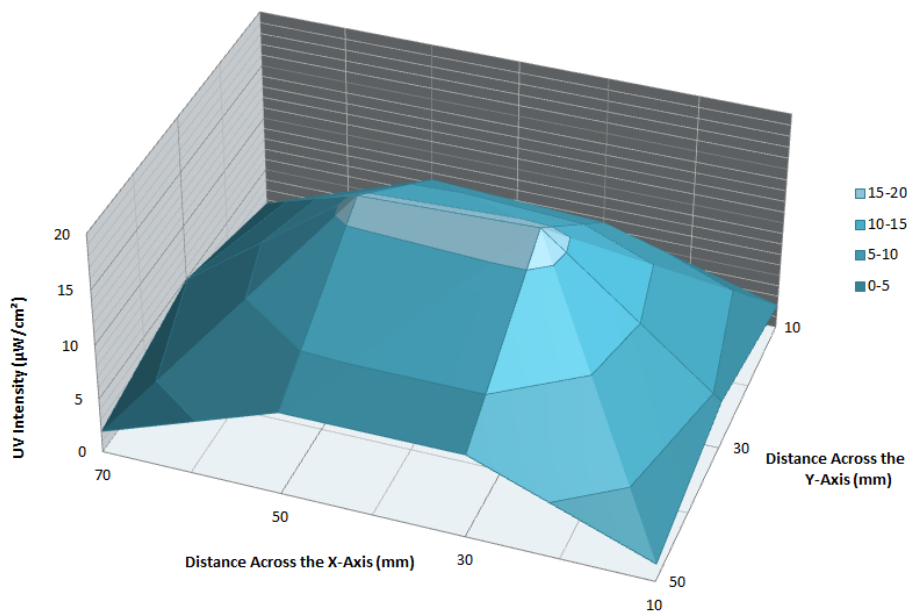
Figure 3.13.   Intensity map of UV light projected from the DLP system

The values measured in addition to a basic exposure, proved this light configuration to be ineffective in the initiation of an efficient curing reaction in the liquid photopolymer. At the intensity measured above, accounting for the required critical exposure energy, it would require a 432 second (7 minutes and 12 second) exposure to initiate curing on the surface of the photopolymer. This value of time would then dramatically increase to penetrate to full cure depth due to the continued absorption of light by the photopolymer. Following this result, the potential to use white light projection in place of a 365 nm light source was assessed to avoid problems with the high UV filtering of the projector system.

The aim of this experimental development process was to produce a low cost, flexible system capable of producing high quality substrates. The issues encountered with ultraviolet projection could be overcome with an expensive, high resolution DMD chipset from Texas Instruments, specifically designed for application with UV light, however this would require significant investment in the product itself and an optical array for image processing.

3.1.5 White Light DLP Projection

Although UV light and UV photo-sensitive materials are commonly used in Stereolithography systems, acrylate-based broad-band materials have been developed for use by hobbyists that are sensitive up to 440 nm, a source wavelength found abundantly in images projected from standard white light DLP's, as shown in the DLP projection spectrum in Figure 3.14. No alterations would therefore be required to the projector to expose the material using a white light source. The ineffective intensity of ultraviolet light projected from the modified system prompted a change to resins: Spot-A Materials Low Viscosity Resin, MakerJuice Labs G+ and Makerjuice Labs SF. These materials are sensitive to a higher UV and blue light wavelengths, up to 440 nm, the lower end of the visible (white light) spectrum. Spot-A Materials LV in particular has an ~70% lower viscosity, 50 cps [182], compared to 150-180 cps of 3D Systems Accura 60 [170], to aid in the deep dip recoating process present in the top-down Stereolithography system. In addition, all broad-band resins possess glass transition temperatures at least 22 °C higher than the 58 °C specified for 3D Systems Accura 60, enhancing their compatibility with conductive material deposition and thermal curing methods to be introduced in Chapter 5. White light projection does however demonstrate one major disadvantage as it produces a broad range of wavelengths across the spectrum of visible light.

A new high definition projection system was sourced to enable the development of the white light exposure capability. The resolution of this DLP projector can be simply calculated from the projectors resolution and the minimum size of projection area that can be focused. The HD projection device has a resolution of 1920x1080 pixels which, when projected onto a surface at its

minimum projection distance of 150 mm with minimum projection area 80 mm x 60 mm, results in a single pixel size and therefore theoretical resolution of 55 μm.
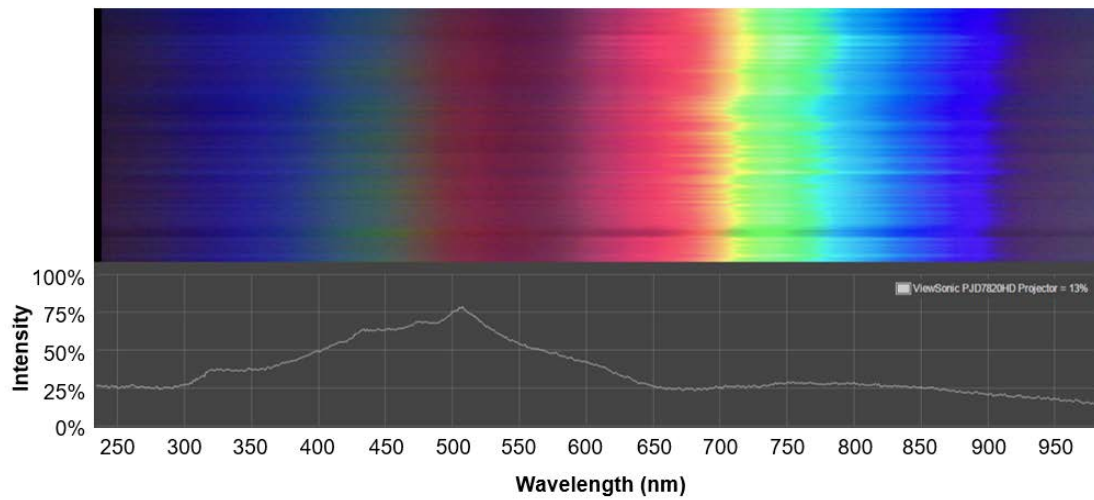
Figure 3.14.   Spectral analysis of ViewSonic PJD7820HD Projector [183]

Spectral analysis of light produced by the standard DLP source shows a peak of 75% at 500 nm wavelength but only 38% at 365 nm, making it apparently suitable for use with conventional 365 nm sensitive resins however, the necessary overexposure to certain wavelengths may cause a t-topping effect [184]. This light intensity was proven to be insufficient to initiate curing of the aforementioned 365 nm resin. A higher intensity of light is emitted between 380 nm and 440 nm making this projector more suitable for curing broad-band photopolymers.

A broad-band resin is sensitive to wavelengths of light between 350 nm and 440 nm, however its sensitivity differs across that range as shown in Figure 3.15. This leads to differing speeds of curing dependent on the wavelength of exposure which can result in residual stresses in resulting specimens.
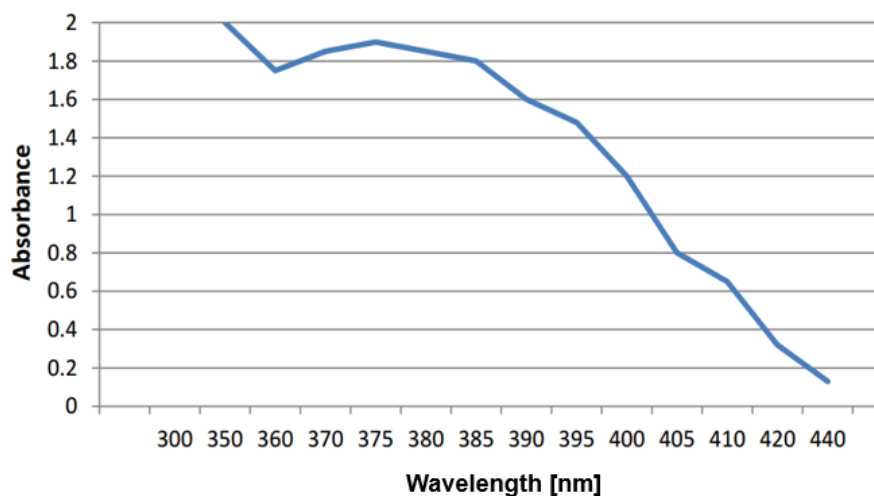
Figure 3.15.   MakerJuice Labs G Resin absorbance at different wavelengths [185]

An inconsistent curing rate limits the process resolution and causes residual stresses within the fabricated parts resulting in geometric inconsistencies manifesting as warping of the samples. When compared to the spectral analysis of the white light projector shown in Figure 3.15, all sensitive wavelengths are projected at differing intensities. Despite these theoretical issues white light has previously proven to be successful and is widely available for use by hobbyists who produce intricate models that are unable to accumulate too much stress or exhibit warping.

3.1.6 Optimisation of White Light Exposure Time

Optimising the exposure time of the projected image ensures that the parts produced are high quality with a high resolution and dimensional accuracy. A number of disadvantageous characteristics have also been associated with overexposure to a light source, including increased stress, brittleness and discoloration [81]. These effects are also observed as the parts age and absorb environmental sources of light through the 'dark reaction' mechanism.

Spot-A Materials Spot-LV resin was selected for use in the development of the white light projection capability of this system. Due to the lack of availability of technical data regarding the resin, the functionality of the system was measured through iterative experimentation of exposure time.

Initial tests around exposure times all demonstrated symptoms of over curing, characterised by, brittle parts firmly attached to the build platform, colour change from clear to pale yellow and, 'stalactite' like structures hanging from the underside of the build platform, shown in Figure 3.16.

These hanging features provide an insight into the degree of overexposure present during this experimentation, measuring 20 mm at 10000 ms, 10 mm at 5000 ms and 6 mm at 1000 ms of exposure to 'white light' from a high definition DLP projector.

Figure 3.16.   Trials conducted with a) 9000 mJ/cm^2, b) 4500 mJ/cm^2 and c) 900 mJ/cm^2 energy doses per layer

Experimentation has shown that reducing exposure time to the lowest value that still results in curing and, reducing the size of the features on the underside of the build platform, limits the brittle nature of the cured resin and prevents significant yellowing of the cured resin due to overexposure. This characteristic is commonly observed after prolonged exposure of the finished part to

environmental UV light sources due to photodegradation. These 'stalactite' structures form due to the projected light penetrating much further into the resin than the surface of the build platform, suggesting that even a 1 second exposure time is too high. The exposure time was halved to 500 ms however this resulted in the final part shown in Figure 3.17.

This ineffective curing could come about for multiple reasons. Firstly, it could result from a low light intensity causing some areas of the projected image to insufficiently polymerise the photopolymer. Secondly, the reflection and scattering of light off the build platform could cause increased exposure to some regions of the resin, overexposing those areas and underexposing others. Finally, the lens array on the projector could also cause a diffraction pattern and therefore cause severe aberration of the projected light [175]. Features were still present on the base of this specimen caused by penetration of the light source through the holes in the build platform and measured 2 mm in length, they provide a contradiction to the suggestion that the exposure time was not long enough.
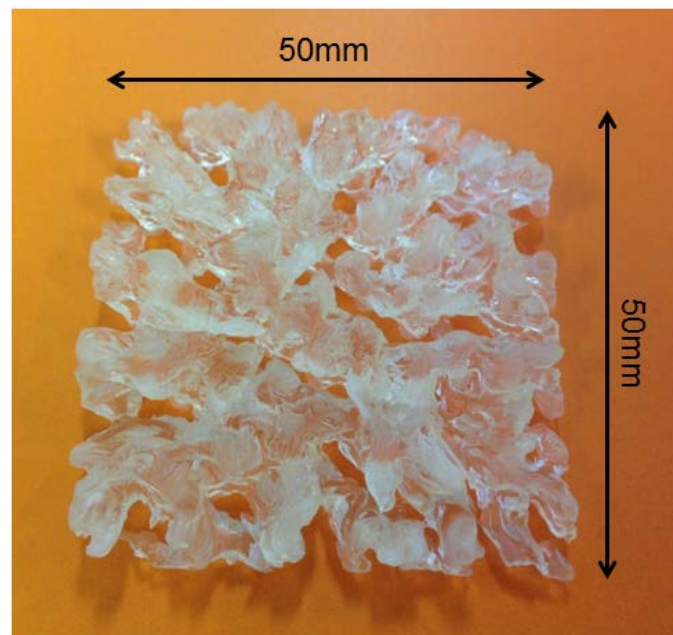
Figure 3.17.   50 mm x 50 mm test substrate produced with an energy dose of 450 mJ/cm^2 per layer

This led to the conclusion that the over exposure demonstrated at higher exposure times is a result of light scattering off the stainless steel build platform, producing multiple exposure doses with only one flash of the projector system. In the case of the 500 millisecond exposure this would explain why areas exposed to direct light failed to cure whereas, those exposed to both direct and reflected light reacted. This conclusion is further justified by the formation of the stalactite-like structures demonstrating that, where there is no reflective surface the light causes curing below the level of the build platform, and therefore the light hitting the reflective surface must have been redirected back towards the source.

Although length of exposure was shown to effect discolouration, it can also be caused by the range of wavelengths being emitted by the projector. Despite being categorised as a broad-band resin it still has a higher sensitivity to wavelengths below 440 nm. Its exposure to a wide band of wavelengths significantly above that value could also cause discolouration and stress.

Two potential ways to overcome the issues with overexposure were theorised. Firstly, the build platform could be changed to a solid, matt surface, preventing the creation of features below the build surface and minimising light reflection. Secondly, overexposure by the broad spectrum of light emitted from the white light projector could be minimised by inserting a bandpass filter.

3.1.7 Solutions to Build Issues with White Light Projection

Addition of a Light Filter

The wide spectrum of wavelengths emitted by the projection source has been identified as one of the issues currently effecting build quality. The inclusion of a filtering element, removing all wavelengths of light above 420 nm, resulted in immediate improvements in quality. Over a 500 ms exposure, the addition of the light filter resulted in a fully cured part of significantly higher quality than previous attempts. A comparison has been made in Figure 3.18, showing the production of a thin photopolymer substrate.

| No Filter | Blue Filter |
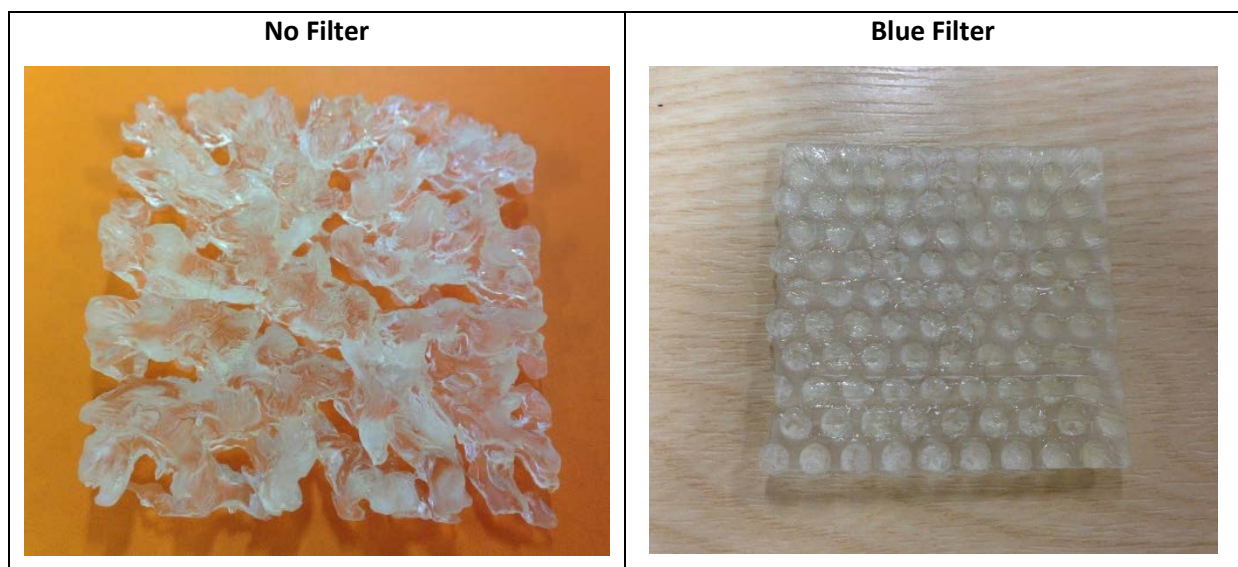
Figure 3.18.   Effect of a light filter on the quality of 50 mm x 50 mm sample at 450 mJ/cm^2 exposure dose

The blue filter transmittance peaks at 410 nm, only 5 nm higher than the peak sensitivity of the low viscosity resin being utilized. The light transmittance of the Comar Optics 390 BG 50 filter at 410 nm is 80%, resulting in the need for a longer exposure time.

Changes in build platform

The use of a perforated build platform caused overexposure manifesting as both additionally cured features beneath the platform appearing as 'stalactite' like structures and over cured sections on the build platform itself as a result of light reflection back off the platform. Attempts to change the platform material improved the quality of parts, creating resolvable features on the surface as shown in Figure 3.19 however, the corners of the part are not properly resolved, suggesting an underlying issue with the projection system optics such as aberration.

Perforated Stainless Steel	Polypropylene
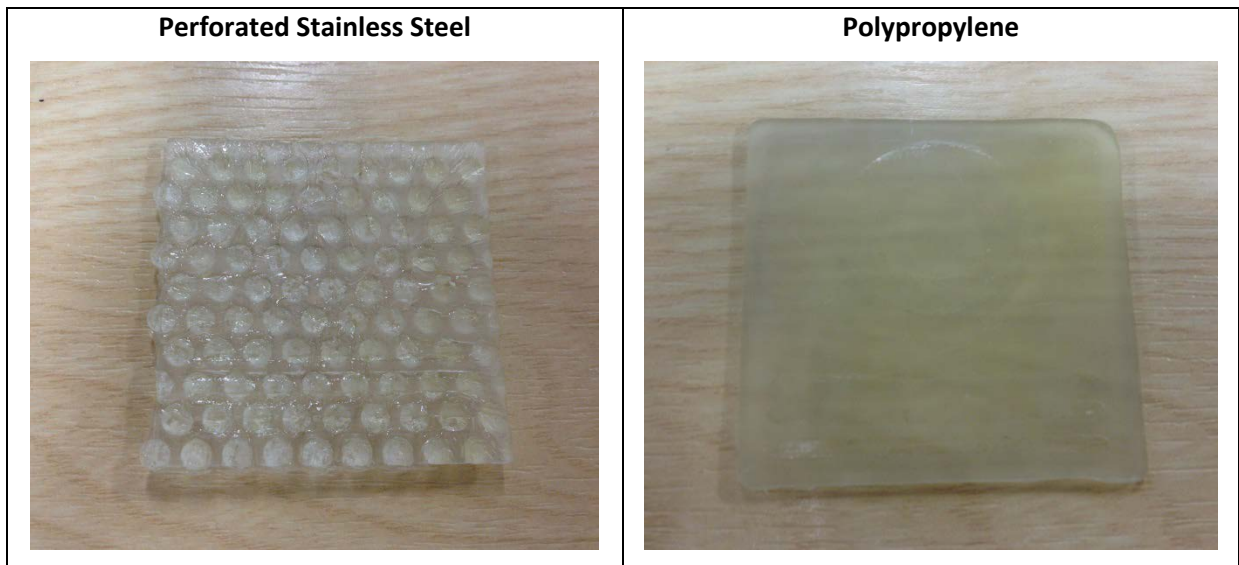
Figure 3.19.   50 mm x 50 mm test samples fabricated with energy doses of 450 mJ/cm^2 per layer produced on different build platforms

Removal of the build platform perforation resulted in the prevention of stalactite structures. The surface finish on the platform was also non-reflective to ensure there was no reflection from the primary light source. This change prevented the penetration of light through the build platform however, due to the increased obstruction of resin flow during recoating, it resulted in an increased surface height, causing a doming on the surface shown in Figure 3.20. This dome is completely formed on the second layer and then continues to increase in height with the designed thickness of the part.
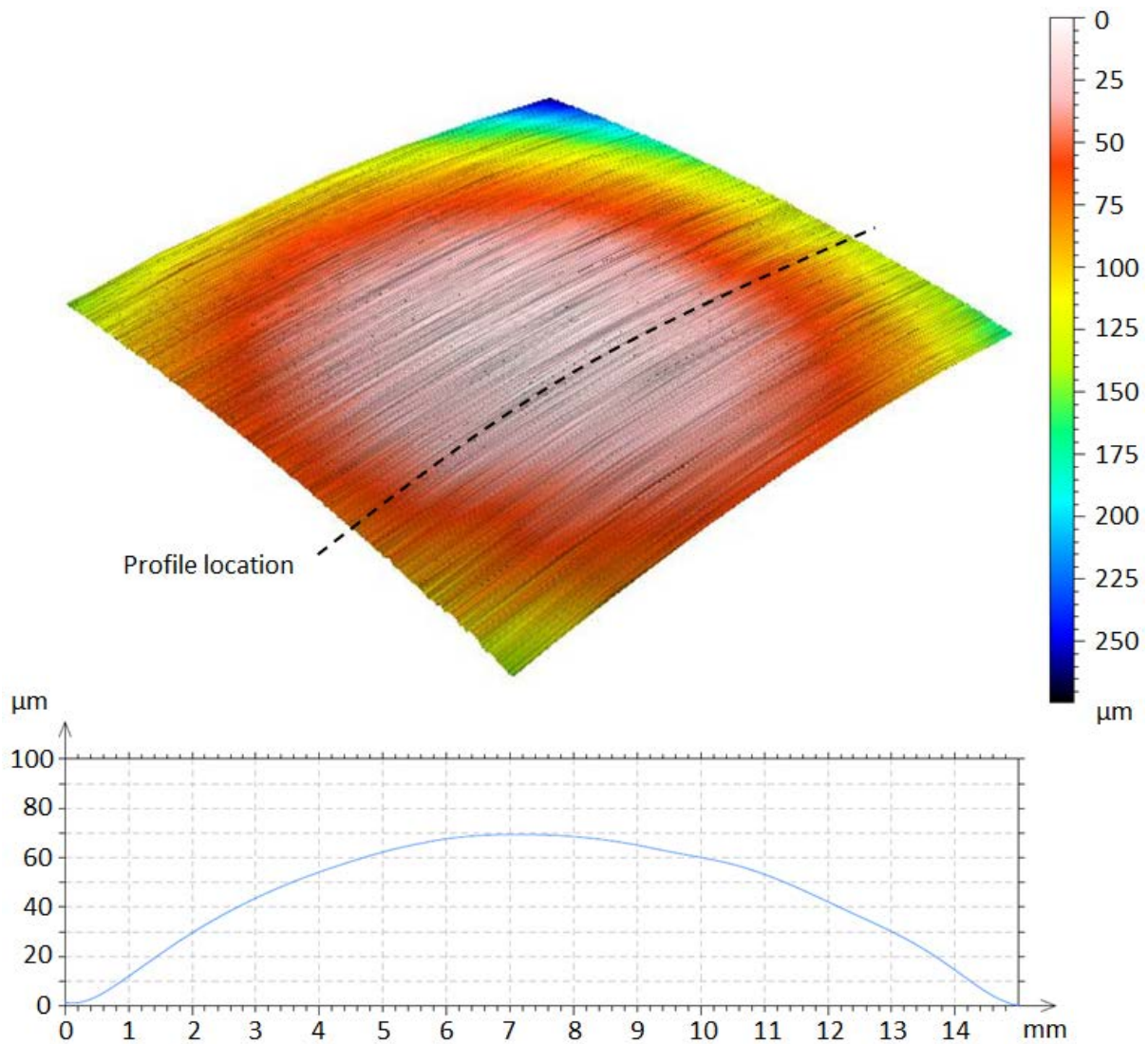
Figure 3.20.   Surface profile measurement of the surface of 20 layer thick substrate produced via top-down Stereolithography

From an average surface profile of the substrate a 70 µm distance has been measured from the lowest point to the highest point on this substrate over a 15 mm square area, equating to a variation in surface height of 0.7 times the layer thickness. A Gaussian low-band filter designed to identify waviness of the surface was used to filter the surface profile from scan data collected by a Talysurf CLI 2000 laser scanning system. This resultant surface is highly unsuitable for use in the deposition of electronic circuitry as this research aims to print conductive tracks with a height of <50 µm. Increasing the surface area proved to reduce this doming affect however, substrate sizes greater than 20 mm x 20 mm were not considered suitable for the development of this research due to the loss in image resolution from increased exposure time. Increased z-wait times were also trialled in an attempt to reduce this doming on the upper surface however these were unsuccessful. This doming

effect shown in Figure 3.21, also previously referred to as a 'meniscus' has been observed by Kataria [186], Kataria and Rosen [153] and, Choi *et al.* [87].
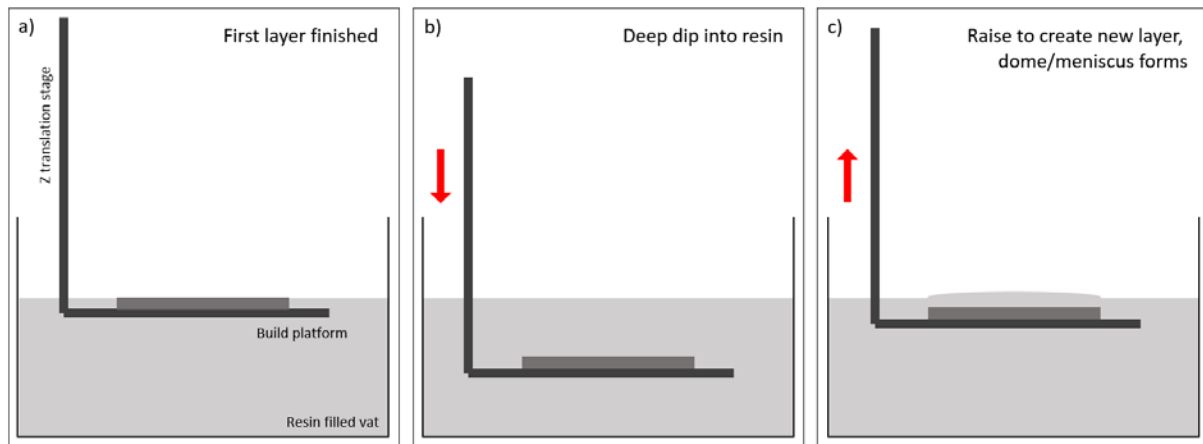
Figure 3.21.   Three stages of deep dip recoating, a) completion of previous layer, b) Deep dip into resin and c) raising platform to create new layer, resulting in the formation of the domed surface

It also formed a body of research conducted by Renap and Kruth [93] who showed that doming was exhibited during most recoating processes including blade recoating whereby entrapped volumes of uncured material resulted in an increased layer thickness despite the blade pass.

Despite some issues, resin was successfully cured to the build platform in 50 μm layers on top of one another to create a three dimensional product. The projection and mechanical systems integrated successfully using the chosen firmware and software. That said, level surfaces could not be created using the top-down method. The only solution to this problem in this build orientation would be the addition of a recoating mechanism, sweeping across and planarising the top surface however, this option had already been discounted due to its lack of compatibility with the embedding of components proposed in Chapter 1. The resolution of the process could not be proven and small features could not be resolved due to both the recoating and DLP optics issues.

3.2   Bottom-up DLP SLA Multilayer Substrate Production

To overcome problems with the top-down Stereolithography setup, a new process orientation was presented. Bottom-up Stereolithography relies upon a means of exposure from underneath the vat to produce parts upside down on the build platform [67]. The method of production is the same as that used in top-down methods whereby resin is selectively cured on a layer-by-layer basis to produce the part, however this occurs through the underside of a build vat, in an opposite orientation to that shown in Section 3.1. A diagram of the proposed setup is shown in Figure 3.22.
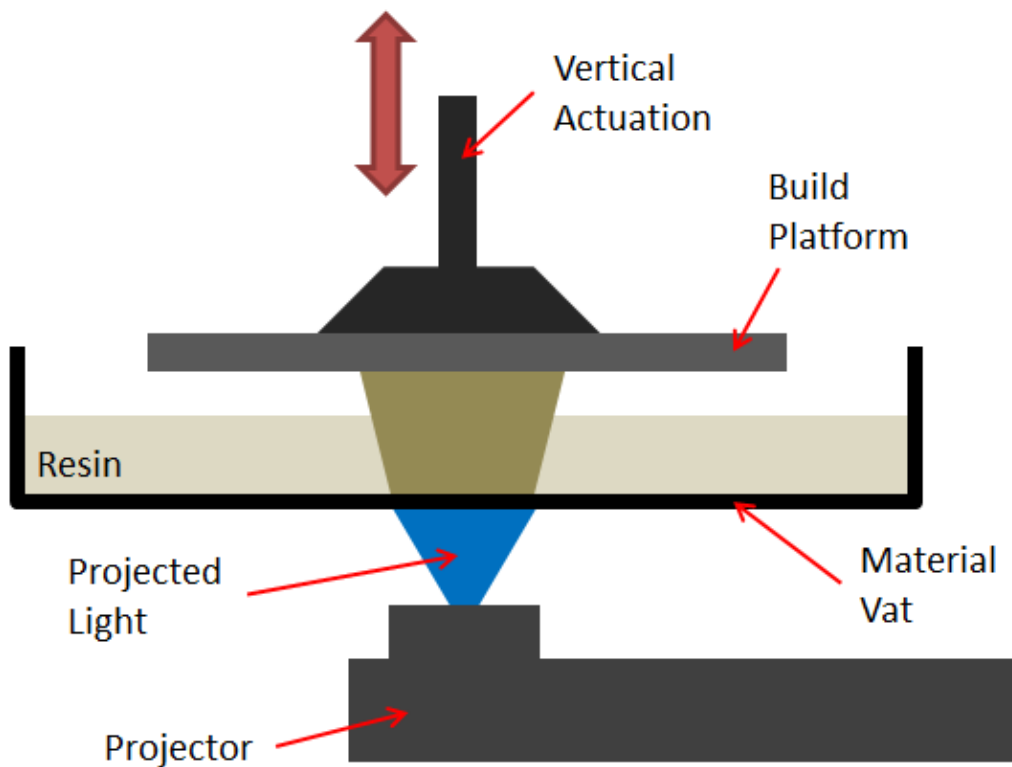
Figure 3.22.   Diagram of bottom-up Stereolithography process

This process has a number of advantages over top-down methods discussed further in Section 2.3.2, especially in the manufacturing of small parts that require a high resolution. This method requires subtle changes in exposure time dependant on layer thickness but optimisation experiments can be conducted to calibrate the machine for a variety of layer thicknesses to ensure they are fully cured and sufficient layer adhesion has been achieved. This functionality makes bottom-up Stereolithography a self-recoating process. This recoating process is also made possible by the addition of a thin film of PDMS on the UV transparent base of the vat, ensuring that the cured resin does not adhere to the glass surface and resulting in a high quality surface finish. These extra transmission surfaces can however result in light scattering which in turn, can impact image resolution. With no x, y-axis movement capability, alignment can be achieved through the repositioning of the build platform after each build and each layer can be created with one movement of the z-axis, allowing all others to be fixed.

This method requires thick embedding layers to encapsulate circuitry, with the shape determined by a single exposure and complex external geometries having to be created before embedding takes place. Stresses on the photopolymer are increased due to the difference in exposure energy absorbed by the bottom surface of the vat and the thick layer adhesion interface up to 2 mm below the surface. However, during the production of multi-layer substrates this method does not allow

the embedding of electronics using individual 100 µm layers as the components would collide with the base of the vat. In addition, changes in substrate orientation are required. Embedding can be achieved using bottom-up projection using the method detailed in Section 6.1 however this may cause the build-up of residual stresses on the substrate.

3.2.1   mUVe3D Stereolithography System

A mUVe3D 1.5 DLP Stereolithography system, shown in Figure 3.23, was sourced providing a highly versatile research machine that can be easily modified and retrofitted with components to make it suitable for this research due to its open source nature. This system was customised by removing a number of structural supports that were causing re-alignment issues and minimising the number of moving parts to increase the repeatability of movement. A new, smaller, detachable build platform was created to allow integration with other AM processes and, this build platform was mounted within a slot mechanism with a locating screw to ensure it was precisely re-positioned after every removal. Finally, a depth gauge micrometer was added to the system, designed to allow the height of the build platform at its home position to be accurately altered. This allowed part-built geometries to be reinserted and positioned at a predetermined height for embedding and further processing.
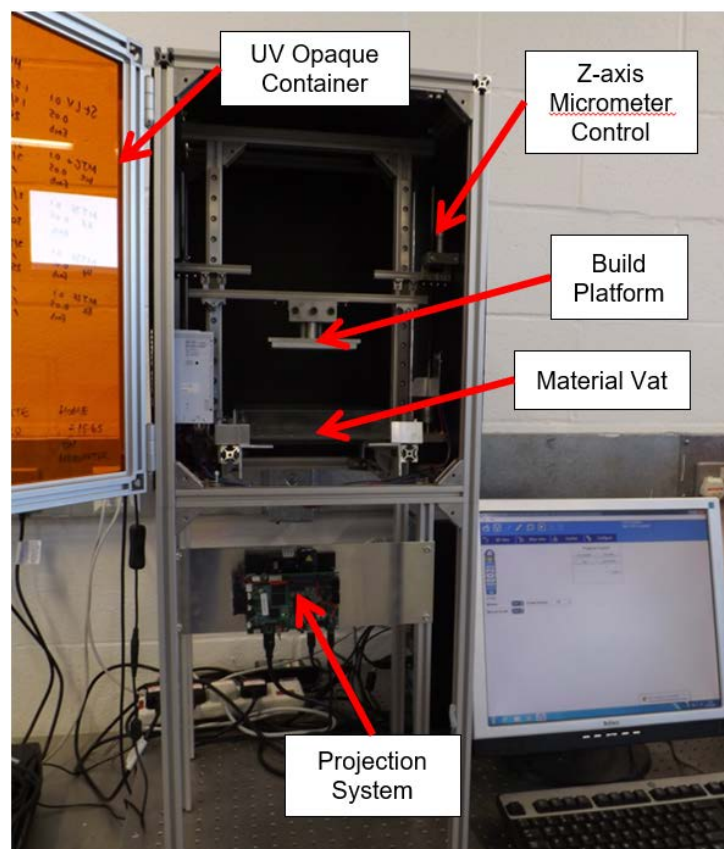
Figure 3.23.   Customised mUVe3D Stereolithography apparatus

The versatility of this system spans further than the internal arrangement. The universal projector mount also allows alternative LED exposure sources to be swapped, providing the potential to integrate an ultraviolet light source into this system. The projection distance and projection area can also be altered, resulting in the potential to create larger parts at the expense of increased pixel size if necessary.

3.2.2 Projection Systems

Selection of a suitable projection system plays a significant role in the production of an accurate substrate with a high resolution. As shown in top-down production, a standard high resolution DLP projector could be used to cure resins whose photoinitiators are sensitive above the ultraviolet spectrum. However, testing in Section 3.1 showed significant issues when curing a large area with such a wide range of wavelengths including warping.

A new 405 nm DLP Lightcrafter™ 4500 projection unit, designed to project smaller areas was sourced from Texas Instruments. The pico-projector in Figure 3.24, built with a 0.45 WXGA chip set is capable of displaying at a resolution of 1280x800. Light projected at 405 nm can be projected at a high enough intensity to cure broad-band resins with a wide absorbance range up to 440 nm. At its minimum projection distance, determined by the smallest distance at which it can be fully focused, the projected image area is 140 mm x 87 mm. This resulted in a theoretical resolution of 109 μm in both x and y axes, calculated by dividing the minimum projection area of 140 mm x 87 mm by the display resolution. This system resolution is later proven through experimentation in Section 3.2.4. It could also be reduced through the application of a high definition DMD or changes in the optics.
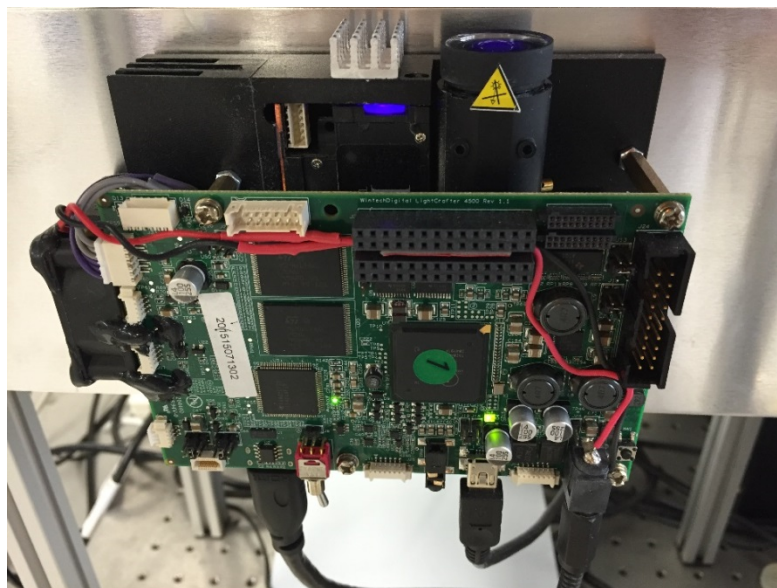
Figure 3.24.   DLP Lightcrafter E4500MKII UV projection module

A 1 W UV light emitting diode has been fitted into this projection module to provide the capability to cure photopolymers traditionally used in laser based systems. The spectrum of light produced by the LED is very narrow, ensuring a higher intensity of UV light.

The GUI Software shown in Figure 3.25 was provided to complement this projection system and facilitate, among other things, control over the intensity of the LED and therefore the projected light. Through this control mechanism, the intensity of the LED can be tailored by inputting values of between 0 and 255 to control its supply current. These nominal values are a result of the primary function of these projection modules as normal full colour projectors, colours created through a combination of differing intensities of the three primary colours, sources of which are normally mounted in the three LED locations.
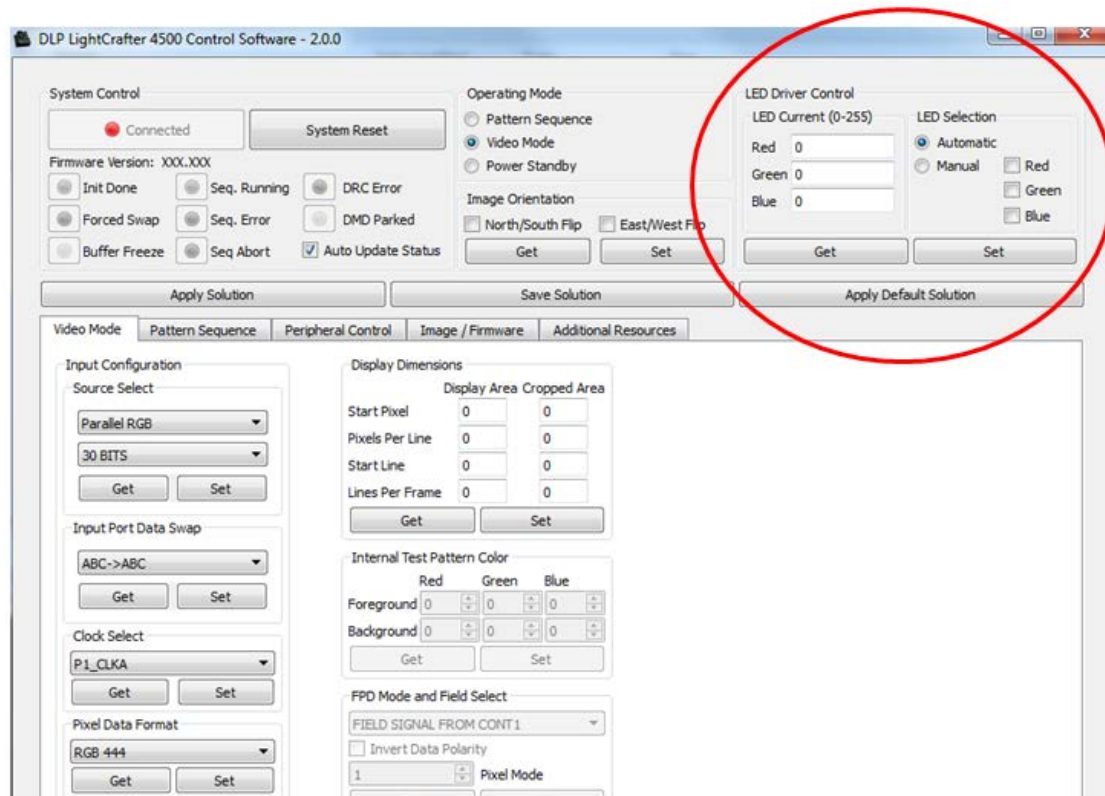
Figure 3.25.   UV projection intensity control software

As standard, this projector was run at an intensity that was measured as approximately 30% of its maximum. It produces a default value of 76 mW/cm^2 at the projection lens, which is reduced to an average of 0.981 mW/cm^2 across the projected area on the base of the vat after passing through the PDMS layer. At full intensity, the same projector produces an intensity of 252 mW/cm^2 at the lens and 3.16 mW/cm^2 on the base inside the vat with the PDMS layer in place. The standard intensity was used to characterise this process for two main reasons. Firstly, at high projection intensities, the antistiction PDMS layer on the base of the vat degrades more quickly, resulting in its failure after

only 4-5 hours of printing. At the default intensity, in excess of 100 hours of printing over a 3-4 month period has not resulted in any observed damage to the PDMS layer. Secondly, DMDs are not designed to be exposed to light below 420 nm as damage can be caused to the mirror coating reducing their longevity. This combination of reasons led to the projection intensity being limited to 30% of its maximum intensity.

3.2.3 Bottom-up Ultraviolet Light Distribution

To ensure uniform curing across the entire build platform an intensity map was created using UV detection apparatus, to determine how much of a drop in intensity there is between the centre and perimeter of the projection area inside the vat with the PDMS layer in place. This also helped to find the optimum position on the platform in which to build parts. This position can be identified by analysing the intensity map and the shape of an array of test samples produced in a matrix across the platform, paying particular attention to the feature resolution and shape of the fabricated samples.

To ensure that the intensity did not change over time, the intensity in the centre of the projected image was measured over a 10 minute period to determine time sensitive fluctuations. This helped determine if the projection system required warming up, a period over which the intensity would increase to a peak. It was however proven that no such period was required as the intensity fluctuated by only 6 $\mu W/cm^2$ or 0.6% over a 10 minute period. LEDs achieve their full intensity very shortly after being switched on, unlike UV emitting lamps which require warm up times prior to machine operation.

The projection area was then split into a grid with 10 x 10 mm sample areas, providing a more accurate intensity map than the top-down projection equivalent and, to facilitate the larger projection area. Using rulers and a set square, the UV sensing probe was positioned in the centre of each of these grid squares and a measurement of UV intensity captured. By recording a measurement in each grid square, the intensity map in Figure 3.26 was produced showing that the intensity at the perimeter of the projection was up to 300 $\mu W/cm^2$ lower than at the centre. The intensity pattern is tilted to one side, resulting in inconsistent perimeter intensity and, the front of the projection, at low x and y distances, was 32% less intense than the peak value of 1091 $\mu W/cm^2$.
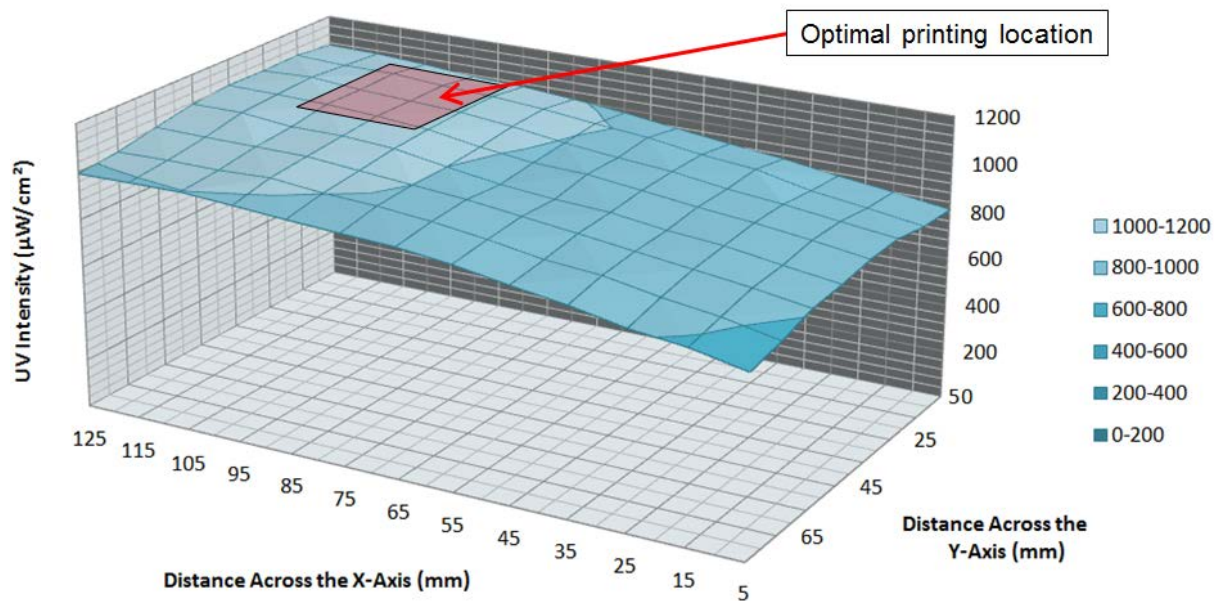
Figure 3.26.   Intensity profile across the UV projection area in the bottom-up orientation

The drop in intensity at the perimeter can be explained by the incoherence of the light source and lack of collection and collimation within the optics of the projector. LED light sources do not emit directionally, the light is spread out and only a certain percentage is captured with higher levels from the centre of the source of projection, a property that is then mimicked when projected onto the base of the transparent vat.

The difference between the intensity at the front and back of the projected image can be explained by the projection offset. Like most other DLP systems this projector is designed with an offset, allowing it to be mounted on a ceiling or table and project onto an offset surface (eg. a wall) without interference. This therefore means that the light making up the top of the image has further to travel to the projection surface from the lens, giving it more distance to dissipate and therefore, reducing the intensity, a phenomenon described partially by the inverse square law. The tilt in intensity is therefore caused by projection offset. Further system development could be conducted by tilting the source to account for the intensity offset and, recalibrating the projection control software to account for resulting dimensional errors in the projected slices. This would result in equal irradiation across the entire projection area.

The intensity map showed that despite some significant variation in projection intensity, the variation over a 20 x 20 mm build area in some locations is minimal and therefore suitable for 20 mm x 20 mm substrate production. However, for future scaling-up of the process to allow a larger build area a complete redesign of the optics would be needed.

The test specimen in Figure 3.27 was designed to determine the accuracy of specific build locations on the platform. With this system being developed to produce substrates no larger than 20 mm x 20 mm, the identification of the optimum location could be conducted by producing an array of the same test specimen spread across the build envelope.
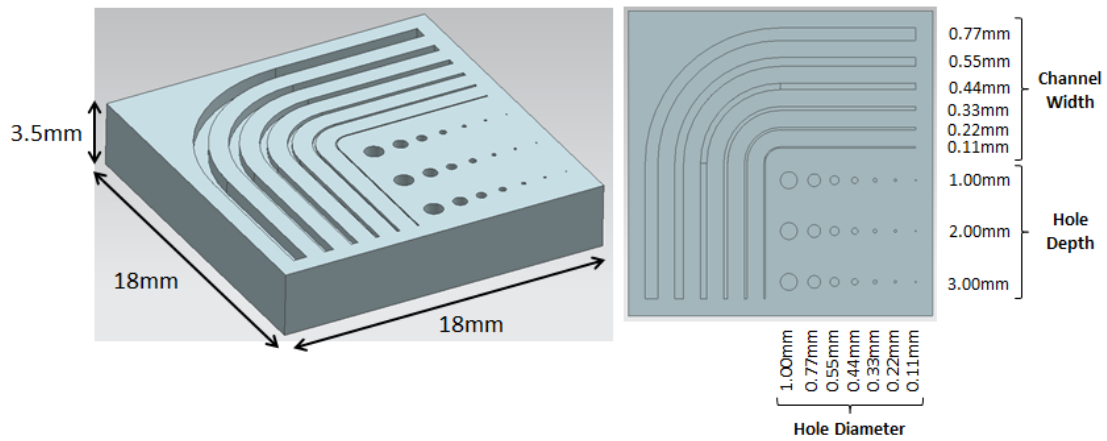
Figure 3.27.   Intensity drop off test specimen design

The design includes 1:1 aspect ratio channels and holes, both of which range in size from 1 mm to 110 µm, the smallest of which is equal to the calculated resolution of the projection system. Sample sizes of 18 x 18 mm in a 5 x 3 matrix were fabricated simultaneously equally spaced across the projection area and evaluated. The array in Figure 3.28 was fabricated with 100 µm layer thickness, however a 50 µm layer thickness was also used to provide an extra variable for assessment of build quality.

☐ Specimen comparisons made in Figure 3.29

☐ Specimen comparisons made in Figure 3.30
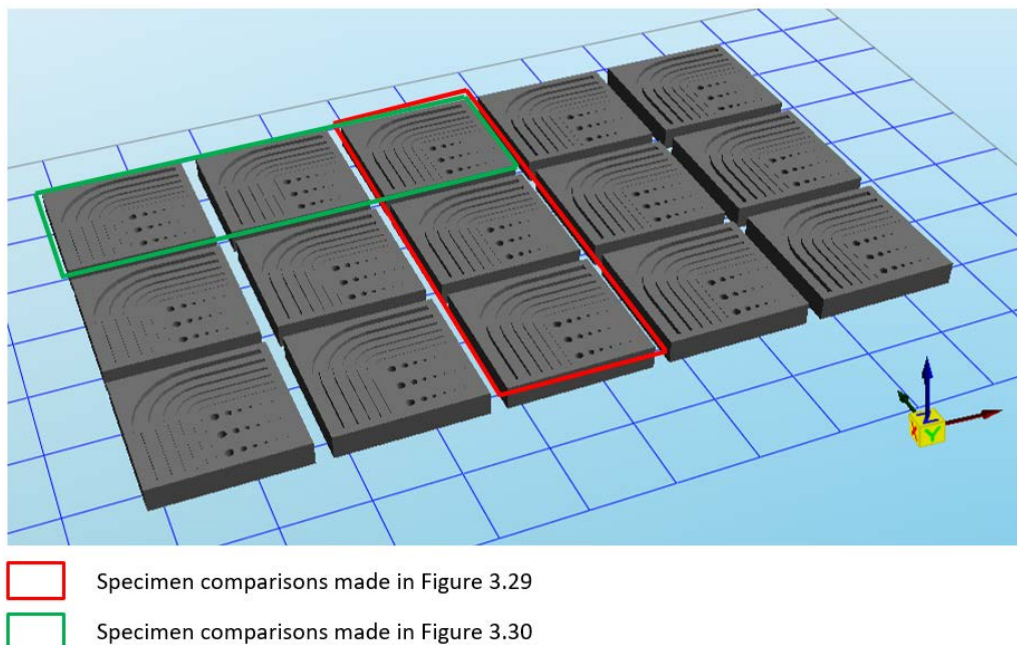
Figure 3.28.   Virtual array of test specimens spread across the projection area

Observation and analysis of the fabricated specimens showed that fabrication in the highest intensity areas with little projection offset resolved the smallest features with a channel as narrow as 110 µm being created. The projection offset caused slanted edges and blurred features with channels in the x direction shown in, demonstrating a reduced resolution compared to those printed in the y direction.
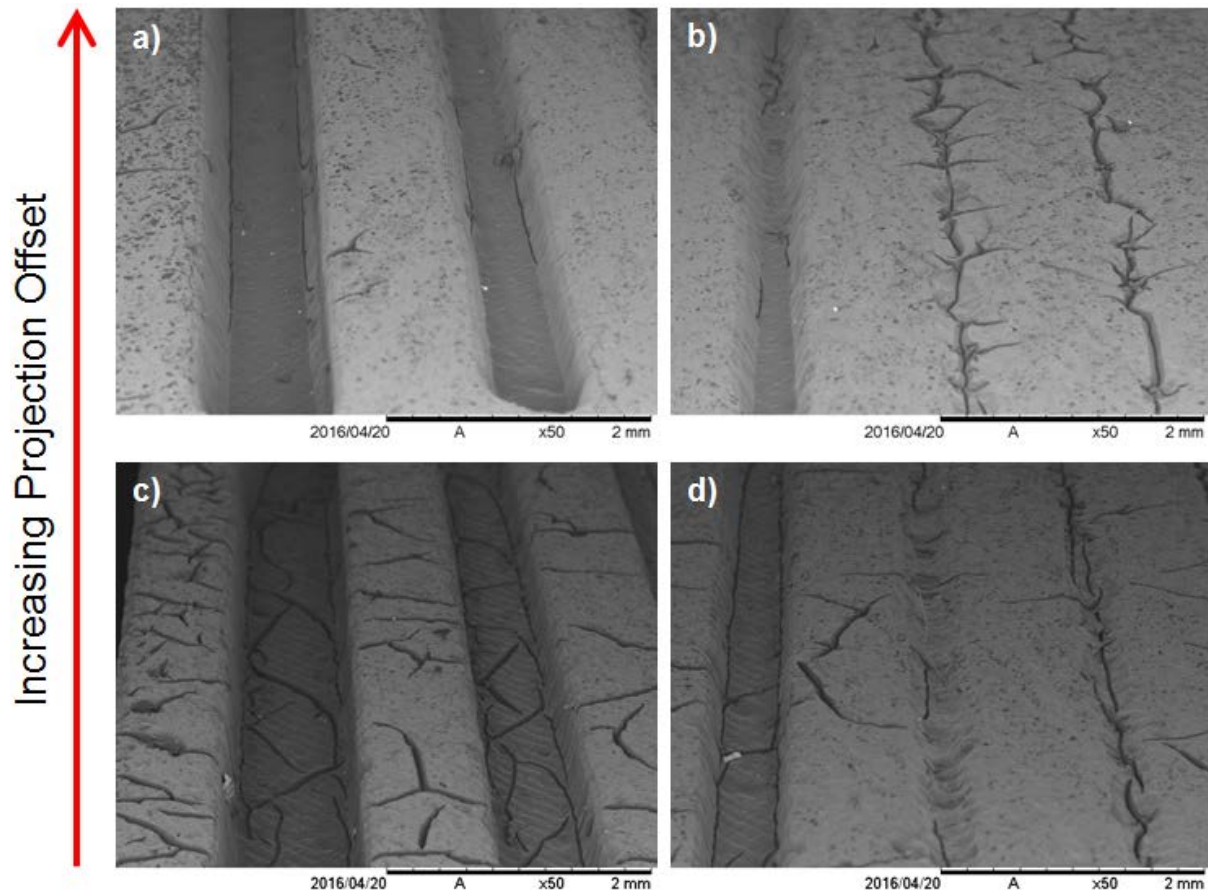
Figure 3.29.   SEM image showing effects of build location on x-axis build resolution of a) 770 µm and 500 µm wide (left to right) channels at high projection offset; b) 440 µm, 330 µm and 220 µm (left to right) wide channels at high projection offset; c) 770 µm and 500 µm (left to right) wide channels with no projection offset; d) 440 µm, 330 µm and 220 µm (left to right) wide channels with no projection offset

The resolution is seen to increase as the x-axis distance from the projector reduces. The channels 440 µm and above in width are all well resolved with 330 µm and 220 µm features visible on the substrates printed closest to 0 on the x-axis in Figure 3.29(d). Increasing x distance has resulted in poor resolution and slanted walls of the 440 µm channel as well as the appearance of tapering in Figure 3.29(b) caused by diminishing projection intensity. Unresolved features appear as cracks, resulting from the exposure of under cured resin to the cleaning solvent. Images of channels produced in the y direction shown in Figure 3.30 exhibit a more severe drop off in feature quality.
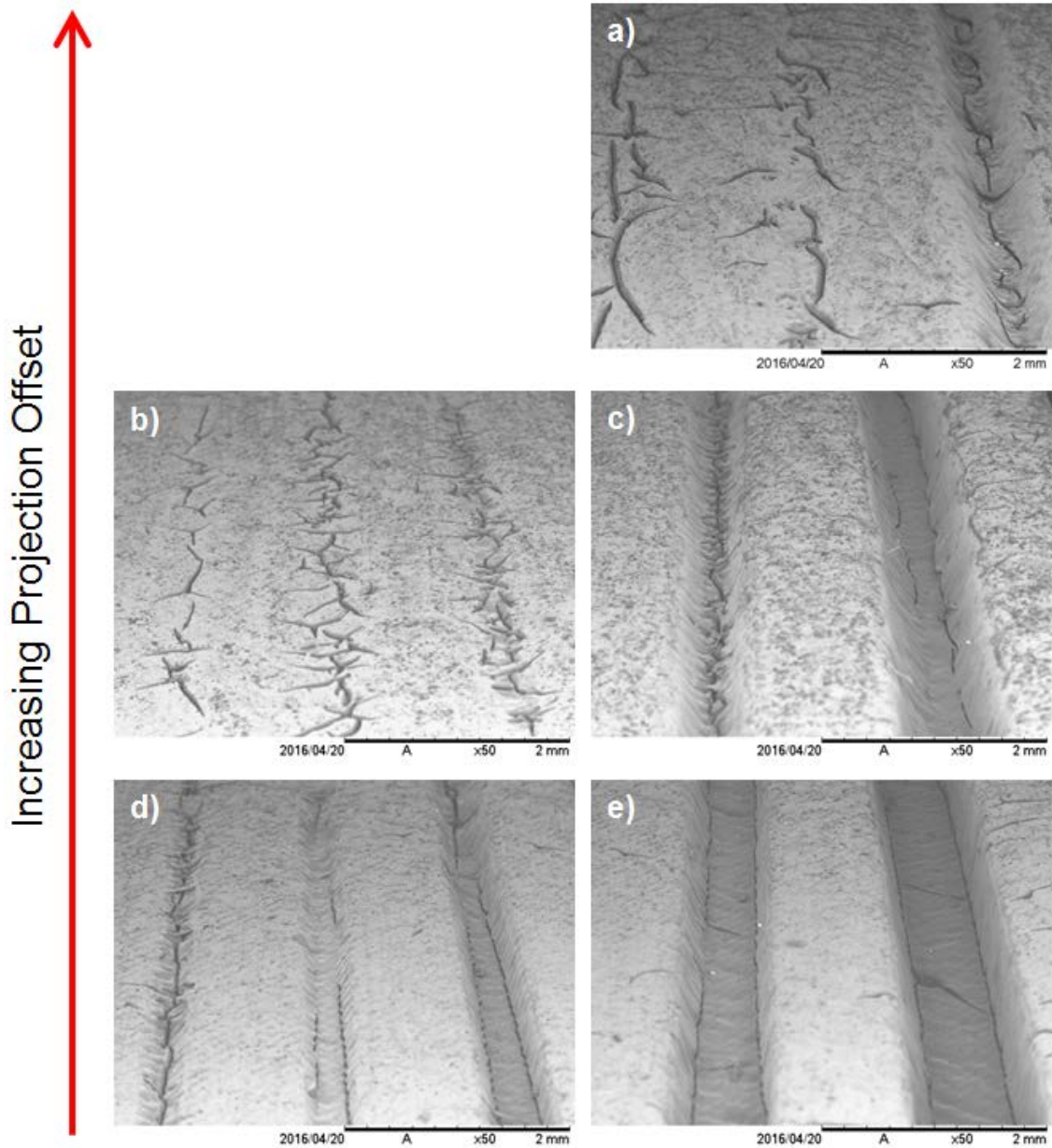
Figure 3.30.   SEM image showing effects of build location on y-axis build resolution of a) 770 µm and 500 µm (right to left) wide channels at high projection offset; b) 440 µm, 330 µm and 220 µm (right to left) wide channels at small projection offset; c) 770 µm and 500 µm (right to left) wide channels at small projection offset; d) 440 µm, 330 µm and 220 µm (right to left) wide channels with no projection offset; e) 770 µm and 500 µm (right to left) wide channels with no projection offset

Reducing light intensity quantified in Figure 3.26 prevents the fabrication of high definition features in certain locations on the build platform. This is the reason for such a significant improvement across Figure 3.29 with the 770 µm features poorly resolved at the top (Figure 3.30(a)) but the appearance of a channel as small as 220 µm in images at the bottom (Figure 3.30(d)). The same effect is evident on samples produced on the extremes of the y-axis. The highest resolution was achieved close to the projector, in a location that was shown during UV mapping to be subjected to the highest intensity of light. This location is the area at which the light hits the base of the vat at the

lowest offset angle in both x and y axes, an area large enough to produce 20 mm x 20 mm substrates for electronics deposition. Figure 3.31 presents both the high and low offset of light from the projectors causing differences in feature resolution in this study.
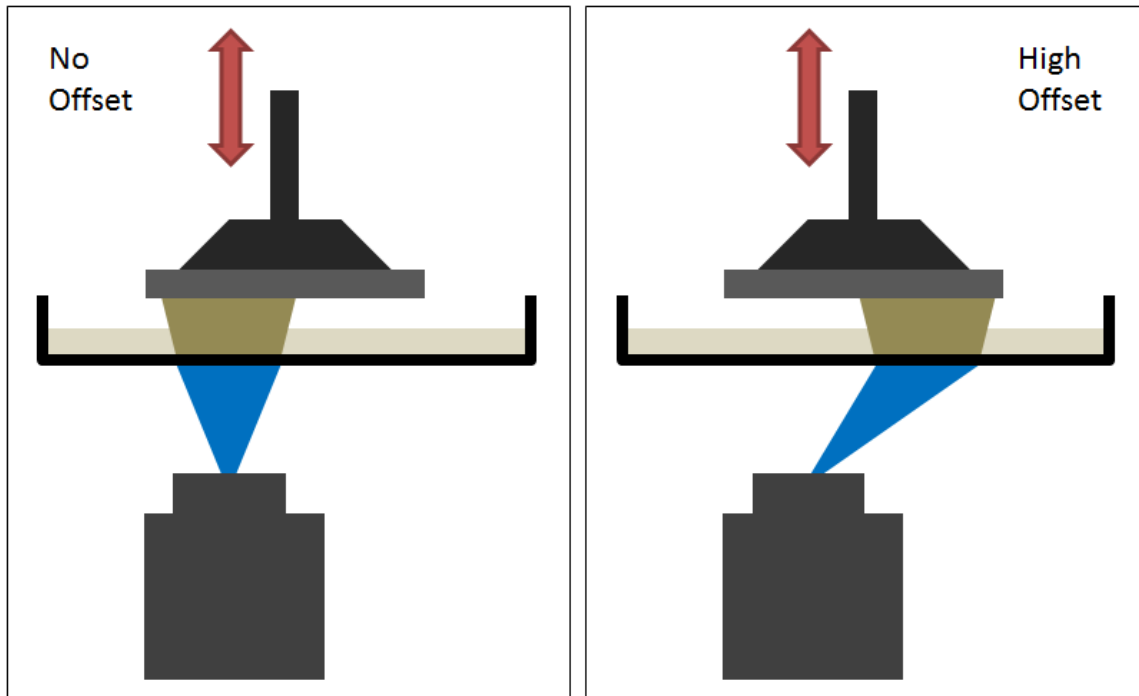
Figure 3.31.   Representation of high and low projection offset in bottom-up SL system

Cracks forming on the test samples were also observed as a result of incomplete curing of the photopolymer surface in particular when features have not been resolved. This lower exposure dose, caused incomplete polymerisation which resulted in the parts swelling and cracking during the subsequent solvent rinsing stage. This observed issue is investigated and methods to overcome it are demonstrated in Chapter 4.

3.2.4   Resolution Testing in X and Y Axes

Having identified the most favourable location on the build platform, the maximum theoretical projection resolution in this location can be calculated using the projected image size, the projector resolution and Equation 3.

Pixel size was calculated at 109 µm in both the x and y axes, over a 140 mm x 87 mm projection area. This individual pixel size is a calculation of the smallest resolvable feature and can be validated via experimentation. The test specimen shown in Figure 3.32(a) was designed with an array of channels with widths increasing in 5µm increments. Once fabricated, these specimens were measured using the Taylor Hobson Talysurf CLI 2000 contact free laser surface profiling system and after analysis the process resolution could be identified. As the resolution is in the order of 22 times higher than 5 µm,

a number of adjacent channels will measure the same width before the width increases by one increment of the resolution. The value by which the width increases and the number of identical adjacent channels multiplied by 5μm would both provide the projection resolution. By using this method and simply changing the build orientation of the test artefact, resolutions in both the x and y axes were determined. The specimen in Figure 3.32(b) was then used to confirm the resolution by printing channels with widths corresponding to multiples of a single pixel dimension.
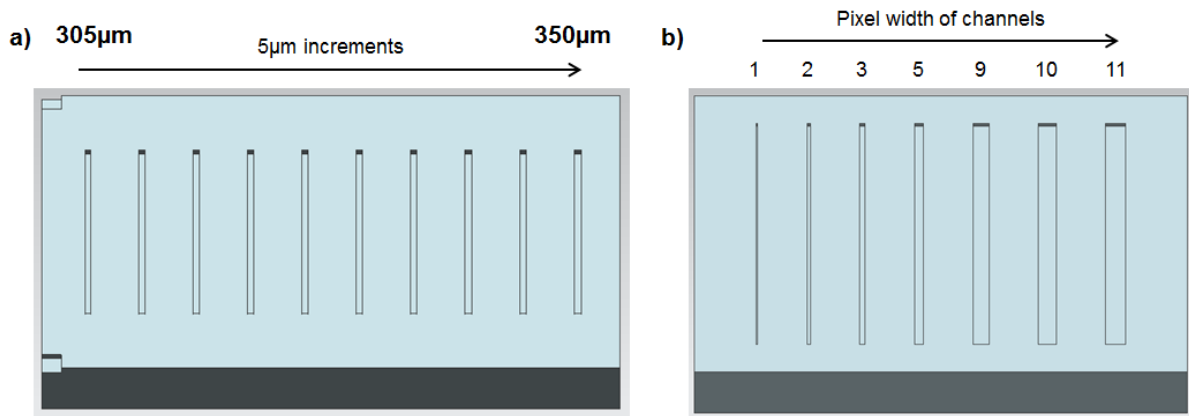
Figure 3.32.   Resolution test sample designs a) for determination and b) for confirmation

The average width of the tracks in sample (a) increased by between 105 μm and 110 μm every 20 to 22 channels, equating to an experimentally determined resolution of between 100 μm and 110 μm at the highest resolution point of the projection area. This has been confirmed by measurements taken from sample (b), presented in Figure 3.33.
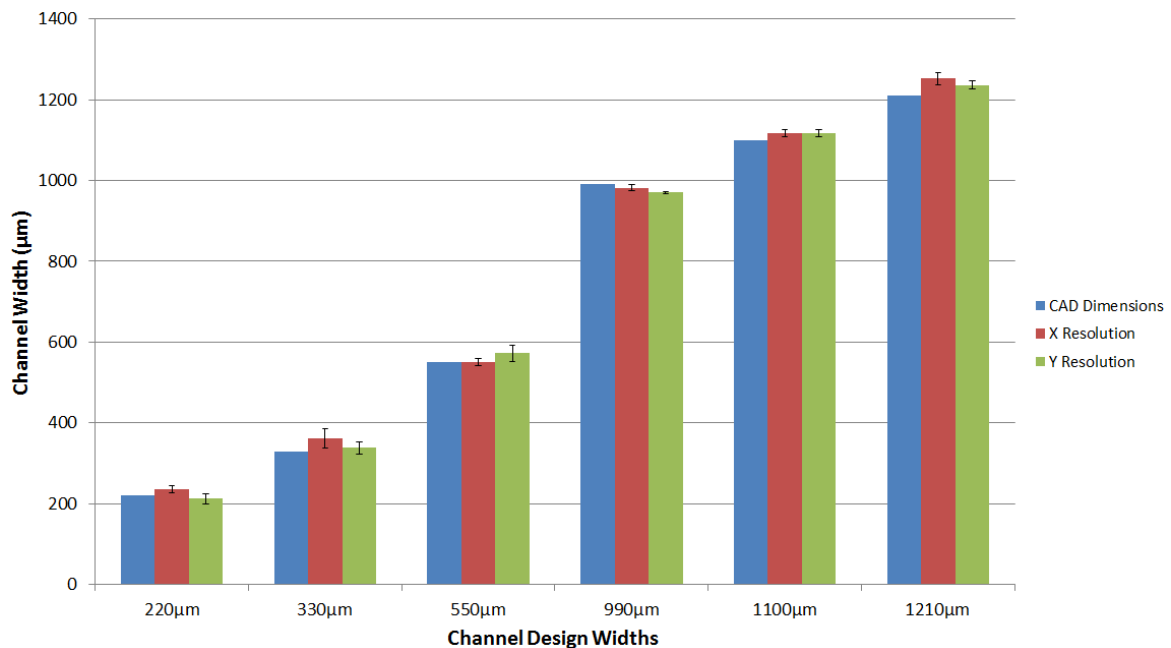
Figure 3.33.   X and Y axis resolution of SLA apparatus compared to CAD dimensions

The measured dimensions of these features printed in both x and y directions have been measured and plotted alongside their designed dimensions. Features built in the x-axis all measured within 10%

of the design dimension. This in comparison to features built in the y-axis which proved more accurate with measured dimensional errors no greater than 4%.

3.2.5 Resolution Testing in Z-Axis

The z-axis movement is controlled through the Creation Workshop control software and is determined by the minimum step size of the motor. A number of factors, most importantly the suction resulting from the proximity of the build platform to the base can impact the z-axis layer thickness. A test specimen has been designed, consisting of five steps increasing in thickness by one 100 µm layer thickness. These artefacts range from 10 layers thick, 1 mm, to 25 layers thick, 2.5 mm. Data processing of a surface scan from the Taylor Hobson Talysurf CLI 2000 exhibited in Figure 3.34 showed an average height increase of 100.95 µm across 72 measurements.
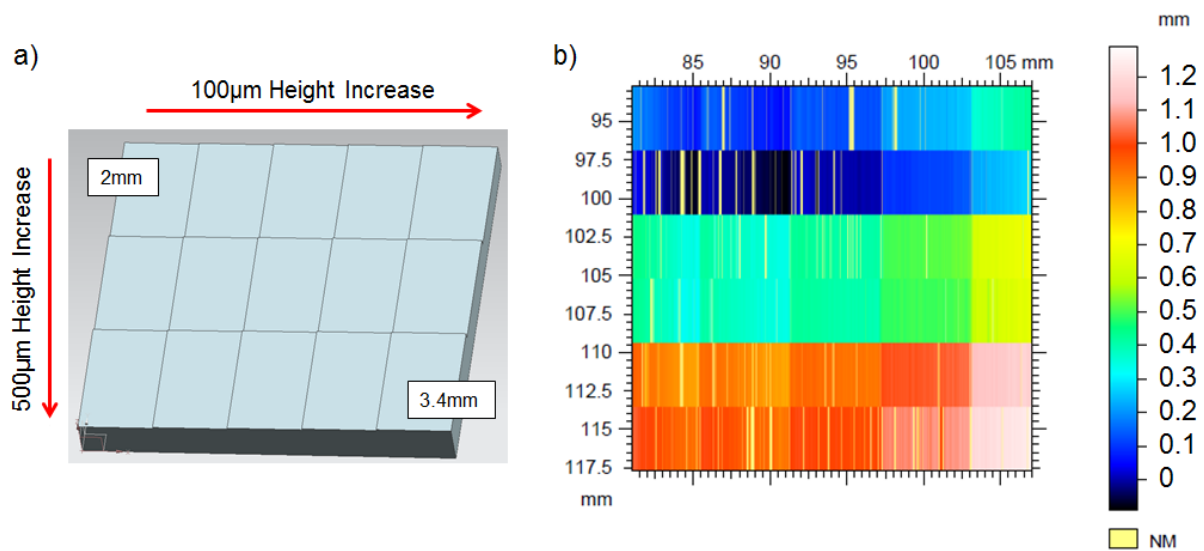
Figure 3.34.   Z-axis resolution test artefact a) design and b) profile scan data

This test specimen proves that the z-axis resolution of this process matches that of the design and, that accurate layer thicknesses can be produced using this bottom-up projection Stereolithography apparatus.

3.2.6 Substrate Surface Finish

A high quality surface finish is necessary for the deposition of conductive materials via dispensing however, it has a greater impact on the surface mount assembly of electronics and packaging of multiple layers of circuitry which would prove particularly difficult on curved surfaces. This was discussed during Section 3.1 with the top-down approach found unsuitable for this application due to the poor planarity of the surface of small substrates. During the optimisation of the bottom-up Stereolithography system a number of 2 mm thick test substrates were produced using both Spot-A Materials LV and MakerJuice SF broad-band resins. These samples were analysed using the Talysurf CLI 2000 to provide surface profiles of substrates produced in the bottom-up projection orientation.

Both these samples were produced using the 405 nm projection source. Over a 15 mm x 15 mm area the difference between maximum depth and height in the Spot-A Materials resin was measured at 25 µm, 45 µm lower than that demonstrated by the top-down projection orientation. This height difference was even lower on MakerJuice SF substrates at less than 6 µm as shown in Figure 3.35.
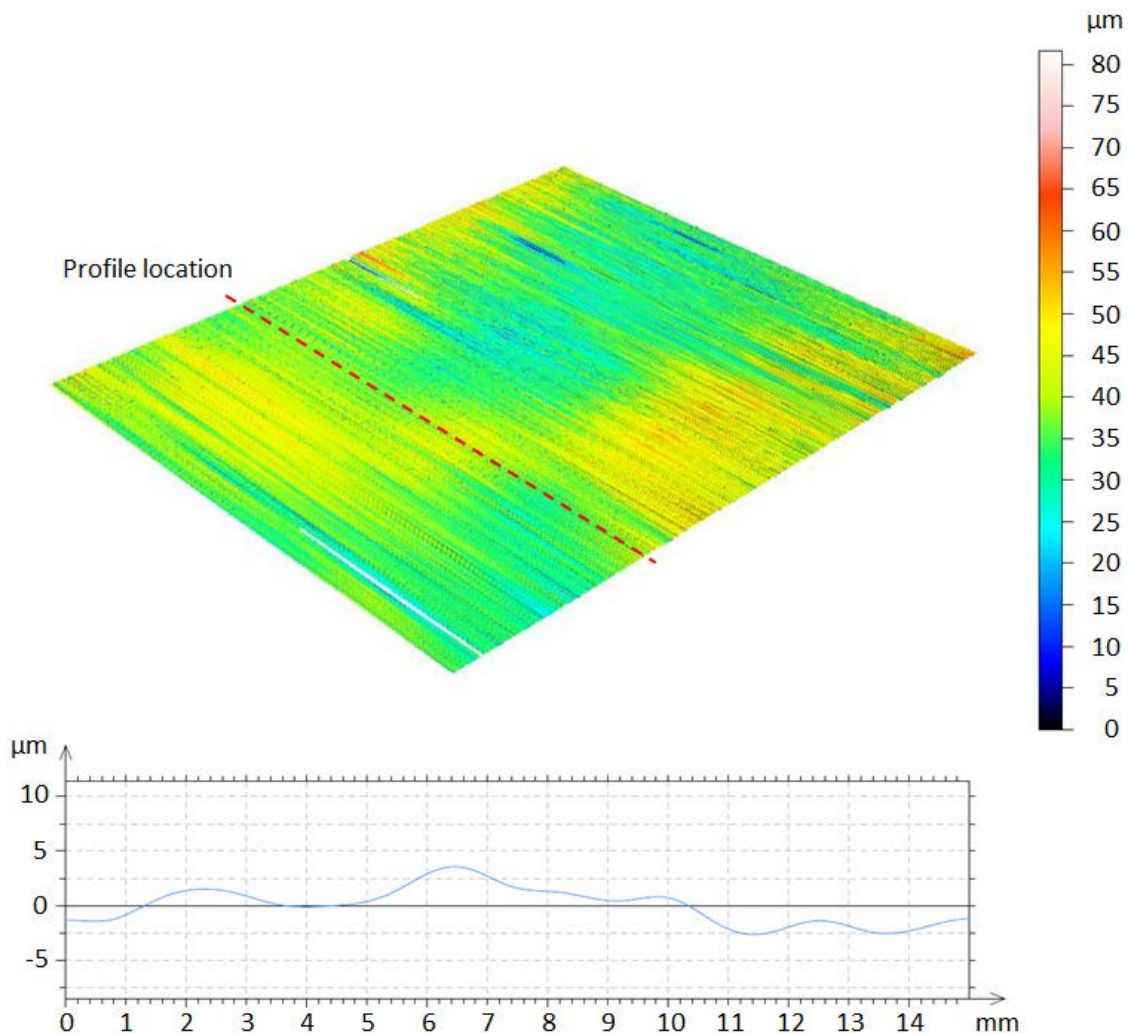
Figure 3.35.   Surface profile scan of MakerJuice SF substrate with overall sample size 15 mm x 15 mm

These results show that MakerJuice SF produces the flattest substrates with the least warping and greatest surface continuity, making it more suitable for application as an electronic substrate. When compared with substrates produced on the top-down system, the flatness is a significant improvement, with the change in surface height of 70 µm demonstrated in Section 3.1, improved to 6 µm in Section 3.2.

An Alicona InfinateFocus microscope was used to measure the surface roughness of the same MakerJuice SF substrate used previously. The Alicona microscope is an optical microscopy system that provides higher resolution measurements than laser mapping and outputs surface roughness

parameters for the quality to be accurately analysed. The measured area was 1.4 mm x 1.1 mm over which a high surface quality is shown in Figure 3.36.
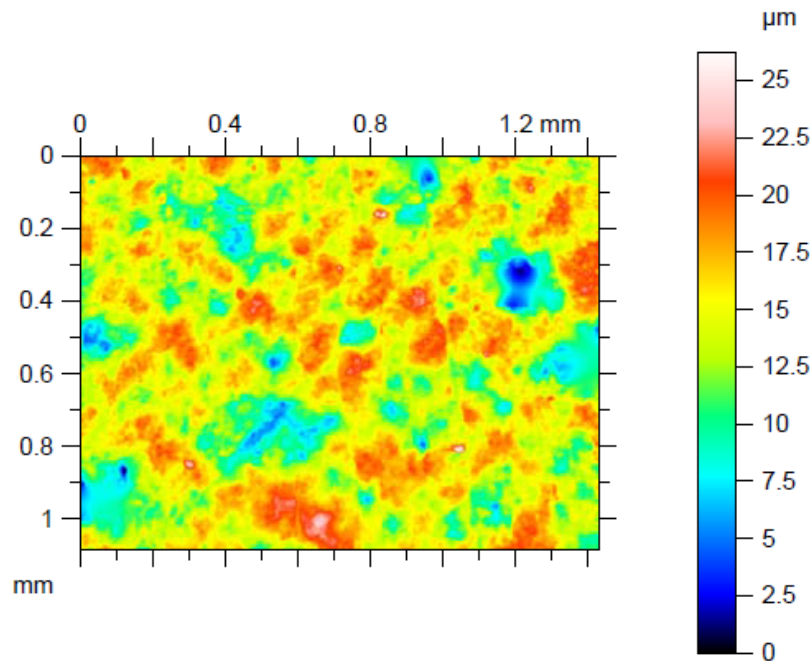
Figure 3.36.   Surface roughness of Makerjuice Labs SF resin substrate

Three surface roughness parameters were also measured by the Alicona system and are defined in ISO 25178 [187] as follows:

- S_a = The arithmetic average of absolute values.
- S_q = The root mean squared.
- S_z = Average distance between highest five peaks and lowest five valleys over entire sample surface.

These three values, especially S_z allow the surface suitability for dispensing to be determined. The surface finish can help predict the reaction of the paste as it contacts the substrate. Table 3.3 lists the surface characteristics of the substrate.

Table 3.3.   Amplitude parameters of resin wafer samples

Sample No.	Amplitude Parameters (µm)		
	S_a	S_q	S_z
1a	2.13	2.76	26.6
1b	2.53	3.2	26.2
1c	3.13	4.12	36.8
Avg. 1	2.60	3.36	29.9

A finer conductor printing resolution produced using smaller nozzle diameters, ~100 μm, requires a lower surface roughness, ensuring that dispensed filaments of material with a consistent profile can be produced without interference from unreliable substrate surfaces. S_a and S_z values in Table 3.3 show a high surface quality that would not interfere with dispensing through nozzles down to 100 μm, demonstrated in Chapter 5.

3.3 Summary

Both top-down and bottom-up Stereolithography methods were evaluated in this chapter for the suitability of fabricating electronic substrates. These substrates are required to be flat with a low roughness, to ensure that conductive material can be dispensed seamlessly onto the surface.

The top-down Stereolithography system custom-built bespoke apparatus was manufactured in-house utilising a conventional DLP projector system with altered UV LED light source. The losses sustained within the projector itself as a result of UV filtering through the various optics elements however created a low intensity output causing excessive polymerisation initiation times calculated in excess of 7 minutes. White light projection in combination with resin sensitive at wavelengths of 440 nm and below were identified as an alternative and tested to determine test specimen quality.

The deep dip recoating method and viscosity of the photopolymer caused a dome to form on the surface of the substrate due to the surface tension of the liquid. Despite the inclusion of light filters to limit the exposure wavelength and iterative exposure optimisation, substrates were all unsuitable for subsequent processing.

The iterative development of this top-down manufacturing method has demonstrated that the achievement of high quality substrates required for the production of electronics via AM methods is difficult without a high intensity dedicated single wavelength light source, an ultraviolet compatible projection platform and a recoating mechanism. The addition of one of these would remove some of the required functionality of the integrated manufacturing system.

Following the poor quality substrates produced using top-down projection, a bottom-up orientation was adopted. This process produces substrates in contact with the transparent base of the vat, therefore showing the potential to produce a flat, higher quality surface than the alternative in Section 3.1. A pre-built system was sourced and its functionality improved including the introduction of a UV pico-projection module. The optimum exposure time was then determined through iterative experimentation, slowly increasing this time period until a well resolved part with sharp edges and accurate dimensions were produced.

The bottom-up process in combination with the UV light source was characterised for the consistency of light intensity across the projection area. This in combination with an array of test specimens produced over the projection area allowed the quality of the identically designed features to be compared by their build location. The optimal build location could therefore be identified. Calculations designed to determine the resolution of the projector and therefore, of the SL process, were verified through the fabrication of samples with varying channel widths, resulting in a confirmed process resolution of ~110 µm in the x and y axes. Z-axis resolution was also confirmed to be 100 µm as specified in the control software.

Finally, non-contact profiling of substrate surfaces was conducted and results analysed for their flatness. These findings could be compared with substrates built on the top-down projection system, proving that substrates produced in Section 3.2 were superior to those in Section 3.1 with average changes in surface height of 6 µm and 70 µm respectively.

4 Mid-Process Developing of Photopolymer Substrates

This chapter will detail the methodology and experimentation conducted to find the optimum mid-processing steps. This includes analysing the type of solvents and suitable exposure time required to effectively clean the substrate without damaging the photopolymer. Substrates cannot be transferred from the Stereolithography apparatus directly into the dispensing system without first removing all the uncured resin. This is to ensure there is no contamination of subsequent processes. The first stage of investigation involves removal of excess resin from the surface of the substrate and build platform via a washing process. This is conducted in a chemical solvent and assisted with ultrasonic agitation. The second experimental stage covers post-build relaxation, baking and UV oven exposure to ensure full crosslinking of the polymer material. The sequence in which these mid-processing techniques will be conducted has been presented in Figure 4.1. This second stage is designed to provide the highest quality surface for the deposition of conductive materials by stopping the substrate from cracking or warping after processing.
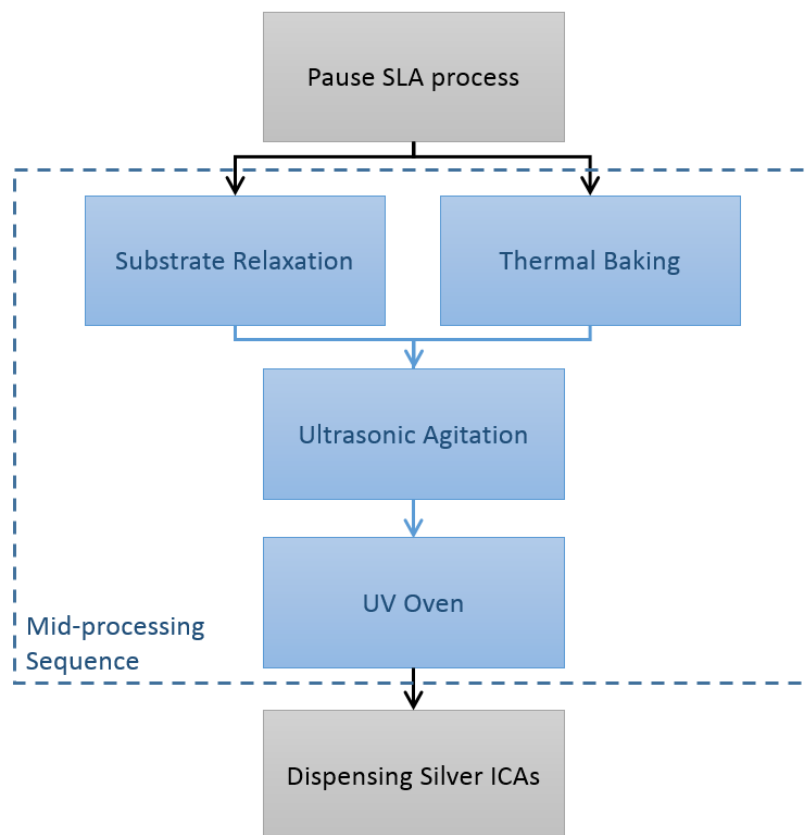
Figure 4.1.   Mid-processing sequence

4.1   Decontamination of Substrates

Solvents are used to remove any uncured resin as excess material cannot be dissolved using water. Stereolithography historically has a relatively low throughput and is also traditionally primarily used for rapid prototyping parts, the volume of parts processed is reasonably small. As a result photopolymer parts are commonly rinsed manually after removal from the vat. Immersion or rinsing using a wash bottle are the most common methods employed. Some machine vendors apply ultrasonic rinsing tanks which are more effective at cleaning out small features and enclosed geometries by means of cavitation effects.

The removal of resin and cleaning of the part requires a solvent which thins and reduces the viscosity of the resin, making it easier to remove from the part. Suitable solvents for rinsing are commonly recommended by the machine vendor but are not necessarily the best solvent to use. To-date there has been no published scientific study investigating the best solvent for rinsing SLA parts and the impact of the solvent rinse. Many solvents will start to swell, cleave and crack parts if the exposure time is too long. There are three solvents that are commonly recommended and used to clean SLA parts (acetone, isopropyl alcohol and methanol). These were tested in addition to five other potential candidates. Qualitative analysis was conducted on the effect of this range of solvents on both flat surfaces and geometric features fabricated using the photopolymer substrate.

All solvent remaining on the substrate surface must be completely dried off prior to the dispensing stage or this would both thin the epoxy and degrade the epoxy in the ICA. The most effective method for drying is the use of a high-pressure clean dry air feed. It is common to observe manual drying of parts using paper towels however this creates both scratches on the surface of the parts and can result in fibres from the paper tissue breaking off and adhering to the surface of the substrate, causing unwanted contamination. As the parts in this process are to be used to produce electronic devices, pressure air drying was only conducted.

Finally, to ensure the fully cleaned 'green' part is completely cured it is placed in an ultraviolet curing oven. Parts are positioned on a turntable to irradiate the sample equally for a predetermined period of time. It is essential that all excess resin has been removed prior to this stage. If the liquid photopolymer is not completely removed from features on the surface including channels, resin remaining in the channels would be polymerised by either post-processing UV exposure or exposure to environmental UV radiation, resulting in a lack of feature resolution.

4.1.1 Solvent Selection for Mid-Processing

Most solvents can be separated into one of three categories; 1) polar protic, 2) polar aprotic, or 3) non-polar. This categorisation can affect their instability and reactivity. Non-polar solvents such as cyclohexane and toluene are typically more aggressive as they require a lower activation energy to reach a transition state [188]. In addition, hydrocarbon solvents such as these can be graded by their Kauri-Butanol value, with a higher value indicating a more aggressive solvent.

The solvent application in Stereolithography post-process rinsing requires close contact and handling by users. As such it is necessary that solvents do not present any significant health and safety hazards to humans and the environment. Pharmaceutical company Pfizer developed the solvent selection guide shown in Figure 4.2 [189] based on three categories, worker safety, process safety and, environmental and regulatory considerations.

Preferred	Usable	Undesirable
Water	Cyclohexane	Pentane
Acetone	Heptane	Hexane(s)
Ethanol	Toluene	Di-isopropyl ether
2-Propanol	Methylcyclohexane	Diethyl ether
1-Propanol	Methyl *t*-butyl ether	Dichloromethane
Ethyl acetate	Isooctane	Dichloroethane
Isopropyl acetate	Acetonitrile	Chloroform
Methanol	2-MethylTHF	Dimethyl formamide
Methyl ethyl ketone	Tetrahydrofuran	*N*-Methylpyrrolidinone
1-Butanol	Xylenes	Pyridine
t-Butanol	Dimethyl sulfoxide	Dimethyl acetate
	Acetic acid	Dioxane
	Ethylene glycol	Dimethoxyethane
		Benzene
		Carbon tetrachloride

Figure 4.2.   Pfizer solvent selection guide for medicinal chemistry [189]

Worker safety analyses potential dangers to the user including carcinogenicity, mutagenicity, reprotoxicity and skin absorption. Process safety examines physical property dangers such as flammability, static charge and potential for high emissions through high vapour pressure. Finally, environmental considerations encompass ecotoxicity, photo reactive potential and ozone depletion potential among others [190]. In addition, the American Chemical Society Pharmaceutical Roundtable composed a list of 'green solvents' based on information about their health and safety characteristics during use as well as issues associated with its interaction with the environment including air, water and as waste [191]. These five characteristics have been graded between 1 and 10, with 10 being highly dangerous, and coloured green, brown and red to denote the degree of danger on a scale of safe, potentially harmful and highly dangerous respectively.

Table 4.1 lists the eight solvents chosen for investigation. Highly dangerous or polluting materials were avoided with green and brown rated solvents graded no higher than 5 for safe use and 6 for disposal chosen. Isopropanol [192], Methanol [193] and Acetone [194] were chosen as they are all commonly recommended by photopolymer vendors for use with their materials and machines. D-Limonene has developed an increasing application in cleaning parts made during fused filament fabrication with polystyrene supports [195]. It has also been used as a paint stripper, to dissolve and remove oil from machine parts and, to remove unpolymerised material from flexographic printing plates after developing [196]. The final four candidates were selected from the list of green solvents and included alcohol (Ethanol), aromatic (Toluene and Xylene) and ester solvents (Tetrahydrofuran).

Table 4.1.   Solvents selected by rating /10 on safety of use and impact of waste

	Name	Safety of Use	Impact of Waste
1	Isopropanol	5	6
2	Methanol	3	6
3	Acetone	4	5
4	D-Limonene	-	-
5	Xylenes	4	3
6	Ethanol	4	6
7	Toluene	5	2
8	Tetrahydrofuran	5	5

D-Limonene was not included in the list of 'green solvents' summarised in Table 4.1 however, work has been conducted proving that the solvent has demonstrated low toxicity in humans after repeated exposure up to a year and even post-ingestion [197], demonstrating its suitability for safe use. It has been shown that rather than dissolving, some cross-linked polymers absorb a volume of the solvent, causing a swelling effect in the polymer [198]. The severity of the swelling is a representation of two forces, free energy of mixing causing the solvent penetration and elastic retractive forces opposing the distortion. Once balanced, the solvent absorption ceases. Parts produced from the MakerJuice SF resin will be analysed for the occurrence of this behaviour, and if present, a solution will be discussed.

4.1.2   Ultrasonic Agitation

This hybrid additive manufacturing approach to the fabrication of electronic circuitry will require the capability to produce high quality surfaces in addition to decontaminated channels and holes in its

adaptation for flip chip packaging and for its application in technologies such as microfluidics. As a result, the function of the ultrasonic agitation process is to thin and remove any excess liquid photopolymer from the surface and related features. Figure 4.3 shows the effect of ultrasonic agitation for the creation of acoustic standing waves and the resultant induced vortices, often referred to as Rayleigh flow. This mechanism provides the required agitation to cause the solvent to flow even in narrow, high aspect ratio channels [97]. These forces have also been used in unrelated applications including the filling of high aspect ratio via holes in PCBs [199].
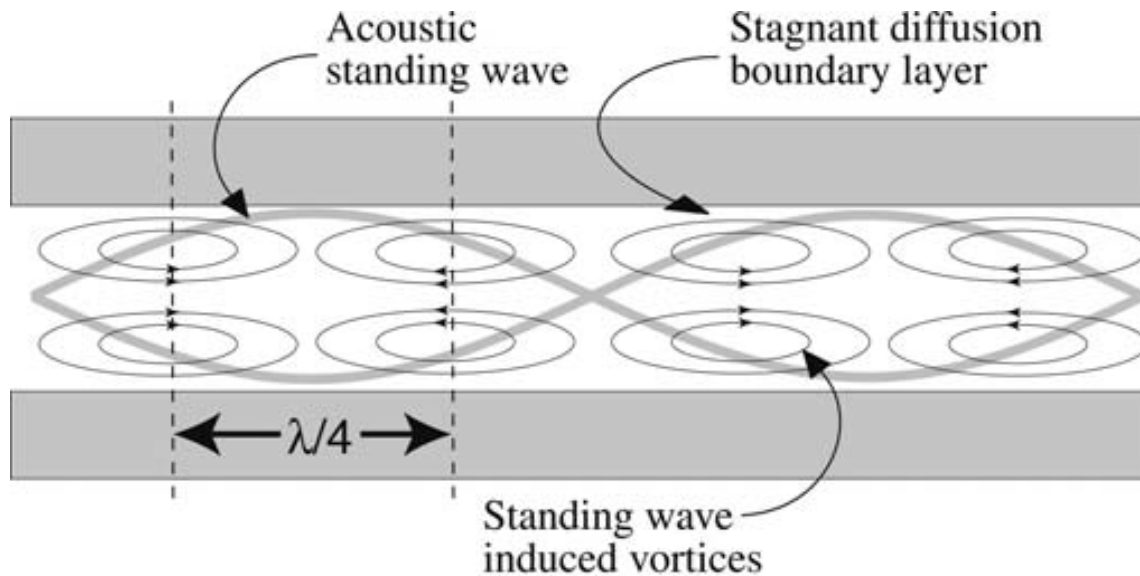
Figure 4.3.   Diagram of acoustic standing wave field and induced vortices [97]

In addition to the turbulence created by acoustic flow, ultrasonic agitation initiates cavitation as a result of the rapid transfer of potential energy to kinetic energy in a very small volume. Thus a large energy concentration is released in the form of pressure and temperature [200].

It is the collapse of bubbles created through ultrasonic agitation that provide its functional significance. As demonstrated in Figure 4.4, at the point when the bubble can no longer sustain its size, it collapses. During the collapse it is estimated that temperatures of 5000 °C and pressures of 2000 atmospheres are created, however, due to the bubble's relative size to the volume of liquid, the temperature is dissipated at an estimated 10 billion°C/s, leaving no lasting impact on the environmental conditions [201].
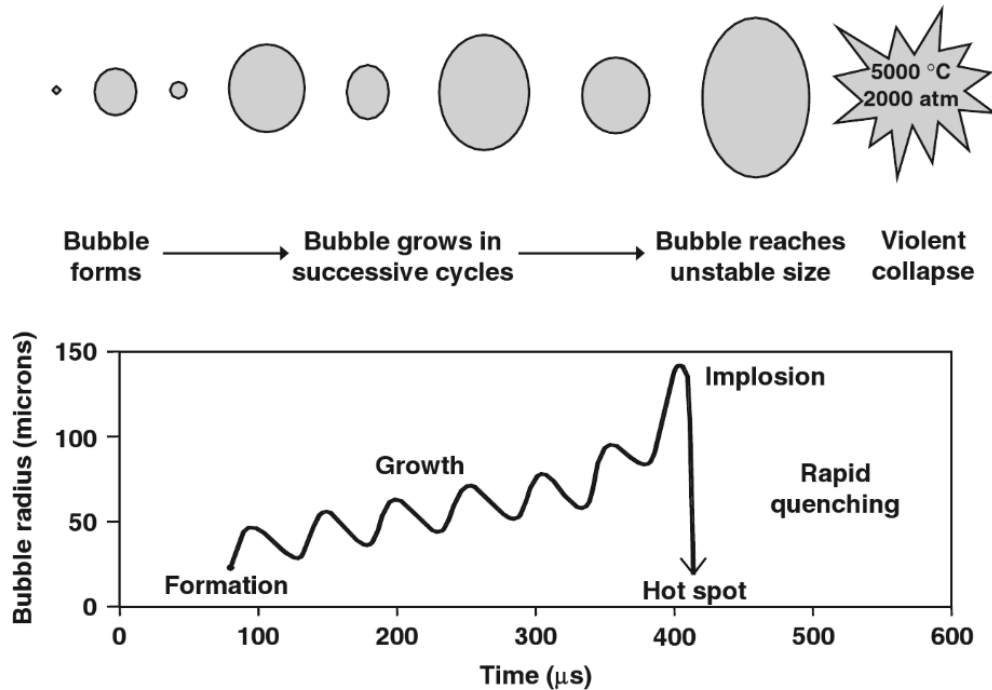
Figure 4.4.   Two representations of the development and collapse of cavitation bubbles [202][203]

The characteristics of cavitation change at different proximities to solid surfaces. At a distance, the cavities or bubbles retain their spherical shape until collapse however, in proximity to a solid surface, collapse is asymmetric and produces turbulence caused by high speed jets of liquid reaching close to 400 km/h that directly impact the surface, therefore creating the cleaning mechanism [204].

Attempts to model ultrasonic systems have provided conflicting data regarding the pressure and temperature created by the collapse of bubbles during the application of sonochemistry. Prasad Naidu *et al.* [205] suggested a final pressure of 78 atmospheres and temperature of 2064 K using model simulations. However, despite these differences in scale, their primary function and its effectiveness is agreed.

Liquid monomers and short polymer chains show a degradation and reduction in viscosity when exposed to cavitation, as a result of van der Waals bonds holding polymer chains together being broken [202]. This proves its potential for use in the removal of excess volumes of liquid photopolymer from the substrate. Ultrasonic agitation has also been shown to initiate and accelerate reactions such as polymerisation and co-polymerisation, as well as changing the reaction pathway in biological, chemical and electrochemical systems [98].

4.1.3   Immersion vs assisted Ultrasonic Agitation immersion

Methods involving immersion or rinsing using a wash bottle lack the capability to penetrate deeply into fabricated features, resulting in dimensional errors and the potential for process contamination.

As explained in Section 4.1.2, the cavitation effect via ultrasonic agitation is a favourable characteristic for the penetration and decontamination of cavities and channels presented for geometrically complex packaging and flip-chip packaging in Chapter 6.

The cleansing of a substrate surface can also be conducted using ultrasonic agitation however, the effects of the cavitation process can be seen as ripple patterns are visible on the surface. A short investigation was conducted to measure and observe the difference between substrates washed using both methods. Figure 4.5 compares substrates washed both using IPA but one is just immersed for 2 minutes and then dried using a standard laboratory blue paper towel versus 2 minutes of ultrasonic agitation and high pressure air drying, more detailed process parameters are detailed in Table 4.2.

Table 4.2.   Table showing process parameters for samples shown in Figure 4.5

	Sample a)	Sample b)
Layer thickness	100 µm	100 µm
Exposure time per layer	12 seconds	12 seconds
Washing method	Ultrasonic agitation	Submersion in solvent
Drying Method	High pressure air	Paper cloth
Solvent	IPA	IPA
Washing duration	2 minutes	2 minutes

The ripple effect can be seen covering the surface of the ultrasonically agitated sample however it is not present on the other. The alternative surface was wiped with a paper cloth soaked in IPA, a process that resulted in the presence of small scratches on the surface with a rougher appearance, shown in Figure 4.5b.

a) Ultrasonic Agitation   A   x500   200 µm   b) Hand Washing   A   x500   200 µm
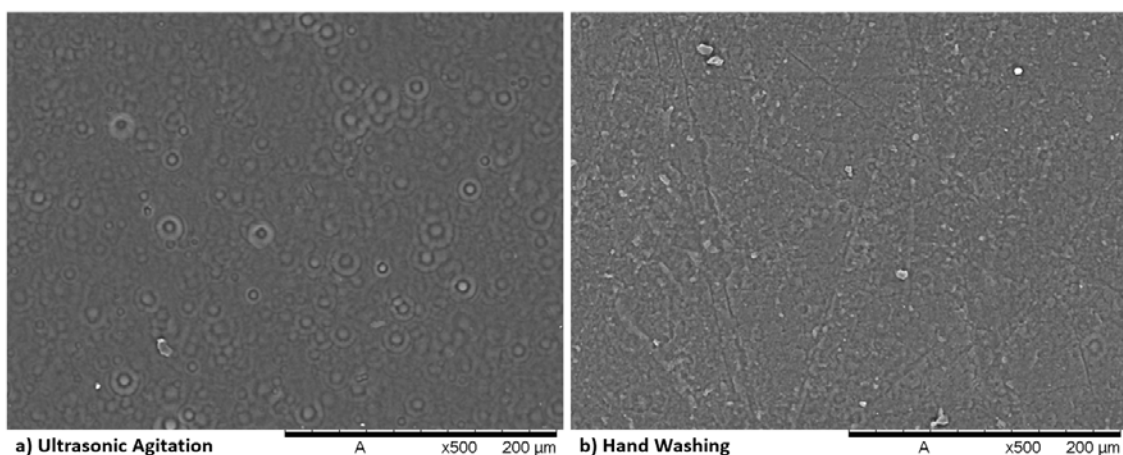
Figure 4.5.   Surface of a) ultrasonically agitated and b) hand washed substrates

Despite the differing appearance of substrates cleaned using different methods, their surface properties are very similar. Values of arithmetic surface average (S_a) measured using the Alicona InfiniteFocus microscope across six samples were 2.32 µm and 3.00 µm for hand washing and agitation respectively.

4.2 Investigating Solvent Compatibility with Photopolymers

Although solvents may clean the surface of uncured resin it is essential that the substrate is not damaged during this process, potentially causing issues during dispensing and sacrificing the quality and functionality of the final part. The interaction between the solvent and photopolymer can vary dependant on the chemical composition and characteristics of the chosen solvent. To select the optimal solvent an experiment was designed to assess the effect of eight different solvents on a cured photopolymer sample over a range of exposure times, the selection of which have been detailed in Section 4.1.1.

The test artefact in Figure 4.6 was designed in Siemens NX 7.5 CAD software with features that allow both quantitative and qualitative analysis to be conducted on the reaction of the cured photopolymer to both the solvent and the time of exposure. The design includes a flat surface to allow both the measurement of surface roughness and magnified imaging and, channels and ridges that can be observed under a Hitachi Tabletop TM3030 Scanning Electron Microscope (SEM) to capture any degradation of sharp edges, the points at which the contact area between substrate and solvent is at its greatest.
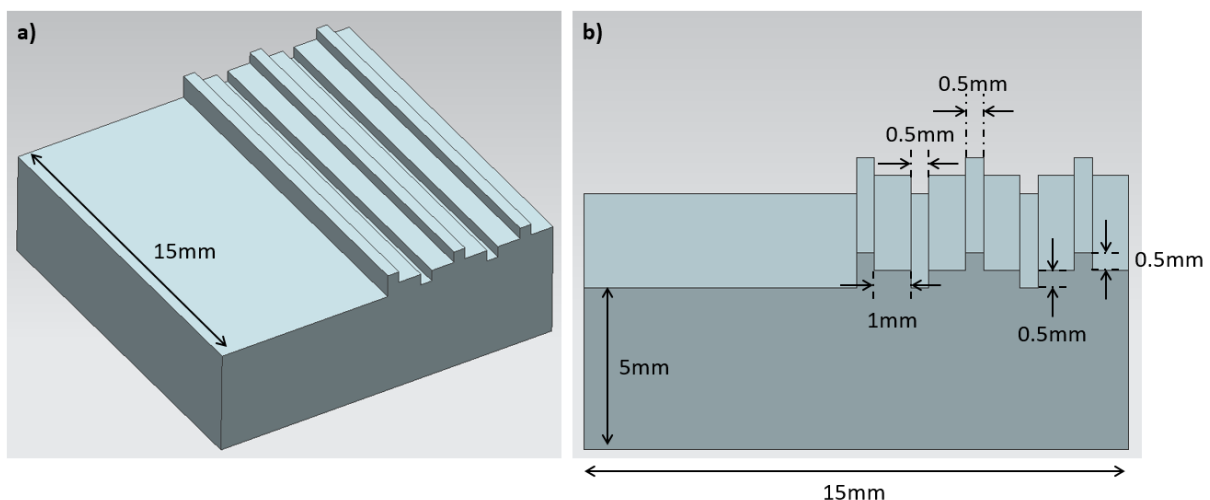
Figure 4.6.   Solvent exposure test artefact a) projection view and b) tilted side view

The eight solvents were tested over 5 minutes, 30 minutes, 2 hours and 24 hours exposure time periods with the 30 minute exposures conducted twice to determine the repeatability of the results. To eliminate the effect of the specimen fabrication conditions on the observed reaction, parts were

produced in batches of nine samples in a 3 x 3 grid on the build platform. Each batch was split between the eight solvents along with one control group, ensuring that only one sample from each batch was exposed to each solvent. The distribution of samples based on the fabrication position in the 3 x 3 grid was also randomised across solvents. These two mechanisms ensure that the effect of any build defects or printer variation can be eliminated from this investigation.

Samples were fabricated using the bespoke bottom-up DLP Stereolithography system before removal immediately after the build process was complete. These samples were then ultrasonically agitated in Isopropanol for 1 minute to clear excess resin from the features, removed and dried using a high pressure air supply. The samples were then placed into empty 50 mL beakers which were subsequently filled with 40ml of solvent. The beakers were covered with parafilm to prevent solvent evaporation over the 24 hours of experimentation. Each sample was removed at its predetermined time interval, excess solvent removed, the surface dried using a pressurised nitrogen source and the entire sample left to dry.

4.2.1   Change in Mass of Photopolymer Specimens

The weight of each set of 5 specimens for each solvent was recorded individually using a Kern PLS 720-3A Electronic Weighing Scale with 0.001 g resolution, immediately before submersion in solvent. The weight was then measured again immediately after exposure and surface drying and, a third time one day later. The change in mass during the exposure to solvent and after 24 hours drying time has been presented in Figure 4.7. All parts showed less than a 0.008 g change in mass over exposure times up to 2 hours in duration, with an average specimen mass of 1.250 g, this is just a 0.006% difference. After a 24 hour period, 5 samples showed an increase in mass, expected to have been caused by solvent swelling, a phenomenon whereby the cured photopolymer absorbs solvent causing geometric distortion and the appearance of swelling. Results suggest that immersion for more than two hours is necessary for the absorption of solvents to begin. Three solvents did not display the increase in mass associated with solvent absorption, with IPA and D-Limonene showing minimal change while Acetone reduced the mass by 0.027 g or 0.02%.
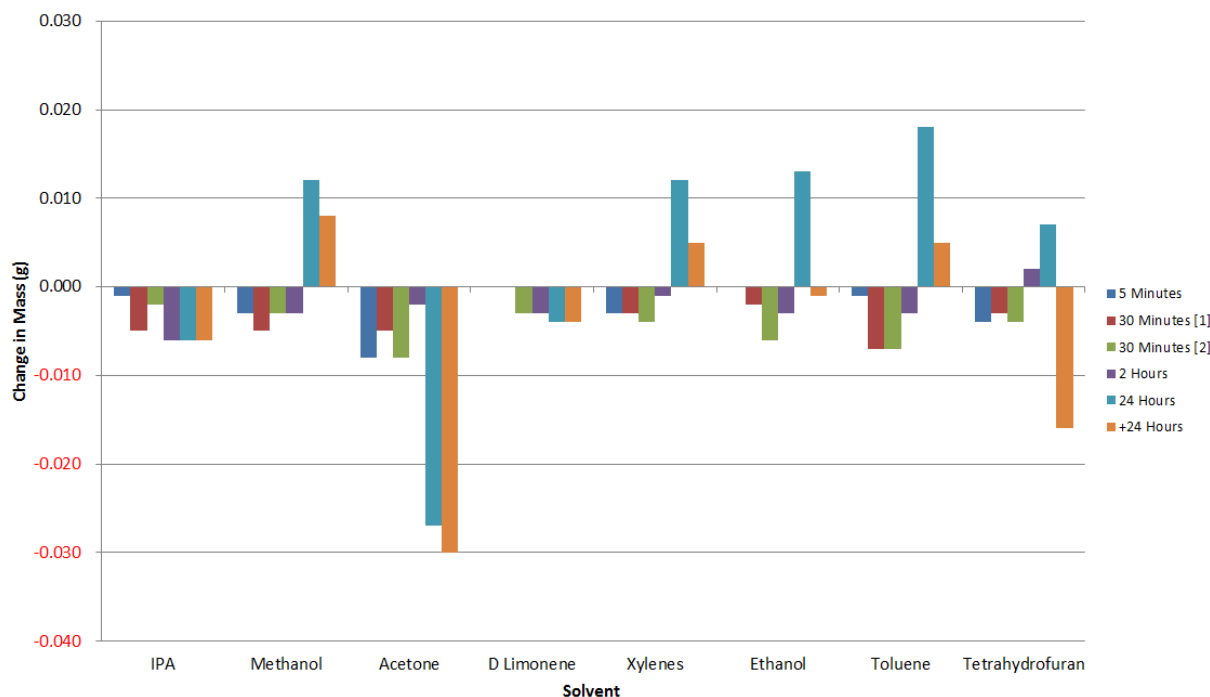
Figure 4.7.   Change in mass of photopolymer specimen during exposure to solvent

The reduction in the weight of the sample immersed in Acetone is a result of the degradation of the sample, characterised by the disintegration of parts of both the surface and ridge features after 24 hours. The same behaviour was observed on the sample immersed in Tetrahydrofuran for 24 hours however, the specimen mass was greater after exposure. This is a result of the weight of solvent absorbed being greater than the material lost.

A further 24 hours of rest after removal from the solvent is shown by the +24 Hour bar in Figure 4.7. Samples saw a widespread reduction in mass with the exception of IPA and D-Limonene which remained constant. This reduction was a result of evaporation of absorbed solvent from the specimens, Tetrahydrofuran specifically saw a decrease in mass of 0.023 g over that day, showing a lower mass than its initial measurement and a manifestation of the removed material.

IPA and D-Limonene demonstrated the least fluctuation in mass and showed a very predictable interaction and behaviour. This would indicate that they are favourable for use in this mid-processing stage. Although the changes in mass measured during this investigation were no greater than 0.03%, this is not an accurate representation of the effect of some solvents on the photopolymer substrates. This will be depicted by SEM images in Section 4.2.2.

4.2.2   Scanning Electron Microscopy of Exposure Samples

Samples exposed to eight solvents for four different time periods were coated in an angstroms thick layer of gold/palladium alloy and examined under a Hitachi TM3030 Desktop SEM. Small features

can be viewed in high resolution and highly magnified images of the surface will allow its quality to be assessed. Exposure of cured photopolymer samples to solvents resulted in observed cracking in a range of severities dependant on the choice of solvent. Control samples that were only ultrasonically agitated in IPA for 1 minute also presented these surface defects although, at the time of submersion into the eight solvents, no surface cracking was present on any specimen. This suggests that all cracking of different severities is a result of the solvent exposure, with that seen on the control samples in Figure 4.8 only appearing 3 to 4 hours after other specimens were submerged.
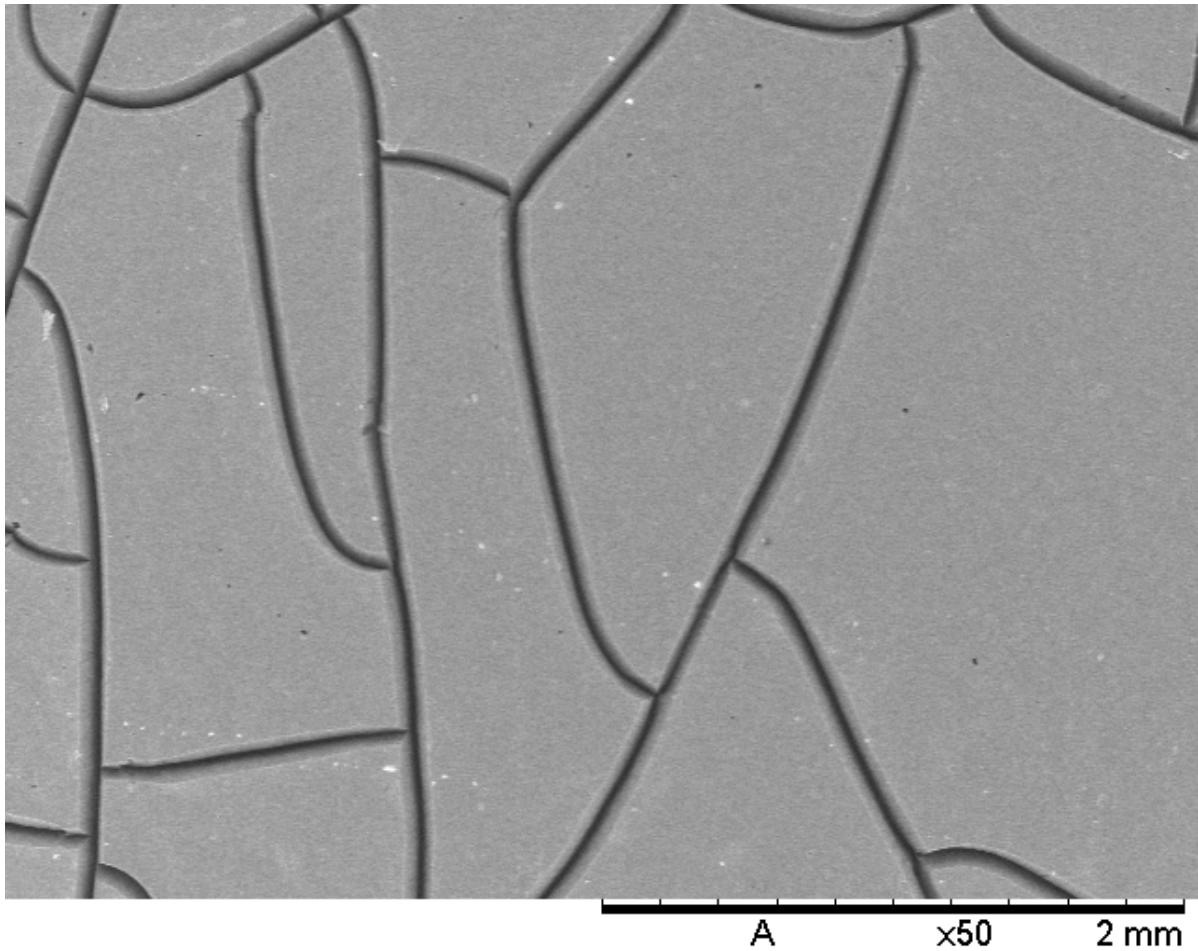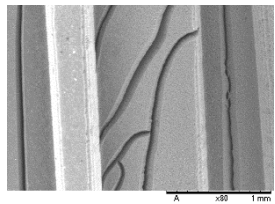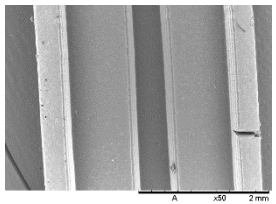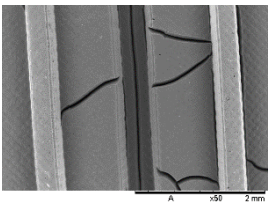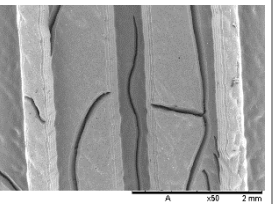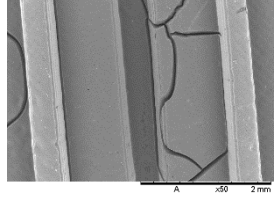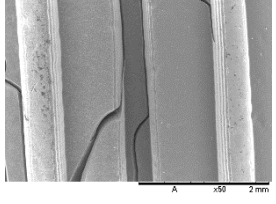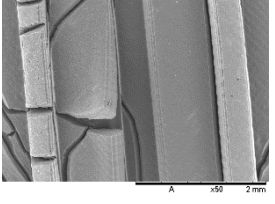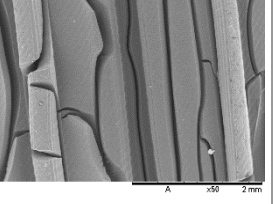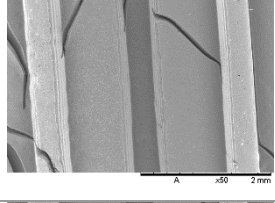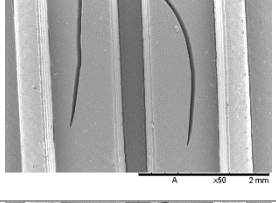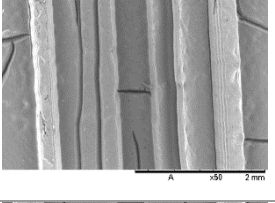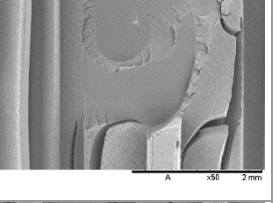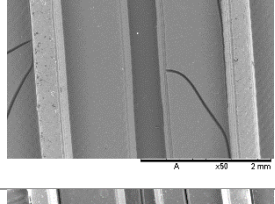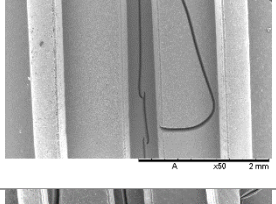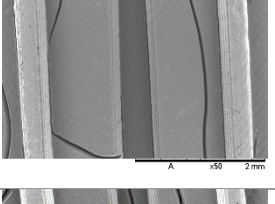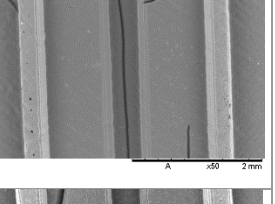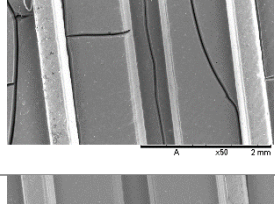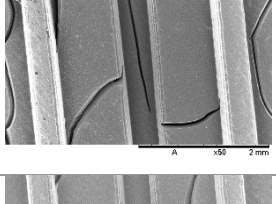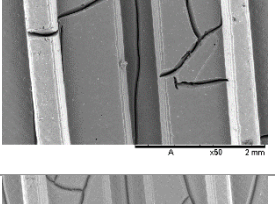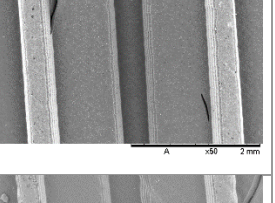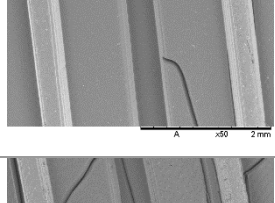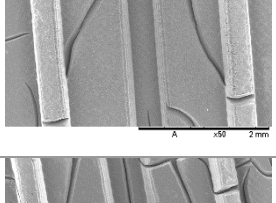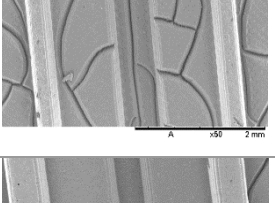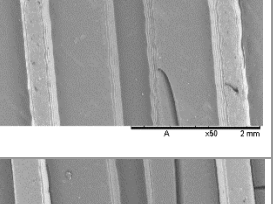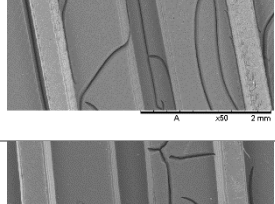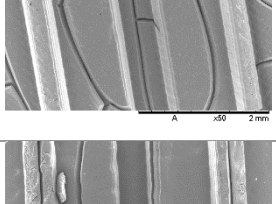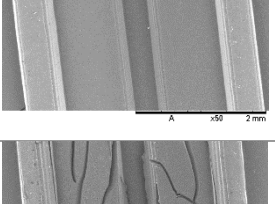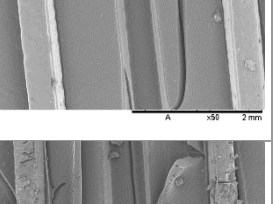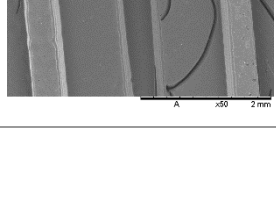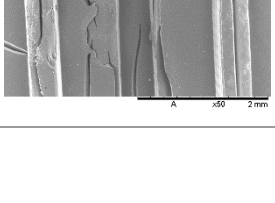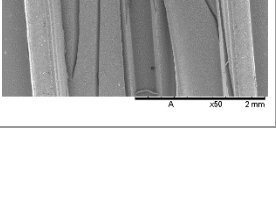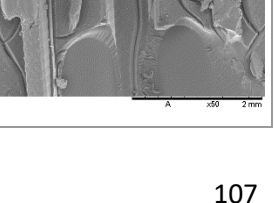
Figure 4.8.   Surface cracking on photopolymer control substrate

 Table 4.3 shows SEM images of all samples tested during this investigation providing a comparison between all solvents and exposure times to those solvents.

Table 4.3.   SEM images of samples exposed to different solvents over four time periods

	5 Minutes	30 Minutes	2 Hours	24 Hours
IPA				
Methanol				
Acetone				
D-Limonene				
Xylene				
Toluene				
Ethanol				
THF				

Both Acetone and Tetrahydrofuran dramatically degraded the surface and ridge features on the specimen as shown in Figure 4.9. This has the appearance of delamination in samples exposed for 30 minutes and 2 hours.
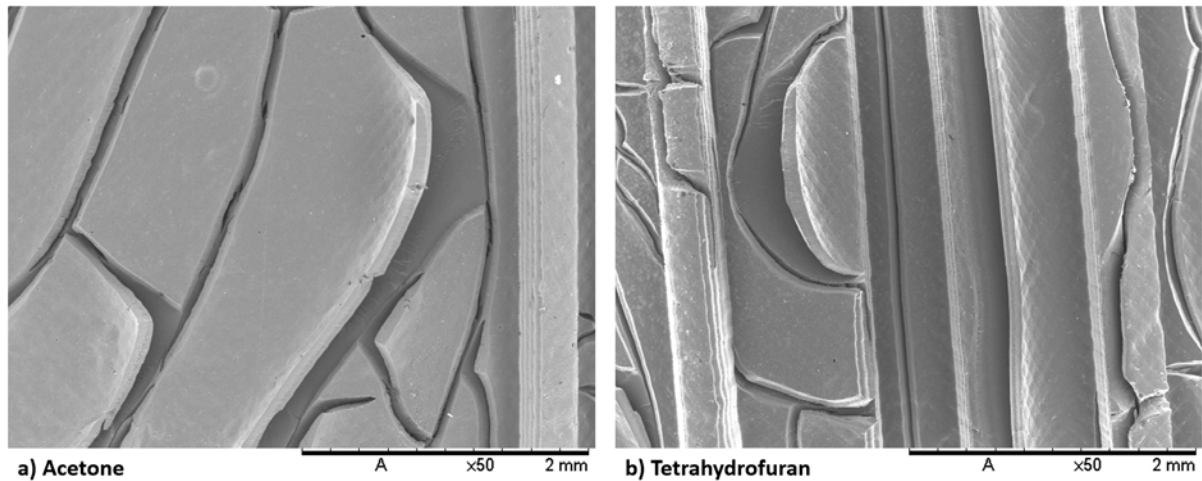
Figure 4.9.   SEM images of samples exposed to a) Acetone and b) Tetrahydrofuran for 30 minutes

After 24 hours this delamination escalated to disintegration of the samples, with the features observed to be bending in Figure 4.9 becoming fully detached from the substrate resulting in the flat surfaces and damaged features in Figure 4.10.
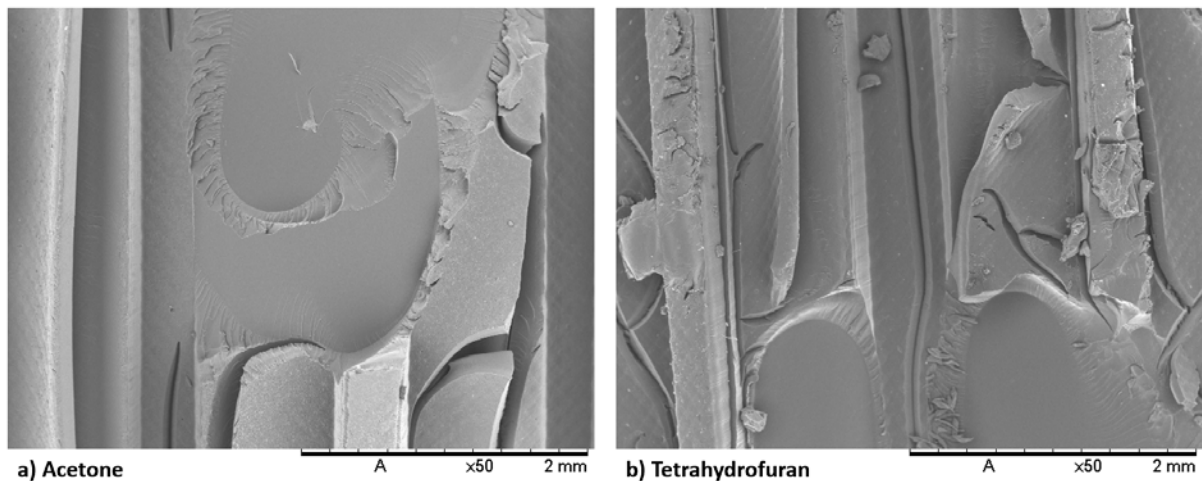
Figure 4.10.   SEM images of samples exposed to a) Acetone and b) Tetrahydrofuran for 24 hours

With such dramatic damage after such a short period of time both Acetone and Tetrahydrofuran were discounted from investigation. Less severe damage was also caused by Methanol, Ethanol and Toluene, all of which showed enhanced cracking propagation on the surface. Raised fragments of photopolymer were apparent, comparable to that in Figure 4.9, without the eventual removal of material. Three solvents, IPA, D-Limonene and Xylenes all produced fissures on the surface, however, no material had lifted from the part. Closer inspection of the channel and ridge features showed

layering resulting from the additive manufacturing process, the definition of this layering can help determine the degree of degradation of these surfaces by the solvent. Features exposed to these three solvents over all time periods still maintained good layer definition on the channel and ridge features as shown in Figure 4.11.
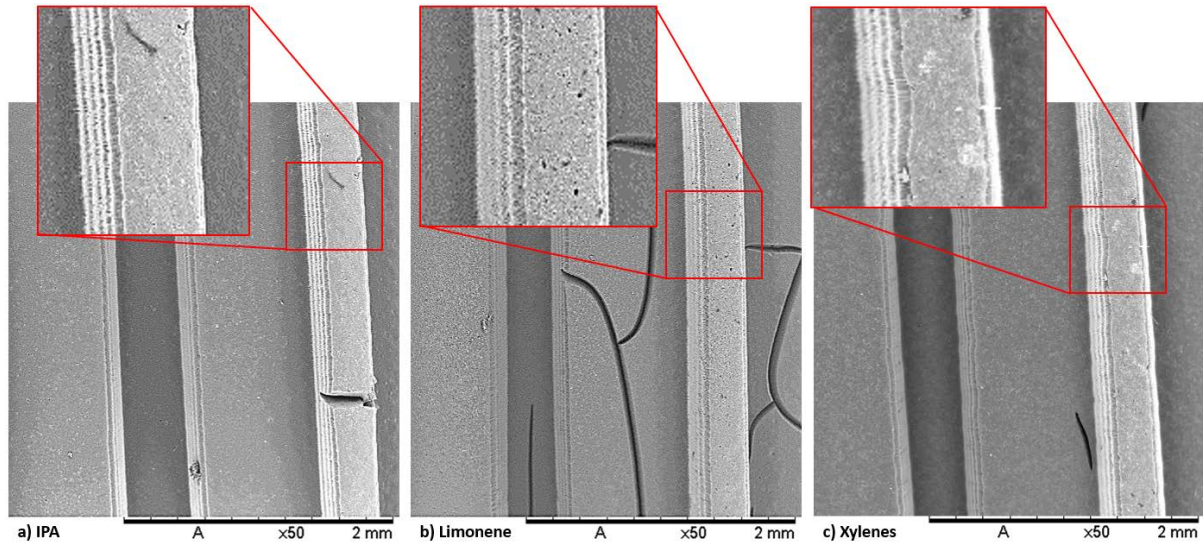
Figure 4.11.   SEM images of samples exposed to a) IPA, b) D-Limonene and c) Xylene for 30 minutes

The solvent in these cases had cleaned the surface but not degraded the photopolymer material, making them suitable for combination with the ultrasonic agitation process. The detail of each 100 µm layer can be seen in Figure 4.11. Xylene has caused minor erosion of the edges of both feature types, resulting in the appearance of a wavy edge. The same effect has been observed at the end of the channels creating small radii on previously sharp edges in x, y and z axes. Figure 4.12 shows that the same phenomenon has not occurred in IPA and D-Limonene samples as layer definition is still visible in these locations.
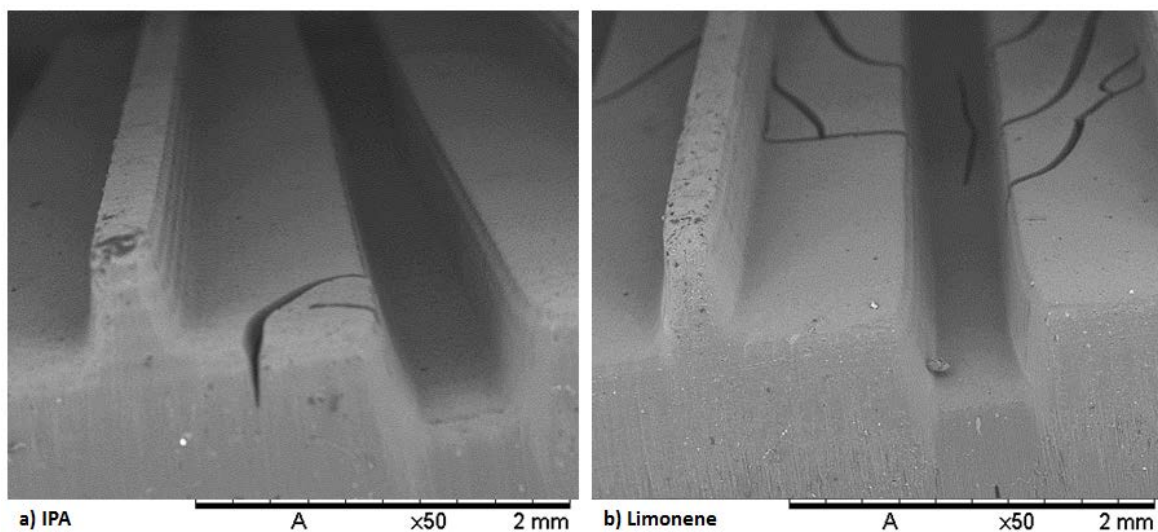
Figure 4.12.   SEM images of samples exposed to a) IPA and b) D-Limonene for 30 minutes

After examination, IPA and D-Limonene have both proven to be suitable for the washing of photopolymers. Both long and short exposure periods in both solvents have caused no measurable or observable damage to the substrate, ensuring that complex geometries can be created and decontaminated without sacrificing accuracy and quality. The cracking of the top surfaces of these substrates has occurred on every sample and it was therefore concluded that this was caused by a characteristic of the fabrication process itself and investigation aiming to reduce the cracking has been presented in Section 4.3.

4.2.3   Surface Analysis of Exposed Substrates

It is essential that a high quality surface finish is achieved on the substrate to prepare it for the process of conductor deposition. Images were taken on the SEM at 400x magnification to capture any defects in the substrate surface as a result of the solvent exposure. Other than the cracking already observed, Figure 4.13 shows that there are no other significant defects in the surface with the exception of small ripple features that are a result of the cavitation effect of ultrasonic agitation.
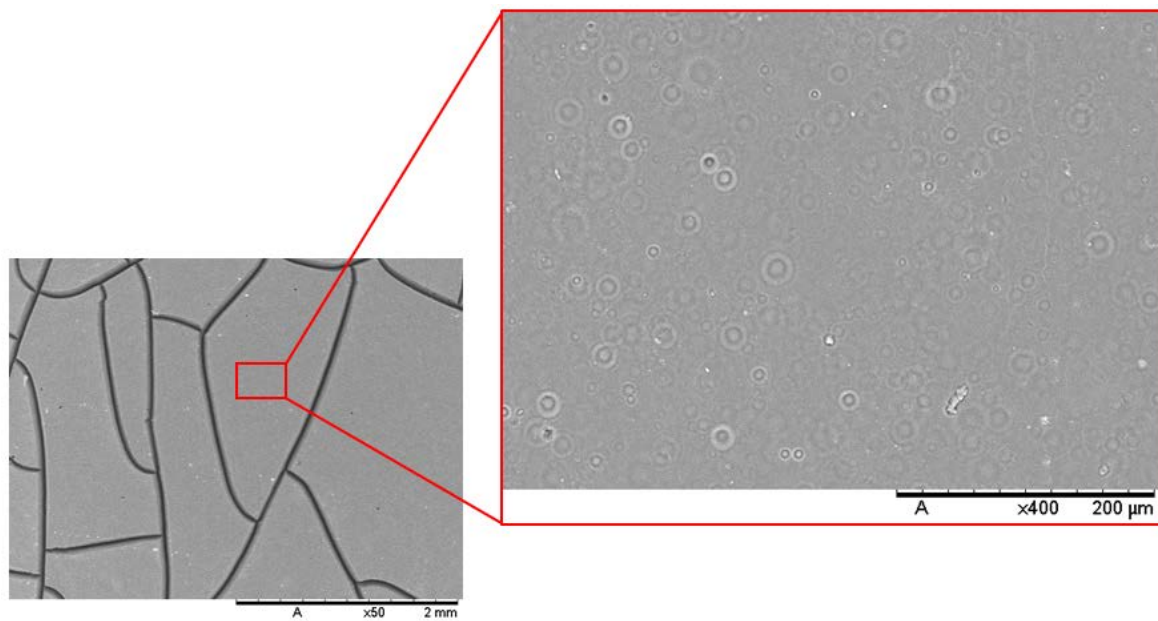
Figure 4.13.   SEM image of sample surface exposed to Acetone for 30 minutes

The effect of this cavitation on the surface roughness can be measured using the Alicona microscopy system by taking the scan of the substrate profile in Figure 4.14. The arithmetical mean height of the surface (S_a) was extracted from the profile data as a quantitative value for the surface roughness. The collection of these values was hindered by the surface cracking however, by selecting 700 µm x 550 µm areas between cracks the post-exposure topology could be examined.

ISO 25178		
Height Parameters		
Sq	1.49	µm
Sp	6.86	µm
Sv	8.13	µm
Sz	15	µm
Sa	1.18	µm

Sq – Root mean square height of the surface
Sp – Maximum height of peaks
Sv – Maximum height of valleys
Sz – Maximum Height of Surface
Sa – Arithmetical mean height of the surface
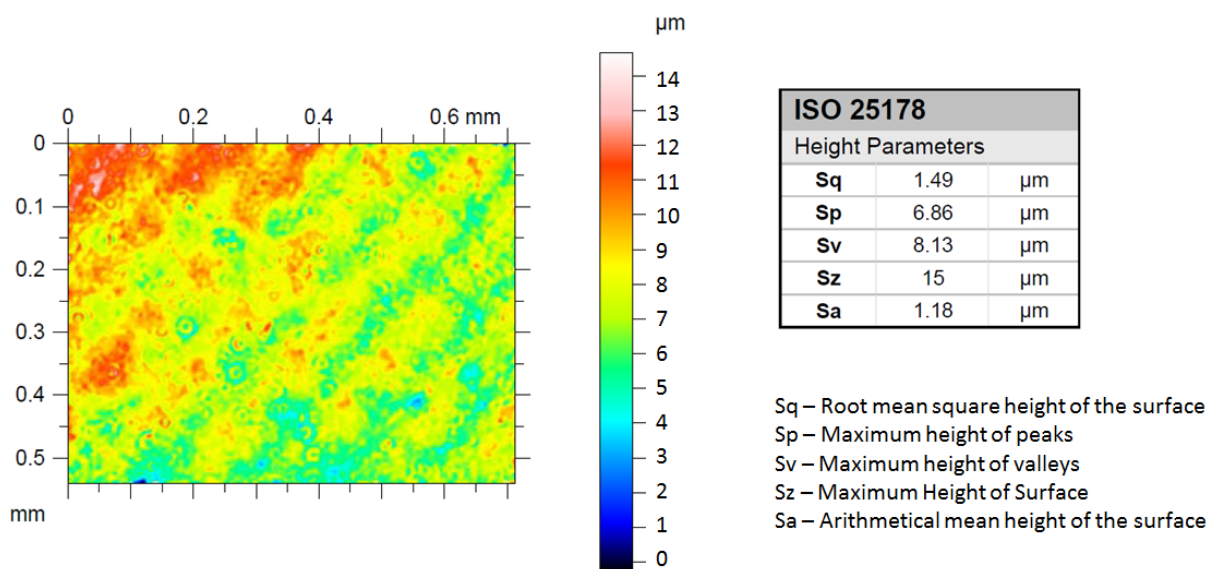
Figure 4.14.   Measured topology of photopolymer surface exposed to D-Limonene for 5 minutes

There was also no observed correlation between exposure time and surface roughness across the entire set of data, showing that the smaller contact area between solvent and sample resulted in the reduction of surface damage compared to the visual observations described in Section 4.2.2.

Two measurements were taken from each sample equating to 10 measurements for each solvent. Measurements taken from the 5 control samples showed S_a values ranging from 1.7 µm to 4.8 µm, an average of 2.84 µm with standard error of 11.51%. IPA, Methanol and D-Limonene samples had standard errors of 0.0785 µm, 0.1030 µm and 0.1264 µm respectively, the lowest among all eight solvents, with standard errors of each measurement calculated by dividing the standard deviation by the root of the number of samples to determine the standard deviation of the sampling distribution of the statistic [206]. The standard error was chosen as it estimates the variation between the sample mean and the mean of a larger population of data. Due to the capability to only sample 5 times this provides a method by which the mean can be extrapolated to a larger number of samples while accounting for the potential variation in the mean resulting from the inclusion of more data. The same statistical analysis has been utilised throughout this thesis to predict the potential variation of the mean as opposed to the deviation of individual samples from the mean.

As there was no consistent relationship across all solvents between exposure time and roughness, time was discounted and the solvent was compared directly to its resulting substrate roughness. This is due in a large part to the degradation presenting in the form of cleaving and cracking and not the actual dissolution of the surface. Roughness average values of all exposure times for individual solvents shown in Table 4.4 corroborate the findings in Section 4.2.2 with IPA and D-Limonene demonstrating the two lowest values.

Table 4.4.   Roughness averages of samples exposed to different solvents

Solvent	Average S_a (µm)	Standard Error (µm)
IPA	2.569	0.0785
Methanol	4.296	0.1030
Acetone	3.727	0.1581
D-Limonene	2.202	0.1264
Xylenes	3.111	0.1807
Ethanol	2.978	0.1687
Toluene	3.538	0.1733
Tetrahydrofuran	7.612	0.3406

On closer analysis of D-Limonene individually, the surface roughness is shown to increase with exposure time, with an approximate increase of 80% from 2 µm to 3.6 µm between 2 hour and 24 hour samples. This is further validated by the average maximum peak heights and valley depths (S_z) which are significantly lower than any alternative between 5 minutes and 2 hours. This was the only solvent demonstrating these responses therefore making it one of the most suitable for mid-processing alongside IPA to create a high quality surface. Further experimentation can therefore be conducted with IPA and D-Limonene to determine firstly, which of the two solvents results in the least crack propagation and secondly, what development techniques can be used to the same effect.

The use of Stereolithography to produce reactors for flow chemistry applications has previously required the examination of photopolymer compatibility with solvents. Epoxy resin specimens were exposed to a number of common organic solvents for 30 minute, 60 minute and 24 hour time periods and the change in weight measured to quantify degradation. Dichloromethane, tetrahydrofuran and methanol all produced a high degree of degradation while ethyl acetate, butanol, isopropanol and diethyl ether had a lesser effect. Increases in weight over the 24 hour exposure period were also exhibited, alongside the photopolymer deterioration during exposure [207]. This corroborated the findings of the experimentation discussed during this section showing photopolymers to be chemically unstable and susceptible to swelling and degradation whether epoxy or acrylate based formulations [208].

4.3 Substrate Surface Development

During traditional electronics manufacturing, development refers to the removal of photoresist material by a solvent or solution. This occurs after the photoresist material has been selectively

exposed to ultraviolet light using a mask to produce the necessary features. Positive photoresists become soluble on exposure to light while negative photoresists do the opposite. The resulting insolubility of negative photoresist materials is caused by the ultraviolet initiation of polymer cross-linking in the material. This polymerisation process requires the photoresist to be rested after exposure to ultraviolet light and before development, ensuring that cross-linking of the polymer has finished. This process is initiated by the light source but continues in the irradiated area once the source has been turned off, only ending once the bonding process is complete. Complete cross-linking ensures that exposed material is not removed during development. The use of solvents for the removal of SU-8 photoresist has previously demonstrated polymer cracking [209]. Baking processes have been used to speed up the crosslinking reaction, for example, SU-8 negative photoresist has been demonstrated to have a better shape definition and less surface distortion when baked at 60 °C compared to 95 °C [210].

The high similarity between negative photoresist materials and photopolymers suggest that a similar behaviour could be observed in parts produced during the Stereolithography process. Stereolithography processes utilising laser based exposure techniques have a higher degree of control over the cure depth than DLP projection. During the hypothetical fabrication of a cube using DLP SL, every time a new layer of resin is exposed, all previous layers are also exposed, with the exposure energy decreasing with distance from the projection source. As a result, when the part is removed, the photopolymer on the surface has not finished cross-linking and requires additional time and energy for the cross-linking to be completed. One potential solution is the application of a UV oven, commonly used in SL post processing to ensure complete cross-linking of fabricated parts. This "oven" has no thermal component but instead exposes the sample to a large dose of UV light in a narrow band of wavelengths at approximately 365 nm. This post-cure stage has proven to significantly improve the mechanical properties of specimens compared to parts in their 'green state', with an increase of ~30% in ultimate tensile strength, and may be beneficial for inclusion in the mid-process developing procedure [211]. In addition to this, observations under a scanning electron microscope show the delayed appearance of micro fractures on the surface if a part is washed immediately after fabrication, caused by a reaction of the photopolymer to the solvent, preventing sufficient polymerisation. These cracks begin to appear approximately 3 or 4 hours after washing.

4.3.1   Mid-processing of Substrates to Reduce Surface Cracking

The effect of substrate relaxation and thermal baking were analysed on the appearance of surface cracks with the aim to reduce or eliminate their appearance. Samples with identical designs were

fabricated in 10 batches. Each batch was processed as referenced in Table 4.5, with samples subjected to one of four relaxation periods or a thermal exposure, both methods were introduced in the mid-processing flow chart in Figure 4.1.

Table 4.5.   Parameters of Development Investigation
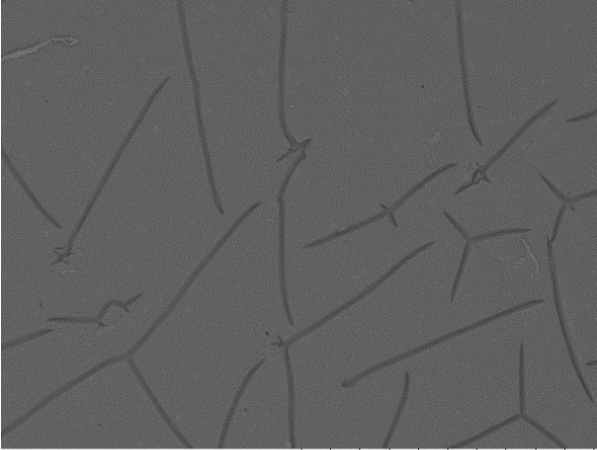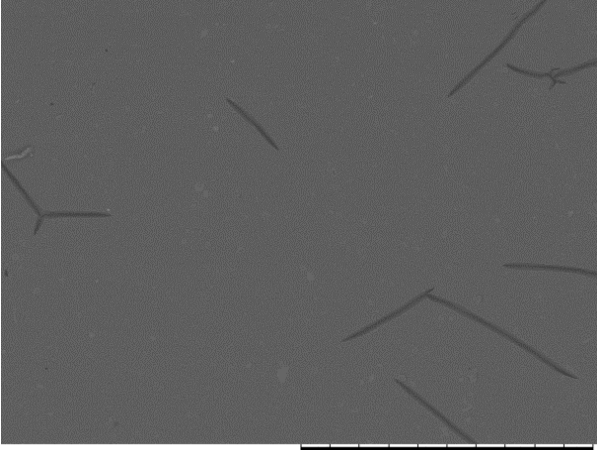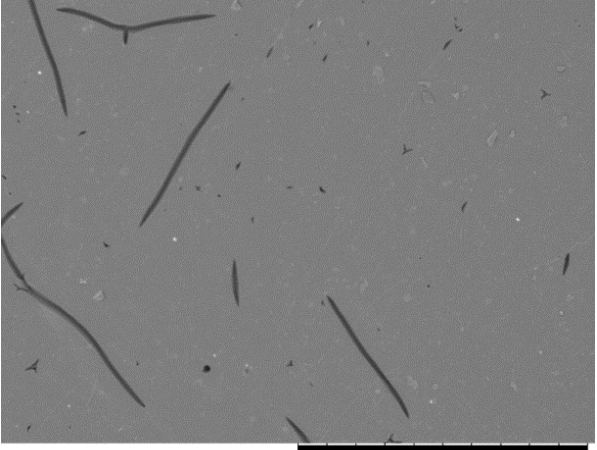
Batch	Solvent	Relaxation Time	Thermal Baking Time
1	IPA	-	-
2	IPA	10 minutes	-
3	IPA	20 minutes	-
4	IPA	30 minutes	-
5	IPA	-	15 minutes (60 °C)
6	D-Limonene	-	-
7	D-Limonene	10 minutes	-
8	D-Limonene	20 minutes	-
9	D-Limonene	30 minutes	-
10	D-Limonene	-	15 minutes (60 °C)

Once the sufficient relaxation or thermal baking times had been conducted, the first 5 batches were subjected to 2 minutes of ultrasonic agitation in IPA and the second 5 samples in D-Limonene. They were then dried with a high pressure air feed before half the samples from each batch were placed into a UV oven for 30 minutes. This allowed a comparison to be made between samples that had been subjected to both photoresist processing techniques, UV oven exposure and washed in both solvents selected in Section 4.2.

4.3.2   Scanning Electron Microscopy of Developed Substrates

The addition of both extra time and energy into the substrates has, in all cases, demonstrated a reduction in the severity of the surface cracking. A relaxation time of 10 minutes resulted in significantly less surface cracks however, 20 and 30 minute relaxation times did not provide any further reductions. Baking the substrate for 15 minutes resulted in a change in the mode of the crack propagation, originating from a number of single points, creating 'star-like' fissures on the surface. Table 4.6 shows five samples that were not exposed to additional UV light, were agitated in D-Limonene and were subjected to each of the five experimental development methods.

Table 4.6.   SEM Images showing the effect of development techniques on cracking

Development Technique	Sample SEM Image
None The substrate was fully fabricated and on completion immediately removed from the vat. It was then ultrasonically agitated for 2 minutes in D-Limonene, removed and dried with a high pressure air source.	
10 Minute Relaxation The substrate was fully fabricated and on completion, left to relax for 10 minutes before removal from the vat. It was then ultrasonically agitated for 2 minutes in D-Limonene, removed and dried with a high pressure air source.	
20 Minute Relaxation The substrate was fully fabricated and on completion, left to relax for 20 minutes before removal from the vat. It was then ultrasonically agitated for 2 minutes in D-Limonene, removed and dried with a high pressure air source.	

30 Minute Relaxation The substrate was fully fabricated and on completion, left to relax for 30 minutes before removal from the vat. It was then ultrasonically agitated for 2 minutes in D-Limonene, removed and dried with a high pressure air source.	
15 Minute Bake at 60 °C The substrate was fully fabricated and on completion, immediately removed then baked for 15 minutes at 60 °C. It was then ultrasonically agitated for 2 minutes in D-Limonene, removed and dried with a high pressure air source.	
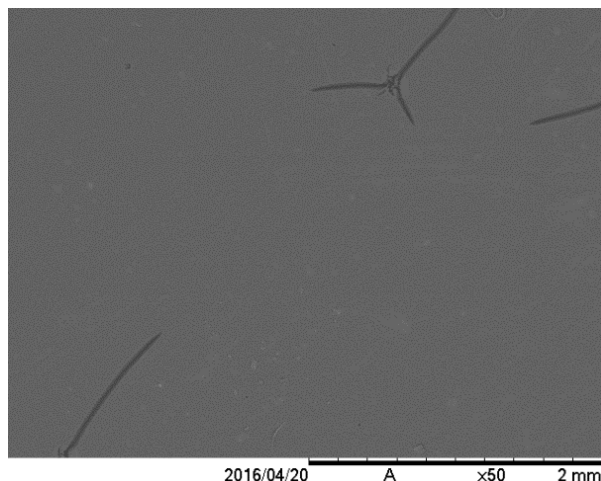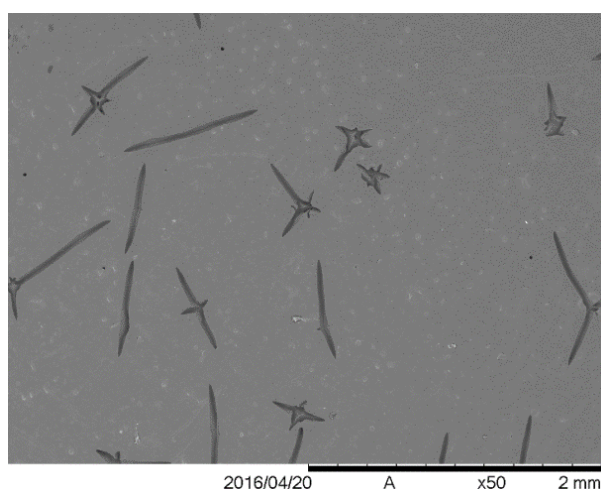
The most effective method used to reduce surface cracking was identified as the additional UV oven curing stage. This UV oven stage is conducted immediately after rinsing, ensuring complete crosslinking of the polymer before the solvent has the time to react with and crack the surface. With the source of the cracking identified as incomplete cross linking of polymers in the photosensitive material, Table 4.7 shows that additional exposure to UV light has resulted in a reduction in the appearance of surface cracking in samples exposed to IPA and, in the case of samples agitated in D-Limonene, the cracking was dramatically reduced.

Table 4.7.   Images showing reduction in surface cracking density after UV oven exposure

	IPA	D-Limonene
No UV		
UV		
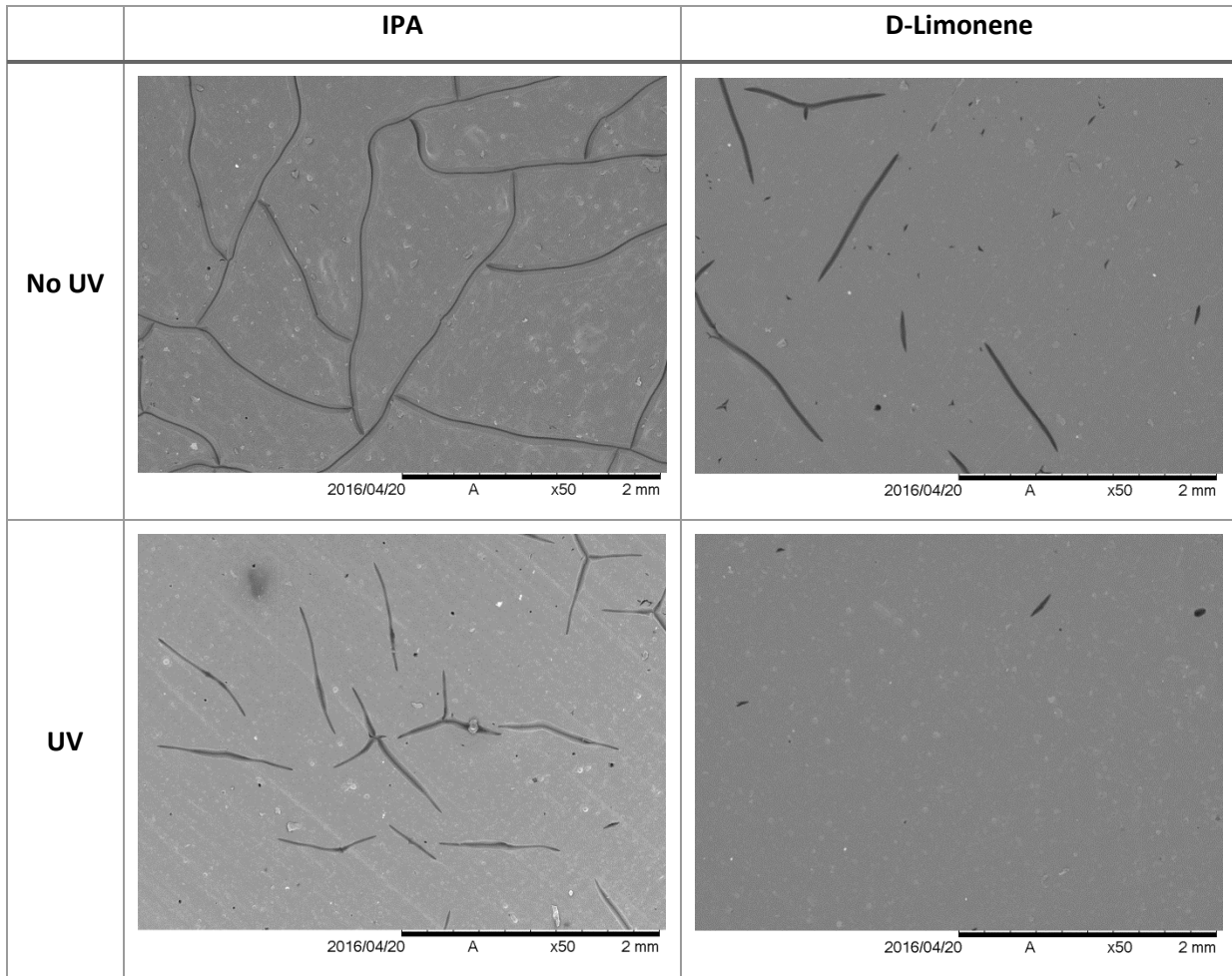
Complete cross-linking has significantly reduced the permeability of the substrate surface to solvents, resulting in a significantly lower cracking density. Over a 2 minute agitation period D-Limonene has also demonstrated a less aggressive reaction with the photopolymer than was shown during prolonged exposure in Section 4.2, creating a more favourable surface for subsequent processing. Although baking has previously been used to encourage the complete crosslinking of parts produced in Stereolithography, its effect has not been examined and quantified [212]. Contrary to this, literature presented in Section 2.3.3 suggests that once polymerisation of photopolymer resins have been initiated by UV light, it cannot be reinitiated or sped up by heat energy.

4.3.3   Surface Roughness of Developed Surfaces

The surface roughness of each sample has also been assessed to determine if the choice of development technique can be used to improve the surface quality, making it suitable for the deposition of conductive materials. Results of a comparison between IPA and D-Limonene are presented in Table 4.8.

Table 4.8.   Surface roughness data (S_a) of developed surfaces

Technique	Surface Roughness (µm)			
	IPA	IPA + UV	D-Lim	D-Lim + UV
0 Min Relaxation	14.33	6.37	3.75	4.11
10 Min Relaxation	7.54	3.49	5.20	2.64
20 Min Relaxation	9.25	4.27	2.28	3.79
30 Min Relaxation	9.30	7.27	3.88	2.5
15 Min Baking	13.63	6.38	4.45	2.83
Average	10.81	5.56	3.91	3.18

Two surface development parameters have been shown to have an effect on the surface roughness of the substrate during this experimentation. Firstly, D-Limonene produced a significantly lower S_a value, more than 50% smaller than IPA across all relaxation and baking specimens. This value then decreased further after additional ultraviolet light exposure in a UV oven. An additional 30 minute UV exposure resulted in a 50% reduction in S_a value on samples exposed to IPA and a 20% reduction in S_a on the samples exposed to D-Limonene, resulting in average values of 5.56 µm and 3.18 µm for IPA and D-Limonene, respectively. There is however no measureable difference in surface roughness (S_a) or average peak to valley distance (S_z) as a result of increasing relaxation time or with the additional thermal baking process.

4.4   Summary

To ensure an efficient transition between substrate fabrication via Stereolithography, material dispensing of isotropic conductive adhesives and surface mount assembly, a development procedure was required that removes any contaminants and optimises the surface quality. Ultrasonic agitation has been evaluated and compared with manual rinsing techniques, proving that this form of assisted agitation is beneficial to this development process.

Experimentation was conducted within this chapter to determine the effect of eight specially selected solvents on a cured photopolymer artefact, which after characterisation using surface analysis and SEM techniques, were assessed for their compatibility with the resin. Significant cleaving and cracking and, in some cases delamination of the photopolymer surface was observed, allowing a number of candidate solvents to be removed from contention. IPA and D-Limonene were shortlisted for further experimentation having demonstrated the lowest surface roughness values and no negative effects on the substrate.

Two photoresist development techniques were adopted for use on liquid photopolymer substrates and tested in an attempt to eliminate surface cracking. Both relaxation and baking processes demonstrated a reduction in cracking and, with the addition of UV oven curing in combination with agitation in D-Limonene, the cracking was almost completely eliminated. This development process resulted in a maximum 50% reduction in surface roughness of substrates agitated in IPA, however the S_a value of developed substrates agitated in D-Limonene was still 14% lower than IPA.

The optimised findings resulted in a development procedure whereby substrates were left to relax for 10 minutes, agitated in D-Limonene for 2 minutes and placed in a UV oven for 30 minutes, producing a substrate with high quality surface finish and no surface cracking while minimising the processing time.

5 Fabrication of Electronic Circuitry

The second digitally driven process used in this hybrid manufacturing approach is the deposition of conductors to enable the fabrication of high-resolution circuitry. This system will be designed to print conductive materials onto photopolymer substrates produced using the method introduced in Chapter 3. These conductive materials will take the form of tracks, z-axis through-layer connections and surface mount device interconnects which will be compatible with surface mount assembly technology, allowing components to be positioned immediately after dispensing and thermally cured in position.

Figure 5.1 outlines the four stage process of printing electronics.
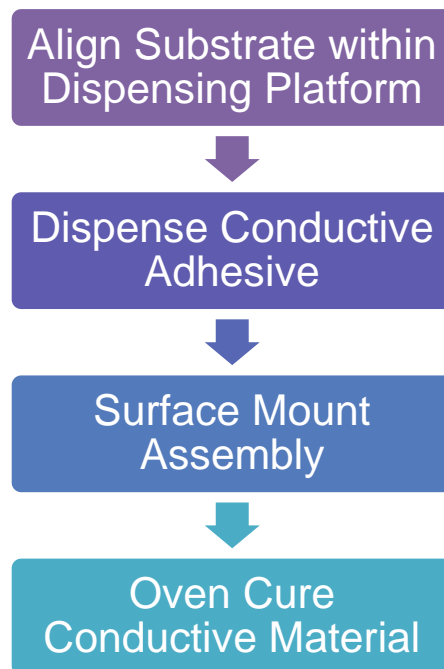
Figure 5.1.   Four stage process for printing electronics

The three objectives of this chapter are to develop and characterise a digitally driven dispensing method for:

- The production of circuit traces on the substrate surface with the smallest width achievable.
- Generation of vertical connections between the layers in order to enable the fabrication of multilayer electronic circuitry.
- Compatibility with surface mount electronic assembly.

Deposition of conductive materials onto photopolymer substrates has previously required the creation of channels on the substrate surface to control material flow [83]. Conductive materials with a high viscosity that exhibit shear thinning will be used to attempt to deposit conductors on a

flat surface without the use of additional features. In addition, experimentation will aim to minimise the track width to facilitate an increase in density and minimisation of the footprint of circuitry. A higher density of electronics can also be achieved by process integration with surface mount assembly. SMDs are available down to 01005 packages with resistors of this size measuring 0.01" x 0.005" (0.4 mm x 0.2 mm) however, the size that can be used is limited by the resolution of the dispensing process used to produce component interconnects. The higher the resolution, the smaller the SMD that can be used.

The successful development of bottom-up Stereolithography capability during Chapter 3 has limited the potential to print via holes in Stereolithography substrates for the production of multilayer electronic devices. The embedding of circuitry in a thick layer of material requires z-axis through layer connections to be fabricated before embedding, as freestanding three-dimensional structures on the substrate surface.

This chapter presents the function of the dispensing system and the selection of conductive materials. The printing of conductive materials will be systematically characterised by changing a combination of parameters including pressure, nozzle inner diameter and print speed. Profile shape of conductive tracks printed using these variables will be analysed to determine their effect. In addition, alternative through-layer conductive connections have been developed for use in multilayer electronic systems produced using additive manufacturing. These take the form of freestanding conductive pillars built simultaneously with the conductive tracks and component interconnects. Finally, the electrical performance of the conductive materials cured using different regimes will be assessed through their resistivity.

5.1   Dispensing Mechanism

5.1.1   Musashi Dispensing Hardware

A Musashi Shotmaster500 dispensing system with a SuperΣCMII pneumatic actuator was used to deposit conductive materials. The system combines a dispensing head and pneumatic actuator, movement mechanism, laser surface mapping, control software and design software for the development of test pattern designs.

The dispensing head provides the functionality to fit a variety of standardised nozzle diameters fitted with the industry standard luerlock threads. Material is fed to the nozzle by means of a disposable syringe and plunger, with the dispensing process actuated by pneumatic force. A suck back mechanism also exists within the pressure controller to ensure no leakage of material from the nozzle once actuation has ceased.

A gantry system provides x-axis displacement across the build envelope and, z-axis height control. The movement in the y-axis is provided by movement of the build platform itself. The Musashi system also contains a feedback mechanism in the form of a laser system to map the surface profile of the programmed dispensing path before the dispensing process is initiated. Alterations in the z-axis will automatically be made during deposition based on the surface mapping to ensure a constant nozzle-substrate relationship. This system has a specified resolution of movement of +/- 5 µm over a 500 mm x 500 mm x 80 mm build area. Before dispensing the z-axis height is calibrated using a contact sensor to ensure the distance from the substrate is correctly controlled. The system setup is shown in Figure 5.2.
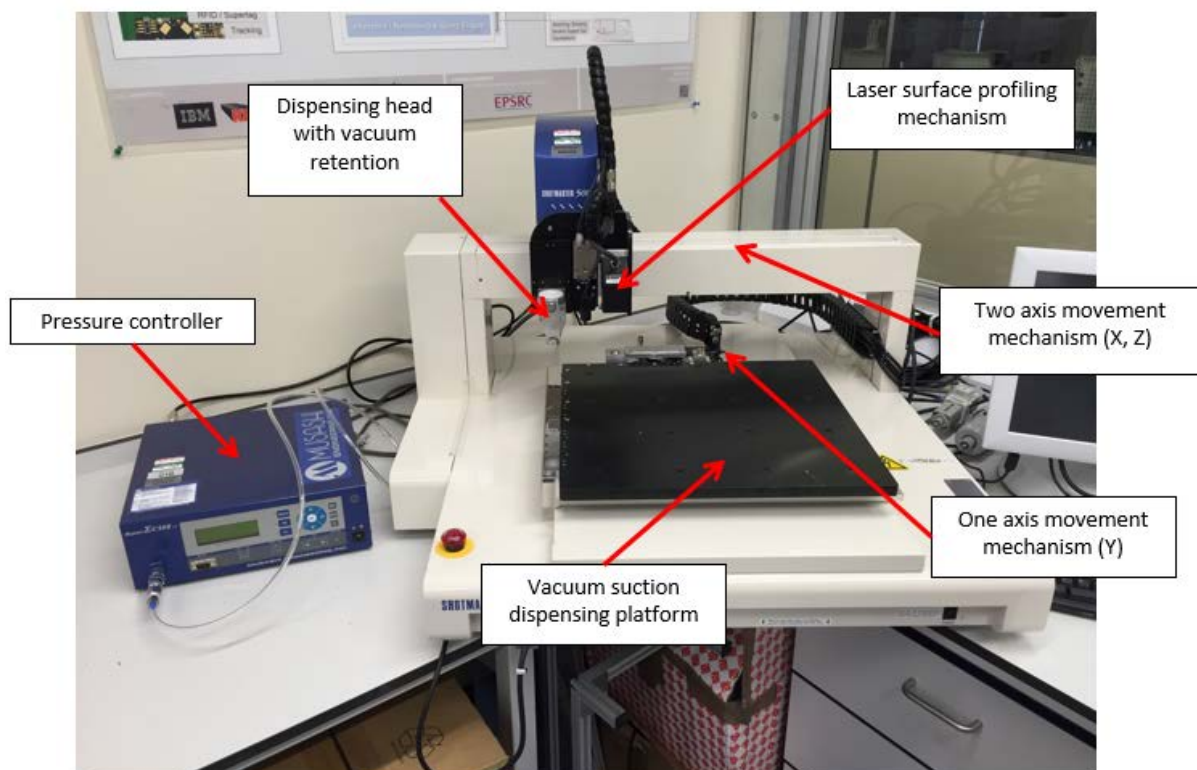
Figure 5.2.   Musashi dispensing apparatus

The build platform has the capability to hold the substrate in a fixed location using vacuum suction applied to the base of the substrate through perforated holes within the platform itself. A camera is mounted beside the dispensing head is used to align the substrate to the dispensing nozzle with an accuracy of 5µm.

5.1.2   Musashi Dispensing Design and Control Software

The Musashi system uses dedicated design software called MuCAD IV. This software allows print and point-to-point motion speeds between 0.1 mm/s and 300 mm/s to be attributed to specific features ranging from simple lines to filled shapes. Designs can be produced in x, y and z axes and feature

dimensions altered in the programming code using both incremental and absolute coordinate systems. From this drawing, a diagram of the tool path is subsequently generated. The design and coding functions have been shown in Figure 5.3.
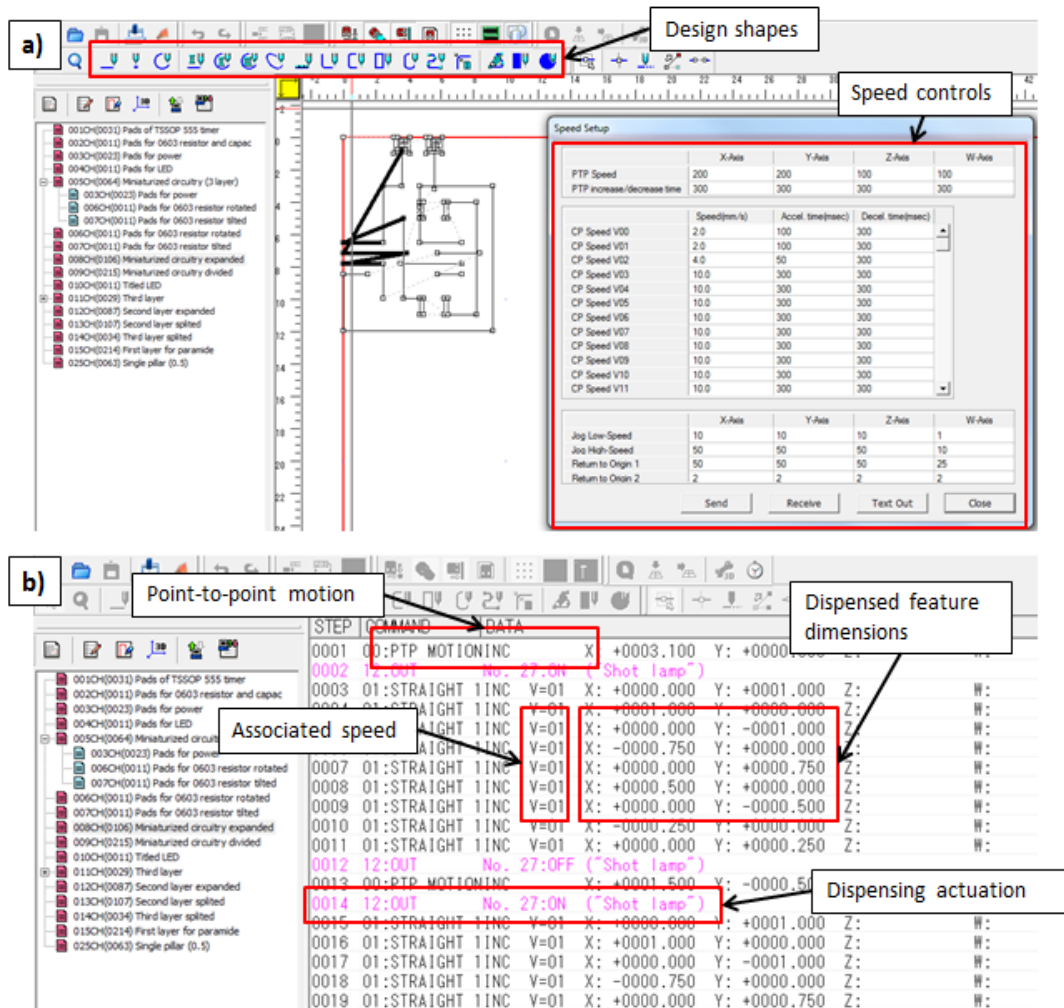
Figure 5.3.   Musashi MuCAD software a) design and b) programming functions

After the part has been designed and a print speed and nozzle path determined within the CAD software, separate control software is used to program the printing parameters. These include print gap, substrate alignment, printing offset and if required, the pattern and pitch of an array of features to be printed, as shown by the screen capture in Figure 5.4.
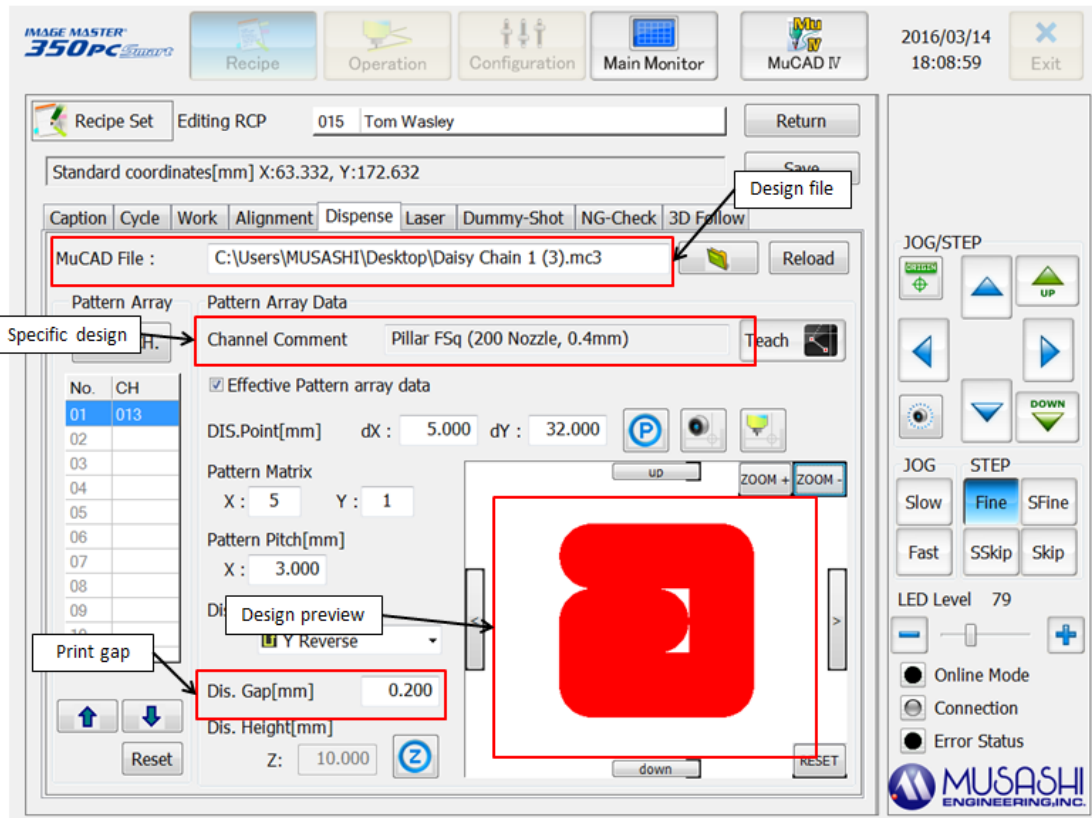
Figure 5.4.　　　Musashi control software

The dispensing pressure controller can be set independently of the software with values between 30 kPa and 500 kPa, both before and during the printing process. The printing medium is manually primed to the nozzle orifice by pressurising the syringe before the dispensing process is initialised. The following procedure is conducted before printing is initiated:

- Design features selected and dimensioned in MuCAD
- Print and point-to-point motion speeds selected
- Designs uploaded into the control software
- Dispensing parameters selected
- Camera used to align and set the print head to the origin
- Printing pressure selected
- Material primed within nozzle
- Nozzle height calibrated
- Printing initiated in autonomous fashion

5.2 Materials

Conductive inks and pastes are the first of two material types that can be used to dispense conductive tracks. The dispensing characteristics of each of these materials can be adapted through

an increase or decrease in the loading of metallic particles, with more viscous formulations referred to as pastes and lower viscosity alternatives as inks. The disadvantage of these materials is their need to be sintered at high temperatures, far exceeding the temperature resistance of photopolymer substrates used in the context of this research. This process evaporates the solvent material and fuses the particles together to create a dense track of conductive material [131]. It is this requirement alone that makes these materials unsuitable for application in this hybrid approach. Further background has been presented in Section 2.4.1.

Isotropic conductive adhesives (ICAs) are the second material group suitable for dispensing. Conductive epoxies are traditionally used to bond surface mount electronic devices to copper pads on a PCB. ICA materials are commonly deposited through narrow orifices or patterns in dispensing, stencil or screen printing processes [213]. The most important characteristic that separates epoxies from metallic micro or nanoparticle inks is the availability of materials that can be cured at low temperatures by the mechanisms described in Section 2.4.1, making them the most encouraging option in the context of this project.

The properties of a number of commercially available epoxies from different suppliers were analysed for their suitability for integration with cured photopolymers. Key material characteristics evaluated were conductivity, viscosity, thixotropic index, maximum particle size, particle type and recommended curing regimes.

The substrate has a glass transition temperature of ~100 °C, above which the surface of the cured photopolymer has been proven to degrade, and therefore the epoxy must cure at a temperature lower than this threshold. The relationship between curing temperature and curing time is inversely proportional and as such, a lower temperature will result in extended curing times [123]. Some conductive epoxies are capable of curing at room temperature however this can take up to 3 days and will not achieve the optimal electrical properties for this material. The curing regime should be optimised to produce the most advantageous electrical properties possible in the shortest timeframe without damaging the substrate.

The viscosity of the epoxy plays a significant role in its dispensing onto a substrate. Too low a viscosity would result in leaking from the dispensing nozzle and slumping of conductors deposited on a flat surface, an occurrence that has previously been controlled through shaping of the substrate surface [165]. Ideally, the paste will have a high enough viscosity to sit on the flat surface of the substrate without spreading. Too high a viscosity would also prevent the material from flowing smoothly through the nozzle, creating either an interrupted flow or no flow. The chosen material

must therefore demonstrate shear thinning, resulting in a drop in viscosity during the deposition process but returning to its previous state after the fact [214][215]. The thixotropic index of the epoxy is related to the viscosity and describes the ability of the dispensed track to hold its shape. It is loosely related to the strength of the forces on the surface and the viscoelasticity of the dispensed track preventing it from collapsing and spreading across the substrate surface, a higher index combined with suitable viscosity will improve track accuracy.

Wettability of the conductive epoxy will determine how well the material reacts to contact with the surface of the substrate. Insufficient wetting would result in either inconsistent or a total lack of deposition on the surface. A lower print gap would exert a greater downward force onto the substrate, helping to improve the wettability.

The particle size of the conductive epoxy determines the minimum nozzle size through which the material can be dispensed without clogging [11]. This also influences the minimum track width. Recommendations from the nozzle supplier indicated that nozzle inner diameters should be at least 10 times higher than the maximum particle size of the material.

Table 5.1 shows the properties of two shortlisted ICAs. Of all epoxies evaluated, they have an equally low specified resistivity of 0.005 Ωcm at 23 °C when subjected to a curing regime of 80 °C for 3 hours, this compared to the bulk resistivity of 1.59×10^{-6} Ωcm and 1.68×10^{-6} Ωcm for silver and copper [216].

Table 5.1. Important ICA selection properties of 2 shortlisted materials [13][217]

	Name	Max. Particle Size (µm)	Viscosity (cPs)	Thixotropic Index	Curing Regimes	Volume Resistivity (Ωcm)
A	Epotek E4110-PFC	≤20	50000-60000	3.3	1 hr @ 120 °C 3 hr @ 80 °C 6 hr @ 45 °C	5×10^{-3}
B	Epotek EJ2189	≤45	55000-90000	5.2	15 min @ 150 °C 1 hr @ 100 °C 3 hr @ 80 °C 72 hr @ 23 °C	5×10^{-3}

The first of the two candidate material types is a silver particle filled isotropic conductive adhesive, Epotek E4110-PFC (material A), consisting of a specified maximum particle size of ≤20 µm. This material is supplied in two parts [13]. Separately both parts have shelf lives of 1 year however, once

mixed in the recommended 3:1 ratio, the pot life is 2-3 hours at room temperature, after which the material will become too viscous due to its low temperature curing characteristics. Epotek EJ2189 (material B) is also a silver filled isotropic conductive adhesive however, the silver is in the form of flakes rather than particles. Material B has a specified larger maximum flake size at ≤45 μm, is also comprised of two parts, part A is silver filled and part B is an epoxy binder [217]. This second material is mixed at a 10:1 ratio, has the same shelf life as the alternative material however, its slower curing rate than material A results in a pot life 1 hour longer at room temperature.

Before dispensing, materials were carefully mixed using a microbalance accurate to 0.001 g, precisely weighing parts A and B to the specified ratio in a polymer container. These parts were then mixed using a stainless steel spatula for 5 minutes, ensuring they are complete combined. This material can then be transferred to a syringe and subsequently loaded into the dispensing apparatus. Immediately after dispensing (within 5 minutes), samples were cured in a Lenton WN60 thermal oven using natural convection (no fan), limiting the time over which slumping of the dispensed features could occur. This oven is capable of reaching temperatures up to 300 °C however, due to the aforementioned limitations of the substrate material, 100 °C will not be exceeded and a range of values up to this maximum will be investigated.

To allow preliminary assessment of the ICA, both materials were mixed and samples deposited on photopolymer substrates for analysis under a SEM. Both the surface and cross sections were analysed, with the latter achieved through mounting samples in a 2 part epoxy and lapping and polishing the resulting specimens perpendicular to the conductive tracks to reveal a cross sectional view of the features. Images of material A on a Hitachi TM3030 Desktop SEM shown in Figure 5.5 suggest that the maximum particle size of the silver particle filled ICA is greater than specified.
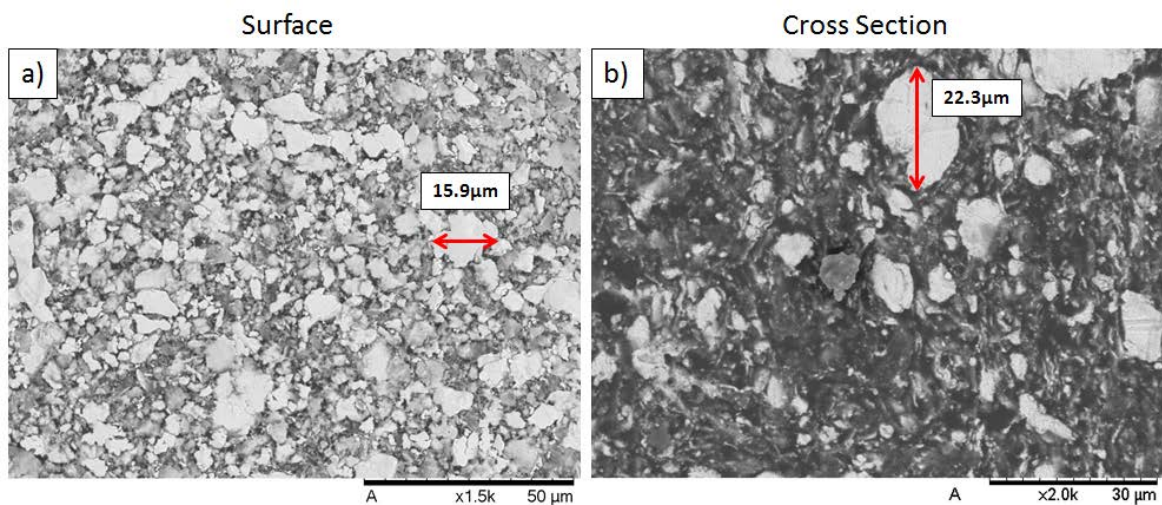
Figure 5.5.   SEM images of cured samples of material A a) surface and b) cross section

A wide variety of particle sizes were observed in the SEM images, one example in excess of the specified maximum particle size. These images show a very low frequency of large particles however, Epotek do not publish particle size distributions of their materials to corroborate these observations as the information is proprietary. Comparable images were taken of material B showing the maximum observed flake size to be 25 µm, as shown in Figure 5.6, lower that the actual value specified on the datasheet. This could again be a result of a low frequency of particles of maximum size distributed throughout the ICA.
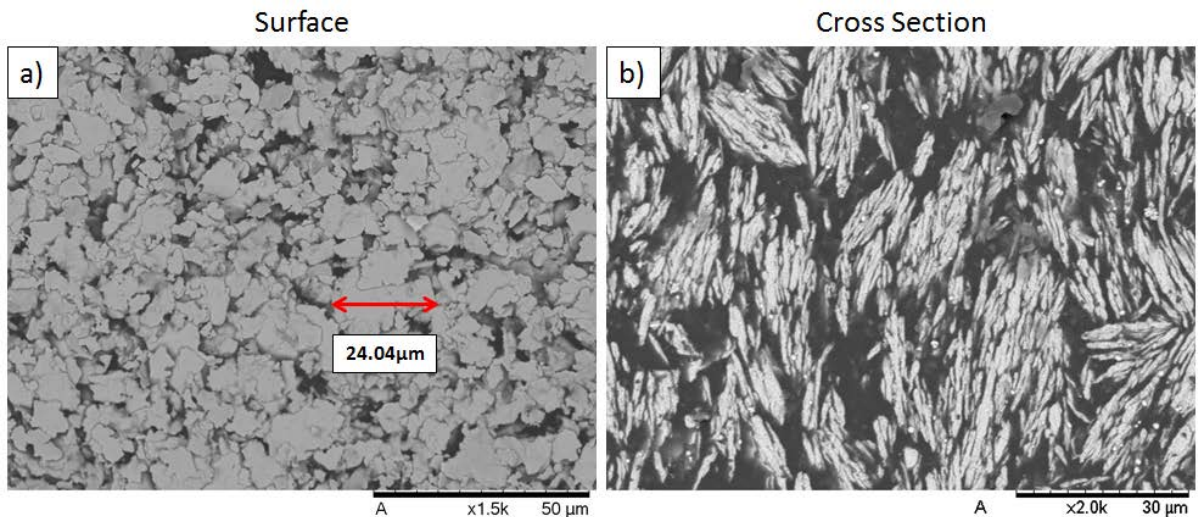
Figure 5.6.   SEM images of cured samples of material B a) surface and b) cross section

There is also an observed difference in the shape of the flakes versus that of the particles in both orientations. Theoretically, after curing the particle filled ICA should display a lower conductivity than its flake filled counterpart. This is due to the more intimate contact of overlapping flakes compared to adjacent particles, a contact that is displayed by the overlapping flakes in Figure 5.6 [123]. This theory has been explored in Section 5.5 through the determination of the measured resistivities of both conductive materials.

5.3   Dispensing of Conductive Traces

The dispensing characteristics of materials A and B were tested initially with paper as a substrate. Paper is both inexpensive, and has suitable surface characteristics for adhesion and wettability of the material. Paper allowed a wide variety of designs to be tested and optimised with ease and low cost. Although tracks were successfully produced on paper, solvent from the epoxy was absorbed into the porous substrate as shown in Figure 5.7, suggesting that the same thing could occur on a photopolymer substrate. This could cause the epoxy to create channels and sink into the surface and, possibly improve the adhesion of the epoxy to the substrate.
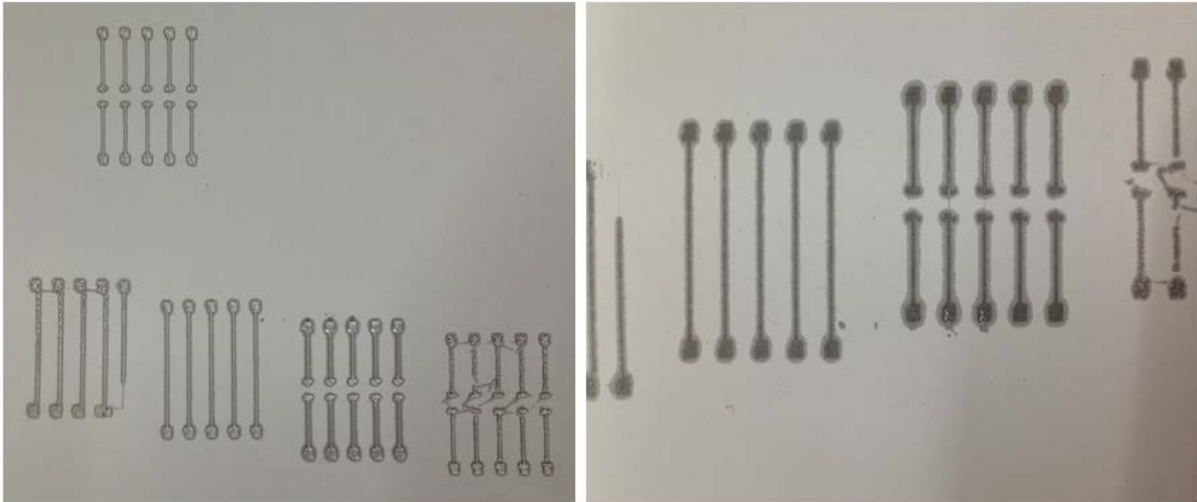
Figure 5.7.   Images of uncured 40mm long ICA tracks during dispensing tests on paper substrate

A study was conducted to characterise the interaction between the ICA and photopolymer substrate. A small quantity of each conductive adhesive was mixed and dispensed using the Musashi system to produce 30 mm x 30 mm substrates with five basic tracks shown in Figure 5.8, both of which demonstrated good wettability. ICAs were deposited using a 200 μm nozzle inner diameter and minimal material slump was observed during the dispensing process due to the relatively high viscosities and thixotropic properties.
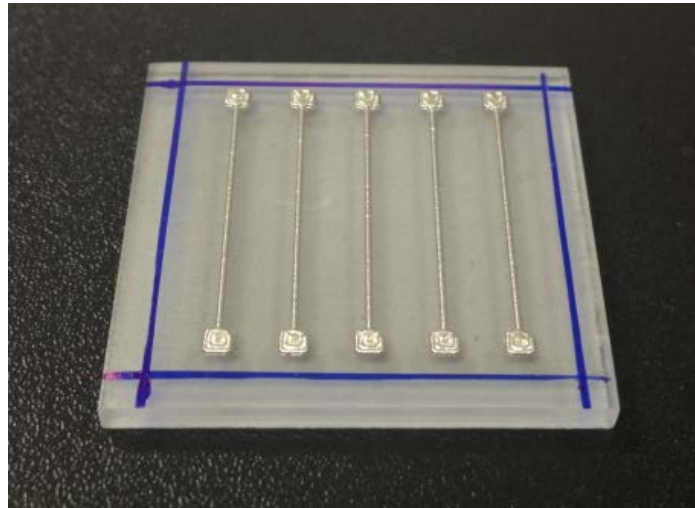
Figure 5.8.   Photopolymer/cured ICA interaction substrate

Following the visual evaluation of the wet conductive tracks, they were thermally cured at 45 °C for 6 hours as per the manufacturer guidelines and then the physical and electrical properties assessed. Once the curing cycle was finished, the epoxy could still be indented using multi-meter probes, indicating that the material was not fully cured. A value of resistance in the order of 1kΩ was also measured across the conductive tracks, 100 to 1000 times higher than what is expected of the cured ICAs.

After observing the absorption of ICA solvent by paper during testing, cured sample tracks of both materials A and B were cross sectioned and examined under a scanning electron microscope to determine whether there is any additional interaction between the conductive material and the photopolymer substrate. The interfaces between ICAs and the photopolymer substrate are shown in Figure 5.9.
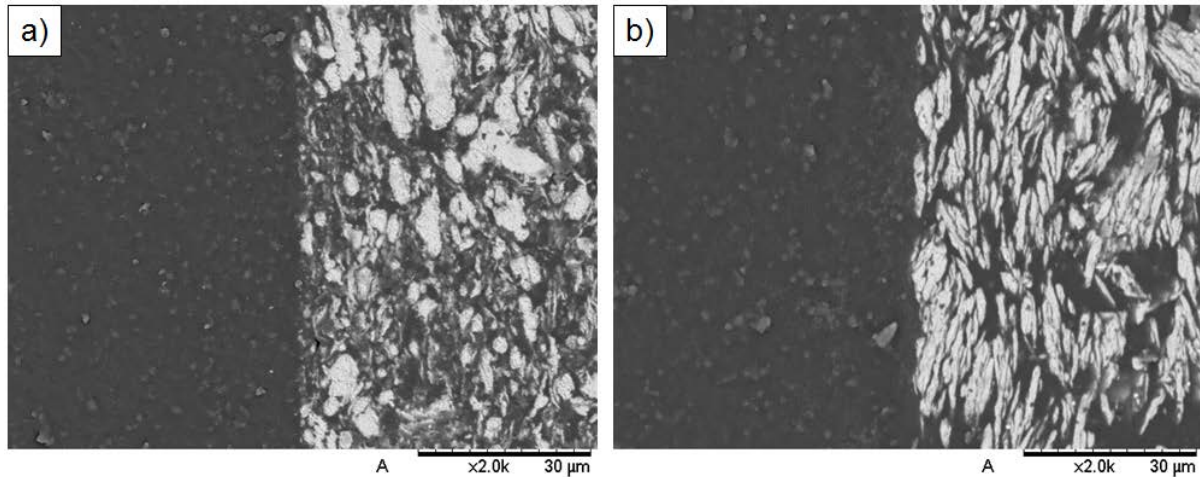
Figure 5.9.   Interaction between photopolymer substrate and cured materials a) A and b) B

Images of the interface show no reaction of the substrate to the ICA with clean boundaries between the silver filled conductive material and substrate. No penetration of the solvent into the photopolymer has been observed, suggesting that it was all evaporated during the curing process.

5.3.1   Determination of Experimental Parameters for Track Dispensing

Initial experimentation to create simple conductive traces demonstrated the capability to deposit conductive epoxies as smooth, continuous lines with minimal slumping.

To optimise the dispensing process, an investigation was carried out to determine the most advantageous combination of parameters. The four most important variables were identified for characterisation: conductive epoxy; nozzle inner diameter; print speed and pressure. Print gap was kept at a constant ratio of 1:1 with the nozzle inner diameter as the theoretical diameter of the dispensed material exiting the nozzle. Initial experimentation was then conducted to determine the minimum and maximum pressures at which each epoxy would print. This investigation gave the limits for the full experimental design. Musashi Engineering, the nozzle supplier recommend a 10:1 ratio however, experimentation demonstrated that both chosen materials could be deposited through a 100 µm nozzle despite the specified maximum particle sizes of ≤20 µm for material A and ≤45 µm for material B.

Material A has a higher viscosity and as such, had a larger range of printing pressures from 50 kPa to 250 kPa for the 250 µm nozzle, 50 kPa to 450 kPa for the 200 µm nozzle and 250 kPa to 450 kPa for

the 100 µm nozzle. This makes the data comparable but also shows that a narrower dispensing orifice requires a higher pressure to produce the same profile from a smaller nozzle. Pressures outside these ranges would result in excessive material deposited or, as shown in Figure 5.10, inconsistent trace profiles. The same results can be achieved with high or low values of print speed.
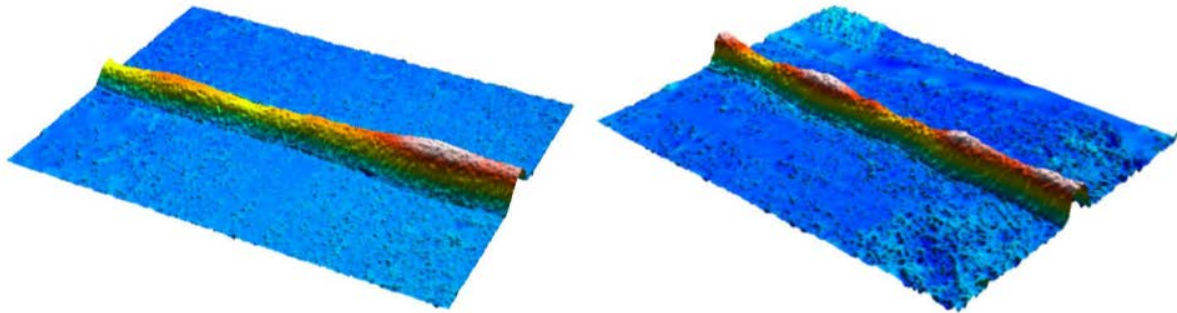
Figure 5.10.   Inconsistent cured track profile resulting from high print speeds of 9 mm/s and pressures of 150 kPa

Material B has a lower viscosity and therefore has an experimental pressure range between 30 kPa and 90 kPa. The same 1, 3, 5 and 7 mm/s print speeds were also used for both epoxies. These pre-determined printing parameters are listed in Table 5.2. All combinations of these values will be investigated and presented with the exception of those resulting in inconsistent deposition or track widths above 1 mm.

Table 5.2.   Experimental print parameters for track dispensing investigation

Nozzle ID (µm)	Print Speed (mm/s)	Print Pressure (kPa) for Material A	Print Pressure (kPa) for Material B
100	1	100	30
200	3	150	45
250	5	200	60
	7	250	75
		300	90
		350	
		400	
		450	

5.3.2   Characterisation of Dispensing Parameters for Conductive Traces

Tracks were dispensed in 10 mm long lines, in groups of three from which six measurements of cross sectional area, width and height could be taken and compared. All track data was taken after thermal curing for 3 hours at 80 °C in a Lenton WN60 thermal oven. The array of tracks is shown in

Figure 5.11. These tracks were produced on glass, providing an optically clear, high quality surface eliminating a potential variable from experimentation.

Figure 5.11.   Array of cured tracks dispensed during process characterisation through all three nozzles in materials A and B

The aim of this investigation was to produce smooth uniform traces with the smallest track width possible. Three-dimensional geometric and contour data of the conductive tracks was collected using an Alicona InfiniteFocus microscope in order to evaluate the properties of the traces.

Material A produced a smoother trace after thermal curing, most likely due to the difference in particle size and particle shape between the two pastes. The inconsistencies in the surface of material B can be seen in Figure 5.12(b) and are attributed to the shrinking of the epoxy resin around larger flakes in a lower viscosity material, creating large craters in the traces and therefore increasing their roughness. The same cannot be seen in Figure 5.12(a) printed in the higher viscosity material A as small particles can be packed closer together, hence the smoother appearance. The cross sectional profiles of these tracks also show that material A retained a more consistent profile shape whereas, material B demonstrated material slumping characterised by the flatter profile and steeper side walls. It is also evident that, rather than forming a peak at the highest point of the track cross section, this material is distributed across the volume of the track, resulting in a wider, flatter track profile.
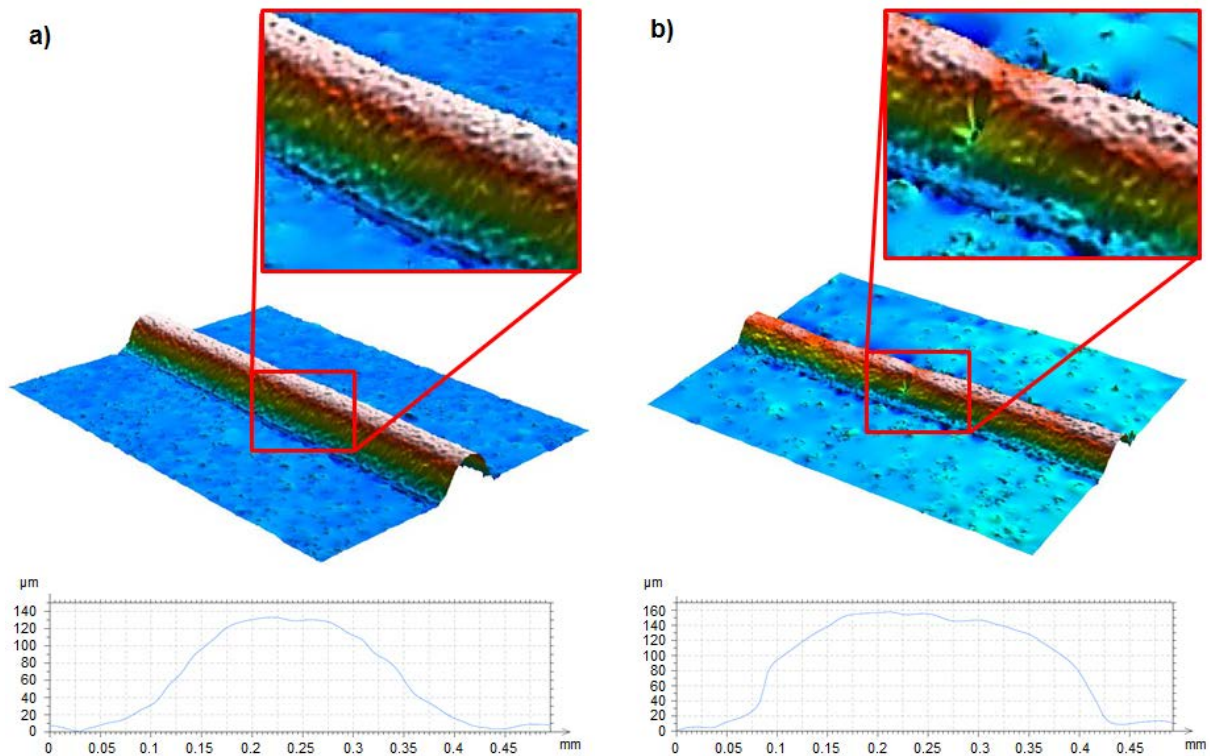
Figure 5.12.   Comparison of appearance between cured tracks printed in material a) A at 400 kPa and 5 mm/s and b) B at 60 kPa and 5 mm/s

The characterisation of the relationship between nozzle diameter, print speed and printing pressure of material A showed a minimum trace width of 170 µm could be achieved from a 100 µm diameter nozzle. This relationship has been displayed in Figure 5.13.
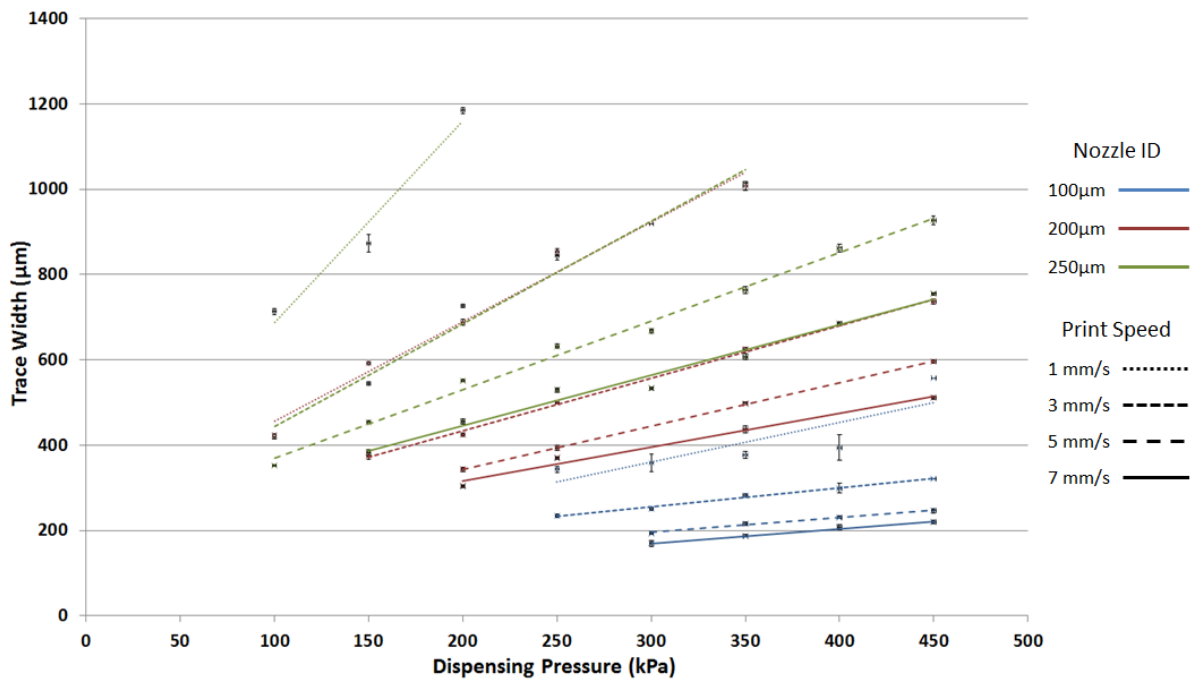
Figure 5.13.   Material A relationship between printing pressure, speed and nozzle diameter on track width

Increasing nozzle diameter and pressure increased the volume of material deposited therefore producing wider and thicker tracks. An increase in print speed reduced the track width since the material is dispensed for a shorter time over the same distance. Figure 5.14 shows the same relationship in material B, however the printing pressures were approximately 75% lower. With the 100 µm nozzle, material B track profiles were found to be inconsistent and were therefore not plotted.
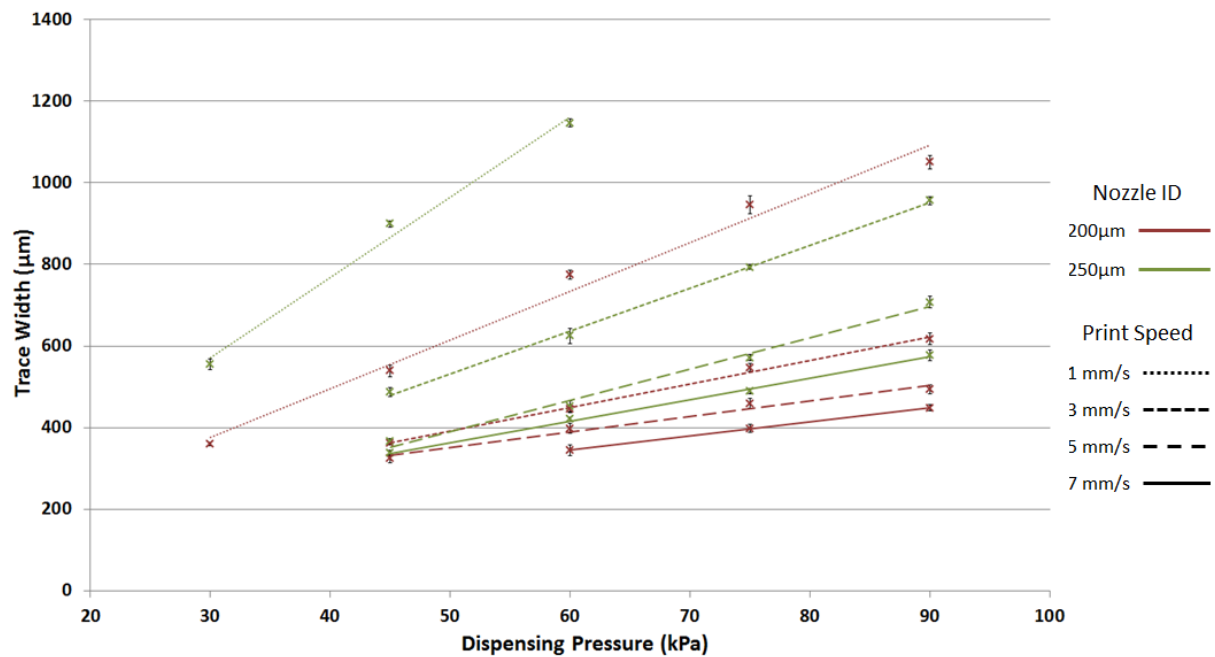
Figure 5.14.   Material B relationship between printing pressure, speed and nozzle diameter on track width

The effect of pressure on track widths had a resulting visual effect on the appearance of the traces. Figure 5.15 shows how the track profile changed with increasing pressure from 150 kPa to 450 kPa. Both the width and height increased however, the track height is also effected by print gap. This is substantiated by the flatter profile of the tracks at higher pressure deposition.

At a 1 mm/s print speed, an increase in pressure of 150 kPa from 300 kPa through a 100 µm nozzle resulted in a 56% increase in trace width while a 250 µm nozzle showed an 86% increase in width over the same increase in pressure. The same relationship between pressure and trace width has been displayed by different samples in Figure 5.15, with a total width increase of 97% across five samples.
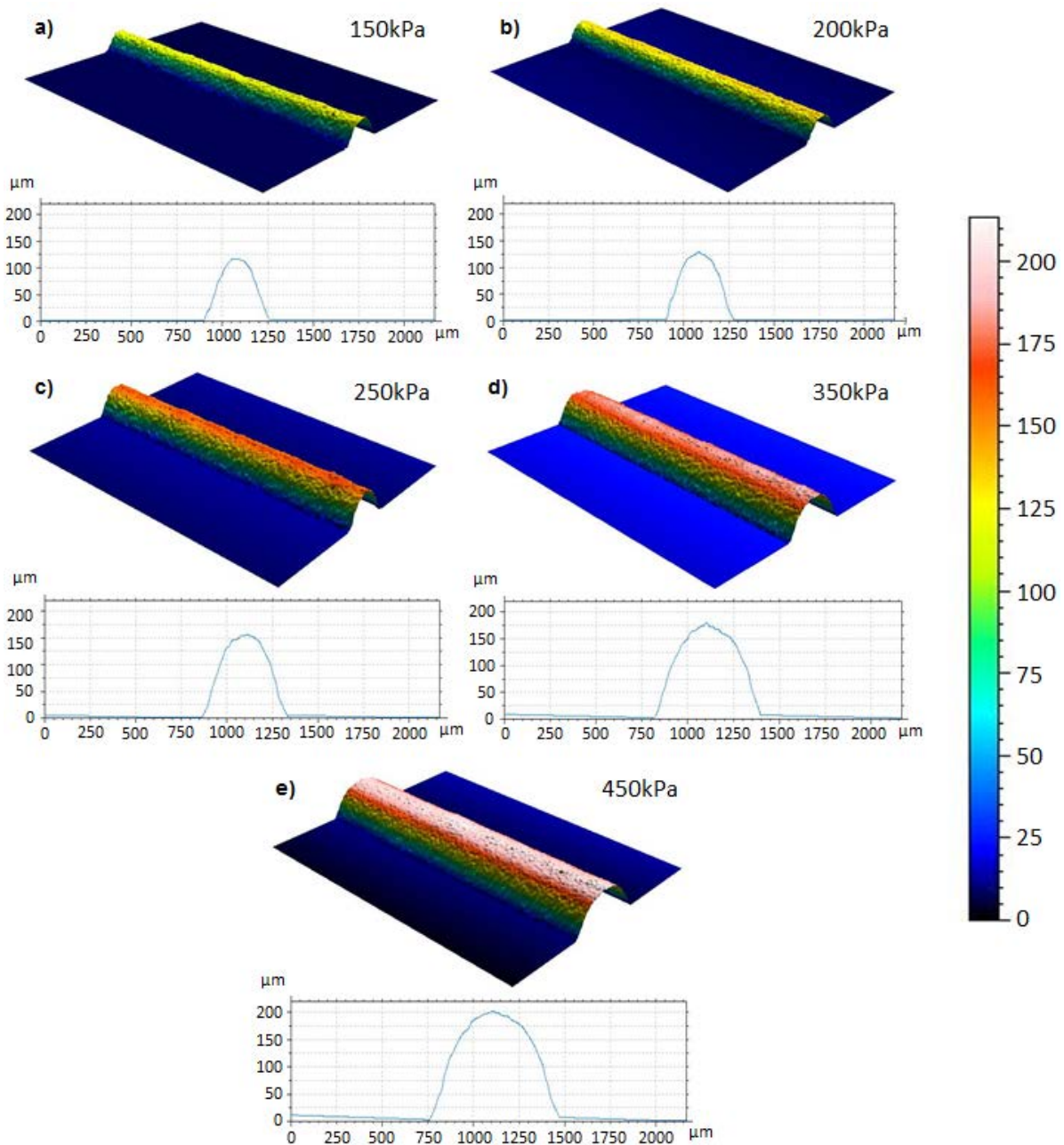
Figure 5.15.   Profiles of cured traces printed through a 200 µm nozzle at 3 mm/s in material A at pressures of a) 150 kPa, b) 200 kPa, c) 250 kPa, d) 350 kPa and e) 450 kPa

The printing parameters at which the smallest track widths were created using each nozzle type were determined and recorded in Table 5.3. This data shows that traces printed through the 100µm nozzle produced the highest trace width/nozzle diameter ratio of 1.69, compared to the lowest of 1.41 demonstrated by the 250 µm nozzle.

Table 5.3.   Parameters proven to produce narrowest consistent cured conductive traces for all three nozzle sizes in material A

Nozzle Size	Pressure (kPa)	Speed (mm/s)	Track Width (µm)
100µm	300	7	169
200µm	200	7	304
250µm	100	5	352

Sets of height and cross sectional area data for material A mimic the relationships demonstrated by the track width, as do those taken from material B, albeit with much lower printing pressures required. The lower viscosity of material B also explains the lower track height on traces when compared to material A. Parameters in Table 5.3 were used to print the traces shown in Figure 5.16.
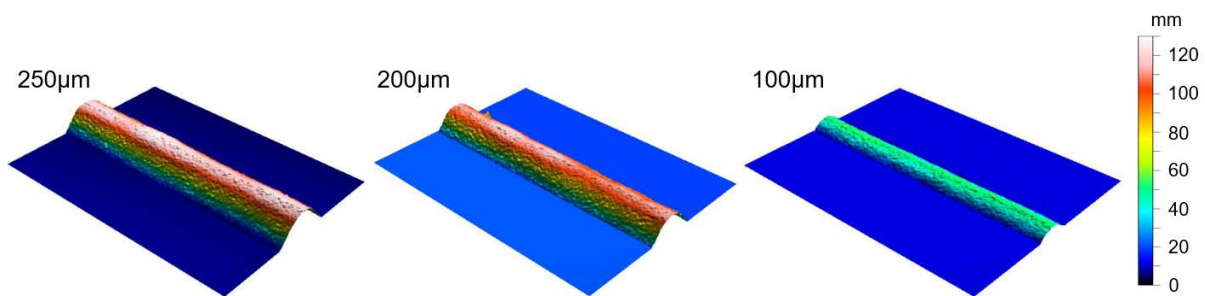
Figure 5.16.   Smallest cured tracks produced by 250 µm, 200 µm and 100 µm nozzles in material A

Table 5.4 compares the height of traces which had similar widths and showed that material B, the lower viscosity ICA, produced track heights approximately 25% lower than material A

Table 5.4.   Comparison of aspect ratios of cured tracks of the same average height printed in materials A and B

Nozzle Size (µm)	Material A		Material B	
	Height (µm)	Aspect Ratio	Height (µm)	Aspect Ratio
100	130.5	0.331	95	0.234
200	152	0.360	154	0.282
250	162	0.387	169	0.348

These lower track heights and aspect ratios were caused by slumping of the material post dispensing and prior to being thermally cured. Through experimentation, the optimal parameters for the dispensing process to create the smallest possible track width, height and cross sectional area was the 100 µm nozzle and material A printed with 300 kPa of pressure at 7 mm/s.

The deposition of conductive traces for integration with Stereolithography substrates has previously achieved line widths between 200 µm and 250 µm [129], controlled by channels on the substrate surface however, this research has reduced this width by 25% to 170 µm and enabled them to be

deposited directly onto the surface without a mechanism for flow control. Trace heights of 130 µm also show a reduction in trace height as channel depths of 400 µm were previously used to contain the conductive ink [83]. This characterisation of the dispensing process has therefore shown improvements in resolution of the dispensing process for application on photopolymer substrates. There is no previous work dispensing ICAs on photopolymer substrates and therefore comparisons can only be made with lower viscosity inks.

Traditionally, stencil printing is used to deposit solder paste onto copper pads on the PCB in order to conduct surface mount assembly of components. Much in the same way as the printed ICAs used during this experimentation, solder pastes exhibit a degree of slumping when the stencil is removed and the paste is no longer contained. The deposition of SMD interconnects using material dispensing therefore only demonstrates one disadvantage over stencil printing and that is the process resolution, slumping is demonstrated by both solder pastes and ICAs however, material dispensing enables fabrication of circuitry in one digitally driven printing process with the capability to iterate designs between prints without manufacturing new templates.

5.4 Dispensing Freestanding 3D Pillars for Z-axis Interconnects

Traditionally z-axis vias in electronics are typically manufactured by a combination of subtractive and additive methods. Holes are produced in the board and then electroplated to provide the conductive pathway between layers. Additive manufacturing methods can fabricate a hole in the substrate without subtractive machining methods however, the method of encapsulation proposed in this hybrid system prevents the creation of a high resolution via hole. This section presents a novel method of overcoming this issue to connecting multiple layers of circuitry through the z-axis via the deposition of three dimensional, freestanding pillars. The technique takes account of the viscoelastic nature of the ICAs which do not readily slump after printing. The pillars can then be embedded with a small protruding contact at the top of the structure on which subsequent printing of conductive features can begin as shown in Figure 5.17. Pillars are therefore required to stand taller than the embedding layers are thick, with 2 mm identified as the maximum prerequisite.
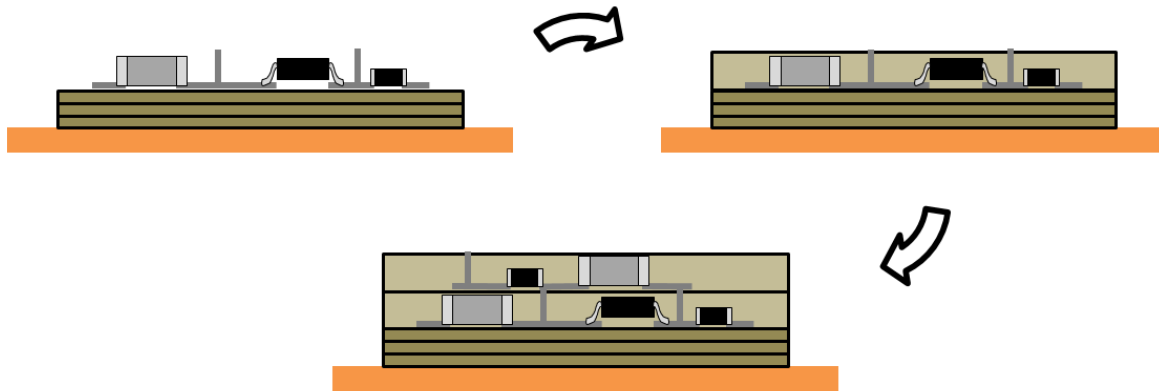
Figure 5.17.   Function of freestanding pillars as through layer connections

To reduce the electronic footprint of any circuit a reduction in the pitch of conductors is required. Pillars of a fixed height and minimal pillar diameter would enable this reduction in pitch.

5.4.1 Pillar Design

Multilayer pillars were designed and machine movements defined in the MuCAD software discussed in Section 5.1.2 . Four pillar designs were considered as shown in Figure 5.18 which included a filled square, filled circle, hollow circle and single dots, all of which would be dispensed over multiple layers, one on top of the other.
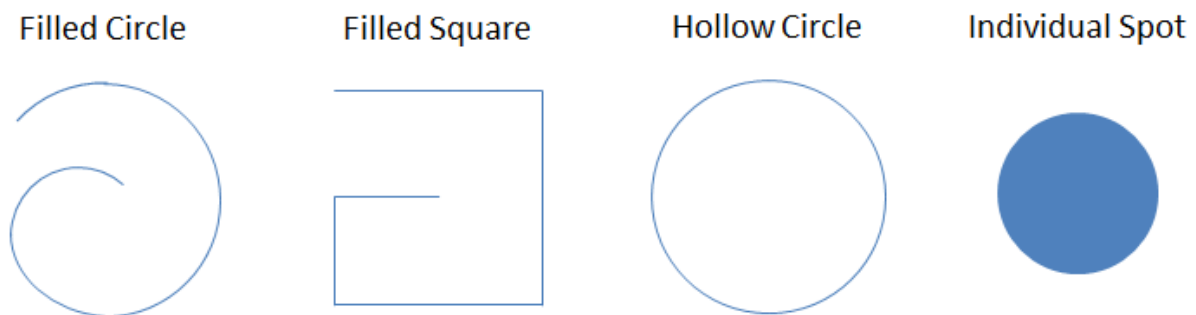
Figure 5.18.   Pillar design considerations

The filled circle appeared identical to the filled square after dispensing due to the rounding of fine feature corners and the round nozzle shape. The hollow circle increased the chance of voids in the structure after thermal curing. Finally, individual spots provide no structural stability during the vertical build process and, there is no motion in x and y axes to move the material away from the nozzle orifice causing pressure induced widening of the pillar. Therefore, the filled square pattern was chosen as the most suitable design to progress further.

This filled square tower structure has been designed specifically for each nozzle diameter, with their dimensions reducing proportionally with the nozzle internal diameter. The 250 µm nozzle design

comprised of a filled 500 µm wide filled square with 7 subsequent layers of the same pattern dispensed one on top of the other, shown in Figure 5.19.
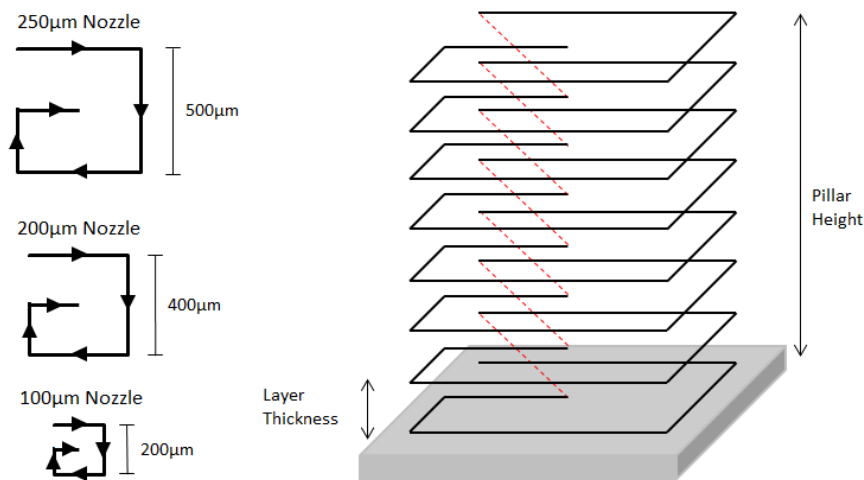
Figure 5.19.   Pillar design and nozzle path

Traces in section 5.3 produced with material A using a 250 µm nozzle demonstrated an average slump in height of ~10% therefore, for the 250 µm nozzle, each layer was moved 225 µm in the z axis, allowing for a 10% slump in each layer of material and resulting in a designed height of 1.8 mm. The 200 µm nozzle ID is 20% narrower than the 250 µm option and therefore, all elements of the design were therefore reduced proportionally with a 180 µm layer thickness and 400 µm design width. The same proportional reduction in dimensions was used to create the design for the 100 µm nozzle.

5.4.2   Feasibility Experimentation

Initial experimentation was conducted to determine a number of capabilities of the system, identify the limits of print speed and pressure and any potential issues when dispensing freestanding structures using either of the silver based conductive materials. Throughout all pillar dispensing experimentation, the mixing process was kept identical to that used in Section 5.3 and all samples were cured at 80 °C for 3 hours immediately after deposition.

Due to the freestanding nature of these z-axis interconnecting pillars, a high aspect ratio needs to be achieved however, the slumping previously demonstrated by material B would suggest that material A would be more suitable. This conclusion is experimentally proven through a comparison of the pillars in Figure 5.20 with those printed in material A.
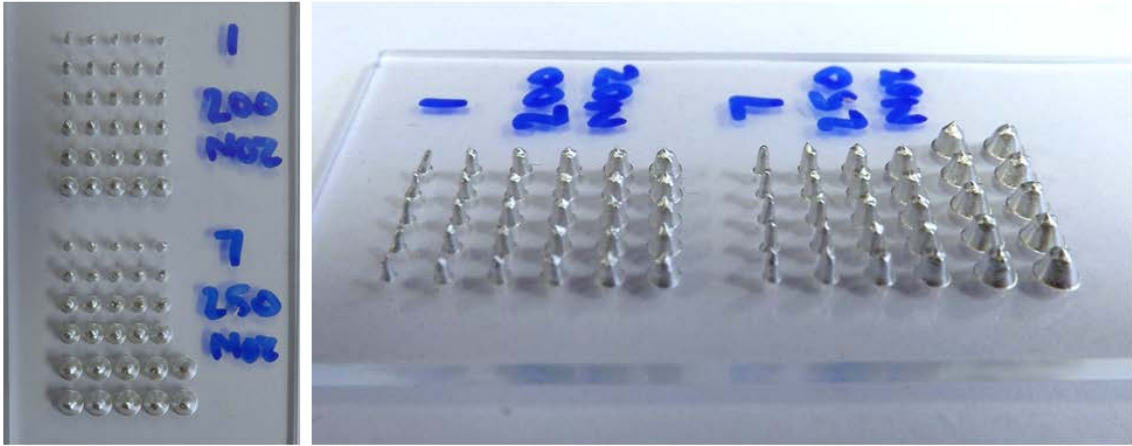
Figure 5.20. Array of pillars printed in material B

The dispensing design was kept constant for both ICAs and therefore the structures produced in both materials could be directly compared. To ensure the pillars printed from materials A and B were comparable, build speed was kept constant but the printing pressure was unique for each material in order to take into account the viscosity differences. Figure 5.21 demonstrates a greater slumping in material B, categorised by its lower peak pillar height than material A.
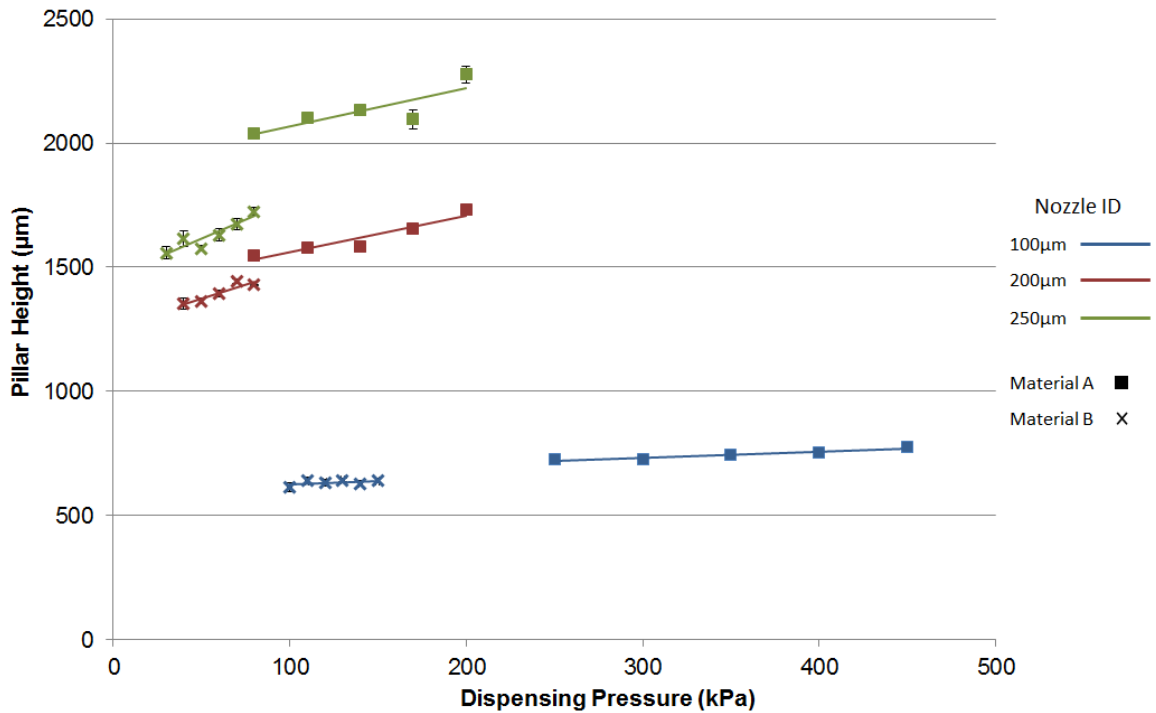
Figure 5.21. Comparison of pillar heights printed using materials A and B

As shown in Figure 5.22, this relationship is validated by the pillar width, starting with similar minimum diameter in both epoxies but, peaking with a diameter increase of 28% with the 250 µm nozzle and 13% with the 200 µm nozzle. This data indicated material A was better suited for high aspect ratio freestanding pillar dispensing.

140
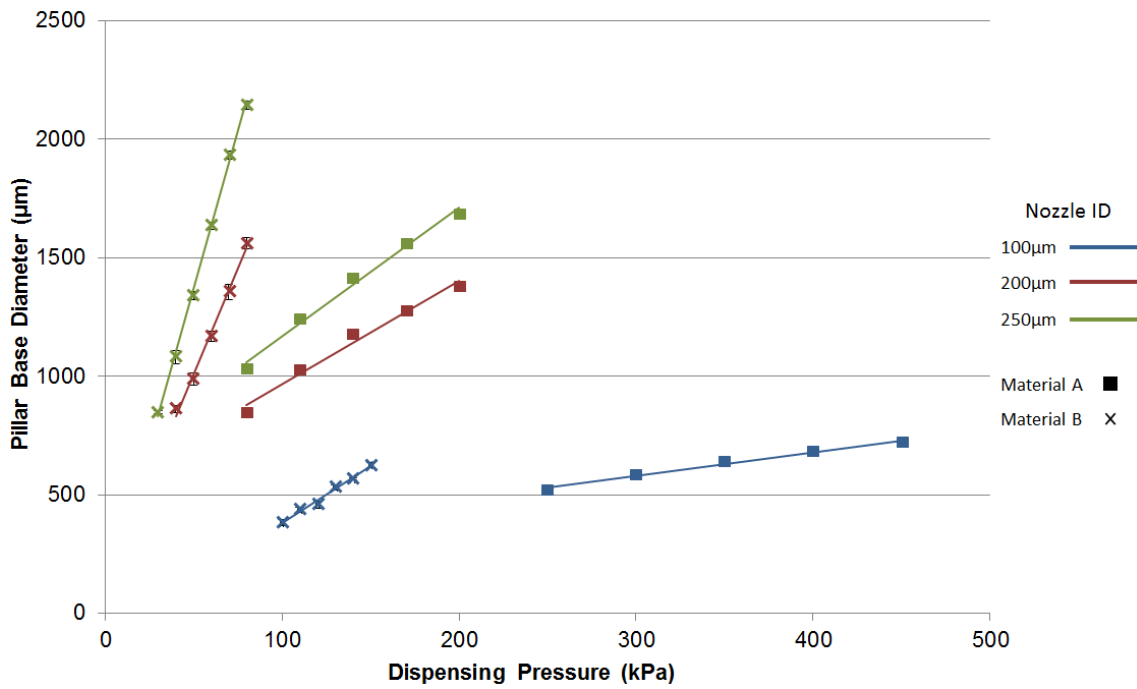
Figure 5.22.   Comparison of pillar base diameters printed using materials A and B

Finally, Figure 5.23 shows the pillar aspect ratio plotted against the diameter, demonstrating that on pillars with comparable base diameters, aspect ratios produced by material A were higher.
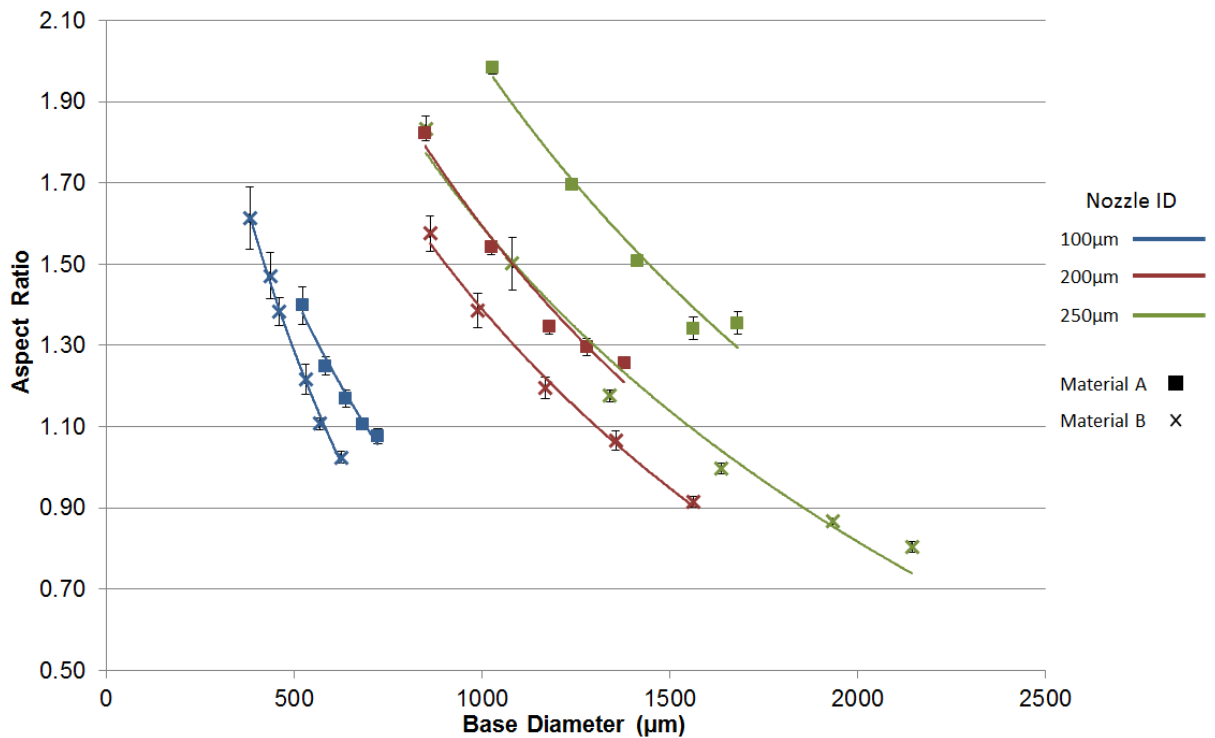
Figure 5.23.   Comparison of aspect ratio at comparable base diameters of pillars printed in materials A and B

During preliminary experimentation, pillar designs were trialled and issues exposed as a result of exceeding the maximum speed at which material can be dispensed, causing the machine to skip alternate layers and produce an undersized pillar. By reducing the point-to-point motion speeds of

the dispensing head in x, y and z axes, the movement time between layers was increased to above the minimum actuation time. Layers could then be printed as designed, one after another to the required height. The reduction in size of the design for both 200 μm and 100 μm nozzles requires the further reduction in point to point movement to facilitate the shorter distances between the end of the previous layer and start of the next.

Observations of the dispensing procedure, shown in Figure 5.24, highlighted significant interactions between the dispensing nozzle and material at the upper limit of the print speed and lower limit of printing pressure.
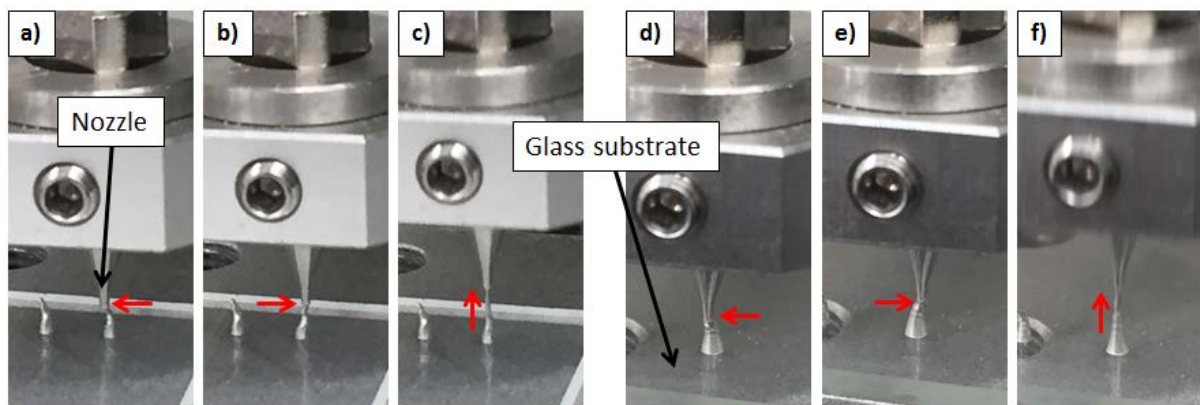
Figure 5.24.   Interaction between nozzle and pillar at a-c) low pressure and d-f) high speed

Under low pressure (Figure 5.24(a)-(c)) and high speed (Figure 5.24(d)-(f)) conditions whereby insufficient epoxy is exiting the nozzle, the top peak of the pillar attaches to and mimics the movement of the dispensing head. This changes the pillar structure and results in a tail at the peak as the epoxy is stretched upwards during detachment. In some circumstances this tail is large enough to fall to one side under the influence of gravity.

5.4.3   Characterisation of Pillar Dispensing Process

A set of optimised experimental parameters based on an initial investigation were determined for use in the characterisation of pillar dispensing in material A. These individual variables are listed in Table 5.5, and all combinations were investigated to determine the relationship between these parameters however each nozzle ID will be used in combination with its proportional design.

Table 5.5.   Experimental printing parameters for pillar dispensing

Nozzle ID (μm)	Pillar Design	Print Speed (mm/s)	Print Pressure (kPa) for 200/250 μm Nozzle	Print Pressure (kPa) for 100 μm Nozzle
100	500μm	1	50	200
200	400μm	3	80	250
250	200μm	5	110	300
		7	140	350
			170	400
			200	450

Higher pressures are required for the 100 μm nozzle and therefore a separate range of values were selected for this experimentation. Pressures in both ranges are within the range required to deposit material while avoiding the interaction shown in Figure 5.24 and ensuring excess material is not dispensed.

Three collections of features were printed, one with each nozzle size before they were thermally cured and measured using the Alicona InfiniteFocus Microscope. The three dimensional data from this measurement system was then processed to extrapolate pillar diameter and peak height information. Figure 5.25 shows the array of printed pillars in material A with each set of six rows corresponding to a different print speed and each of those six rows produced using a different printing pressure, creating five samples for each different combination of print parameters.
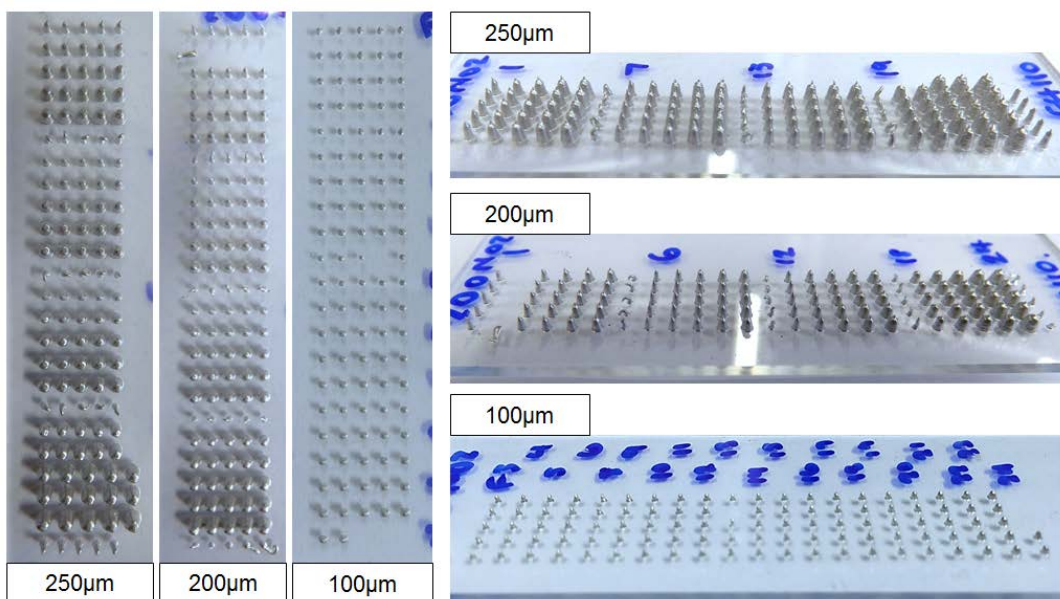
Figure 5.25.   Array of pillars printed in material A using different dispensing parameters

Musashi control software allows the printing of a pattern of features thereby allowing five pillars to be created with each separate set of parameters. This provides enough data to determine standard deviation and error within the data.

On analysis of the pillar array the most noticeable trait of these structures is the change in diameter from base to peak. This is caused by slumping as a result of both the viscosity of the material and the weight of multiple layers printed on top of one another, this slumping is however less severe than material B. Figure 5.26 shows SEM images of pillars produced using a 200 µm nozzle, 3 mm print speed and pressures of 140 kPa and 170 kPa. It demonstrates tapering from base to peak and also shows very little layer detail in the structures, with the expectation that individually dispensed layers would be more defined. This is a further result of agglutination and slumping due to the material rheology.
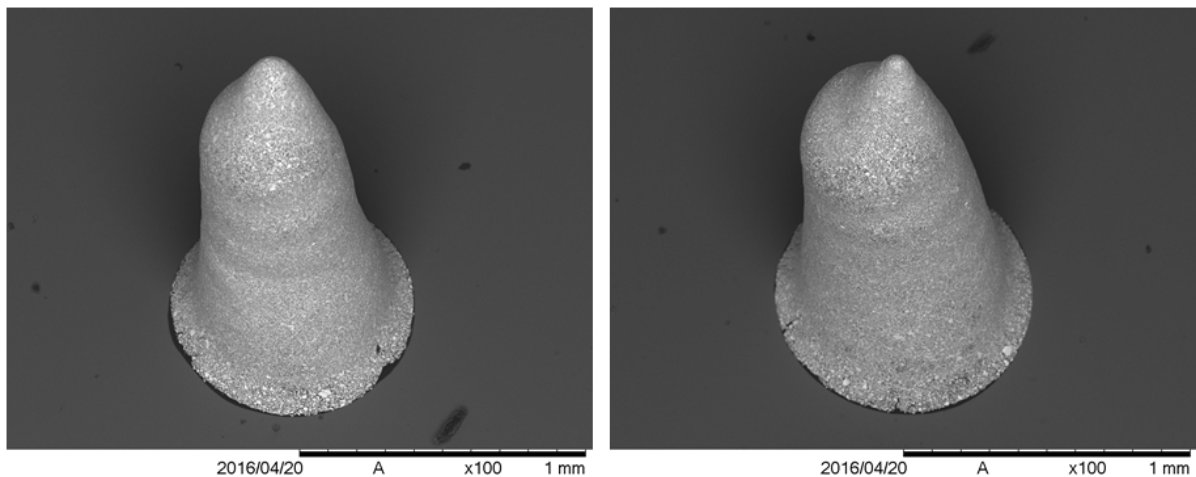
Figure 5.26.   SEM images of pillars printed in material A

The base diameter of the pillars is a function of the volume of material dispensed which, in section 5.3.2, was shown to be controlled by a combination of the printing speed, pressure and nozzle size and is so again when printing vertical structures. The effect of these parameters on pillar appearance is displayed in Figure 5.27(a)-(c), with gradual decreases in pressure, nozzle size and print speed respectively.
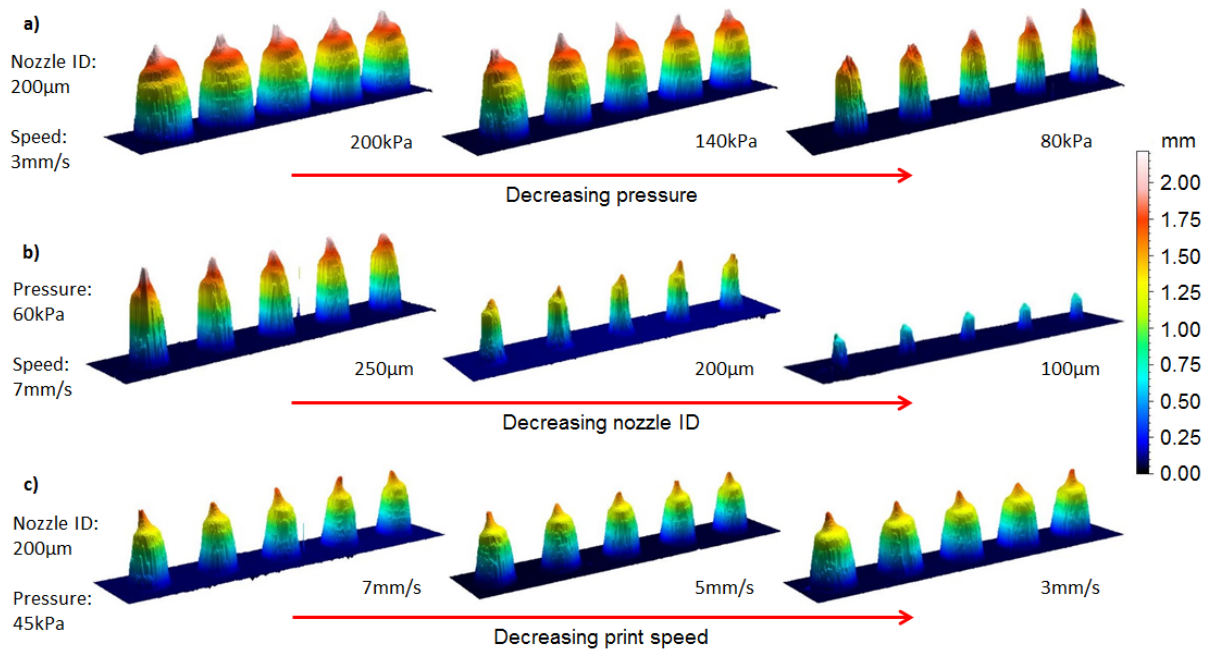
Figure 5.27.   Visual differences caused by a) decreasing pressure, b) decreasing nozzle size and c) decreasing print speed in material A

As expected the largest pillar diameter was created with a 250 μm nozzle and pressure of 200 kPa, exceeding 2 mm in height, evidence of which is presented in Figure 5.28. With an experimental mandate to minimise the diameter of the pillars, the 100 μm nozzle produced the smallest pillar base diameter of approximately 500 μm. This dimension has been produced at speeds of 5mm/s and 7mm/s with respective printing pressures of 250 kPa and 300 kPa. As the pressure increases the rate of increase in diameter reduces due to the fixed design width. This can be explained by diameter increase being a result of pressure exerted on the material by itself during deposition and under the force of gravity with subsequent layers printed vertically. Figure 5.28 compares diameters of pillars printed using 200 μm and 250 μm nozzles. Printing pressure increases with base diameter, however, the rate of increase in diameter begins to level off at higher pressures.
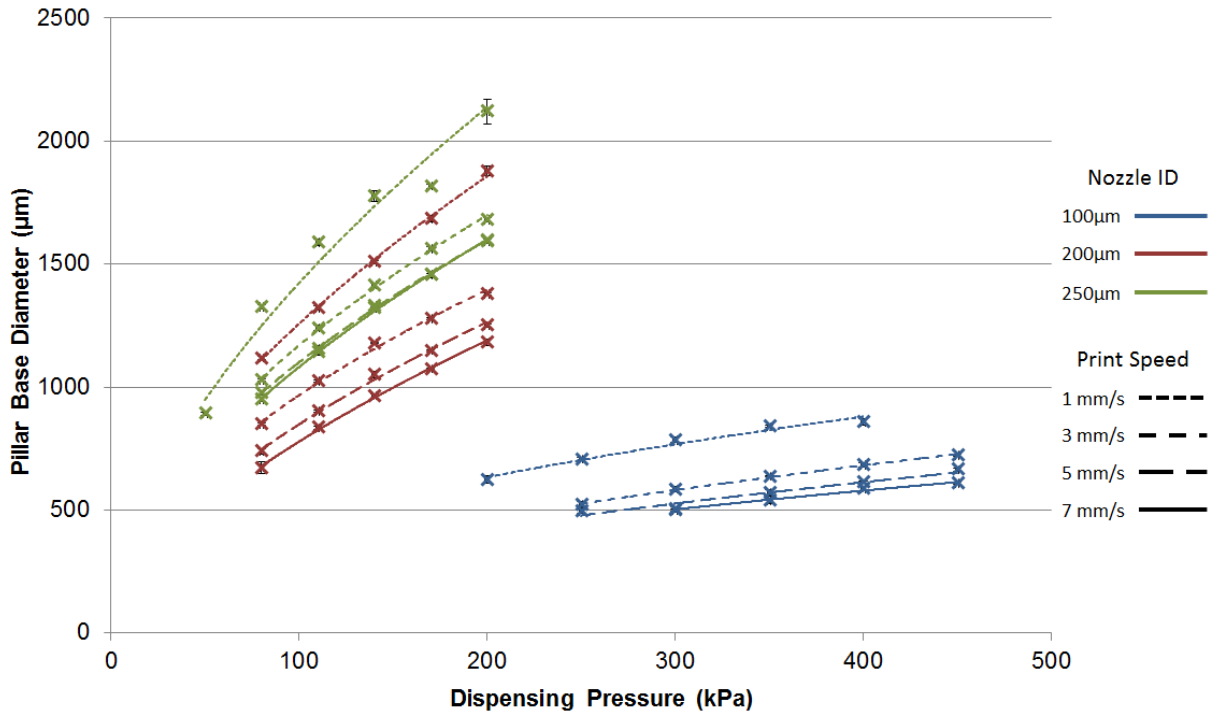
Figure 5.28.   Relationship between dispensing pressure, 200 μm and 250 μm nozzle IDs, print speed and diameter in material A

Unlike pillar data shown in Figure 5.28 for the 200 μm and 250 μm nozzle, data shown in Figure 5.29 for the 100 μm nozzle has a minimum diameter of more than twice the designed pillar width, resulting in a lower aspect ratio.
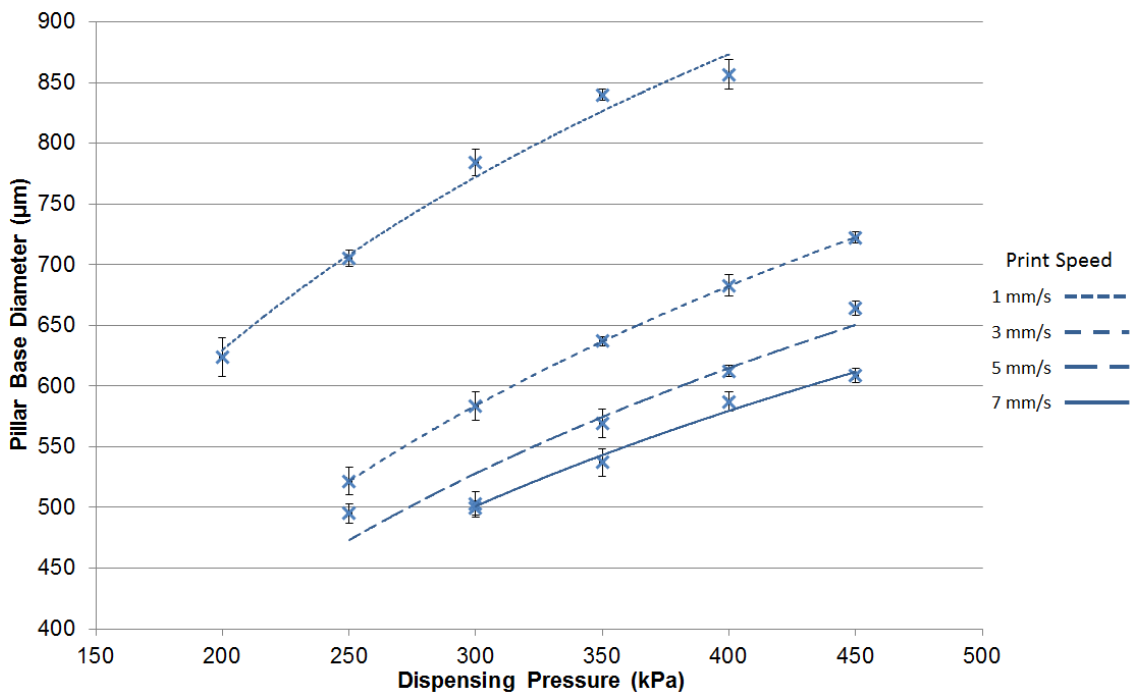
Figure 5.29.   Relationship between dispensing pressure, 100 μm nozzle ID, print speed and pillar diameter in material A

The highest aspect ratio achieved was approximately 1.4, the lowest of the three dispensing nozzles. This limitation is a result of the design height. An increased design height has the potential to produce higher aspect ratio pillars with a narrower base than both 200 μm and 250 μm nozzles. This increase would be dependent on the capability of the material to support the weight of that above it with such a small diameter. However, the designed diameter could be increased to improve the pillar stability. As it stands, with a height of 719 μm this pillar would not be sufficient to create contact through the proposed minimum 1.2 mm embedding layer. Increased volume of material also results in pillars with a lower aspect ratio. Figure 5.30 shows that both the larger nozzles exhibit the same trend with similar aspect ratios achieved while diameters of pillars produced using a 200 μm nozzle are approximately 200 μm smaller. Shorter and narrower pillars show great potential in the minimisation of this multilayer approach, reducing the electronic footprint.
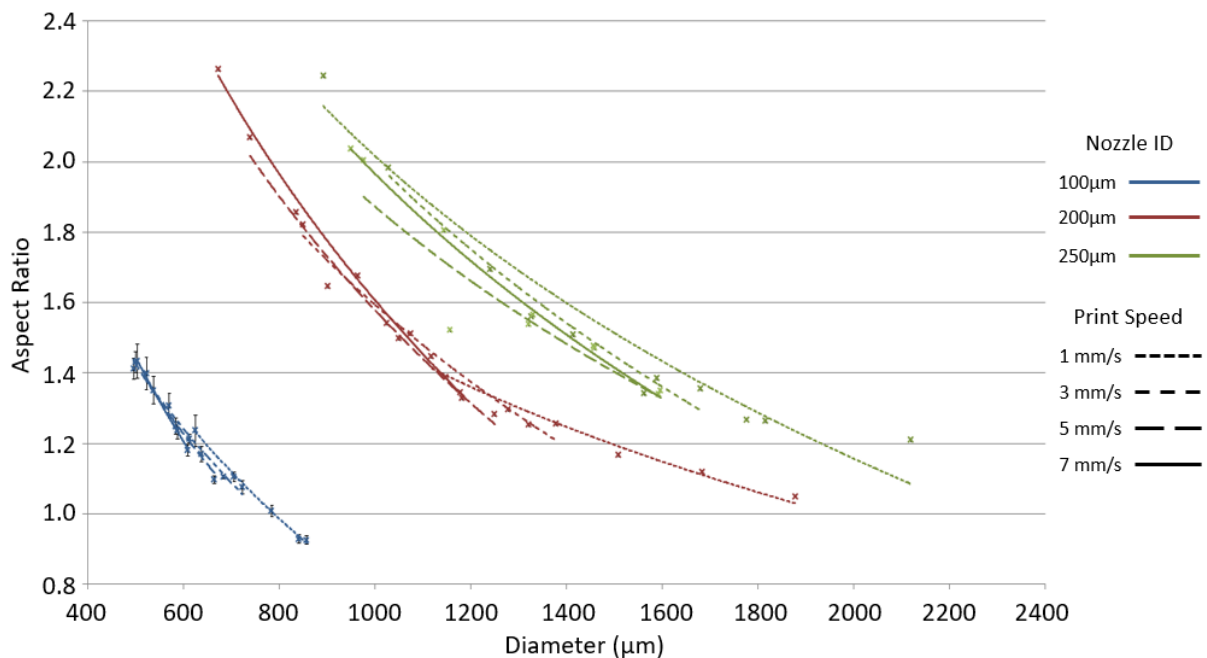
Figure 5.30.   Relationship between diameter and aspect ratio of pillars printed in material A

These diameters increase due to higher volumes of material deposited that spread out wider on the substrate and on subsequent layers. The same relationship has been discovered when dispensing with a 100 μm nozzle, however, as a result of the narrower nozzle orifice, aspect ratio does not increase as quickly with the decrease in pressure.

Two larger nozzles produced a tail feature left on the very top of the pillar, produced when dispensing stops and the final direction of material mimics that of the nozzle as it is moved upwards in the z-axis away from the structure.
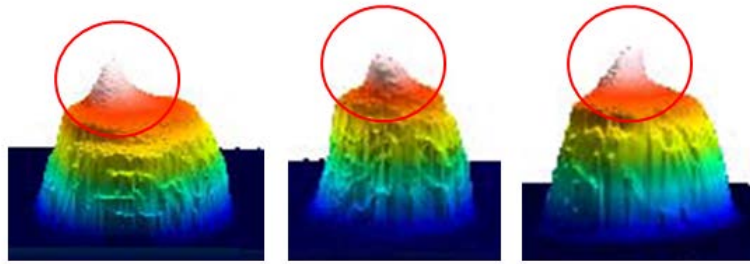
Figure 5.31.   Tail features on pillars caused by upwards motion of the 250 µm nozzle

The small 100 µm nozzle does not create these tails as the volume of material being dispensed is significantly lower, also explaining why the average pillar height was lower than its design. This nozzle also showed minimal height increase with increasing pressure with only a 10% increase between 1 mm/s and 7 mm/s.

The layer by layer freeform fabrication capability of additive manufacturing techniques has previously facilitated the production of three dimensional, off-axis via holes ~1 mm in diameter which can be pumped with conductive inks to form conductive connections between electronics components on multiple planes [83]. Conversely, the creation of structures designed to penetrate subsequent layers of circuitry has been discussed before, whereby trapezoid wedges 12.7 mm x 2.03 mm x 1.52 mm in size were produced to connect adjacent layers [94]. These structures however covered a large area on the substrate and were therefore not suitable for the minimisation of the electronic footprint, in contrast to the capability of the freestanding pillars introduced during Section 5.4 with base diameters of ~500 µm. Additionally, this method requires just a single ICA printing and thermal curing process whereas, to ensure a prefabricated via hole is completely filled to create electrical contact between layers, multiple filling cycles would be required to account for loss of volume due to evaporation and shrinkage of constituents of the conductive inks during curing.

5.4.4   Normalisation of Results for Material Volume and Print Area

Experimentation throughout Section 5.4 has been conducted to determine the maximum height and minimum diameter achievable using the two chosen commercially available isotropic conductive adhesives and three different nozzle sizes (250 µm, 200 µm and 100 µm), each with their own design proportional to the nozzle size. The aim was to maximise the aspect ratio of conductors on the substrate surface and therefore, two parameters that resulted from the variation in design dimension, printing pressure, print gap and nozzle ID size were not included in the investigation; namely, the volume of material deposited and the area over which it was printed. Both these variables do directly affect the pillar dimensions, larger print areas and printed volumes increase the pillar diameter and provide the material capability to produce taller standing structures. It was

148

however concluded during the experimental design that these responses would be controlled through printing pressure.

Dimensions produced through individual nozzles cannot however be directly compared using the printing pressure as a variable. Normalisation of the data to account for volume of material would therefore be required to make this data directly comparable. Microscopy could be used to determine the volume of each printed feature and therefore, the average volume of material deposited for each feature printed with each set of different parameters. By plotting volume against height, diameter and aspect ratio, results produced by different nozzles and using different dispensing parameters can be directly compared using material volume as a common variable. This may prove individual dispensing parameters such as nozzle size, printing pressure and print speed to be irrelevant despite their effect on dispensed volume known to be significant. Determining the relationship between volume and conductor dimensions will show whether there is a linear relationship between volume and individual dimensions or if reductions in nozzle size and changes to other variables are beneficial.

With changes in print design for individual nozzles, the area over which the material is deposited changes. This was designed to account for increased volumes of material resulting from differing nozzle sizes as printing through a larger nozzle over a smaller area, would not form precise sequential layers and was therefore not a viable option. This does however increase the diameter of the printed pillars, reducing the aspect ratio but, it is not the sole variable affecting the diameter as the material behaviour also affects the dimensions. The control over the diameter using different print areas is limited by the slumping of the material, which accounts for significant increases compared to the designed pillar sizes. Although increased diameter is considered detrimental, it provides increased structural stability facilitating increased pillar height. This explanation is supported through the data presented in Section 5.4.3 showing that increasing print area results in increased height and therefore, the optimal combination of print area and material volume would result in a pillar of the required height and the smallest possible diameter.

5.4.5   Pillar Cross Sectional Microscopy

Pillar samples were mounted, ground and polished in an epoxy substrate to the centreline of the pillar structures. The resulting surface was then examined and captured using both a Nikon Eclipse MA200 inverted microscope and an OGP Smartscope Flash 200 microscope. Material A demonstrates a higher abundance of voiding within the pillar structure, located at its core as shown in Figure 5.32. This results from both the manual mixing process used to combine the two parts of the adhesive and the square-helix pillar design. The higher viscosity of the ICA prevents full agglomeration of the material and traps the gas within the structure, stopping it from escaping.
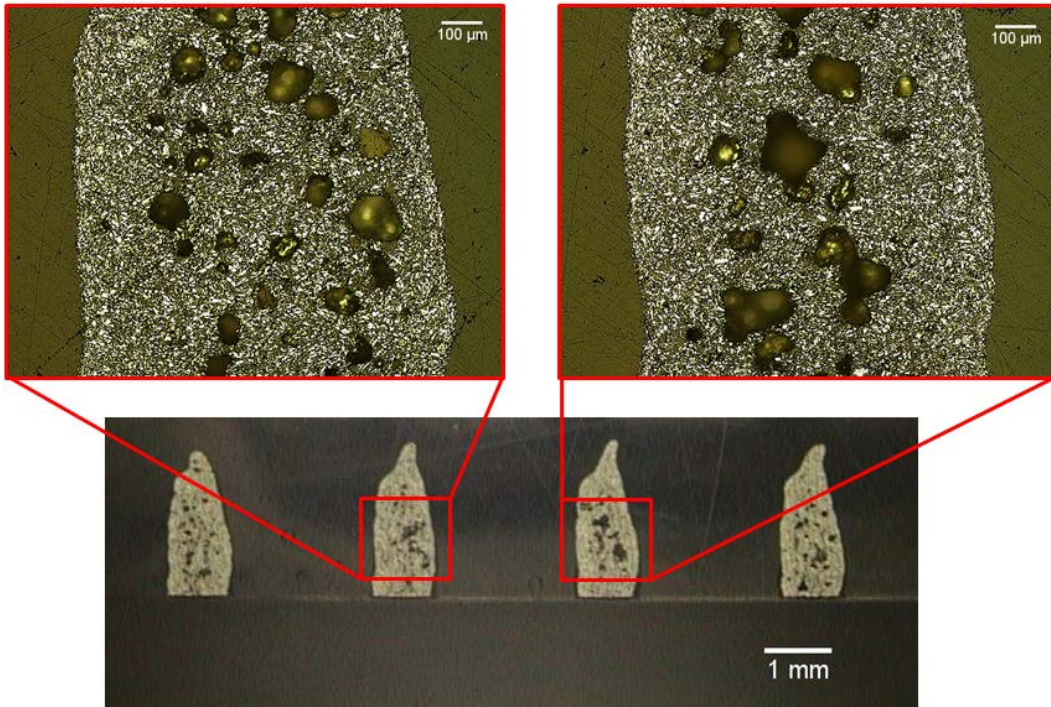
Figure 5.32.   Cross sectional microscopy of pillars printed in Material A

Comparable images in Figure 5.33 show significantly less voiding in the centre of the pillar structures produced in material B. The lower viscosity not only provides an easier escape route for the trapped gases but the increased slumping effect also results in greater coalescence of the ICA and therefore, smaller and less abundant voiding.
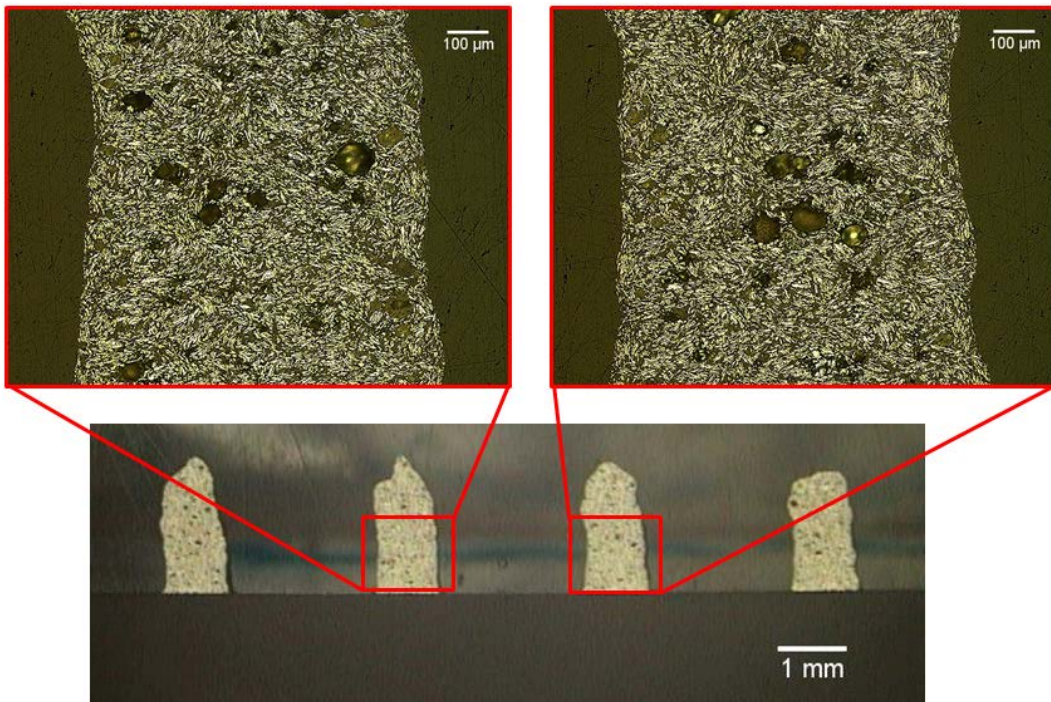
Figure 5.33.   Cross sectional microscopy of pillars printed in Material B

150

Fully dense pillar structures could be produced using either material however a degassing process would be required to remove the gas incorporated into the epoxy during the manual mixing procedure, insertion into the material syringe and the deposition process. This could be conducted by vacuum degassing at any or all of these stages, most importantly once the structure has been printed as all trapped air can be removed in one procedure. The elimination of voiding would increase the volume of conductive material while maintaining the external pillar dimensions, therefore increasing the conductivity of the structure.

5.4.6   Maximising Pillar Aspect Ratio

Following the characterisation of the pillar dispensing process, iterative experimentation was conducted at room temperature using the optimum printing parameters determined in Section 5.4.3 and reintroduced below. Alterations were made systematically to the design height to produce structures with the highest aspect ratio possible that can be applied in multi-layered printed electronics. The design height was increased one layer at a time until the material could no longer support itself, typically causing it to topple over. 250 µm, 200 µm and 100 µm nozzles were used in this experimentation, with the expectation that each would result in different printed pillar characteristics of height, diameter and aspect ratio. With an increase in nozzle size the diameter of pillars also increases therefore, a limit of 1 mm was set on the pillar diameter, outside which any pillars would be discounted as too large. Base diameters larger than 1mm would result in an undesirable increase in the footprint of the circuit, becoming disproportional to the track widths and heights produced using the same nozzle. All experimentation was conducted using materials A and B, allowing one final conclusive comparison to be made between their comparative structural capabilities.

To maximise the pillar height while reducing base diameter, the 10% slump allowance was removed from the design. After analysis of results during characterisation, a pressure of 90 kPa was used to print at a speed of 5 mm/s through a 250 µm nozzle, which previously resulted in a base diameter slightly less than 1 mm. The design prints a total of 8 x 250 µm thick layers in a 500 µm x 500 µm filled square configuration. After dispensing the first design, subsequent pillars were printed with a print height 1 layer higher than the previously successful feature. The height was incrementally increased with five pillars printed at each height until the pillar structures collapsed, proving that the limit had been reached, therefore determining the maximum pillar height that can be consistently produced by each nozzle diameter. The dimensions of the pillar were then measured both to ensure the base diameter is within the 1mm upper limit and to determine the aspect ratio. The resulting profiles are shown in Figure 5.34.

For the 250 µm nozzle the highest aspect ratio was achieved from 16 printed layers. Any value in excess of this caused the pillar to collapse under the weight of itself. At 3.801 mm in height and with a base diameter of 0.979 mm, the aspect ratio was 3.88. The designed height of this pillar at 16 layers is 4 mm, with the 0.19 mm difference explained by the slumping effect resulting from the viscosity of the isotropic conductive adhesive.
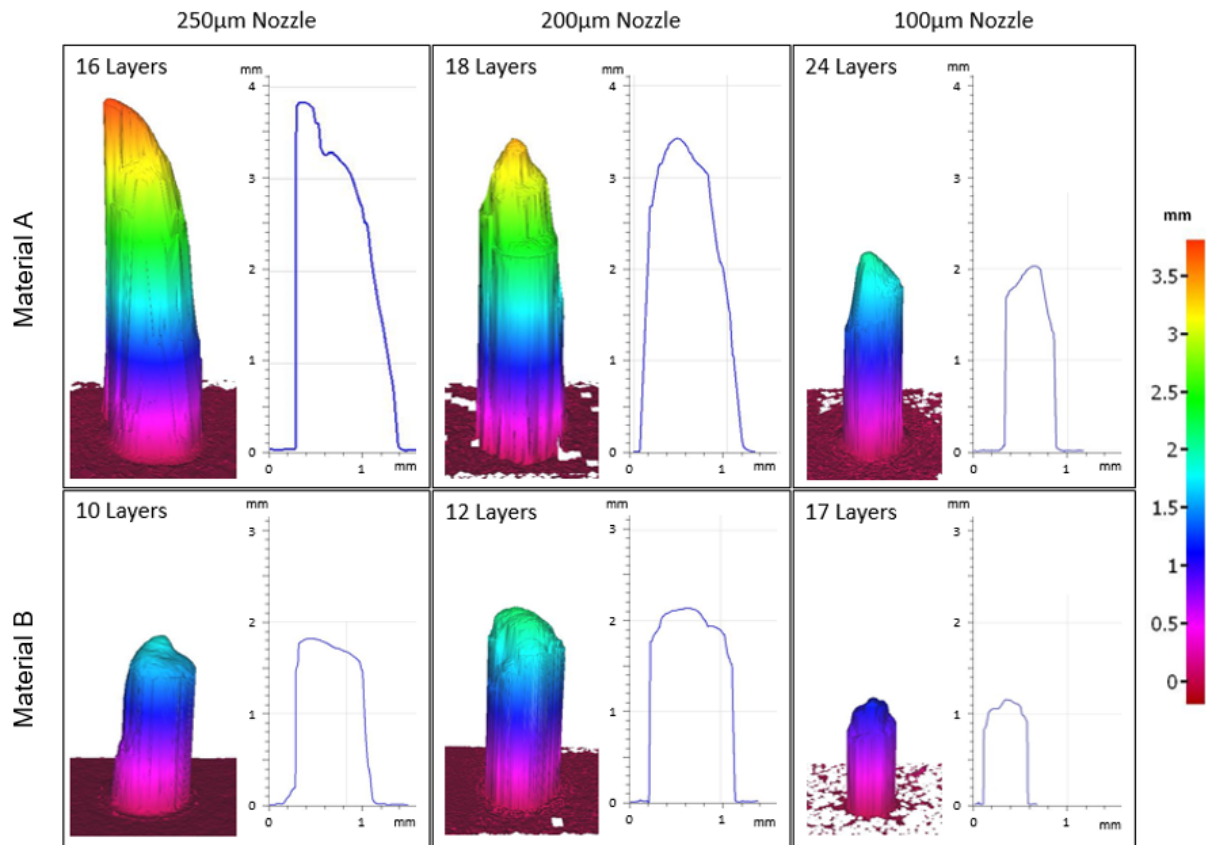
Figure 5.34.   Comparison of the tallest pillar profiles produced using both materials and all three nozzles

The same experimentation was conducted with the 200 µm and 100 µm nozzle IDs to determine any differences in capability. The combination of material A with the 100 µm nozzle produced a 24 layer pillar with an aspect ratio of 3.68 which, despite not being the highest, was in excess of 2 mm in height at a 550 µm base width, allowing it to penetrate the thickest proposed embedding layer while minimising its footprint. The same MuCAD designs were used for these nozzle sizes, again with the 'slump allowance' removed, making the print gap identical to the nozzle ID. Resulting dimensions, number of layers and aspect ratios are detailed in Table 5.6. They have also been compared to their equivalent structures printed in material B.

Table 5.6.   Summary of maximum aspect ratios with pillar dimensions

Nozzle (μm)	Material	No. of Layers	Height (μm)	Base Diameter (μm)	Aspect Ratio
250	A	16	3801	979	3.88
	B	10	1800	1016	1.77
200	A	18	3437	1079	3.23
	B	12	2163	1028	2.10
100	A	24	2033	553	3.68
	B	17	1175	488	2.41

All nozzle sizes produced features higher than the designs in the characterisation process. A maximum of 16 layers were printed using the 250 μm nozzle while 18 could be deposited using the 200 μm nozzle before the structures became too unstable to stand upright, examples of which are shown in Figure 5.35. With a greater layer thickness and base width the 250 μm nozzle was therefore able to produce the highest pillar with the highest aspect ratio.
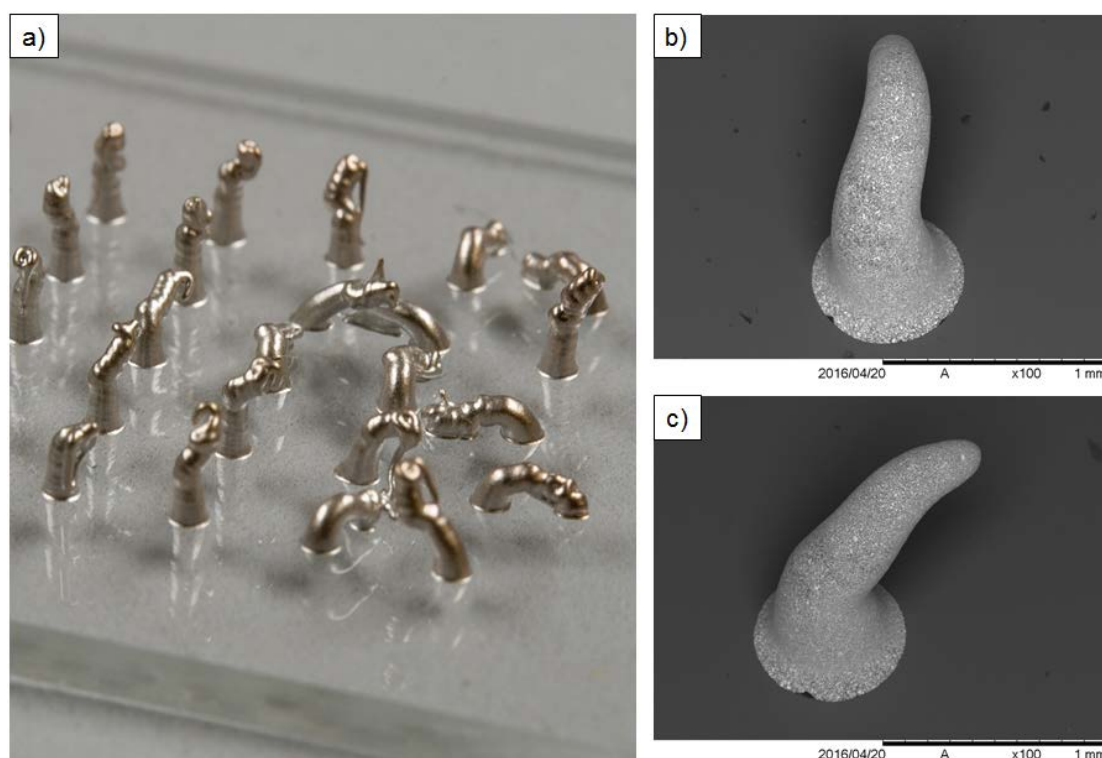
Figure 5.35.   Images of material A pillars printed through a 200 μm nozzle a) partially and fully collapsed due to structural instability; b) SEM image of partially collapsed pillar; c) SEM image of almost fully collapsed pillar

The failure is a result of the pillar becoming unable to support its own weight, causing leaning of the pillar followed by eventual collapse.

5.5 Generic Dispensing Guidelines for ICA Materials

The characterisation of conductor dispensing introduced and evaluated during Sections 5.3 and 5.4 can only be considered repeatable with a pneumatic dispensing system, identical nozzles and the same materials. This is because the internal structure of the nozzles may differ, with different tapering angles to the tip or chamber diameters, changing the flow of material. Additionally, although material viscosities can be closely matched, different materials will display alternate degrees of shear thinning and wetting behaviour, affecting the way they flow through the nozzle and interact with the surface. Table 5.7 introduces generic guidelines for the control of each printing variable that can be followed to aid in the successful deposition of ICA conductors onto photopolymer substrates.

Table 5.7.   Generic guidelines for ICA deposition on photopolymer substrates

Variable	Guideline
Pressure Actuation	Material viscosity should be considered when choosing the actuation method. Pneumatic actuation requires a lower viscosity material than solid state alternatives. It also has a 'suck back' mechanism, creating negative pressure after dispensing and resulting in no leaking from a pressure accumulation.
Dispensing Nozzle Type	A short nozzle tip ensures that the material does not clog in the orifice. Needles should be avoided as a higher pressure is required to deposit material through the needle element and there is a longer distance where clogging can occur. Tapered nozzles to an orifice provide the best solution and reduce the chance of blockage.
Point to Point (P2P) Motion Speed	P2P speed should be kept as high as possible as a reduced 'tailing' effect has been observed with faster nozzle retraction. The type of conductor (e.g. conductive pillars) can require a reduction in the P2P speed as the actuation speed may not be fast enough to keep up with the system movement, printing alternating layers.
Nozzle ID	The choice of nozzle inner diameter is often limited by the maximum particle size of the material. Nozzle manufacturers recommend ratios of between 5:1 and 10:1, nozzle diameter to maximum particle size however, through experimentation, a ratio of 2.1:1 has been proven using Material B in this study. Providing an effective method of cleaning the nozzles has been identified, testing is the most effective way to determine the minimum ID applicable.

Dispensing Pressure	A range of pressures over which the material can be dispensed through each nozzle ID needs to be determined. Pressures outside of these result in no/excess material flow or, in the context of this process, inconsistent deposition creating irregular cross sectional areas on traces and reduced pillar heights. The optimal pressure and speed combination can then be determined for the chosen material.
Print Speed	Print speed is related closely to pressure as higher speeds can be combined with higher pressures to create conductor dimensions similar to those produced at lower speeds and lower pressures. Extremes in print speed can result in poor/no wetting of material to the substrate at the high end, while too low a speed results in the unwanted accumulation of a large volume of material deposited over a short distance, increasing the size of the conductor. This range of effective speeds needs to be identified for new materials.
Print Gap	Theoretically, the extruded material takes the form of the nozzle orifice, resulting in dispensed 'filaments' of the same diameter. No investigation of print gap was conducted during this study however, it is recommended that a 1:1 ratio, print gap to nozzle ID, is used as no apparent contact between the nozzle and material was observed at this distance.

5.6 Optimisation of Thermal Curing Regime for Conductors

The recommended rapid curing regimes for both epoxies cannot be followed as they prescribe temperatures above that which the substrate is capable of withstanding. The specifications refer to the epoxy's ability to cure at lower temperatures however, curing in these conditions had not been previously optimised. Investigation with both epoxies around cure temperature and curing time was conducted and the resultant resistivity of the cured tracks measured.

Table 5.8 shows the analysis of specified curing data allowing the determination of three suitable curing regimes by comparing those of both epoxies recommended by the manufacturer and finding common characteristics. The low glass transition temperature of the photopolymer substrate meant limiting the temperature to ~100 °C.

Table 5.8.   Table of manufacturers recommended and chosen curing regimes

No.	E4110-PFC Spec		EJ2189 Spec		Chosen Regimes	
	Temp (°C)	Time (hrs)	Temp (°C)	Time (hrs)	Temp. (°C)	Time (hrs)
Low	45	6	23	72	45	6
Med	80	3	80	3	80	3
High	120	1	100	1	100	1
V High	n/a	n/a	150	0.25	x	x

Curing regimes were selected as shown in Table 5.7 and tested on uniform tracks dispensed on photopolymer substrates. The effect of the difference in curing regimes was shown through the calculation of changes in volume resistivity of the tracks. The resistivity of the tracks was calculated using Equation 6.

$$\rho = R\frac{A}{L} \qquad\qquad (6)$$

ρ = resistivity

R = resistance

A = cross sectional area

L = length

Unlike the preliminary work which was designed to provide a basic understanding of the behaviour of the conductive materials, resistance is not a suitable unit for comparison. This is because it is significantly affected by the volume of material dispensed, thereby requiring identical track dimensions to provide a relevant comparison. Volume resistivity is calculated using both the cross sectional area and length, therefore accounting for both variables that could cause significant differences in resistance measurements.

Sample length can be designed into the dispensing file, ensuring that the total length of the track is known and cross sectional area can be computed using specially designed Matlab code. Finally, resistance of the track is measured using a four-point probe with the probes positioned in identical locations every time a measurement is taken as shown in Figure 5.36.
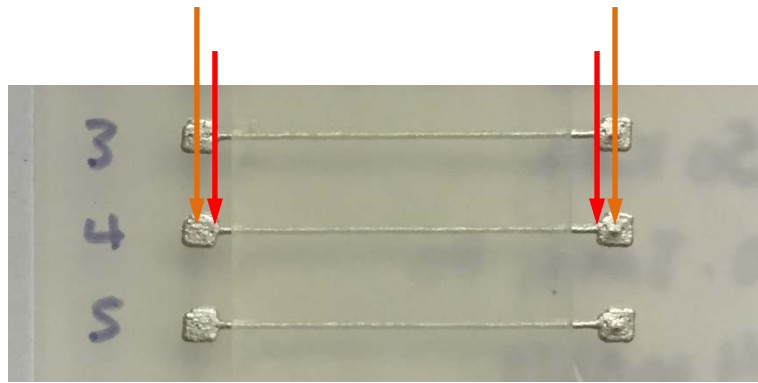
Figure 5.36.   Four point probe measurement positions on 20mm long conductive traces

Outside probes were placed in the centre of the pads and internal probes were positioned at the very ends of the conductive track, ensuring that the measured distance is as close to 20 mm as possible.

After microscopy raw coordinate data was extracted from profiles of the conductive traces taken on the Alicona. This data was inputted into a piece of MatLab code designed to provide the cross sectional area of the trace.

The MatLab code is designed to process the raw data in a number of stages:

1. Raw data is read and formatted into a matrix that can be represented in a 2D or 3D image.

2. The user defines an area either side of the conductive trace to be removed from the coordinate data matrix, reducing the data processing load and keeping the track profile data.

3. Full data profiles at each x-axis coordinate interval were processed and levelled using data from the scanned substrate.

4. Z=0 is then defined from the level of the substrate surface and calculation performed to determine the cross sectional area of the track above that surface for each x-axis interval.

5. Computed cross sectional areas along the full length of the track are then averaged to provide one value of cross sectional area.

The raw data can be interpreted and output in both 2D and 3D formats shown in Figure 5.37 and Figure 5.38, both of which illustrate the input coordinate matrix.
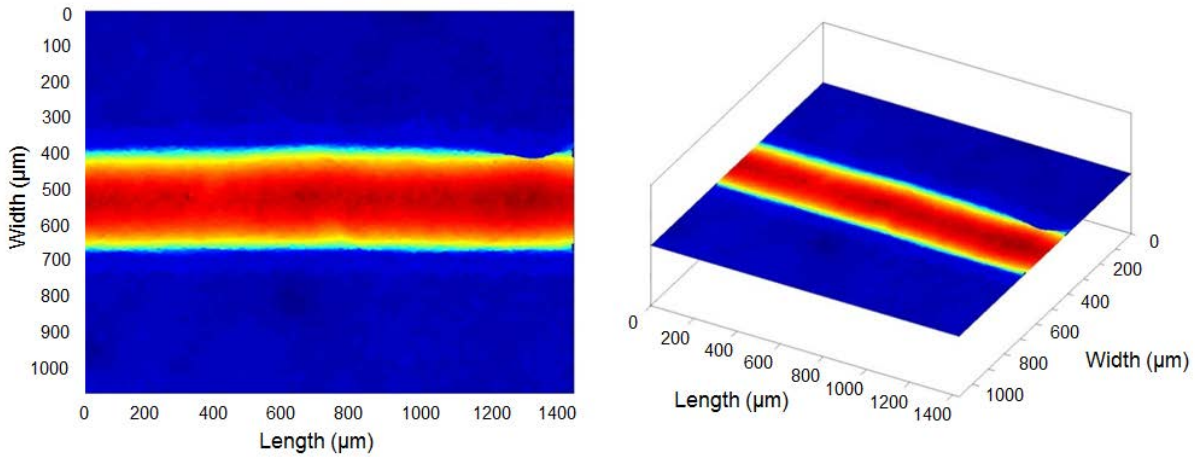
Figure 5.37.   2D representation of tracks produced in Matlab

The 2D representation uses a colour based profile to show differences in z coordinates, however Figure 5.38 gives a useful visual assessment of the track profile.
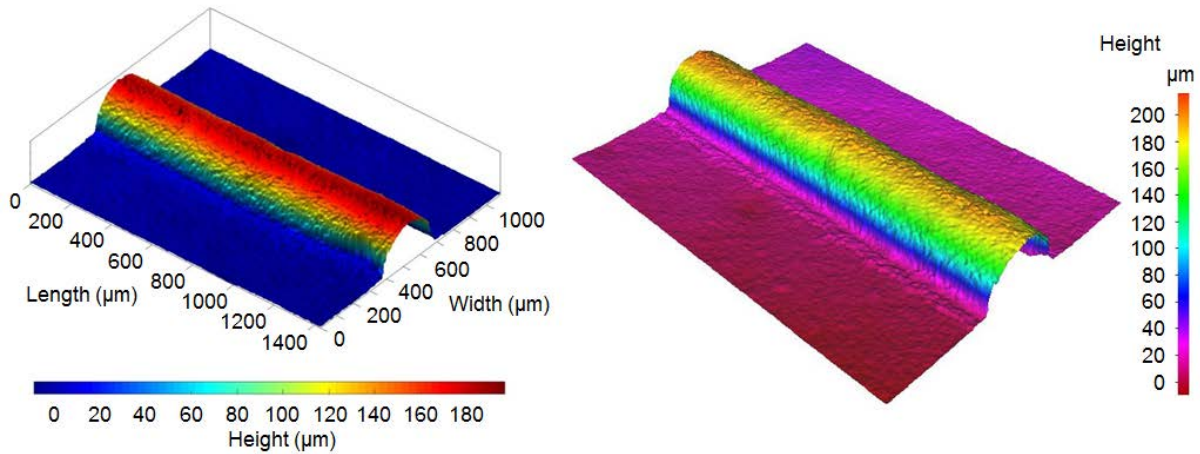
Figure 5.38.   3D representations of tracks generated a) in Matlab and b) on the Alicona Microscope

Three-dimensional representations produced on Matlab do not differ to those produced on the Alicona InfiniteFocus microscope, with a comparison made in Figure 5.38. This data analysis tool has ensured that the calculated resistivity values are as accurate as possible and small profile errors are accounted for.

Conductive epoxies behaved as expected with increasing curing temperature resulting in a lower resistivity of the material. The resistivity difference between the two materials is negligible with exception to the 6-hour regime where material A had a much higher resistivity. The error bars displayed in Figure 5.39 show that the result of curing was consistent across a number of samples, indicating that the process is highly repeatable.
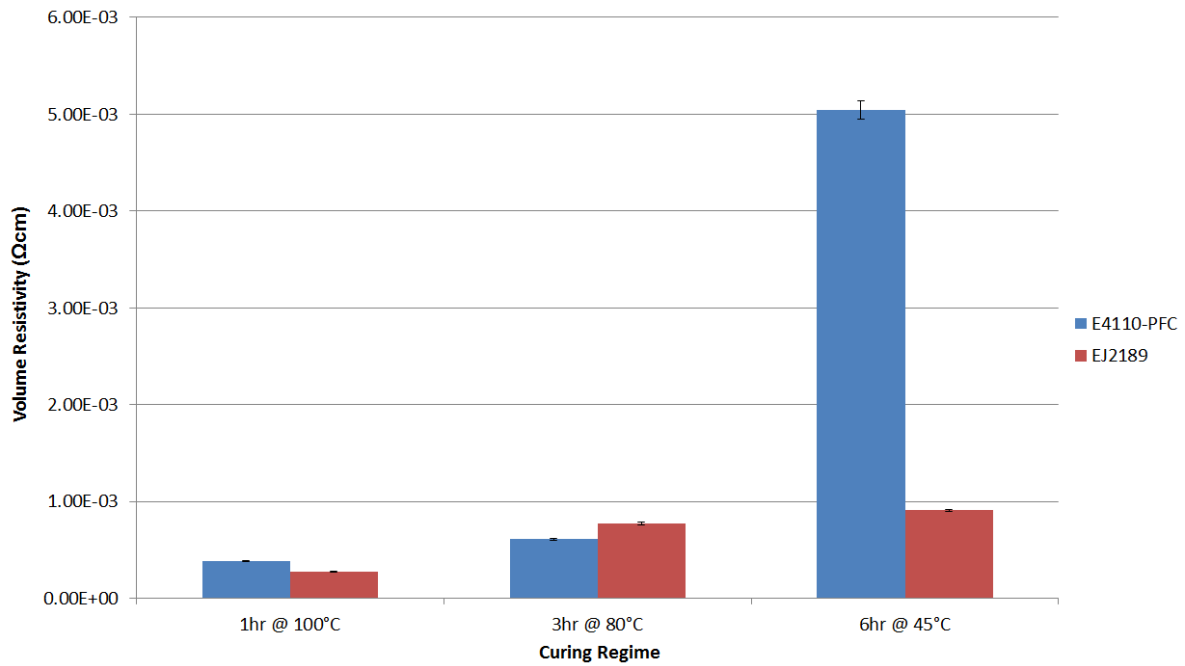
Figure 5.39.   Volume resistivity of three curing regimes on two epoxies

The volume resistivity of these conductive tracks was found to be an order of magnitude lower than the Epotek datasheet specifications, details of which are presented in Table 5.8. This can be explained by the manufacturer underestimating its performance on the specification, therefore ensuring that the material will always exceed expectations.

Table 5.9.   Comparison of specified vs measured resistivity values of conductive epoxy

Curing Regime			Resistivity (Ωcm)	
Source	Temp. (°C)	Time (hours)	E4110-PFC (A)	EJ2189 (B)
Specification	80	3	0.005	0.005
Testing	80	3	0.000609	0.000776
Testing	100	1	0.000381	0.000275

In either scenario, both materials A and B have specified resistivity values of 5×10^{-3} Ωcm when measured at 23 °C after a curing cycle of 3 hours at 80 °C. Under the same conditions, as shown in Table 5.8, both materials had respective resistivity values approximately 10% of that value while, increasing the curing temperature to 100°C halved the resistivity again. This compared with the resistivities of bulk silver and copper of 1.59×10^{-8} Ωm [15] and 1.68×10^{-8} Ωm [14] respectively. Resistivity values from this experimentation are higher than the nanoparticle silver inks previously dispensed and sintered on photopolymer substrates which exhibited a minimum volume resistivity of 2.7×10^{-7} Ωm [83]. These inks were sintered by laser processing therefore fusing nanoparticles and creating a higher conductivity than conductive adhesives can achieve.

5.7   Summary

A Musashi Shotmaster500 dispensing system was used to print isotropic conductive adhesive materials to create conductive tracks, SMD interconnects and through-layer conductive pillars, facilitating the fabrication of multi-layer electronic circuits. This dispensing platform was combined with a pneumatic actuator, providing accurate control of the printing pressure, and a computer system with control and CAD software, allowing custom design files to be uploaded and a wide variety of dispensing parameters to be controlled, including print speed and print gap. A laser surface mapping module also allowed the topology to be profiled and followed maintaining a constant print gap.

Two isotropic conductive adhesives were chosen for their material characteristics. Their viscosity, thixotropic value, resistivity and recommended curing regimes were assessed for their compatibility with a photopolymer substrate. Epotek E4110-PFC (material A) and EJ2189 (material B) ICAs were selected, both exhibited high enough viscosities to prevent dripping through the dispensing nozzle, thixotropic values which would result in any printed structures holding their geometry with minimal slumping and finally, curing temperatures below the ~104 °C glass transition temperature of the substrate.

The capability of the system to dispense traces using both ICA candidates was evaluated using an experiment designed to compare the effect of nozzle ID, printing pressure and printing speed on the height, width and cross sectional area of the subsequent trace profiles. The width and height of the tracks can be decreased through three mechanisms, firstly, decreasing the nozzle ID, secondly, increasing the printing pressure resulting in the deposition of a greater volume of material, and finally, reducing the print speed therefore depositing a greater volume of material per unit of length. The smallest track dimensions were printed at 300 kPa and 7 mm/s through a 100 µm nozzle.

A novel method was developed to create through layer conductive connections between multiple layers of circuitry stacked vertically. Freestanding pillars were designed and printed in a layer-by-layer fashion to produce a structure that could connect adjacent planes. Further dispensing characterisation was conducted to determine the effect of nozzle size, printing pressure and printing speed on the height and base diameter of the pillars. These structures could then be minimised to facilitate reduction in electronic footprint within the embedded electronic system. An iterative investigation was also conducted to produce the maximum achievable pillar height through each nozzle. A maximum aspect ratio of 3.81 was achieved, with a height of 3.8 mm and diameter of 0.98 mm. A 100 µm nozzle was also used to produce a 2.04 mm high pillar with a diameter of

0.55 mm, making this nozzle capable of producing all circuitry required to produce multilayer circuitry with embedding layer thicknesses of 2 mm.

The thermal curing regimes for both ICAs were investigated to reduce the resistivity of the conductors while preventing degradation of the temperature sensitive photopolymer substrate. Three potential regimes were identified by comparing and combining those recommended by the manufacturer before being tested on 20 mm long conductive traces printed in both epoxies on photopolymer substrates. Using profile data captured through microscopy, a Matlab code calculated the average cross sectional area of each trace, producing values that were used to calculate the resistivity when combined with trace resistance and length. The optimum regime was identified as 80 °C for 3 hours, resulting in resistivity values of both materials one order of magnitude lower than their material specifications.

When combined, the results captured during this chapter can be applied to the fabrication of multi-layer embedded electronics resulting in the minimisation of circuit footprint and components and therefore, package size.

6 Process Integration and Electronic Packaging

The successful combination of multiple manufacturing methods relies upon materials and processes to be fully compatible. The substrate fabrication and dispensing processes must successfully interleave together to ensure that multiple layers of circuitry can be created through alternate production cycles on each system.

This research aimed to produce a hybrid process compatible with current electronic packaging technology including surface mount assembly (SMA) and flip-chip packaging. The deposition of ICA conductors onto the substrate surface has exhibited its capability to produce component interconnects and this chapter will introduce its combination with SMA. The potential for use of this deposition technique at a smaller scale, with a narrower pitch, for printing flip-chip interconnects is also presented. Both AM processes have also previously been characterised and optimised for this application in Chapters 3 and 5 and now, the processes of encapsulation or packaging of the circuitry and the resultant electrical and mechanical properties of the package are evaluated.

This chapter will introduce the progression from surface mount assembly to flip-chip packaging and finally, the embedding of circuitry to create multilayer circuits

6.1 Surface Mount Electronic Assembly

Surface mount assembly (SMA), described in detail in Section 2.1, traditionally places devices onto copper pads on a printed circuit board (PCB). The pads are produced via a combination of photolithography and chemical etching and the solder paste is deposited by stencil or screen printing. These small solder paste deposits ensure surface mount devices adhere to the surface and remain in position until the PCB is passed through a reflow oven, resulting in the fusion of particles and creation of highly electrically conductive connections. Isotropic conductive adhesives present a viable alternative to solder paste for low temperature applications where incompatibility with solder reflow temperatures are exhibited. Curing temperatures lower than 100 °C are required for use with photopolymers due to their low glass transition temperature.

Surface mount devices (SMDs) can be passive, active or electromechanical components and include simple two terminal components such as resistors and capacitors, up to packages with tens of contacts like small outline integrated circuits (SOICs) and ball grid arrays (BGAs). Two terminal SMDs are available in a range of sizes to suit their application from imperial code 2512 to 01005, with further descriptions provided in Section 2.1.

A vast majority of research conducted into hybrid AM of electronics through a combination of stereolithography and material dispensing has used through hole component technology. This allowed components and their legs to be placed into prefabricated trenches and channels and, ink cured in the same structures to create interconnects. The progression of this technique saw the introduction of SMDs which were press fitted into trenches upside down, exposing the interconnects and allowing conductive inks to be deposited into trenches and onto the SMD interconnects before laser curing. The need for channels arises from the low viscosity of the ink and therefore prevents deposition directly onto the surface [83].

The use of isotropic conductive adhesives allows conductors to be deposited on the surface of the substrate as shown in Chapter 5 and therefore, the process introduced during this thesis is able to use traditional surface mount assembly.

To that end, an electronic circuit was produced by combining all production methods described during Chapters 3, 4 and 5. Its fabrication began with the layer by layer photopolymerisation of the substrate material using the Stereolithography process before being cleaned using a combination of D-Limonene and ultrasonic agitation and, being exposed to an additional dose of UV light to reduce surface cracking. Material dispensing was then used to add conductive traces, through layer pillar connections and component bond pads to the substrate surface to create a single layer circuit.. This was done by aligning the substrate under a camera in the dispensing system, setting the origin and using a pre-programmed tool path generated by CAD software to deposit the viscous conductive adhesive onto the substrate surface. Figure 6.1 shows how surface mount components have then been placed directly onto the bond pads created during material dispensing, completing the layer of circuitry and electrical connection. This substrate was then placed in a thermal oven to cure the ICA and secure the components to the surface. 1206 components and a Mini Small Outline Package (MSOP) with dimensions of 3.2 mm x 1.6 mm x 1.1 mm and 4.9 mm x 3.9 mm x 1.75 mm (1.27 mm pin pitch) respectively were successfully positioned on interconnects dispensed using a 250 μm diameter nozzle, proving the feasibility of mounting surface mount devices onto the surface of additively manufactured substrates. The dispensing characterisation experimentation conducted in Section 5.3 proved that achievable conductive trace widths facilitated the use of 0603 SMDs and Thin Shrink Small Outline Packages (TSSOPs) with dimensions of 1.6 mm x 0.8 mm x 0.8 mm and 4 mm x 3.3 mm x 1.15 mm (500 μm pin pitch) respectively. This capability has been demonstrated in Figure 6.1 as it shows a single layer of circuitry with 0603 SMDs and a (TSSOP) mounted on dispensed ICA features. This example has a circuit footprint of 8 mm x 8 mm, improving on the 25 mm x 15 mm circuit achieved with larger 1206 SMDs.
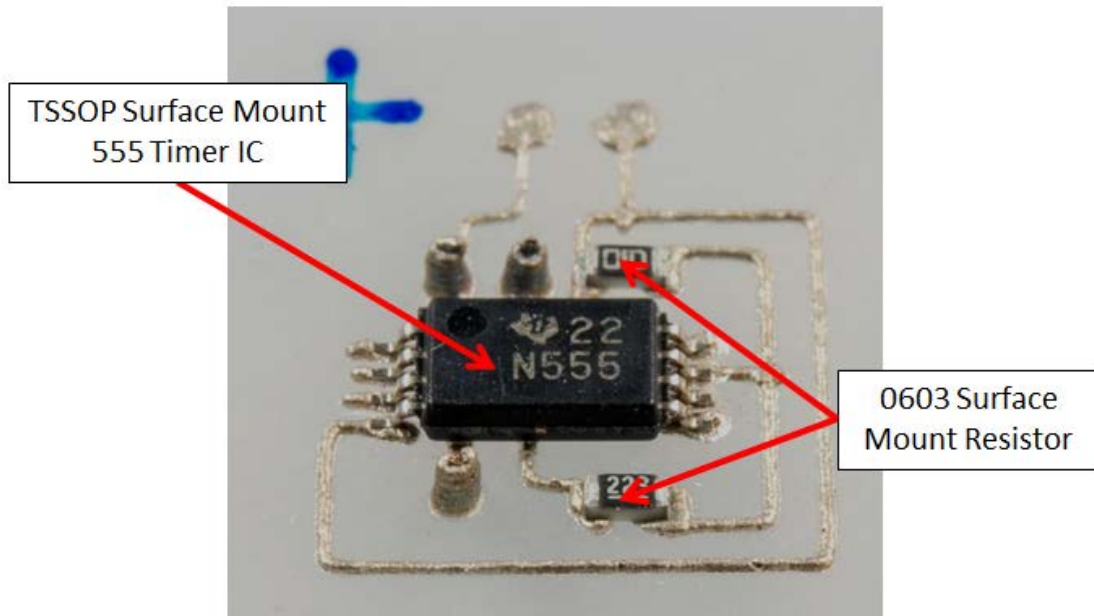
Figure 6.1.   Surface mounting of resistors, capacitors and thin shrink small outline package on dispensed conductors printed on a photopolymer substrate

6.2   Flip-Chip Packaging

The hybrid approach to the fabrication of multi-layered electronics using both Stereolithography and dispensing processes has indicated a resolution high enough to conduct flip-chip packaging of bare silicon die using a photopolymer substrate and conductive epoxy to deposit the interconnections. This process is not compatible with solder based processes as it is conducted at a low temperature (<100 °C) however; this characteristic demonstrates its suitability for application with technologies that require low temperature processing such as liquid crystal displays that are easily damaged by a high temperature reflow process. This method also incorporates a number of the benefits of FC packaging including high density interconnects, reduced packaging footprint, minimised cross-talk and inductance. These advantages were presented in detail in Section 2.1.4.

Flip-Chip on Board (FCOB) and Flip-Chip in Package techniques were explored, using the Stereolithography process to generate the photopolymer substrate, underfill material and embedding / encapsulation of the bare die as shown in Figure 6.2.
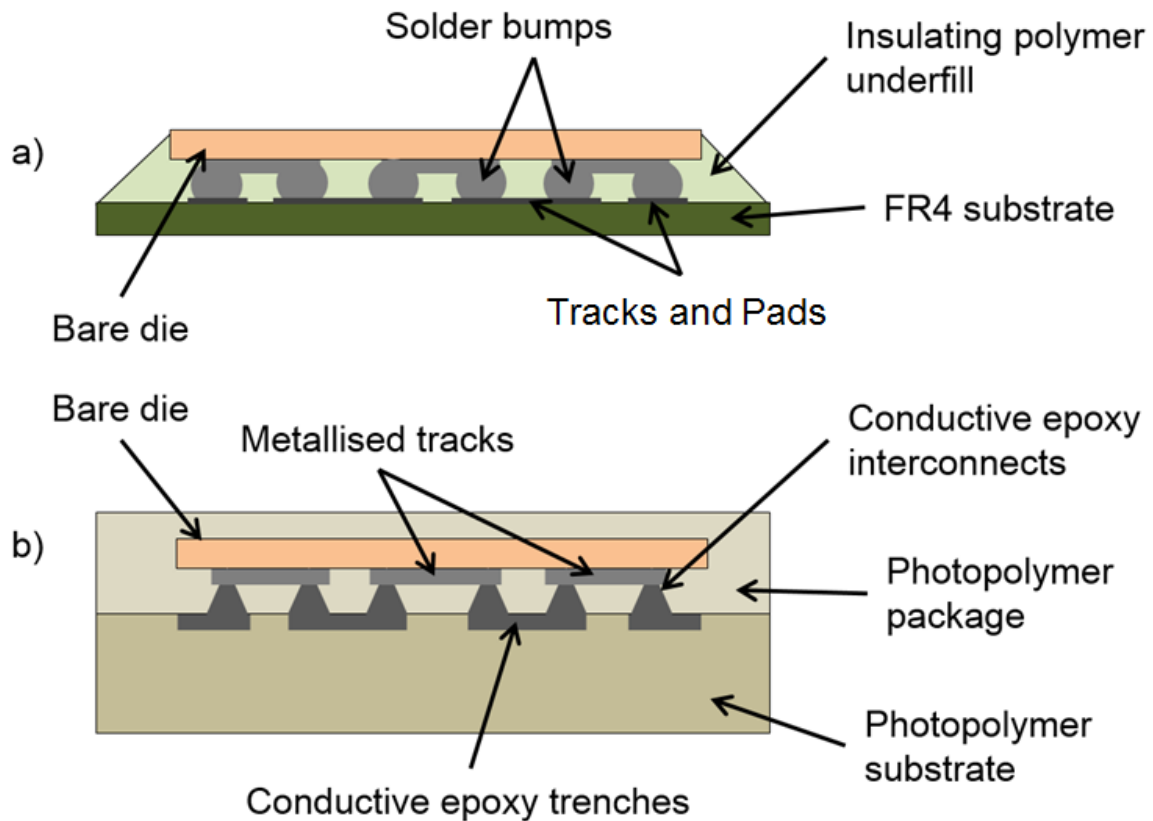
Figure 6.2.   Examples of a) traditional solder based FC on board and b) additively manufactured flip chip packages

The primary goal of this experimentation is to successfully conduct FCOB packaging using Additive Manufacturing. If successful this process could easily be adopted to flip-chip in package. Two methods are proposed in which flip-chip packaging can be achieved through additive manufacturing techniques. Firstly, the Stereolithography process can be used to produce channels in a photopolymer substrate. The digitally driven aspect of this additive manufacturing process allows the channel size to be customised and matched to the chosen die design. These channels can then be filled with a conductive epoxy, thermally cured and the surface polished to ensure a completely flat surface with no trace of excess conductive material. An interconnect bump is then deposited on the end of each of the sunken channels, designed to align precisely with the conductive pads on the bare die and complete the electrical connection as shown in Figure 6.3(a). The second method requires a much greater line dispensing resolution as conductive traces the same length and width as the channels in method one would be fabricated on the substrate surface; this is summarised in Figure 6.3(b).
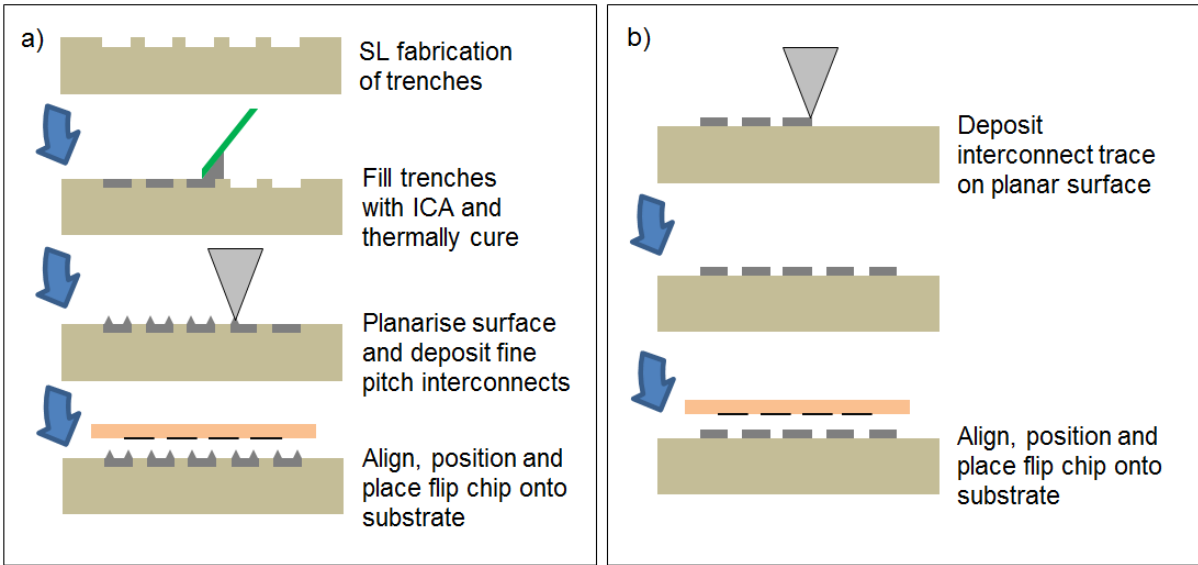
Figure 6.3.   Additive manufacturing FC by a) method 1; b) method 2

Method A provides a planar surface onto which high resolution fine pitch interconnects can be printed, this more closely resembles the conventional FC packaging process and was therefore investigated in further detail. This process was proven using a perimeter pattern daisy chain die. A daisy chain allows each connection to be tested to ensure successful electrical connection has been made between each pad. These patterns also facilitate microscopy of cross sections of a number of connections, providing a determination of the bond quality and repeatability of the process.

Figure 6.4 shows both a schematic and an image of the pattern on the base of a Topline 6.3 mm x 6.3 mm daisy chain perimeter die. An opposing mirrored pattern is required in ICA on the substrate to successfully complete the daisy chain pattern.
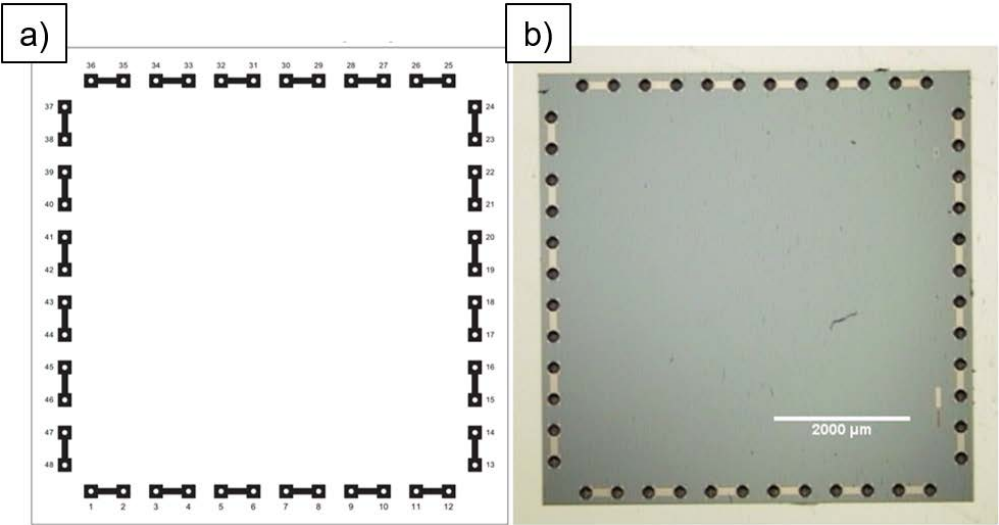
Figure 6.4.   Daisy Chain Flip-Chip Pattern a) schematic and b) micrograph

Figure 6.5 shows the dimensions and pitches of the metalized pads are 457 μm pitch with a diameter of 190 μm. These pads are pre-bumped with 187 μm diameter and 140 μm high lead free SAC (Sn/Ag/Cu) solder bumps as samples without solder could not be sourced.
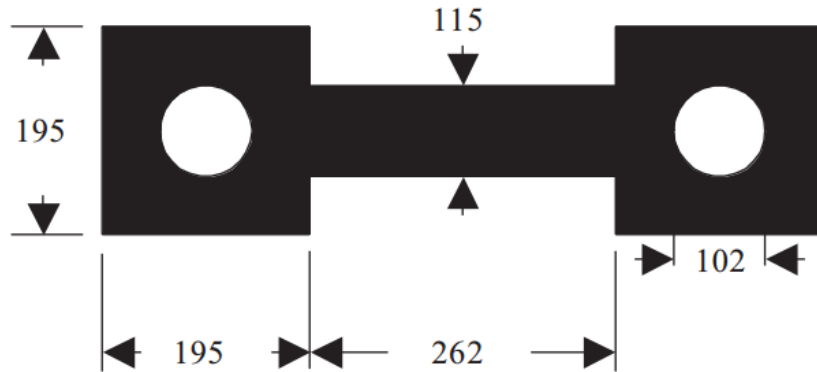
Figure 6.5.   Daisy Chain Pattern Dimensions (microns)

Epoxy deposition could occur by two methods, firstly, the inverse of the flip-chip artwork could be deposited onto a blank photopolymer substrate before the chip is flipped, aligned, placed and thermally cured. Alternatively, the inverse of the daisy chain artwork could be dispensed directly onto the underside of the flip-chip with contact tracks and pads printed on the photopolymer substrate. The chip could then be flipped, positioned relative to the test pads, placed and cured.

6.2.1 Flip-Chip Packaging Substrate Preparation

The high resolution of the Stereolithography system facilitates the layer-by-layer fabrication of substrates with small surface channels. This pattern can be customised to suit the bare die pattern, specifically a daisy chain pattern around the perimeter of the die. The subtracted features on the photopolymer were then filled with epoxy using a doctor blade, sweeping the conductive material across the surface. The capability of the bottom-up Stereolithography process results in flat substrates required to make the material spreading process successful and prevent scratching of the surface. Once the channels have been filled, a fibreless cloth and Isopropyl Alcohol was used to clean some excess material from the surface, leaving epoxy filled features and traces of silver material before being cured. A high degree of accuracy and planarity is necessary to ensure precise alignment can be achieved. An additional lapping and polishing step was conducted to remove any sliver residue left over from the spreading process, and to ensure the substrate is completely flat. The substrate was designed to be polished, with a feature depth of 200 μm, ensuring that defects in the surface up to 100 μm in depth can be removed while enough conductive material remains to create a sufficient electrical contact. This polished surface and the two processing stages leading to the resulting substrate are shown in Figure 6.6(a)-(c), before the interconnects are deposited.
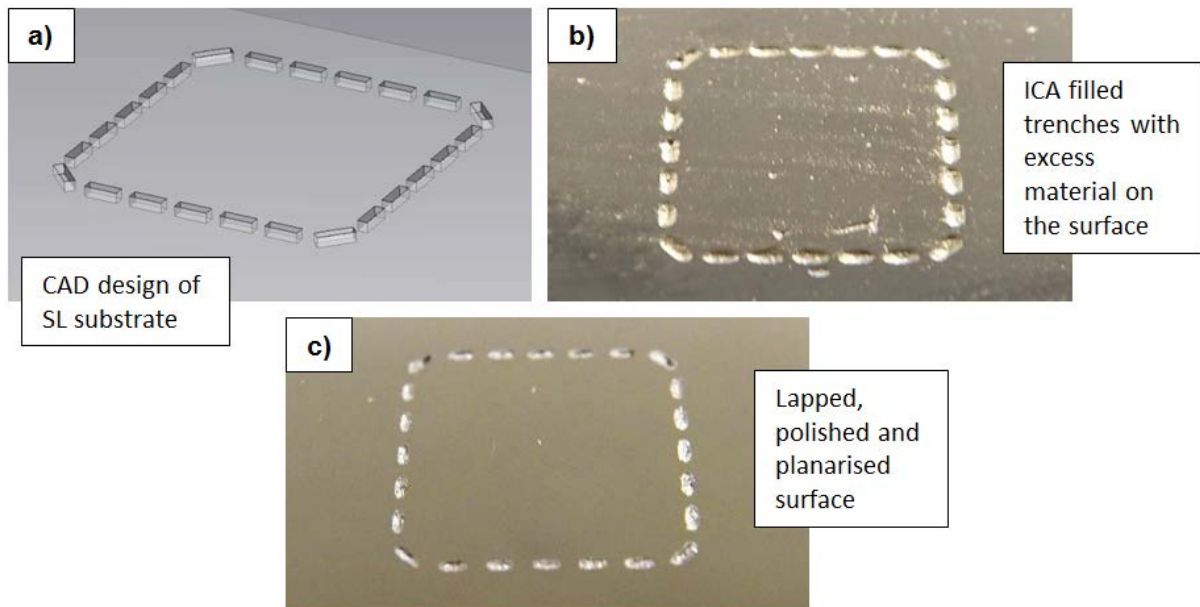
Figure 6.6. Three stages of flip-chip trace development in a photopolymer, a) CAD design of substrate with 600 μm long channels; b) channels filled with ICA; c) filled channels and surface planarised

In this particular application, the channels have dimensions of 644 μm x 200 μm x 200 μm, and require connection with UBM pads 195 μm x 195 μm, as shown previously in Figure 6.5. A high degree of control over bump height and diameter is therefore necessary; to ensure all the interconnections make contact with the bond pads on the die. Also deposits must be limited to a diameter of 300 μm to ensure no shorting occurs between the interconnects.

6.2.2 Characterisation of Dispensing Process for ICA Interconnects

The integrated Musashi CAD package allows the design with dimensions identical to the SL design to be produced. The location of conductive epoxy deposition can be controlled relative to a datum or alignment feature ensuring that bumps are dispensed on either end of each filled channel. Characterisations of the dispensing system and two candidate conductive epoxies were conducted to determine the most favourable printing parameters to produce a suitably sized interconnect. Four different variables were assessed for their effect on the diameter of interconnects including the epoxy, printing pressure, print gap and the printing actuation time. Material, pressure and actuation time, previously controlled through nozzle speed, have all been proven to impact the printed geometry; however, the inclusion of the print gap variable should aid in the deposition of smaller volumes of material as it will contact and wet to the surface sooner therefore, potentially reducing the bump diameter.

Differing material viscosities resulted in differing interconnect profiles, with the higher viscosity material A (E4110-PFC) producing higher sharper conical peaks, caused by an increased tailing effect. Lower viscosity material B (EJ2189) detaches more easily from the nozzle, creating a cleaner break

after dispensing and little or no tail. These characteristics are displayed in Figure 6.7(a) and Figure 6.7(b) respectively.
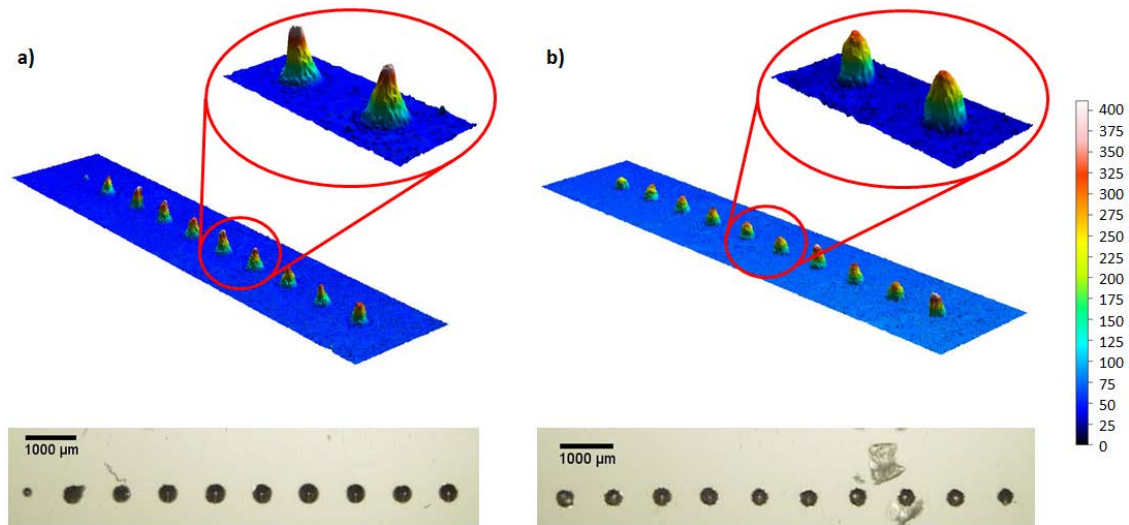
Figure 6.7.   Comparison of interconnect profile in ICA materials a) A and b) B

A wider range of pressures could be used to dispense the higher viscosity material A as the volume of material deposited increases more gradually with increased pressure than in materials of a lower viscosity. This also results in the relationship between bump profile and print gap being more critical, with the material making contact with the substrate surface sooner and therefore wetting faster. This thereby produced smaller features when actuation times and pressures are kept constant, all shown in Figure 6.8. An increase in actuation time showed the same result as that in chapter 5, increasing the volume of material deposited and therefore the resultant bump diameter.
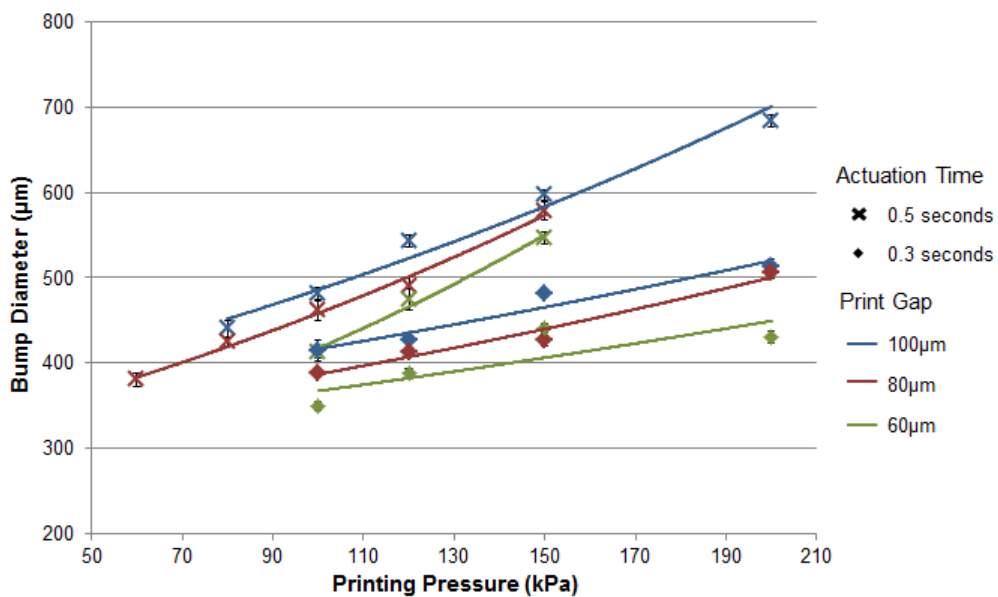
Figure 6.8.   Relationship between interconnect bump, print gap and print actuation time in material A through a 200 μm nozzle

The same experimentation with material B, plotted in Figure 6.9, demonstrated a similar grouping of actuation times however, the print gap demonstrates very little relationship with the corresponding bump diameter. With a lower viscosity and already demonstrated slumping of this material, the material wets easily to the substrate regardless of these tested distances between the nozzle and substrate. Actuation times of 0.2 s and 0.1 s required different printing pressures which negated the time difference, creating interconnects with very similar dimensions.
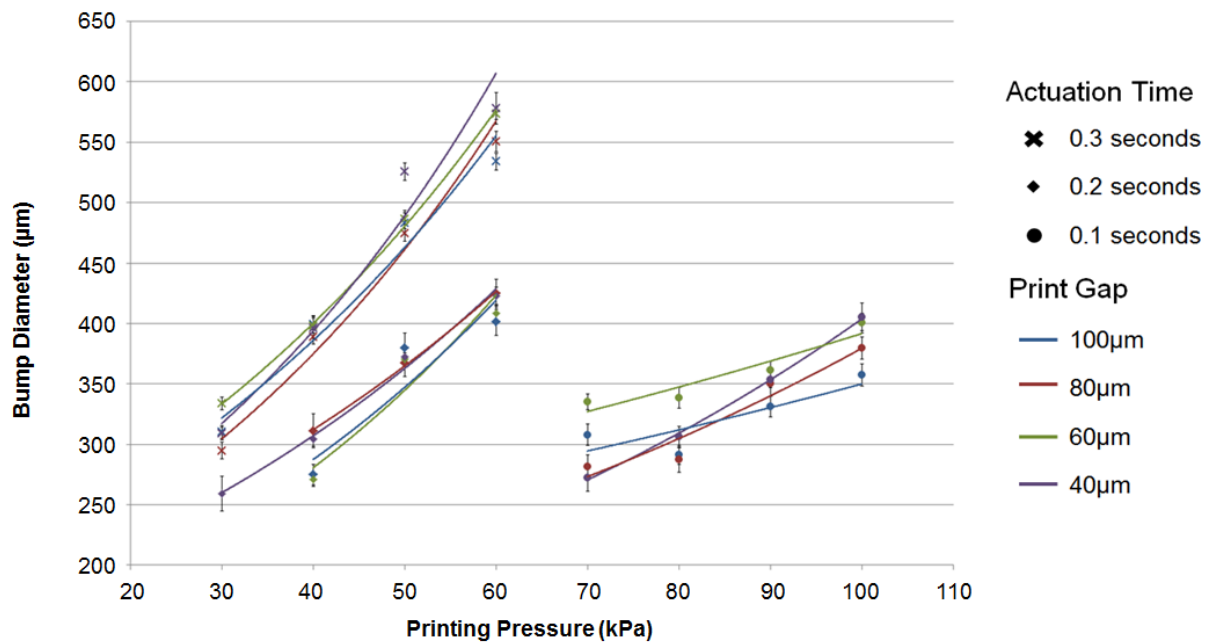
Figure 6.9.   Relationship between interconnect bump diameter, print gap and print actuation time in material B through a 200 µm nozzle

Using a 200 µm nozzle bump heights between 330 µm and 250 µm were achieved, with the addition of a bonding pressure during packaging, the resulting chip standoff was 160 µm and therefore comparable to the 140 µm solder bumps prefabricated on the daisy chain test die. Height and width demonstrate a positive correlation and increases in both can therefore be explained by a greater volume of material deposited.

Changes in pressure result in significant changes in bump diameter as a result of the change in material deposited. Figure 6.10 shows an array of dispensed interconnects produced using three different pressures, 40 kPa, 50 kPa and 60 kPa and, increasing 399 µm, 483 µm and 534 µm base diameters. This shows the significant difference that very small changes in pressure can have on the shape of the interconnect, specifically the base diameter.
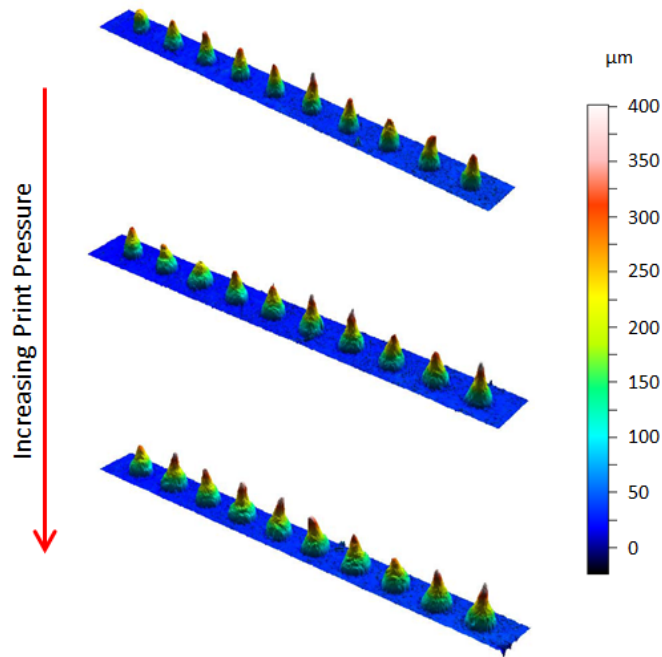
Figure 6.10.   Effect of increasing print pressure from 40 kPa to 60 kPa (top to bottom) on interconnect diameter in material A

Optimally this process would deposit small bump diameter with the highest possible aspect ratio providing a good height standoff and robust connection and, ensuring that all UBM pads make and maintain contact with their uncured epoxy interconnect when the die is flipped.

In order to try and reduce the interconnect sizes further a 100 µm nozzle was also investigated to print the interconnects. The most consistently printed features were produced using a 60 µm print gap, Figure 6.11 shows the relationship between pressure and actuation time through a 100 µm nozzle at a 60 µm print gap.
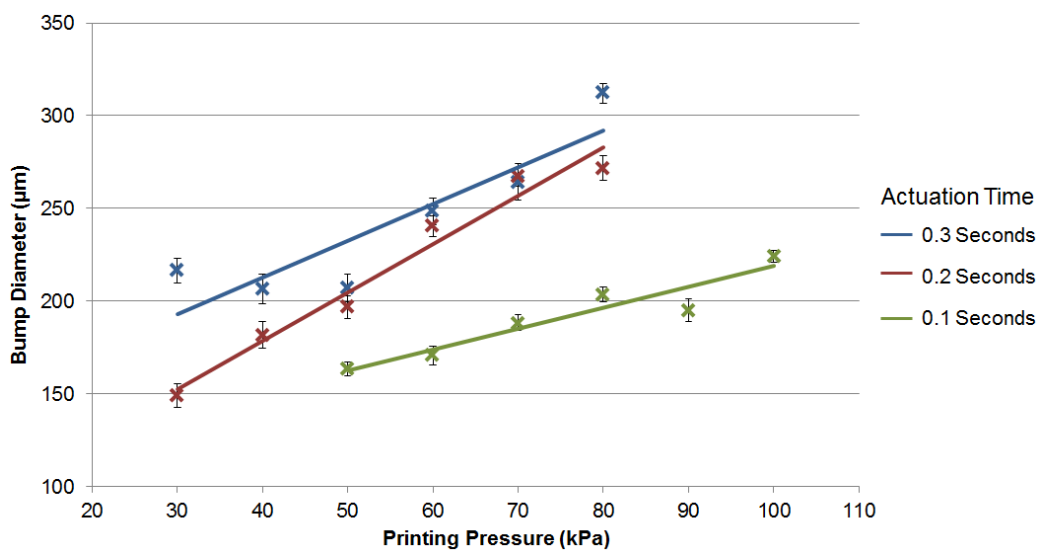
Figure 6.11.   Effect of actuation time and printing pressure through a 100 µm nozzle and 60 µm print gap

171

Figure 6.12 shows the smallest consistent interconnect produced was 149 μm in width and 80 μm in height, produced at a 30 kPa pressure, 60 μm print gap and pressure actuation time of 0.2 seconds. These 80 μm high interconnects would minimise the chip standoff, lower than that achievable using the 187 μm pre-bumped daisy chain test die but provide an avenue for future miniaturisation and for packaging even finer pitch flip-chip devices.
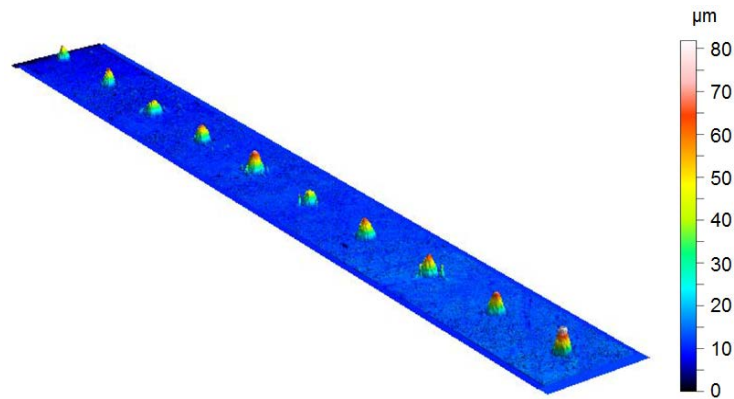
Figure 6.12.   3D profiling and 2D imaging of smallest deposited interconnects produced through a 100 μm nozzle at 30 kPa pressure and 60 μm print gap over 0.2 seconds of actuation

Once optimal parameters were experimentally found, they could be applied to the daisy chain specific design, to ensure than no shorting was observed between interconnects. Glass was initially used as a low cost test substrate with ideal qualities in terms of surface roughness and flatness. After imaging all samples using the same microscope magnification, the interconnect pattern, base substrate with filled channels and bare die with daisy chain pattern could be overlaid. These results demonstrated the alignment that is achievable from integrating these three individual processes. Figure 6.13 shows the overlaid patterns and shows that UBM tracks and pads are connected by the filled channels and interconnects as designed.
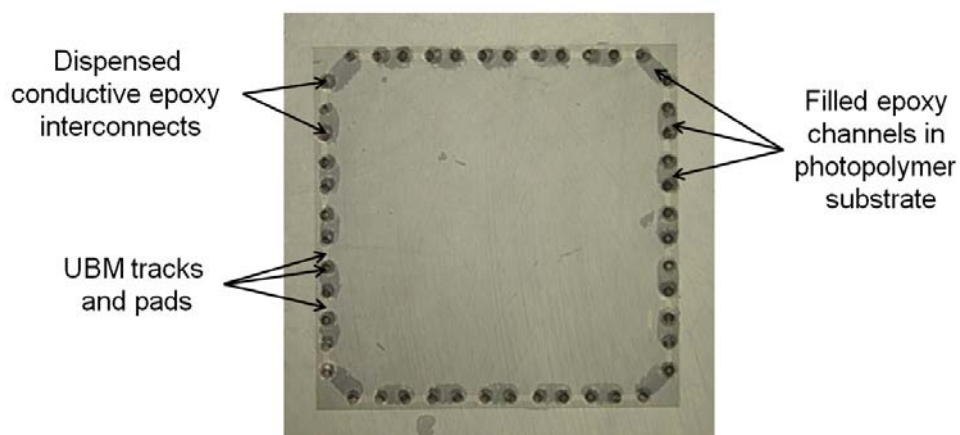
Figure 6.13.   An overlaid image of filled substrate channels, dispensed interconnects and bare die patterning

Further testing of the dispensing pattern was conducted on photopolymer substrates, ensuring that wetting properties of glass and polymers did not differ significantly. This also confirmed that the epoxy filled substrate could be successfully positioned and aligned relative to the dispensing nozzle, and interconnects deposited on either end of the filled channels did not contact the adjacent feature. Figure 6.14 shows a developed daisy chain substrate design that allows the electrical characteristics of interconnections to be tested, providing a method by which faulty connections can be diagnosed.
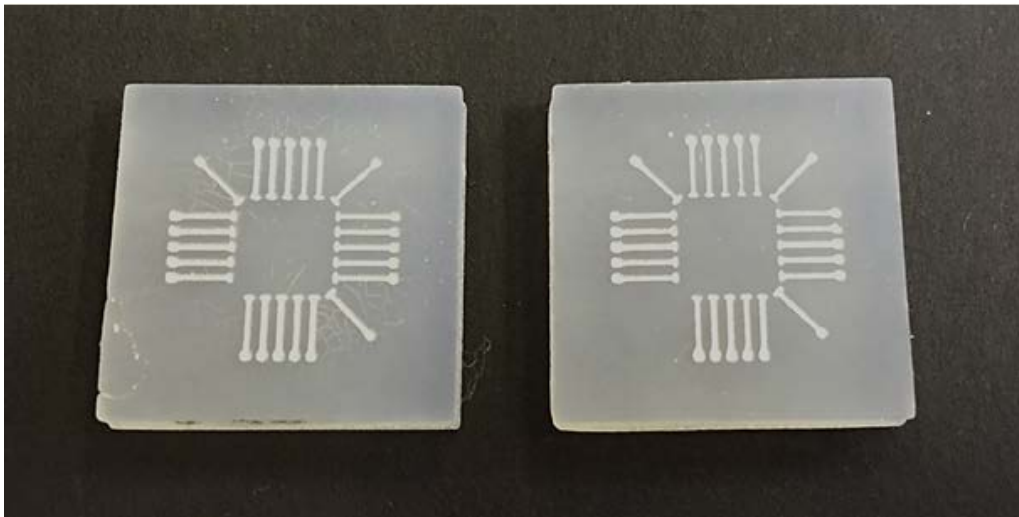
Figure 6.14. Fabricated photopolymer substrate with redistribution tracks for electrical testing

Each filled trench has a conductive redistribution trace and pad connected to it. Using a 4 point probe, the resistance between adjacent pads were measured to determine the quality of the connections. This was in particular to assess if the gap between UBM on the flip-chip has been bridged and to evaluate the electrical characteristics of each interconnection.

In comparison, stencil printing of low temperature ICAs has resulted in the deposition of sub-100 μm pitch flip-chip interconnects through 20 μm orifices at pitches of 90 μm [31]. Deposits with a diameter of ~50 μm and a height of ~15 μm were demonstrated through stencils produced using advanced microengineering techniques [32]. Despite its capability to produce interconnect dimensions 60% smaller than those produced using material dispensing in this experimentation, the process still exhibits a lack of flexibility due to its template driven nature, making it highly suitable for mass manufacturing but not for the low volume, bespoke production for which this hybrid additive manufacturing process has been developed.

6.2.3 Flip-Chip Alignment, Bonding and Testing

Due to the low temperature curing capability of the conductive epoxies, once the interconnects have been dispensed, the alignment of the chips needs to take place within a short time frame. A manual flip chip bonder was used with an optical prism splitter, allowing both the chip and substrate to be

seen through the same eye piece. Micro positioners enable the alignment of the substrate relative to the chip placement arm. The chip, secured to the placement nozzle using a vacuum, can then be placed once aligned by rotating the positioning arm 90 degrees, making the chip and substrate parallel. This mechanism is displayed in Figure 6.15.
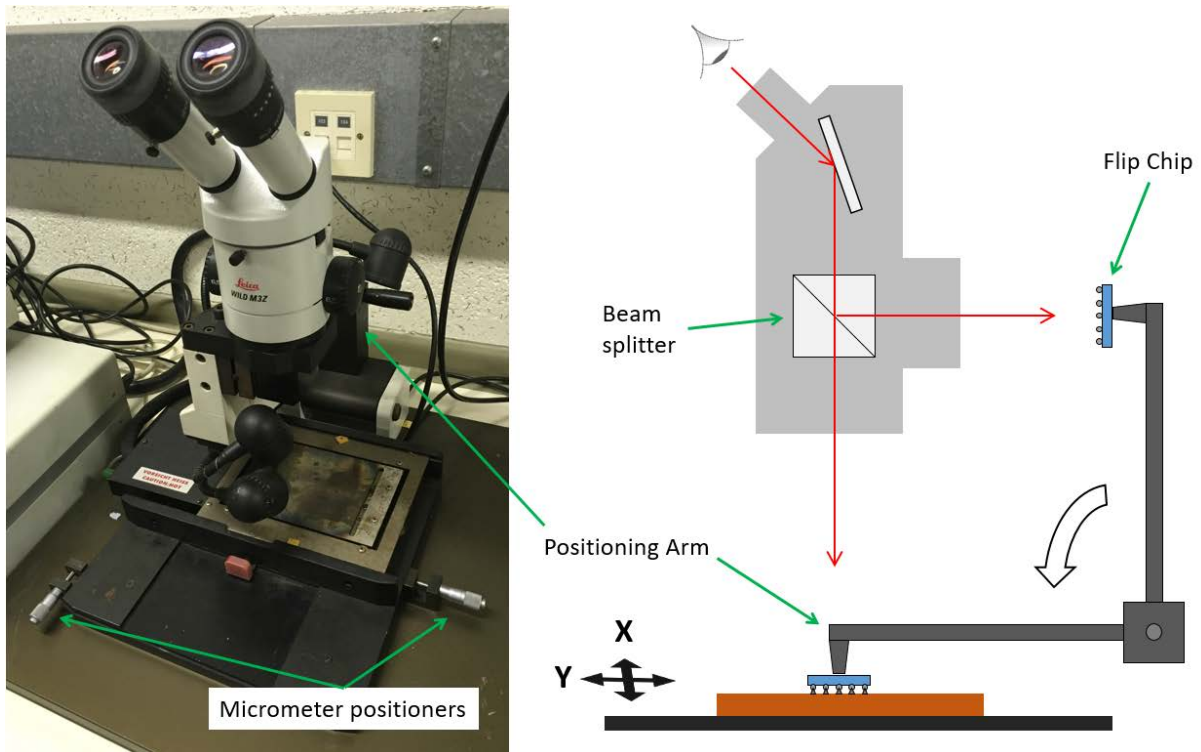
Figure 6.15.   Manual flip-chip alignment apparatus and function

The pressure exerted on a chip after positioning is an important process parameter. Too high a pressure will cause the wet epoxy to spread and contact, creating a short. Too low a pressure may only cause the tips of the highest interconnects to connect as a result of the natural variation of deposited bumps and also creates a very small bonding area to the pads on the die reducing the reliability of the packaged chip. Initially, die were positioned on the surface and subjected to no additional pressure, a second experiment was conducted whereby a placement force of 0.08 N was applied in the centre of the chip after alignment by placing a small weight in the centre of the chip, exerting a uniform force across the chip and corresponding interconnects. The uniform pressure resulted in improved electrical properties manifesting as a reduction in the resistance of the daisy chain circuit. This can also be represented visually through the height of the solder bumps off the substrate surface as shown in images of low and high pressure conditions in Figure 6.16(a) and Figure 6.16(b).
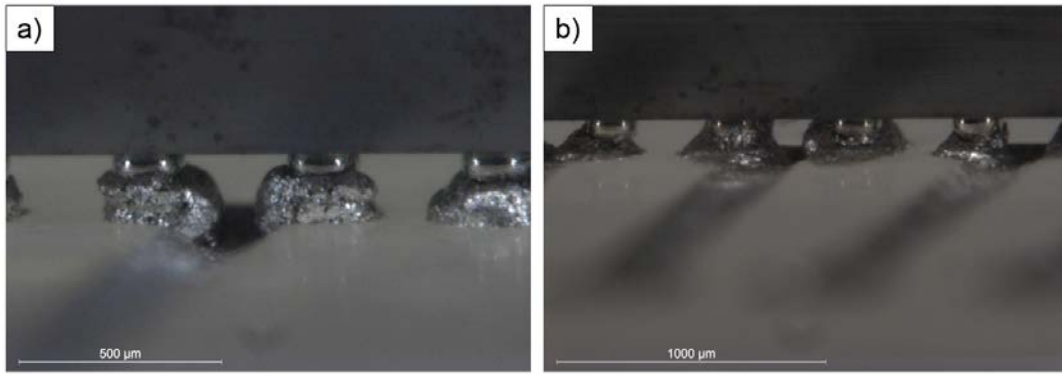
Figure 6.16.   Chips bonded with forcess of a) 0 N and b) 0.08 N

A number of errors during the packaging and positioning process can cause failed connections between UBM and epoxy bumps. The two most common errors are inconsistent deposition of epoxy interconnects, resulting in different bump heights and misalignment of the flip-chip during positioning, reducing electrical contact and increasing the contact resistance. These issues are shown in Figure 6.17(a) and Figure 6.17(b). The deposition process relies upon a consistent flow of material through the printing nozzle and adhesion of the uncured epoxy to the substrate surface, resulting in uniform deposition. In cases where the flow is interrupted or epoxy substrate adhesion is not strong enough, the interconnects are not correctly formed. This results in a low bump height followed by a higher adjacent bump height caused by the additional deposition of extra material which accumulated after previously failed deposition. Inconsistencies in the function of the flip-chip positioning system with prism splitting optics has caused misalignment between the interconnects and UBM. This misalignment has resulted in one of two scenarios, firstly, errors greater than 150 μm result in a total failure to create electrical contact between the UBM and epoxy bump and secondly, a misalignment of between 0 μm and 150 μm creates a reduced contact area and therefore increased contact resistance. As this was a manual alignment method, operator skill was crucial to achieve well aligned interconnects across the full design area.
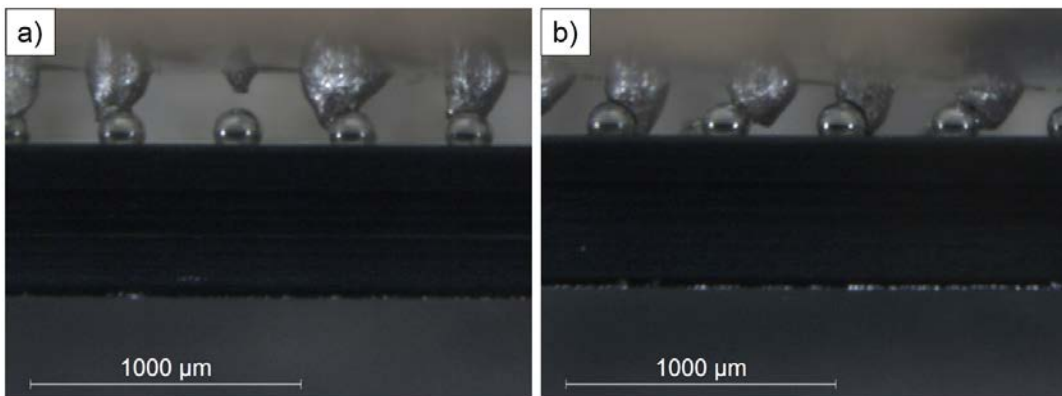
Figure 6.17.   SEM images of a) inconsistent interconnect dispensing; b) chip misalignment

Small inconsistencies in deposition can be compensated for through the addition of a placement pressure when the chip is flipped. This reduces the standoff height and ensures sufficient electrical contact is made between UBM and lower interconnects.

Successful packaging was conducted however, the solder bumps increased both the standoff height and the contact resistance. A coining method was used to remove some of the solder from the metallised pads on the underside of the chip, better simulating packaging of chips without solder bumps which have a planar bond pad and providing a more accurate indication of the contact resistance. Packaging of the flattened bumps is shown in Figure 6.18 with all interconnects successfully aligned.
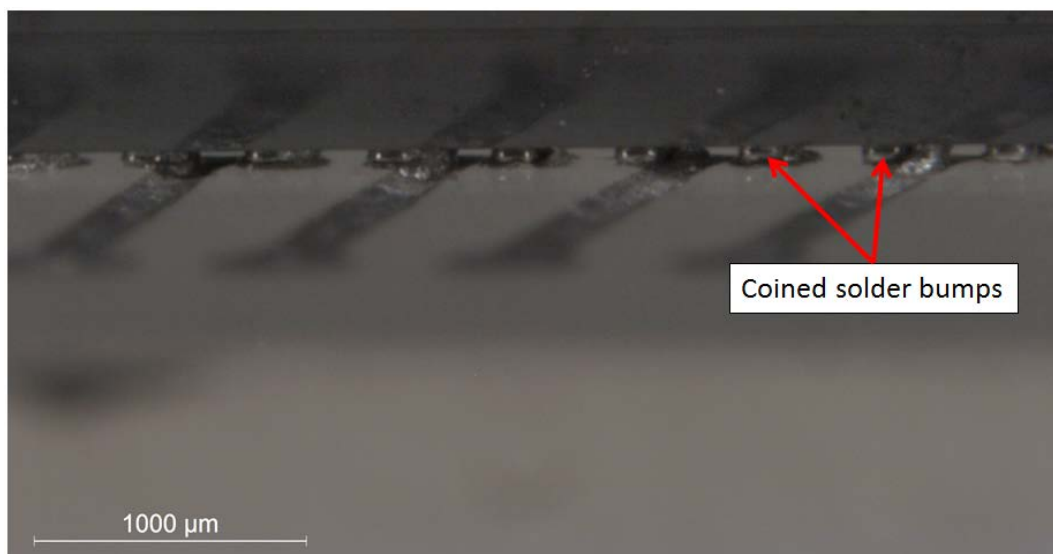
Figure 6.18.   Successful connections made on coined solder bumps

A four point probe was used to measure these resistance values between redistribution traces on the photopolymer substrate in the locations in Figure 6.19. The contact resistance between each of 23 individual adjacent daisy chain interconnections were measured and an average calculated around the perimeter of the entire flip-chip under three different conditions: 1) 0 N bonding force; 2) 0.08 N bonding force; 3) solder removed and 0.08 N bonding force. The average resistance across a single joint reduced from an average of 5.2 Ω down to 3.2 Ω through the addition of the 0.08 N bonding force and further down to 2.3 Ω by removing the excess solder material from the pre-bumped pads.
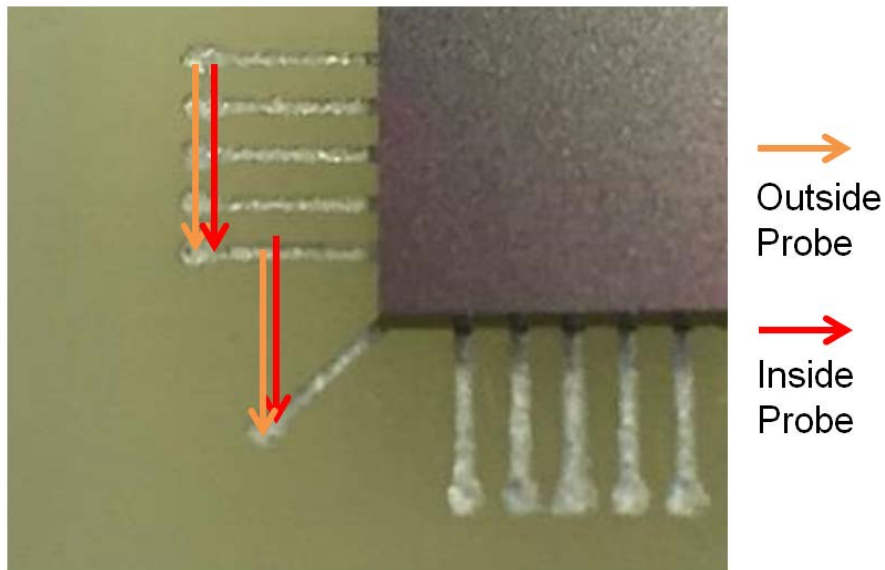
Figure 6.19.   Diagram showing four point probing locations

6.3   Process Integration

Unlike previous studies into hybrid integration of digitally driven manufacturing methods this approach is unique in that it fully encapsulates the dispensed conductive material and electronic components within the substrate material. The bottom-up Stereolithography process presents a number of advantages and disadvantages for embedding electronics. The use of this Stereolithography projection orientation solves a number of limitations of top-down projection and laser based systems. Firstly, there is a high degree of surface quality and planarity of the embedded layer, facilitating the deposition of conductive materials onto the surface for subsequent layers. Secondly, the height of this embedded layer can be precisely controlled, ensuring that freestanding pillars introduced in chapter 5 break the surface and create electrical contact between adjacent layers. Finally, full layers of circuitry including SMDs can be embedded and protected from external environmental conditions.

6.3.1   Bottom-up Embedding

Electronics cannot be directly embedded with a layer-by-layer approach using a bottom-up projection based SL apparatus as surface mount devices would protrude and impact the base of the vat during processing inhibiting individual layer formation. The solution to this issue was to touch the tip of the conductive pillars into the anti-stiction layer on the base of the vat before exposing a thick layer of liquid photopolymer material between the base and substrate surface to fully encapsulate this layer of componentry and circuitry. To polymerise a single thick layer, a long exposure dose was applied, ensuring that the light was fully transmitted through the liquid resin to

the substrate surface to fully attach the thick layer to the original substrate. The embedding process chain is displayed in Figure 6.20.
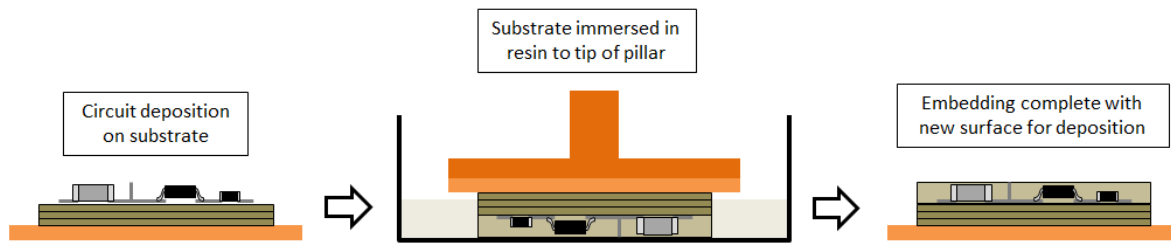
Figure 6.20. Three stage diagram of bottom-up component embedding on a flat substrate

To ensure that multiple layers of electronics can be sequentially embedded, this embedding process was characterised for:

- the compatibility of both SMDs and conductive adhesives with the liquid photopolymer,
- the mechanical strength of the bond at the adhesion boundary,
- stresses in the exposed photopolymer.
- the surface quality of the embedding layer.

Z-axis resolution of this process is limited by the height of the pillars and the height of the components off the substrate, resulting in layer thicknesses up to 2 mm.

In order to achieve the fine z-axis resolution of the 3D photopolymer part a cavity is fabricated prior to depositing the circuitry, conducting the packaging and embedding stages. This process is displayed in Figure 6.21. Base substrates are fabricated with geometrically complex external walls surrounding a cavity with a depth 100 µm greater than the height of the tallest component, therefore requiring pillar heights just less than 100 µm above the external walls. On completion of the substrate build process, the home position is reset to the finishing height, allowing for accurate reinsertion and build continuation from the previous layer without requiring secondary alignment methods. Characterisation of the dispensing process and miniaturisation of the compatible SMDs resulted in the eventual production of 1.2 mm deep cavities containing single layers of electronics.
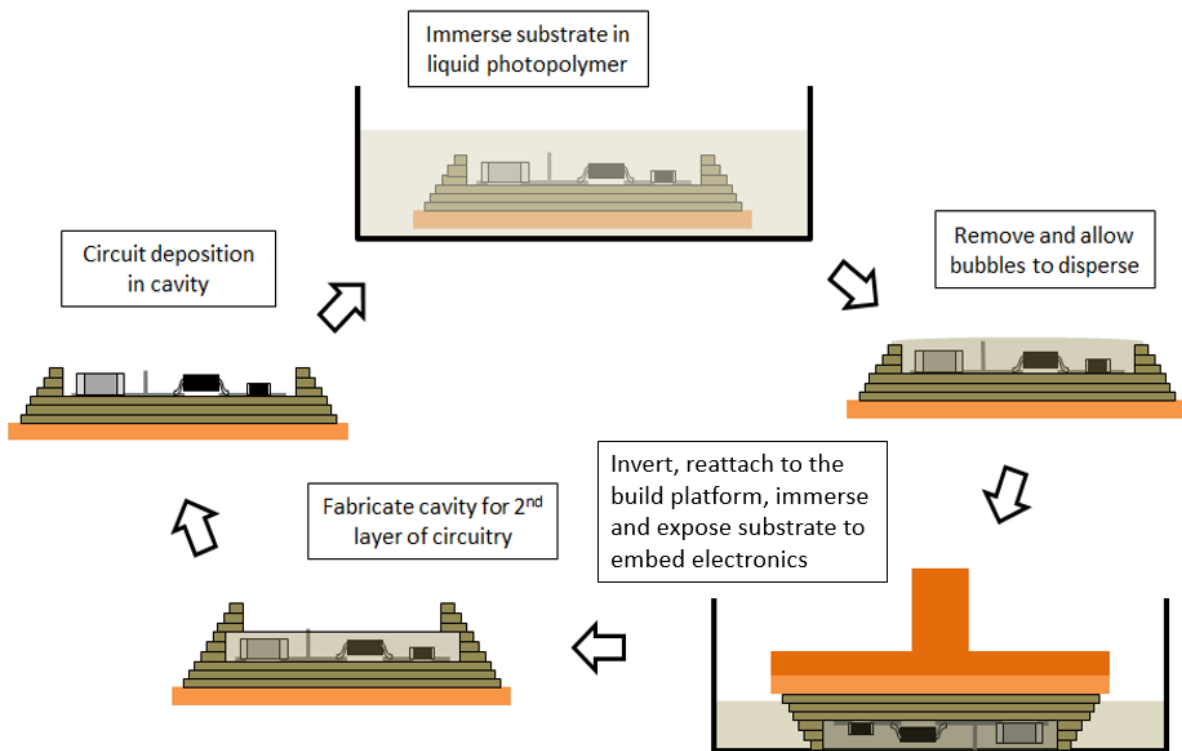
Figure 6.21. Embedding process for complex external geometries

The inclusion of cavities in conjunction with the bottom-up projection orientation has the potential to trap bubbles in the prefabricated cavity. On submersion of the part, air can become trapped in the enclosed volume with no route to escape. Pre-process upright filling of the substrate was found to eliminate not only the bubble entrapment caused by inverted immersion in the resin but also allowed time for the components to be underfilled through capillary action. In conventional flip-chip packaging methods underfill is commonly used to improve the reliability of the interconnects [40]. This procedure entails filling the cavity while the substrate is facing upwards and, providing sufficient time for the bubbles to disperse before inversion and immersion in the full vat of photopolymer. The top surface of the external side-walls can then be positioned on the base by homing the system to the predefined position, resulting in the pillars pressing gently into the soft PDMS layer. The substrate build process can then be reinitiated, with a single long exposure of light on the cavity to complete the embedding process before further deposition of circuitry.
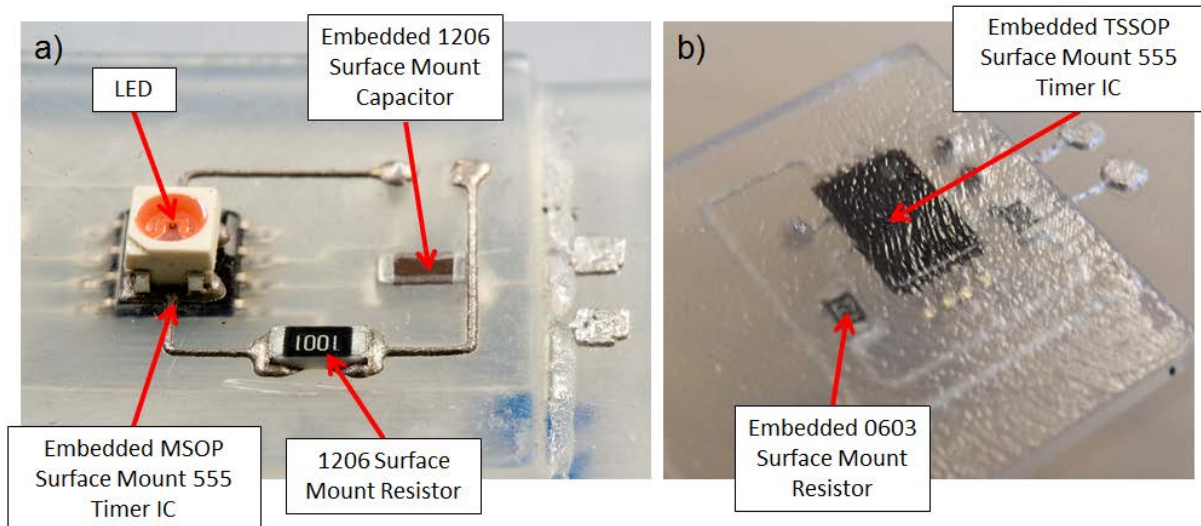
Figure 6.22.   Examples of a) embedded 1206 SMDs with a new circuit layer on the subsequent surface and b) embedded 0603 SMDs

Both embedding methods were characterised by sequentially increasing the exposure time until adhesion was achieved between the substrate and the thick layer. This exposure time was then applied to a full circuit layout with the aim of fully encapsulating the electronics without the appearance of pockets of uncured resin surrounding components. This experimentation resulted in the discovery of minimum times of 90 seconds and 210 seconds at 1050 µW/cm^2 to cure 1 mm and 2 mm thick layers respectively. Figure 6.22 gives examples of embedded components and shows how subsequent circuitry can be added to the embedding surface. The full process can then be repeated to build up complex multilayer embedded electronics. Further explanation and demonstration of the entire process will be given in Chapter 7.

6.3.2   Residual Stresses Caused by Thick Embedding Layers

As previously mentioned, stress reduction is of high importance to ensure both the functionality and quality of parts. Due to the material properties and fabrication mechanism employed within Stereolithography based systems, these stresses can be created through a combination of long exposure times, poor choice of material and design flaws. These effects are further amplified by the inclusion of components into a thick layer of photopolymer, not only causing warping of the substrate as a result of uneven curing rates but also, the propagation of cracks from the sharp corners of the surface mount devices, spanning the entire surface of the embedding layer as shown in Figure 6.23.
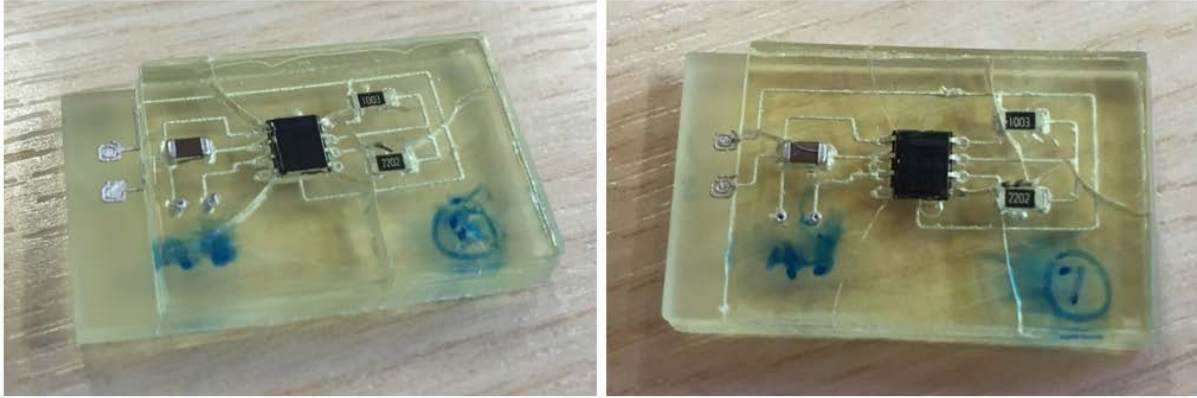
Figure 6.23.   Stress induced cracking in photopolymer substrates

Highly sensitive liquid photopolymers exhibited both cracking and warping, as they absorb more of the light causing overexposure and creating brittle substrates. Materials with a lower sensitivity exhibited none of these stress characteristics, and resulted in the production of a flat surface without cracking and with no observed loss in printing resolution. During the embedding process, the total energy received by the resin on the bottom surface of the vat is greater than that by the resin on the substrate surface due to absorption of the UV light as it passes through the resin. This difference in the degree of curing across the thick layer creates potential for warping and cracking. Figure 6.24 shows samples produced in MakerJuice SF resin, including one with a coloured pigment, to determine the effect of high exposure doses on thick layers with embedded parts in a lower sensitivity material. A simple and fast feasibility study was devised to evaluate the suitability of this approach by using small thin metal offcuts to simulate the inclusion of electrical components. Once proven to work, a circuit layer was embedded using the unpigmented version of this material, allowing enhanced transmission of light through the photopolymer as the pigmented material is too absorptive to cure thick layers.

Figure 6.24.   Embedding in MakerJuice SF Resin without stress cracking

The observations from Figure 6.24, in addition to a change in light source from white light to 405 nm UV light, as discussed in chapter 3, resulted in the fabrication of flat substrates and crack-free embedding using unpigmented MakerJuice SF resin supplied by MakerJuice Labs. This discovery alongside measured characteristics discussed in chapter 3, make this resin well suited for stress reduction and the fabrication of embedded electronic systems.

As previously stated, a reduction in the size of circuitry also enables a reduction in circuitry from 1206 SMD components to 0603. This resulted in a reduction in the required embedding layer thickness from 2 mm to 1.2 mm, reducing the exposure time from 210 seconds to 90 seconds. This decrease in package footprint not only miniaturises the circuit and therefore allows more functionality to be built into the same size part but it also reduces the residual stresses as a result of using thinner embedding layers.

6.3.3   Tensile Strength of Substrate across Exposure Boundaries

A number of characteristics of this embedded layer require investigation to ensure that the substrate produced through flood exposure demonstrates suitable mechanical properties similar to substrates built of thin layers. This investigation used tensile testing to make a comparison between the adhesive strength of layers of a regular thickness and those created during the 1 mm and 2 mm embedding processes. Three tensile testing specimen designs were fabricated lengthways in sets of six, one set without interruption, another with a single 1mm layer exposure over 90 seconds in the centre and a final set with a 2 mm layer exposure over 210 seconds in the centre. This build orientation means that adhesion between layers will be assessed as the force will be applied perpendicular to the layer boundaries. Figure 6.25 shows the design of the test specimen.
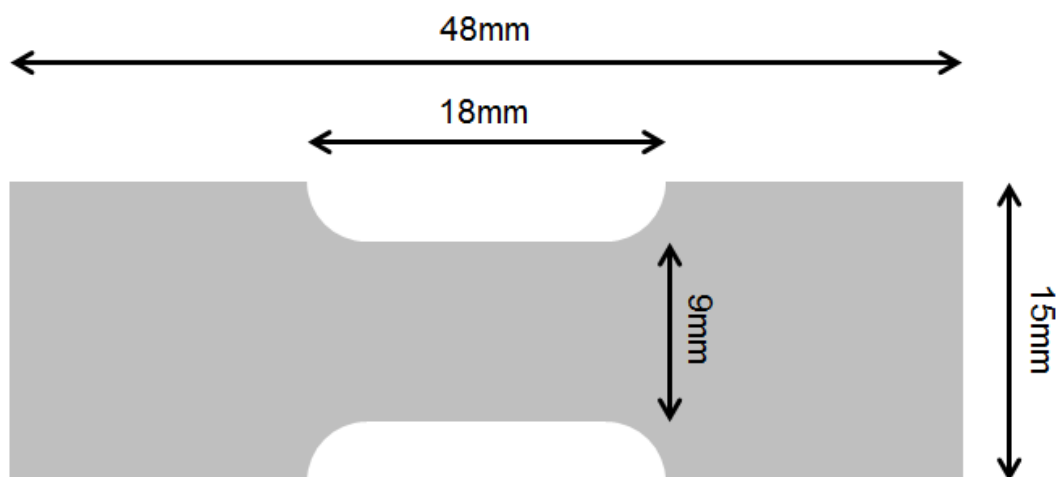
Figure 6.25.   Tensile testing specimen design

Fabricated specimens, examples of which are shown in Figure 6.26 were fabricated and tested. Each specimen was fixed in the jaws of an Instron 3369 Tensile Testing system and a fixed rate increase of

extension was applied at 1 mm/s. This was set to determine both the maximum extension capability of each part and the tensile force exerted on each specimen over that extension length and therefore at failure.
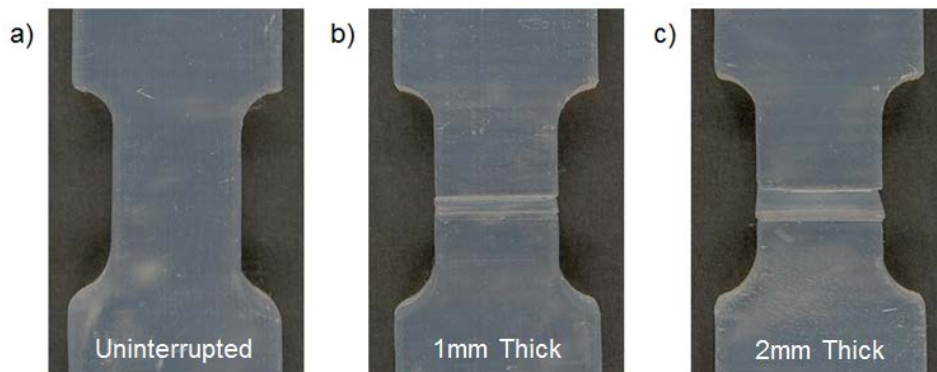
Figure 6.26.   'Dog bones' fabricated a) without interruption, b) with 1 mm thick exposure and c) with 2 mm thick exposure

The thick exposed layer boundaries can be seen in the images in Figure 6.26(b) and Figure 6.26(c), this interface would be the region where potential weakness in adhesion could occur. Data points of plotted failure loads in Figure 6.27 had some spread, however there were noticeable trends, with differences in both maximum load and maximum extension of samples built over all three different fabrication regimes. With increasing layer thickness the tensile strength decreases with the extension of the sample at failure.
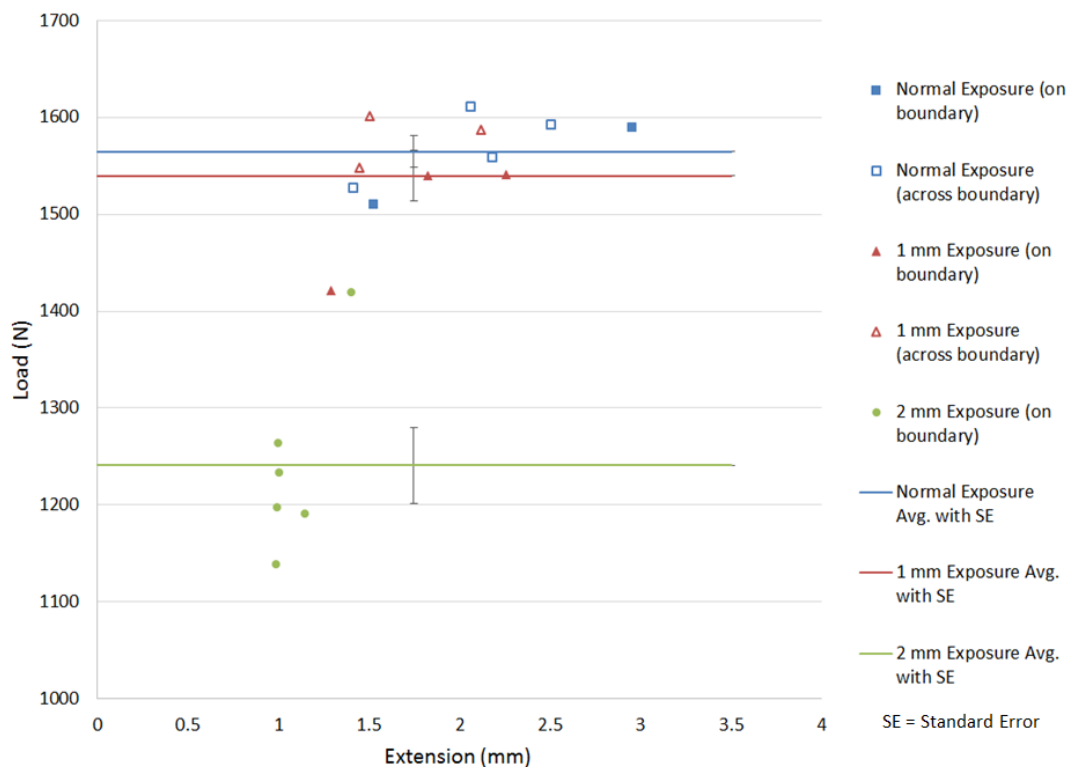
Figure 6.27.   Plot of load vs extension at failure

These results suggest a reduction in strength in thicker layers with the maximum load of the 1 mm exposure being only 2% lower than the uninterrupted samples, compared to 22% over 2 mm. Such a similarity shows negligible negative characteristics as a result of the 1 mm exposure, especially as the maximum average load on the sample at failure was 1540 N, higher than any load that could feasibly be reproduced on the substrate in any application. A number of photopolymer materials including 3D Systems Accura 60 [170] and MakerJuice Labs Substance G+ Resin [185] both specify maximum tensile load bearing capability of ~3000 N in the same size samples as this investigation, twice that presented above. These data sheets do not however specify the orientation of these measurements to the build plane and therefore if the force was applied in line with the build plane the value could increase. Despite these specified values, previous experimentation has shown acrylic based photopolymers to exhibit a tensile strength of up to 15 MPa, translating to the capability to withstand a tensile load of 675 N on the same sample dimensions as above [218]. Values from literature are however affected by a number of build variables including laser power and hatching pattern making the experimental determination and comparison of data between both DLP and laser-based stereolithography difficult [80].

The fracture boundaries specify the location at which the weakness of each specimen is situated. Fractures occur both linearly and across exposure boundaries in a ratio of 2:4 in uninterrupted parts and 1:1 in those with 1 mm thick layers. The fracture mode is also indicated by different point formatting in Figure 6.27. The adhesive strength displayed by the 1 mm layer specimens is almost comparable to a standard 100 µm layer and in half the samples, resulted in the material fracturing across curing boundaries. This proves that cure boundary adhesion of 1 mm thick exposure is comparable to the mechanical strength of the fully built part with continuous 100 µm layers. The non-linear fracture boundaries also show that the adhesion between cure boundaries is equivalent to that perpendicular to those boundaries and therefore, similar to the mechanical strength of the bulk material. The images in Figure 6.28 show that the weaker specimens with a thick 2 mm layer fractured linearly along one of the flood exposure boundaries, proving as expected that the exposure boundary is the primary weakness.
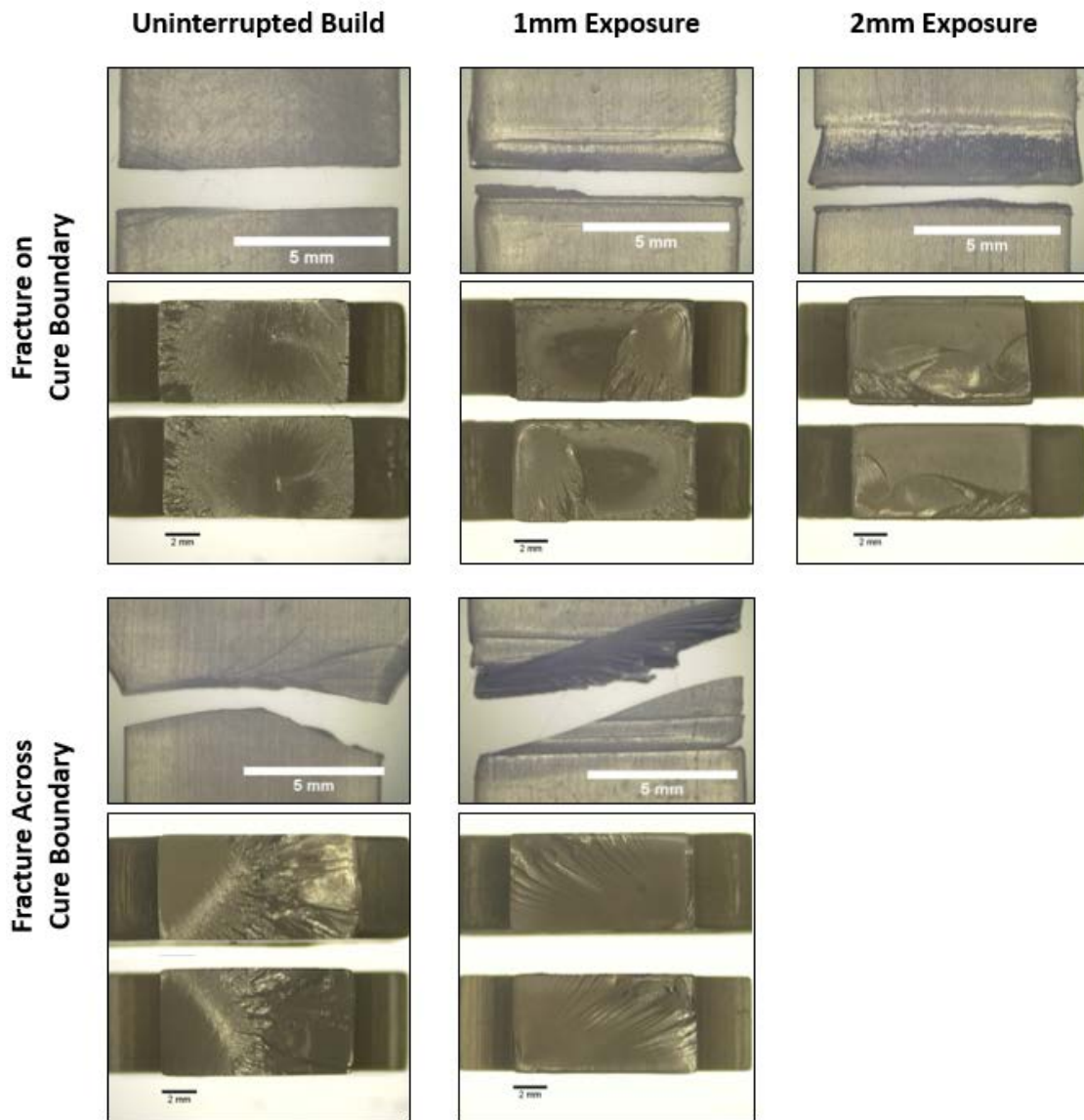
Figure 6.28.   Fracture boundaries in tensile testing specimens

These results provided a basis on which the size of electronics and conductive features could be reduced to facilitate the use of 0603 SMDs, ensuring that the thinnest possible embedding layer can be achieved, without compromising the mechanical properties of the base substrate material or subsequent layers.

6.3.4   Embedded Conductive Tracks

Due to the nature of the encapsulation process, there is the potential for the creation of stresses in the substrate as a result of curing a thick layer of photopolymer. Lopes *et al.* [83] demonstrated that embedding conductive tracks causes an increase in resistivity of the laser cured ink however, without further work, this difference was not quantified. This could be caused by delamination and cracking of conductive material which has minimal elasticity once thermally cured as they do not absorb stresses well.

Test samples were created to determine the effect of the embedding process on the electrical properties of conductive tracks. Samples previously used to determine the resistivity of the tracks in chapter 5 were embedded under a 1.2 mm thick layer of photopolymer before their resistance was measured using a four point probe positioned in identical locations to those in the previous chapter. These measurements in conjunction with the average cross sectional area previously calculated by a Matlab interpretation of surface profile data gathered using the Alicona microscope, allowed the resistivity to be calculated and compared against pre-embedding values in Figure 6.29.
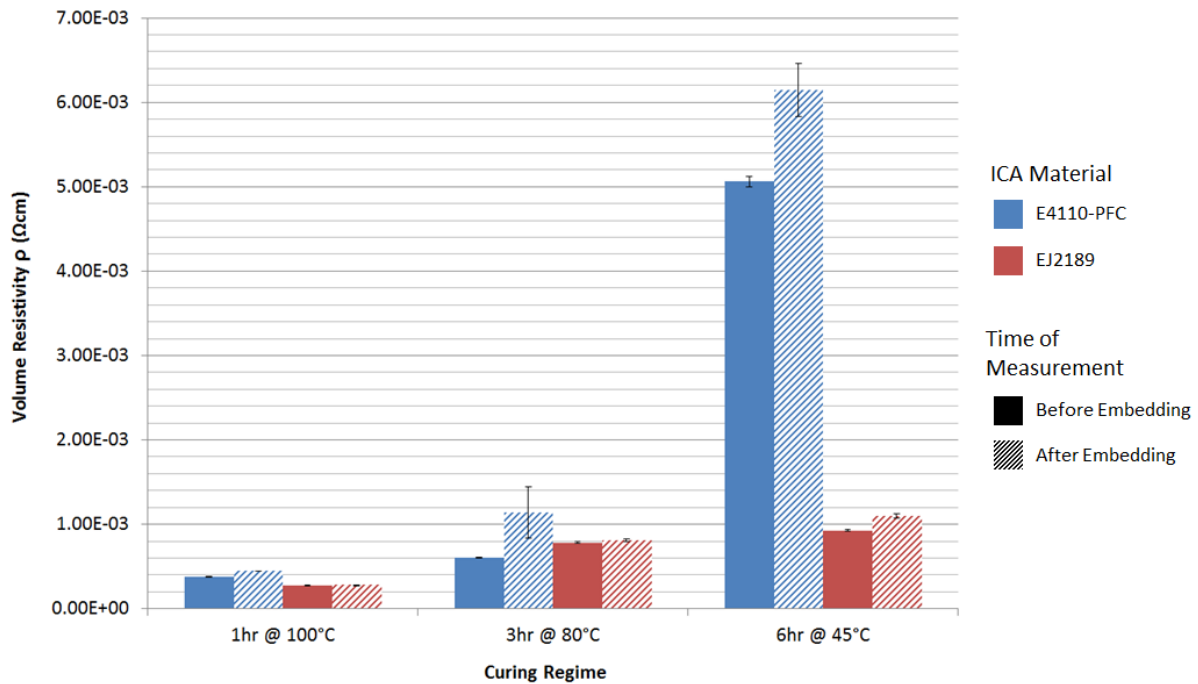
Figure 6.29.   Comparison of resistivities of material A and material B before and after embedding

The resistivity of tracks printed in material A and cured at 80 °C for 3 hours increased by an average of 89% when embedded. This value was only 5% in material B, showing significantly greater compatibility with the liquid photopolymer. The same pattern is evident across the two alternative curing regimes, with material A showing greater increases in resistivity after embedding under the photopolymer. The most probable reason for increases in resistivity of tracks are stresses propagating from the thick layer of cured photopolymer. This could cause cracking of the cured ICA resulting in contact between silver particles being broken. Silver flakes however demonstrate a less severe reduction in resistivity as cracking of the ICA can occur, but due to the shape of the silver filler, flakes can slide across the surface of one another, demonstrating some ductility while maintaining electrical contact.

6.3.5   Surface Quality of Embedded Layer

The surface quality of the encapsulation layer must have a low surface roughness and a planar surface. Although the dispensing system has integrated surface mapping capability, the behaviour of

the ICA material could be affected by small curvatures in the substrate surface, especially under the applied pressure of the SMDs. In addition, surface mount packaging requires a flat surface to contact all pads. As such, analysis of the embedding surface was conducted on both the Taylor Hobson Talysurf and Alicona microscope to measure the surface flatness and roughness. Figure 6.30 shows that the embedding surface mean profile fluctuates by less than 7 µm over the 15 mm x 15 mm measurement area.
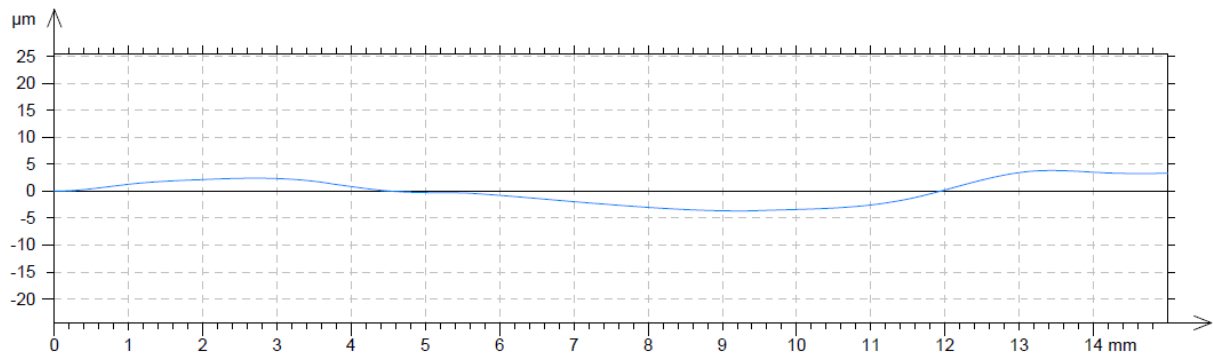
Figure 6.30.   Surface profile of a 1.2 mm thick embedding layer of MakerJuice SF resin

This profile shows suitability for subsequent printing with print gaps at a minimum of 100 µm in the dispensing process, providing enough clearance for consistent printing. The additional laser mapping capability of the Musashi can also account for these small changes in topology. The surface roughness of these samples shown in Figure 6.31 is also very low with a S_a value of 1.09 µm and S_z value of 16.6 µm.
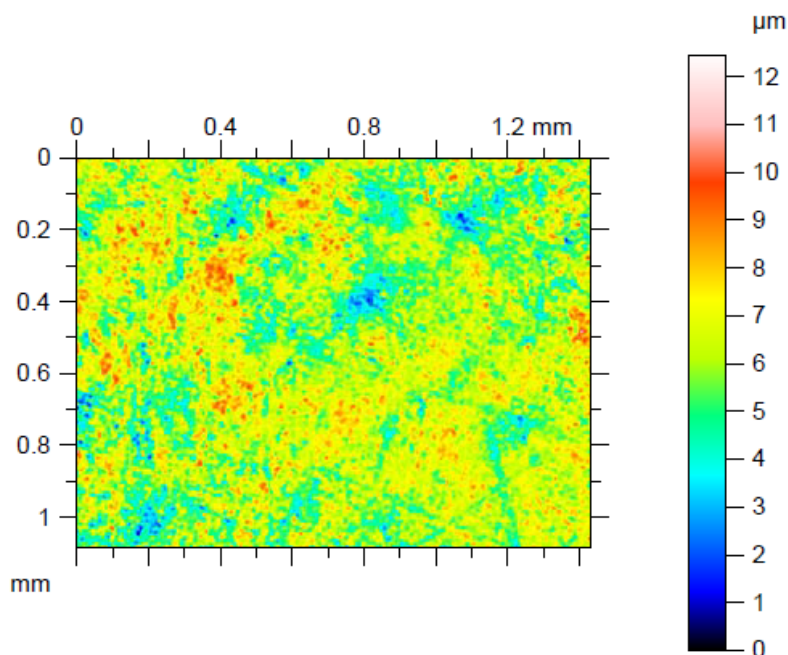
Figure 6.31.   Alicona profile of the surface of a MakerJuiceSF embedded layer

This roughness is lower than that achieved during base substrate fabrication as the top resin layer has undergone a long period of exposure to UV light, resulting in the top surface mimicking the surface quality of the PDMS layer through which the curing is conducted. The increased exposure time also results in fully cross-linked substrate surfaces.

6.3.6   Using Liquid Photopolymers as an Insulating Underfill Material

Traditionally, after flip-chip placement an insulating polymer material is used to fill the void between the chip and the substrate, protecting interconnects from stresses such as shock, vibration and drop. In Figure 6.2(b), the use of the liquid photopolymer to replace conventional underfill materials was proposed, allowing the encapsulation and underfill processes to be conducted simultaneously. The embedding process introduced in section 6.3.1 facilitated this and attempted to ensure that no bubbles remained under the chip. This same concept has already been proven using surface mount devices, where they have been embedded and any remaining air surrounding the components filled with liquid photopolymer. This capability makes this process unique as the substrate material can be used to provide both a surface for the deposition of electronics and the underfill.

To demonstrate this process, assembled flip-chip samples were immersed in the liquid photopolymer and selectively exposed to UV light to encapsulate and underfill the chip. The resulting structure was then mounted in a block of epoxy resin, ground and polished to provide a cross sectional view of the chip and interconnects. This enabled the capability of the liquid photopolymer to fill the cavity underneath the chip to be assessed. These cross sections were imaged using a Nikon Eclipse MA200 inverted microscope.

Figure 6.32 shows a successfully underfilled chip with no bubbles visible around the interconnects or under the bare die. The photopolymer has also been used to form a cap over the bare die, fully embedding it within the substrate material. A faint boundary can be seen where the underfill and substrate interact however, no bubbles can be seen in this cavity.
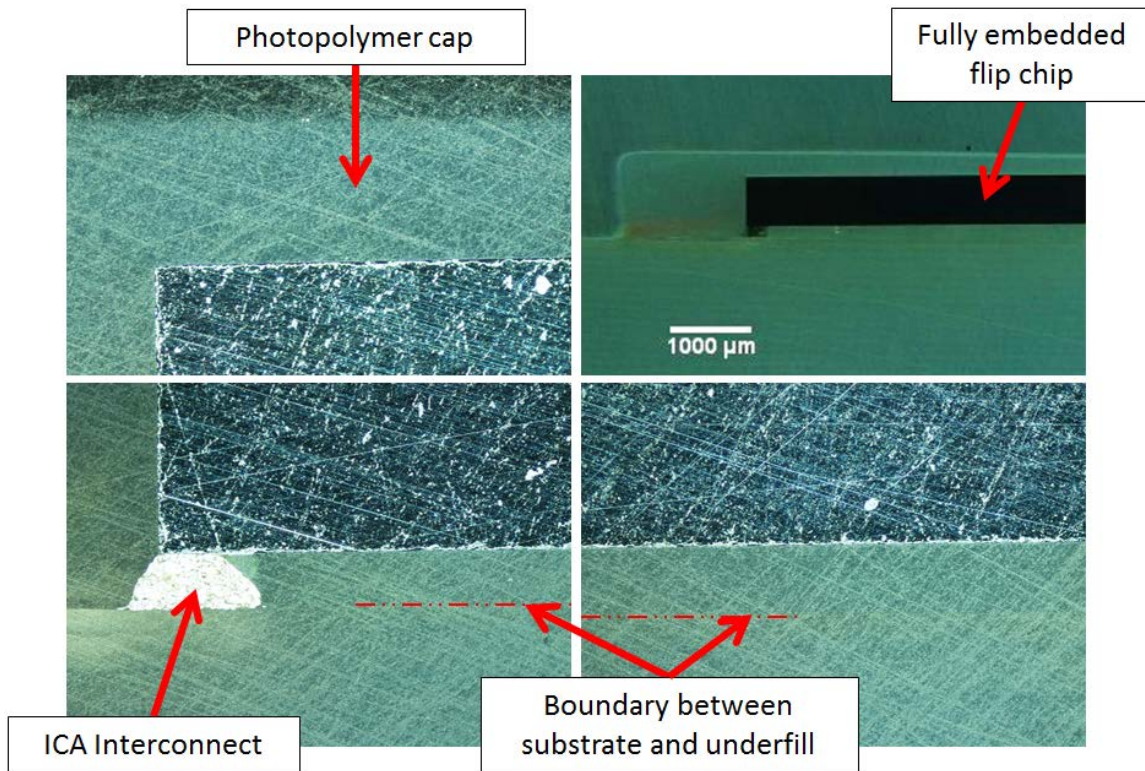
Figure 6.32.   Cross sectional images of successfully underfilled and embedded flip-chip bare die

Figure 6.33 shows a failed attempt to fully underfill a flip-chip. This sample had the solder bumps coined and therefore, the standoff height halved from ~160 μm to ~80 μm.
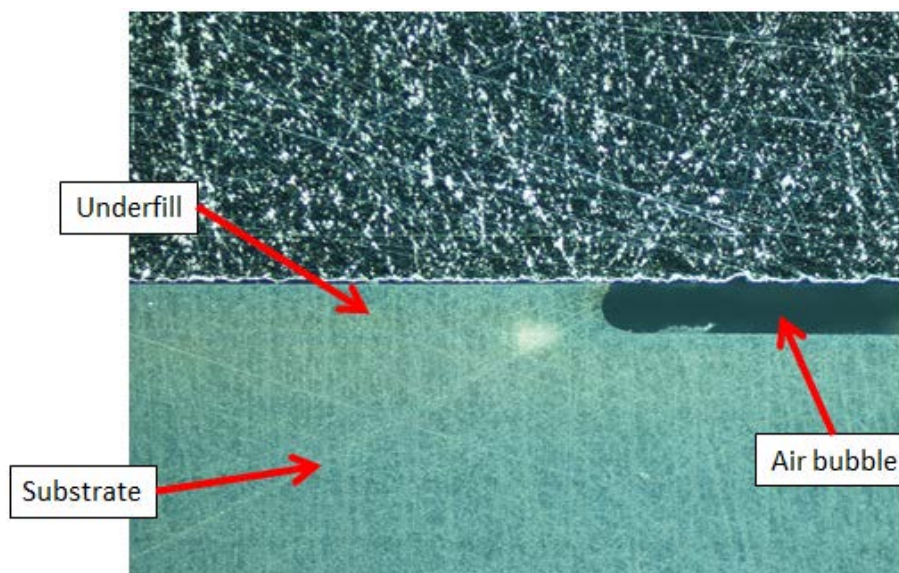
Figure 6.33.   Cross section of unsuccessfully underfilled flip-chip bare die

Under filling is conventionally conducted using capillary forces to completely fill the cavity, a method that could be further explored with a liquid photopolymer before the embedding stage. Similarly, ultrasonic agitation of the substrate while submerged in the resin may also achieve the same result.

6.4   Summary

Packaging of electronic components and dispensed ICA conductors has been characterised and shown as successful. This has included the addition of a surface mount assembly stage whereby packaged components can be mounted to the wet ICA deposited during the dispensing process summarised in Chapter 5. This chapter also showed the capability of this combination of manufacturing processes to conduct electronic packaging on a chip scale with the successful flip-chip packaging of a daisy chain patterned bare die onto isotropic conductive adhesive interconnects on a photopolymer substrate. This was achieved through the development of conductive channels in a photopolymer substrate, fabricated by filling surface trenches on the substrate with ICA, before conductive bumps were created on either end of the trench. Four dispensing parameters, nozzle size, pressure, print gap and pressure actuation time, were investigated with the aim to produce the smallest possible conductive interconnect to align with the metallised pads on the underside of the flip-chip. A minimum diameter of 150 µm was achieved at a pitch of 457 µm. The daisy chain patterned die was then aligned and placed both with and without additional pressure. The contact resistance of each connection was measured resulting in an average value of 3.2 Ω, achieved with a placement force of 0.08 N. Finally, these flip-chips were embedded after which they demonstrated no change in resistance. One chip was also successfully underfilled however, another was unsuccessful.

To facilitate the successful integration of multiple processes, the interaction between separate AM technologies has been assessed. A novel packaging method for multilayer electronics has been explained and testing presented to ensure that the electronics are fully encapsulated in and under filled with an electrical insulator. Liquid photopolymer materials with low sensitivity were proven to be more suitable, resulting in a smooth surface and fully cured embedding layer. Photopolymers with high sensitivity caused stress cracking to propagate from the sharp corners of the embedded components, creating an unsuitable surface for further processing. The adaptation of this process to enable geometrically complex packages to be fabricated has also been explained, allowing the additive manufacturing technique to be utilised to its full potential. Surface roughness and flatness of the subsequent dispensing surface produced in the SLA apparatus was also shown to be higher quality than the base substrate.

To ensure that embedding using a flood exposure method did not sacrifice the mechanical strength of the substrate material the tensile strength of embedding layers at 1 mm and 2 mm depths were compared to uninterrupted builds to ensure that there was no significant weakness in the substrate over multiple layers, the results of which proved that the tensile strength decreases with increased

thickness however, a load in excess of 100 kg would need to be applied perpendicular to the embedding plane to cause failure. Finally, the electrical characteristics of conductors were monitored during the embedding procedure to ensure that their resistance did not increase. Stresses exerted on the substrate during the embedding process could cause cracking of the cured conductive material, creating breaks in the conductivity however, the resistance of tracks at a given length showed only a very small change in resistance and therefore volume resistivity.

This chapter has presented successful testing of specimens produced using the unique combination of manufacturing techniques interleaved during this research. Results have shown that high quality electronic packages on both component and chip scales with good mechanical properties can be produced, catering to a wide range of potential applications.

7 Demonstrators

The vision of this doctoral research was to develop a digitally driven manufacturing process chain that could produce bespoke multi-layered embedded electronics contained within a freeform geometry. The previous experimental chapters have developed the processes and method of interleaving bottom-up stereolithography with dispensing and surface mount assembly. These packages were designed to include conductive tracks, interconnects and z-axis connections, allowing the positioning of components directly onto conductors and electrical connection between multiple layers stacked in the vertical plane.

Feasibility demonstrators were designed to prove this processes capability for producing both single and multilayer systems. A flashing 555 timer circuit was designed as a simple and visual feasibility demonstrator. This circuit contains discrete components (resistors and capacitors), an LED and a Small Outline Integrated Circuit (555 timer chip). Iterative development of five separate demonstrators shows progression from a single layer embedded circuit, to multiple layers, followed by a reduction in the size of both conductive features and electronic components. Finally, the integration of the optimised and minimised circuit design into a pyramid shape was produced. This evolution in complexity and reduction in feature sizes is summarised in Figure 7.1
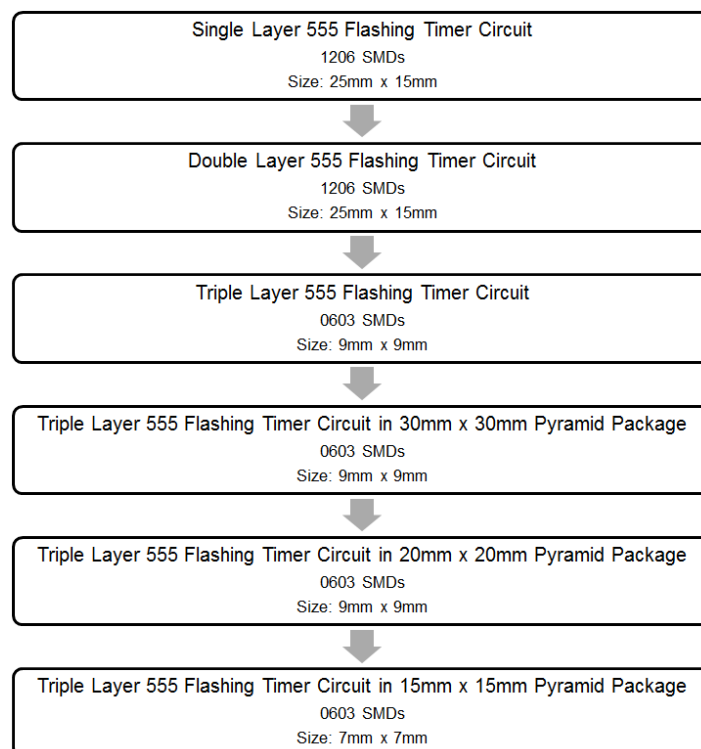
Figure 7.1.　　　Flow diagram of demonstrator evolution

7.1 Single Layer 555 Flashing Timer Circuit

The initial 555 timer circuit was designed over a single layer using 1206 discrete surface mount components. The integrated MuCAD dispensing software was used to design the conductive track layout as shown in Figure 7.2, thereby providing the dimensions for the circuit footprint. This footprint was used to determine the size of the base substrate. Once the substrate was fabricated, the build platform can be removed and the substrate washed using the mid-processing procedure developed in chapter 4 in order to remove any excess liquid photopolymer material. The build platform was then positioned in the Musashi system and the substrate aligned prior to depositing the circuit layer using the parameters determined during process characterisation in chapter 5.
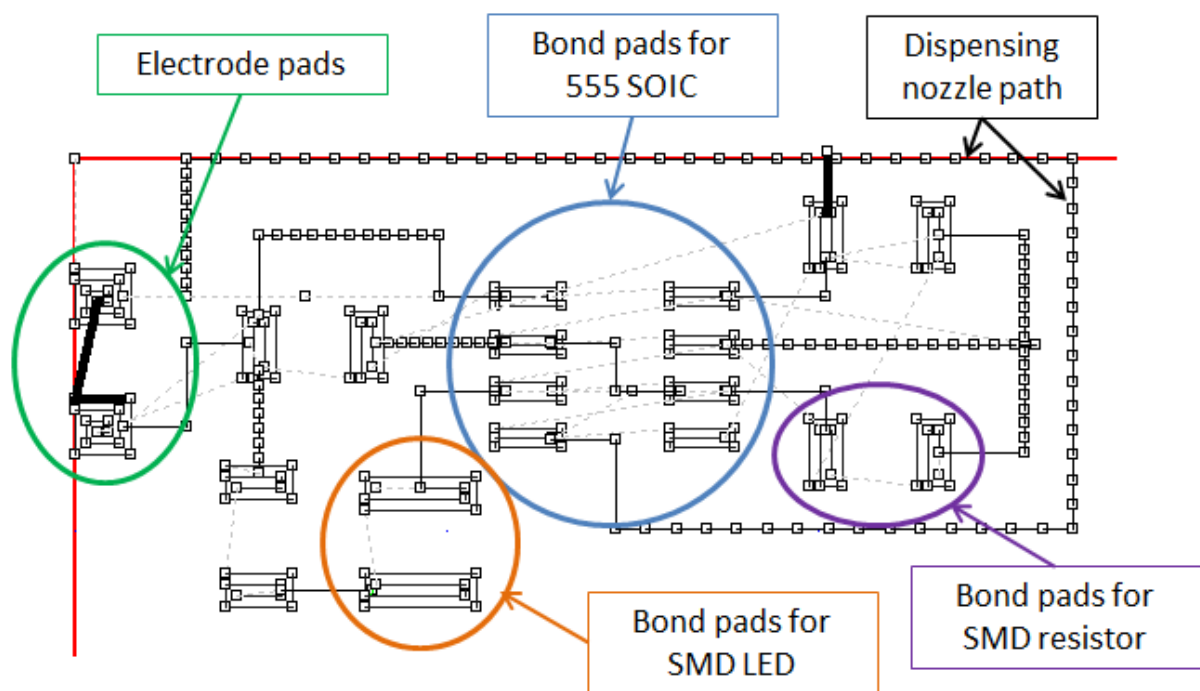
Figure 7.2.   Single layer 555 timer circuit design in MuCAD

Following material dispensing, components were placed onto the wet ICA interconnects before the part was thermally cured for 3 hours at 80 °C. Once cured the substrate with mounted electronics and printed conductive circuitry, still adhered to the SL build platform was re-immersed in the liquid photopolymer. Setting the part alignment and layer standoff height was conducted via two mechanisms. Firstly, the digital design of the embedding layer was positioned precisely over the corresponding area on the substrate within the virtual build environment in the Creation Workshop SL control software. This resulted in the accurate projection of the image onto the vat in the desired location. Secondly, a depth micrometer fastened to the lower limit switch of the z-axis motor was used to raise the home position of the build platform. Its distance from the base of the vat was increased by the thickness of the substrate plus the thickness of the mounted components. This

process prevented contact occurring between the base of the vat and the circuitry and ensured that all components were fully embedded. A long exposure of ultraviolet light projected onto the immersed electronics then cured this embedding layer. For the 1206 components a 2 mm layer was cured, fully embedding the circuit as shown in Figure 7.3.
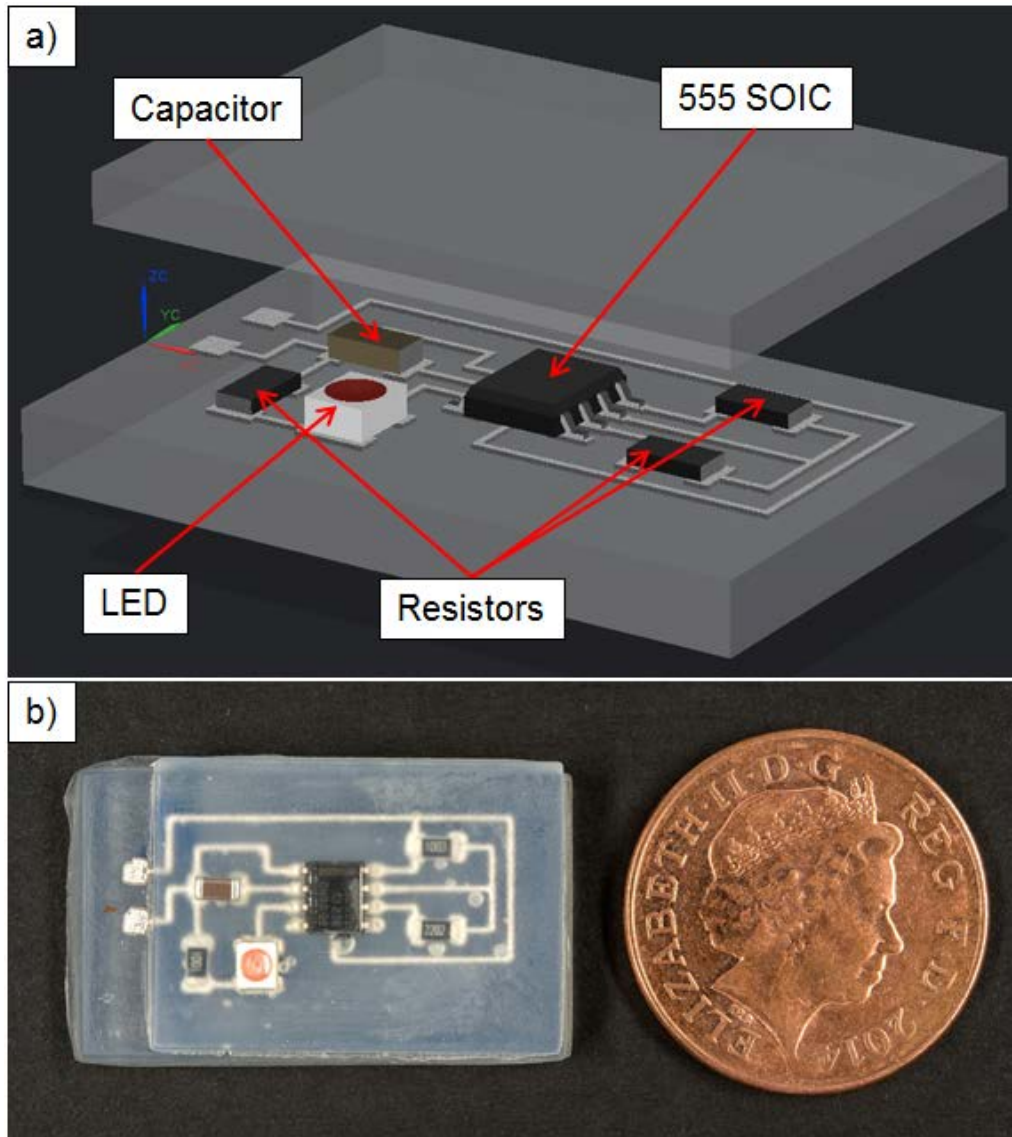
Figure 7.3.   a) Design of and b) fabricated single layer embedded 555 timer circuit

The final product had a footprint of 25 mm x 15 mm, with only the power connections exposed in order to allow a 9 V battery to be connected as a power source. The resultant circuit successfully operated, causing the LED to repeatedly flash on and off. Figure 7.3(b) shows that previously encountered stress related issues have been overcome however, there are a number of air bubbles trapped in the embedded layer as this technique did not use the method developed in chapter 6 to reduce the appearance of bubbles. The resin was left to settle in the vat before the flood exposure

process, as the air is forced out from underneath the components, it moves to the substrate surface in the form of small bubbles that are subsequently all located in close proximity to the components. This fully functioning demonstrator proved the capability of this manufacturing method to produce embedded electronics.

7.2   Dual Layer 555 Flashing Timer Circuit

With the proven fabrication capability, the electronics were now divided into two layers, producing the first demonstration of z-axis connections within a fully functioning circuit. This circuit design was again produced on the MuCAD software. Three separate designs were required: 1) first circuit layer, 2) z-axis connections; and 3) second circuit layer as shown in Figure 7.4. It is essential that both layers have the same dispensing origin to ensure an electrical connection is successfully made between the layers and conductive pillars.
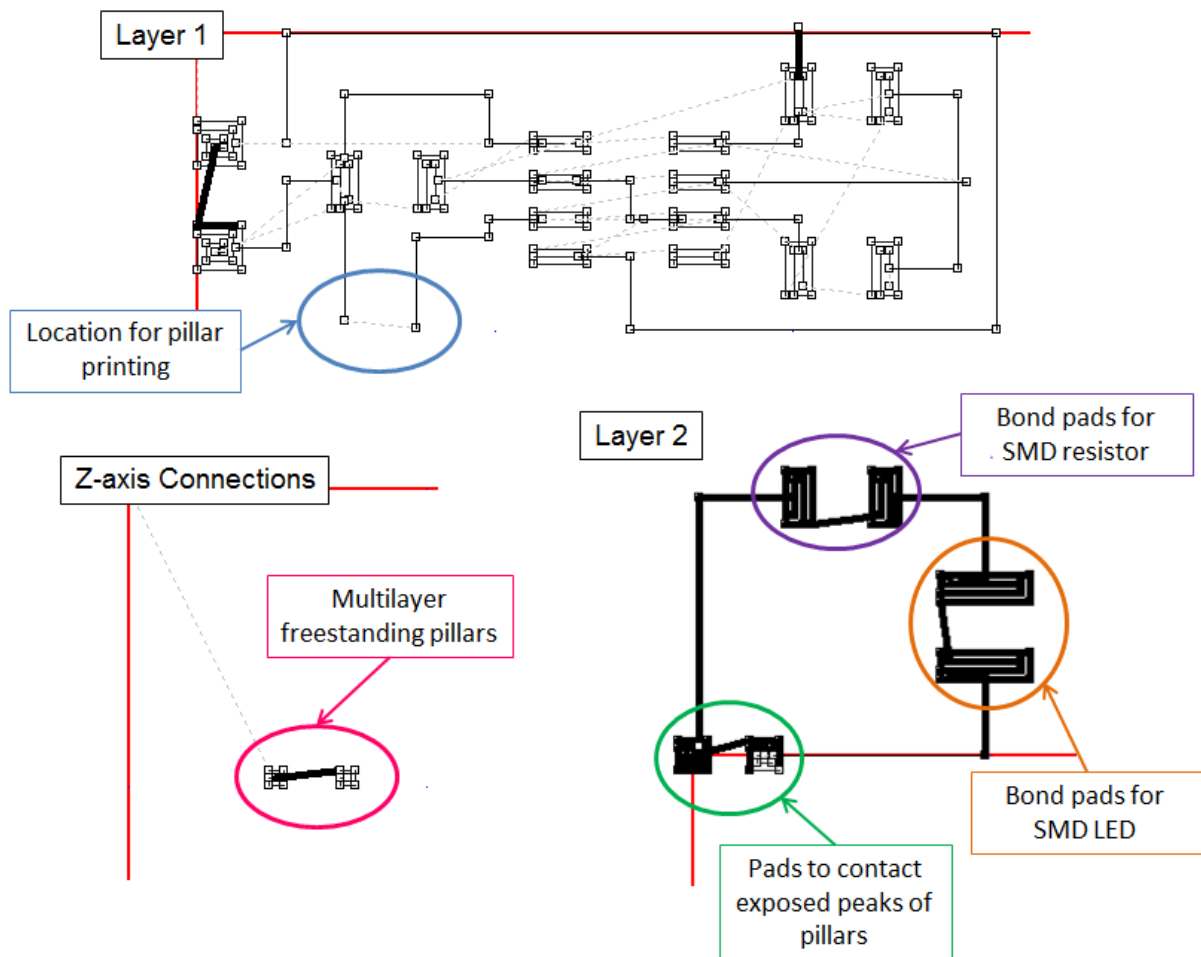
Figure 7.4.   Three MuCAD dispensing designs for two layer 555 timer circuit

The initial fabrication process was identical to the single layer demonstrator, with base substrate production and mid-process cleaning. The first layer of dispensing was then conducted, again

creating tracks and SMD interconnects however, this iteration also required the printing of 3D pillars to create electrical contact with the second layer. Both designs were printed simultaneously, allowing immediate surface mount assembly of components and thermal curing. The first layer was then immersed in the liquid photopolymer and left to settle before being removed. Finally, the home position of the SL z-axis was set with the conductive pillars pushing gently into the PDMS layer in the base of the vat. The resin was then exposed, embedding the first layer but leaving the tip of the pillar exposed on the top surface, as shown in the CAD design in Figure 7.5.
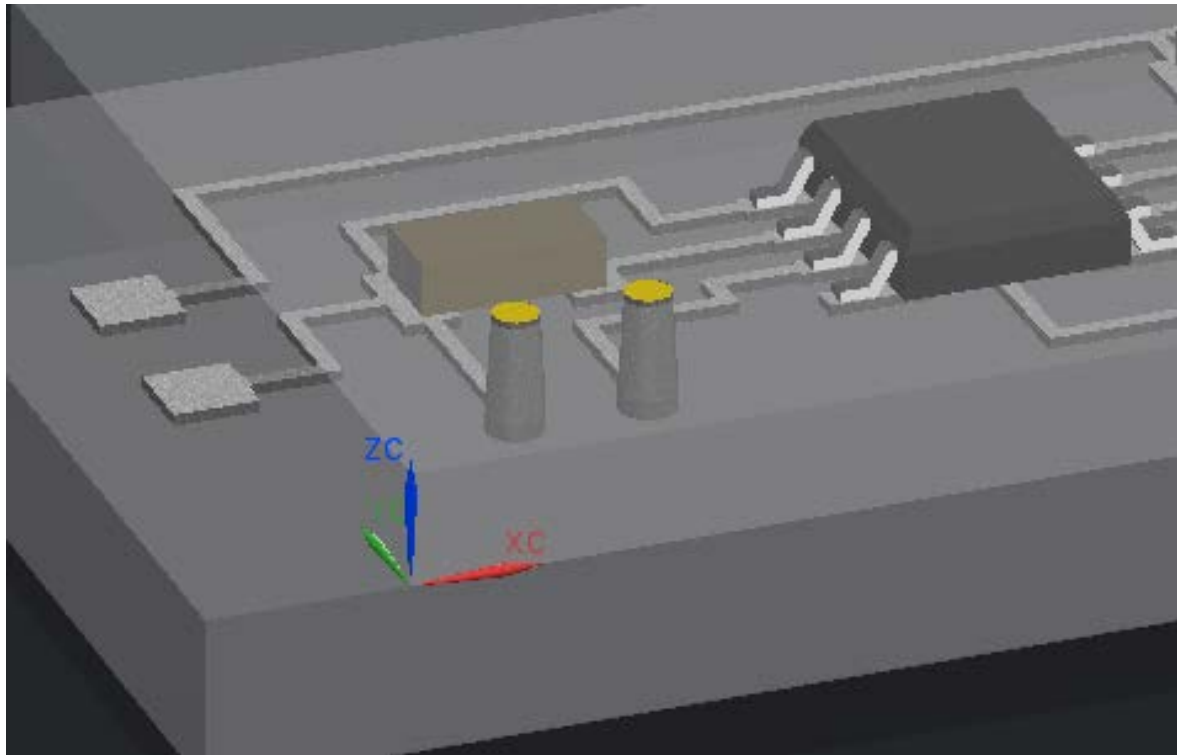
Figure 7.5.   Exposed peaks of conductive pillars

The same deposition process was then repeated to fabricate the second layer of conductive features and package the components as shown in Figure 7.6. After thermal curing the circuit was again submerged in the resin and exposed to a projected image for a prolonged period of time, embedding the second layer. The dimensions of the second embedding layer were reduced to suit the footprint of the second layer of circuitry, designs of which are shown alongside the fabricated demonstrator in Figure 7.6.
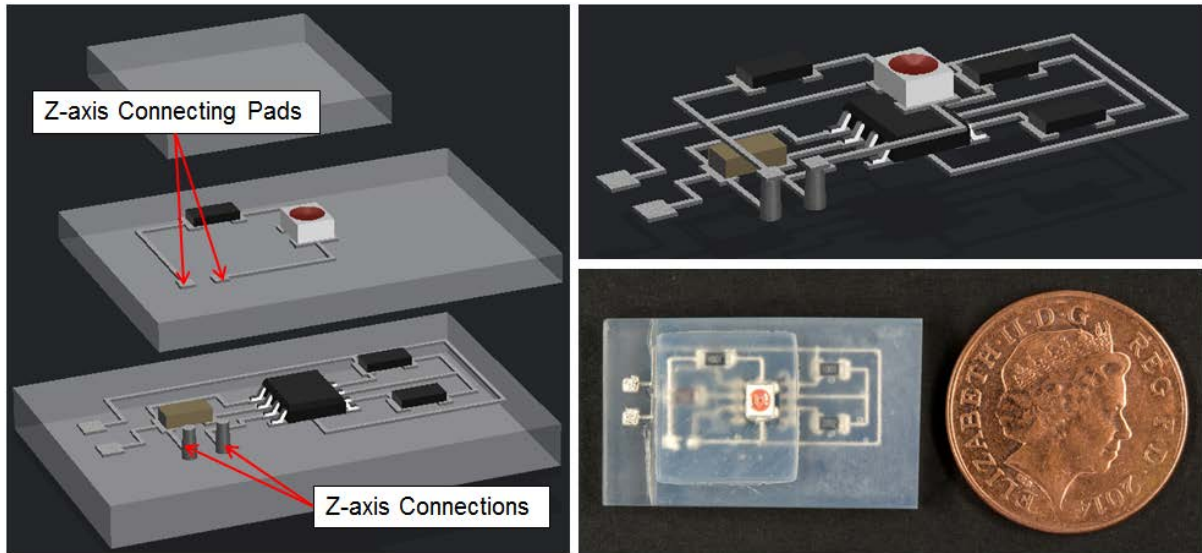
Figure 7.6.   Exploded design, circuit layout and photograph of the 2 layer demonstrator

When attached to a power source, the LED blinks in a set periodic fashion identical to that of the single layer embedded timer. This proves for a basic DC circuit that splitting the circuit over multiple layers did not affect its basic function. An increase in electrical resistance will alter the resistance ratio of the circuit, therefore changing the frequency the LED flashes at.

7.3   Triple Layer Miniaturised 555 Timer Circuit

Characterisation of the dispensing process to enable finer features to be deposited and an increased accuracy of the pick and placement stage for SMDs facilitated the miniaturisation of the circuit footprint. In order to further access the embedding of electronics a 2.5D pyramid was designed. To enable the miniaturisation of the circuit, the size of SMDs was halved from 1206, with a resistor dimension of 3.2 mm x 1.6 mm, to 0603, with a resistor dimension of 1.6 mm x 0.8 mm. Smaller components required a redesign of the circuit layout including the size of the component pads and pitch. In addition another layer of circuitry was incorporated to further evaluate the multilayer capability of this manufacturing process chain. The multilayer design made in MuCAD is shown in Figure 7.7.
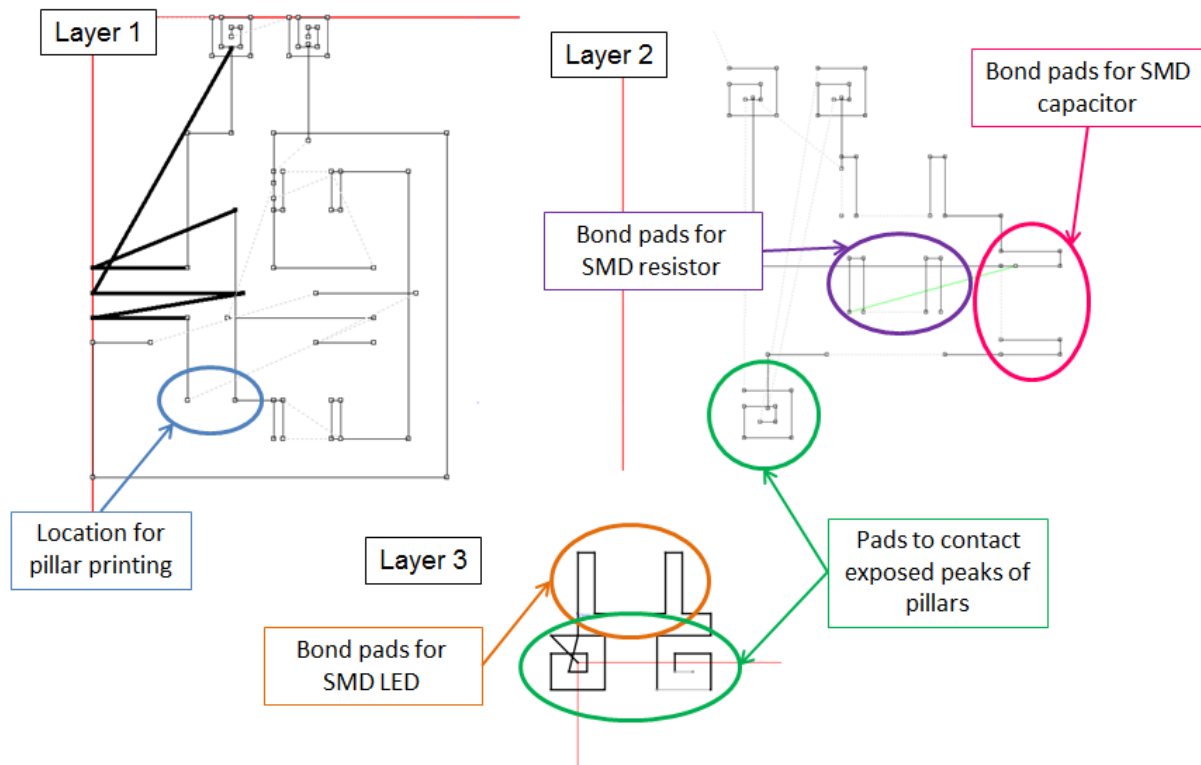
Figure 7.7.   Three layer designs in MuCAD for triple layer flashing 555 timer circuit

The triple layer design kept the same 555 Small Outline Integrated Circuit (SOIC) on the first layer in combination with two resistors. Three pillars were also positioned to connect the first and second layers of circuitry. The second layer now consists of a capacitor and a resistor with another two vertical connections going to the final layer where the LED sits. An exploded view of the multilayer design along with the three dimensional circuit layout and the fully fabricated demonstrator are shown in Figure 7.8. The pitch of the smaller 555 SOIC pins is 650 µm, requiring the density of deposited tracks and interconnects to match these dimensions, made possible through the aforementioned optimisation of the dispensing process. The same manufacturing processes used in sections 7.1 and 7.2 were employed to produce this specimen, consisting of a repeating cycle of substrate production, decontamination, conductor dispensing, surface mount assembly, thermal curing and embedding.
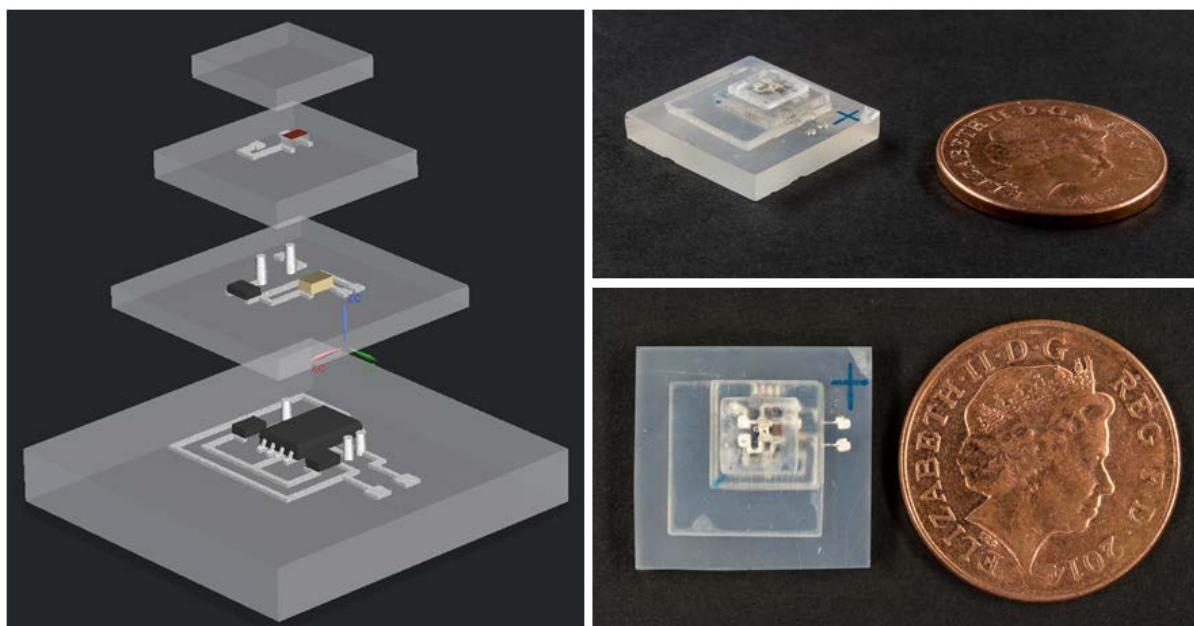
Figure 7.8.　　　　Exploded view, circuit layout and photograph of triple layer, miniaturised 555 timer demonstrator

The footprint of the fully fabricated and functioning demonstrator has been reduced by 70% to 9 mm x 9 mm. The reduction in SMD size has also enabled a reduction in the thicknesses of embedding layers, from 2 mm to 1.2 mm, and therefore the corresponding exposure time required to produce the thick embedding layers was decreased from 210 seconds to 90 seconds. This also further reduced any residual stresses on the substrate caused by the longer exposure time and thicker layers.

These embedded circuit feature sizes are currently in the smallest possible form for this particular type of ICA material. With maximum particle sizes of 20 μm dispensing is limited to a minimum 100 μm inside nozzle diameter, therefore limiting the electronics density. Further investigation of finer particle size distribution pastes could lead to a further reduction in size such as nanoparticle silver pastes as demonstrated by the Lewis group to print features down to 2 μm [11].

7.4　Geometrically Complex Demonstrator

The final demonstration of the capability of this novel manufacturing technique is that of the geometric capability generated through the 3D forming stage of the photopolymer substrate. There are some minor changes to the manufacturing process to facilitate the introduction of complexity to the package, the details of which are discussed in section 6.3.1. No more changes were made to the design and layout of the electronics, the same electronics and dispensing architecture deposited during the production of the demonstrator in section 7.3 were packaged within a traditional pyramid shape.

Embedding circuitry within thick layers of photopolymer limits the geometric freedom in the z-axis due to the large stair stepping caused by the embedding layer. However, this restriction can be eliminated through the production of cavities made from thin layers which are sequentially deposited to the same height as the required embedding layer thickness. This allows the compatibility of this technique with surface mount assembly to be maintained and also the fabrication of unique freestanding z-axis connections to provide the electrical contact between adjacent layers. The base substrate is fabricated layer-by-layer with the external wall geometry containing a central cavity. The circuitry is then deposited, SMDs placed and the layer thermally cured. Liquid photopolymer is then filled into the cavity and left to settle for 5 minutes facing upwards, allowing any trapped air to dissipate. The specimen is finally repositioned upside down in the SL system and submerged within the vat to the top of the cavity. The next stage in the SL build process is then initiated, beginning with one long exposure to cure the filled cavity before the traditional layer-by-layer approach is again used to produce the external geometry and cavity to contain the second layer. This process is represented in Figure 7.9.
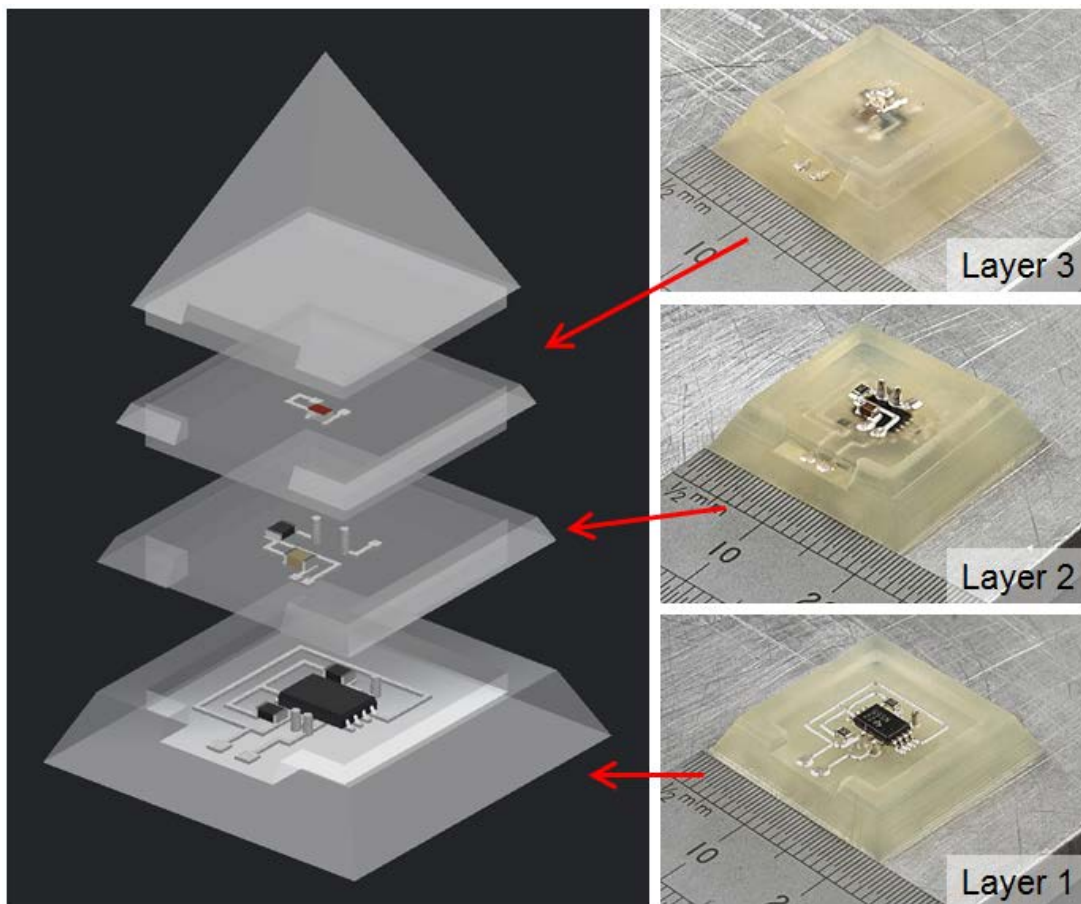
Figure 7.9.   Designed and fabricated examples of pyramids

This cycle was repeated three times before the final immersion in the SL system to build the top of the pyramid structure and fully embedding the last layer of electronics. The completed

demonstrator is shown in Figure 7.10 and Figure 7.11. Only two conductive pads remain exposed to allow a power source to be connected, resulting in the expected intermittent flashing of the LED.
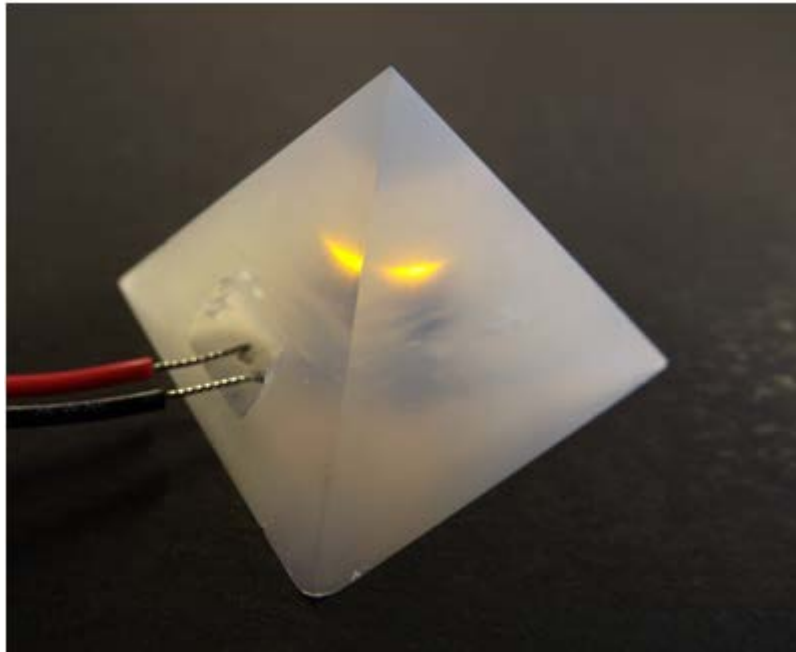
Figure 7.10.   Large pyramid with flashing 555 timer and 30 mm x 30 mm base

Three pyramid demonstrators were fabricated, with the only difference between the size of the base layer which was reduced on the second iteration from 30 mm x 30 mm to 20 mm x 20 mm.
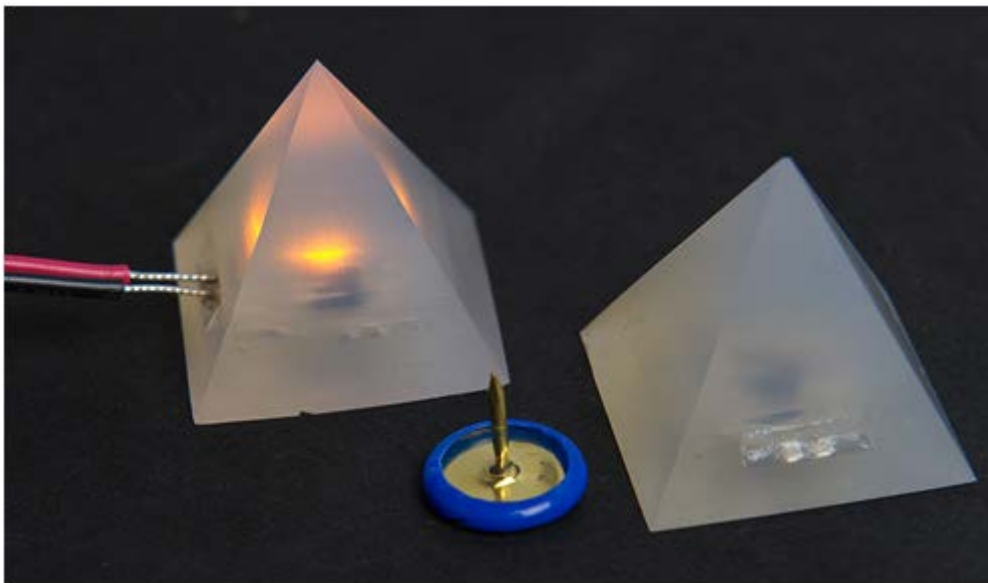
Figure 7.11.   Miniaturised pyramid with flashing 555 timer and 20 mm x 20 mm base

Finally, the pyramid demonstrator shown in Figure 7.12 was produced on a 15 mm x 15 mm base using a 100 μm nozzle and ICA material A, resulting in a significantly smaller circuit layout.
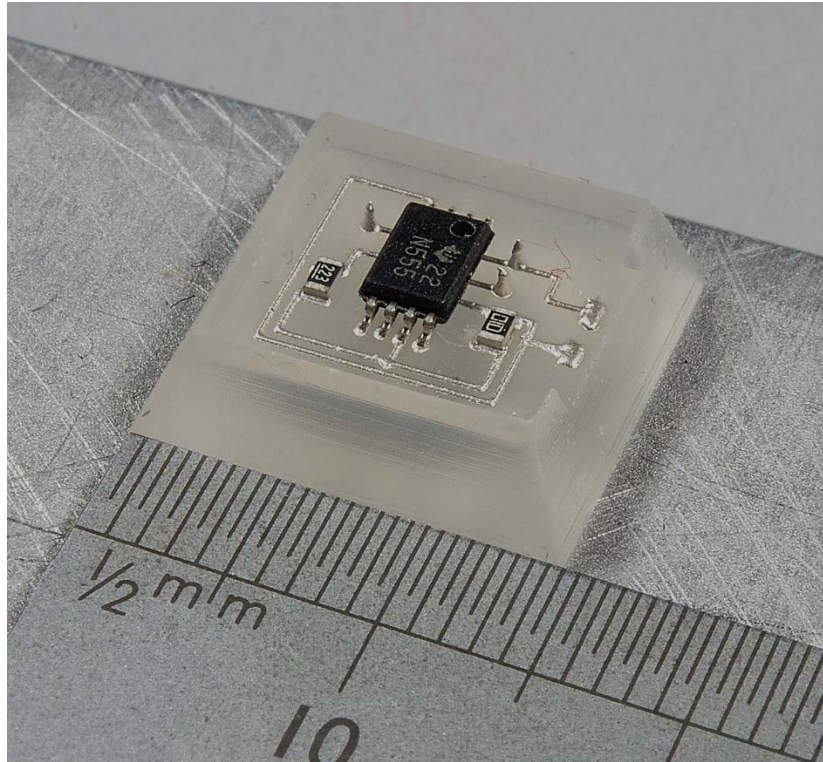
Figure 7.12.   15 mm x 15 mm pyramid base

The size of the IC and SMD components can be further reduced to 0402 or even 0201 and the circuit pattern condensed now that smaller track and pillar widths have been proven in the context of a print layer of circuitry. Recommendations for resolution improvement of the dispensing process will be made in chapter 9.

7.5   Application in Microfluidics

Microfluidics presents a method of processing volumes of fluid between 10^{-9} and 10^{-18} litres causing differences in behaviour that differ from conventional flow theory [219]. These devices reduce reagent use and increase throughput by providing a method of analysing, mixing, heating and separating small volumes of fluid [220].

7.5.1   Microfluidic Manufacturing Background

Microfluidic devices are traditionally manufactured by a combination of additive, subtractive and pattern transfer techniques, the choice of which is dependent on the material. Materials are selected dependent on their compatibility with the fluid and the processing requirements. Fabrication techniques include micromachining, injection moulding, wet and dry etching, soft lithography and in situ construction [221].

Following its wide use in MEMS based processing, silicon micromachining has been applied to the production of microfluidics with Electrochemical Micro-Machining (EMM) demonstrating a resolution of ±1 μm on 50 μm features [221]. Both silicon and glass show high resilience to solvents making it suitable for chemistry applications. However it is also costly and silicon is not UV transparent, demonstrating unsuitability for biological applications [222][223].

Injection moulding alternatives are able to produce parts in high volume at low cost however both resolution and material choice are incomparable to other methods [224]. A master mould or template is also required which itself needs machining [225].

Wet etching offers good control over the etching rate alongside high repeatability. Micro channels are created by eroding solid material using a chemical solution, the rate of which can be controlled by the etchant concentration and etching time. Alternatively, dry etching is a slower process however it works on almost all materials. This process uses ion or photon beams to knock atoms out of the substrate material or, electron beams to heat and vaporise the substrate material producing the final features [219].

Soft lithography was specifically developed for application with biologically compatible materials. A two part polydimethylsiloxane (PDMS) is patterned using stamping, moulding or embossing with the resolution limited by that of the master template [226]. It is cheaper and faster than micromachining and is easy to manufacture [227]. It also encompasses hot embossing that can transfer patterns from quartz or metal plates.

Finally, in situ construction relies upon UV exposure of photopolymers through a mask, defining the channels walls and allowing remaining fluid to be washed away. This is a cheaper, quicker alternative to those presented however, material choice is limited to UV curable polymers. This technology translates closely to Stereolithography, one of a number of additive manufacturing processes used to fabricate microfluidic devices.

All these fabrication approaches are limited to 2.5 dimensions with an improvement to traditional 3D methods significantly increasing the processing cost and the failure rate of the manufacturing process.

7.5.2 Additive Manufacturing of Microfluidics

A number of additive manufacturing techniques have been previously evaluated to fabricate microfluidic devices. Polymer processing techniques including inkjet 3D printing (i3DP), fused deposition modelling (FDM) and Stereolithography (SL) have been assessed for their suitability.

Ink jet printing has proven favourability for the production of enclosed channels in excess of 400μm in width and open channels down to 100 μm in width in multiple materials providing both improved physical and chemical functionality [228]. Examples of these channels are displayed in Figure 7.13. Commercial machinery does however come at a cost 10-100 times higher than SL and FDM alternatives, but batch production in combination with a short build time makes this method affordable for commercialisation. The greatest challenge in the production of micro scale i3DP features is the removal of support materials, a process that will require improvement in order to achieve enclosed channels of the same quality as their open equivalents [229].
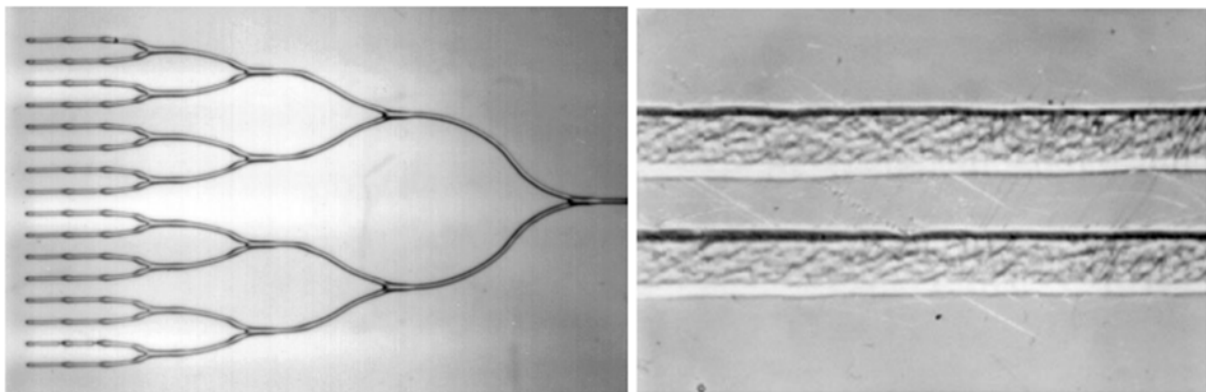
Figure 7.13.   Ink-jet printed a) 100 μm and b) 275 μm polymer lines [230]

Stereolithography has a number of advantages in the production of microfluidics including high resolution and optical clarity through additional polishing. The build orientation can be altered to minimise the roughness of micro channels and improve the flow conditions [74]. Embedded channels down to 300 μm in width can be fabricated without support structures and cleared by pumping through a solvent at a high pressure, ultrasonic agitation and a high pressure air supply, allowing a full microfluidic matrix including ports and measurement points to be fabricated in one build process [231]. Channels smaller than 300 μm cannot easily be cleared of the excess liquid resin, therefore causing the blockage of these features. SL is more convenient, cheaper, faster and has the capability to produce devices with a higher geometric complexity and functionality (Figure 7.14(a)-(f)) than soft lithography and other traditional methods. That said, resins are not currently biocompatible and are not chemically inert to many solvents.
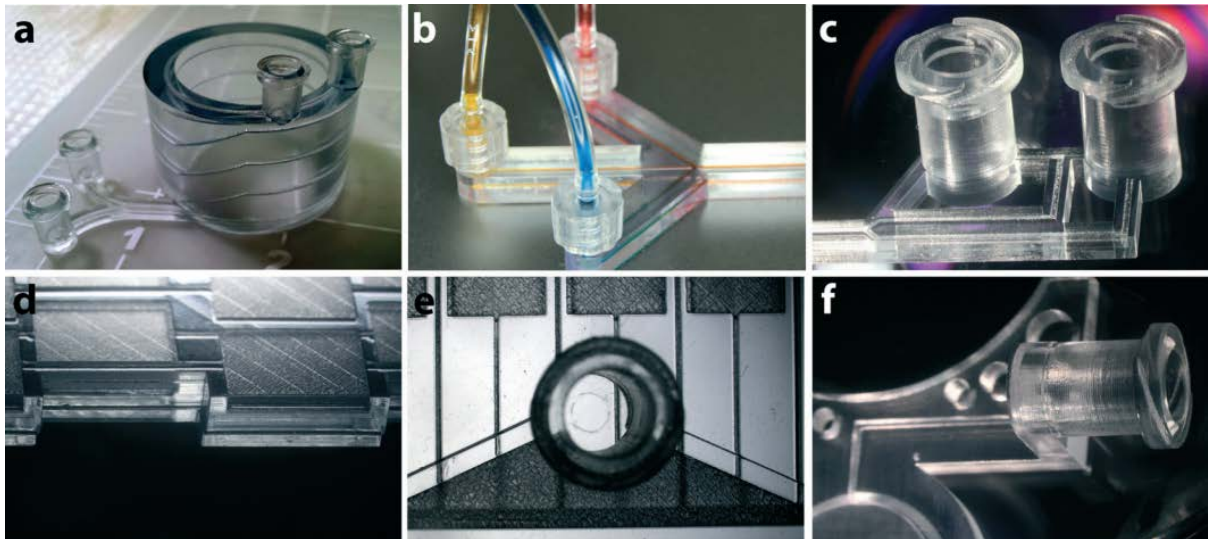
Figure 7.14. Examples of SL manufactured features and devices a) a coil shaped microchannel device, b) interfaces with integrated luer connectors, c) micrograph of the removal of voiding from the footprint of SLA parts, d) closed chambers can be accessed from precisely-defined sidewalls of a device, e) an inlet distributor with a folded geometry and, f) a luer inlet orientated parallel to the plane of the chip [231]

Finally, Fused Deposition Modelling is a simple, low cost and widely available technology for the production of millifluidics, an example of which is displayed in Figure 7.15. There are however inherent limitations including the surface texture caused by the filament and dimensional accuracy, hence it is limited to macro scale manufacturing [232]. In addition,100% fill density cannot be achieved and reaction pressures are severely limited due to the low adhesive strength between printed filaments. The FDM concept does however make the technology compatible with a wide variety of materials promoting its use to extrude multiple materials and produce functional devices using magnetic, flexible and conductive filaments in addition to a number of coloured polymers [233][234]. High deviations in channel width also make printed features very inaccurate [235].
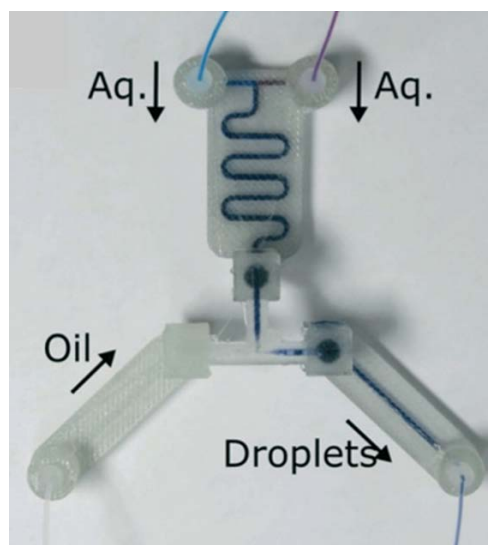
Figure 7.15. FDM printed PLA microfluidic for generating oil-in-water droplets [236]

All presented methods have favourable characteristics for different applications within microfluidics, from cheaper systems requiring less accuracy to high quality, high resolution devices capable of highly accurate measurement. Further development is however needed as additive manufacturing techniques are still incapable of producing accurate and repeatable micro features less than ~500 μm in size. The AM production methods reviewed above all produce microfluidic systems with no integrated functionality. The hybrid approach developed and explained during this thesis allows the integration of additional functionality such as sensing electrodes for monitoring and controlling reactions, actuators for reactions, heating and pumping. This can all be packaged within bespoke geometries and allows the microfluidic network to be optimised for a chosen reaction.

7.5.3 AM Development of a Microfluidic for UV Catalysis

One specific type of reaction conducted in microfluidic devices is UV catalysis. This exposes a solution to a given intensity of ultraviolet light to initiate or speed up a reaction. For the purposes of this application an LED was chosen as the exposure source as they have previously been embedded during this research and provide a compact footprint and can be surface mount assembled. LED's have been embedded in FDM parts designed for microfluidic measurement purposes [237].

The hybrid additive manufacturing developed during this PhD was used to fabricate the entire device including microchannels, circuitry, discrete components and an embedded UV light source to expose the fluid passing through the reaction chamber.

This application required the inclusion of embedded channels, a feature that had not yet been fabricated using this system. The DLP exposure method and poor control over the depth of light penetration caused problems with the accumulation and polymerisation of excess resin in the channels once they had been fabricated. Therefore TESA 4965 clear double sided acrylic tape was used to seal the cleaned channel once built, allowing additional material to be added without flooding the channel and facilitating the creation of ports through which fluid can be pumped in and out of the device.

The movement of fluid through channel features and reaction chambers can be assessed through observation of the flow of coloured die underneath the surface. Samples of the microfluidic channels and reaction chamber geometry were produced, sealed with tape and embedded. Vertical entry and exit ports were built and threaded, allowing the die to be pumped through the structure using a syringe from right to left in the images shown in Figure 7.16. The darker shade of red shows the most direct flow path through the chamber while some die has settled in the sharp corners and flows more slowly through the system.
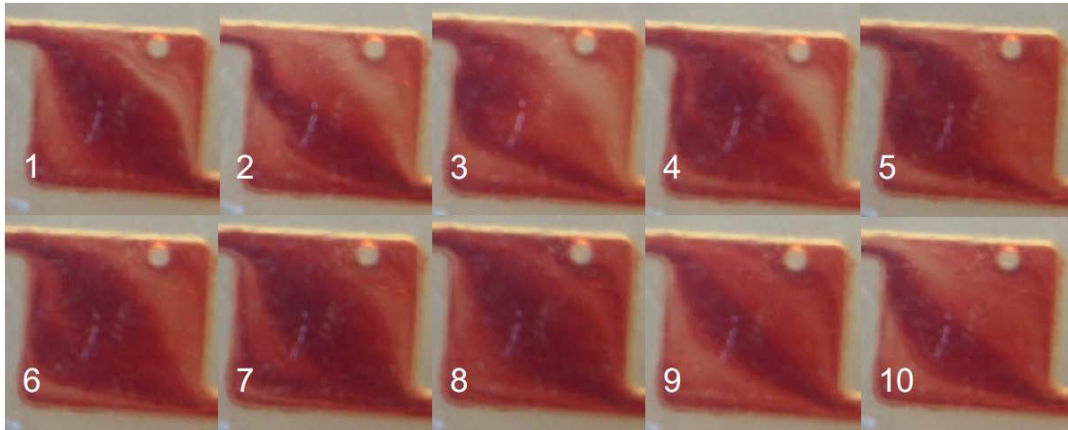
Figure 7.16.   Fluid flow through the 5 mm x 5 mm reaction chamber

The chamber shape has also resulted in the entrapment of a bubble and therefore, further development of this application would involve a redesign of the chamber shape to ensure a consistent flow of material. Some possible re-design options are presented in Figure 7.17. The first shows a mixing chamber with corners removed, aiming to ensure that all fluid flows through the chamber at an equal rate with no areas of stagnation. The second design involves increasing the fluid path distance and since the channel does not enlarge would prevent air bubbles from settling in the reactor. As this method is digitally driven an infinite number of possible channel geometries could be designed including ones that are highly complex and span multiple layers.
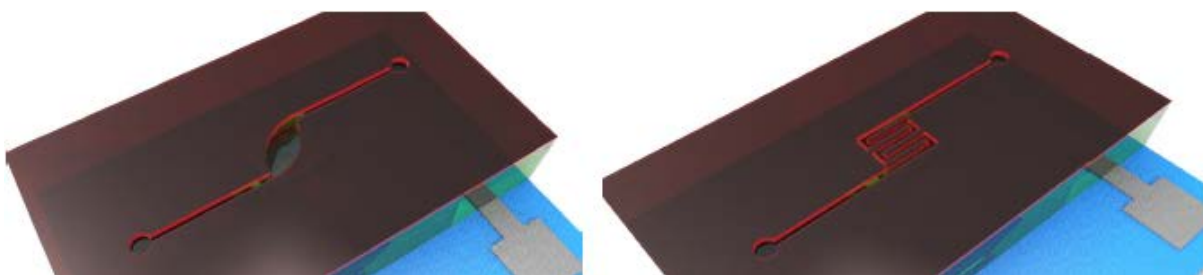
Figure 7.17.   Channel re-design suggestions

Further functionality could be added to this microfluidic device by including measurement points and incorporation of sensors for in-situ process monitoring.

7.5.4   Fabrication Process

The device was designed in multiple build stages each of which has been shown in Figure 7.18. This required the substrate fabrication process to be paused four times during the build process. The build pauses provide the opportunity to print a layer of circuitry, insert a UV LED in a pre-fabricated cavity, position and secure a UV transparent quartz window underneath the reaction chamber and,

seal the microchannel, before each of these features are encapsulated within the photopolymer substrate.
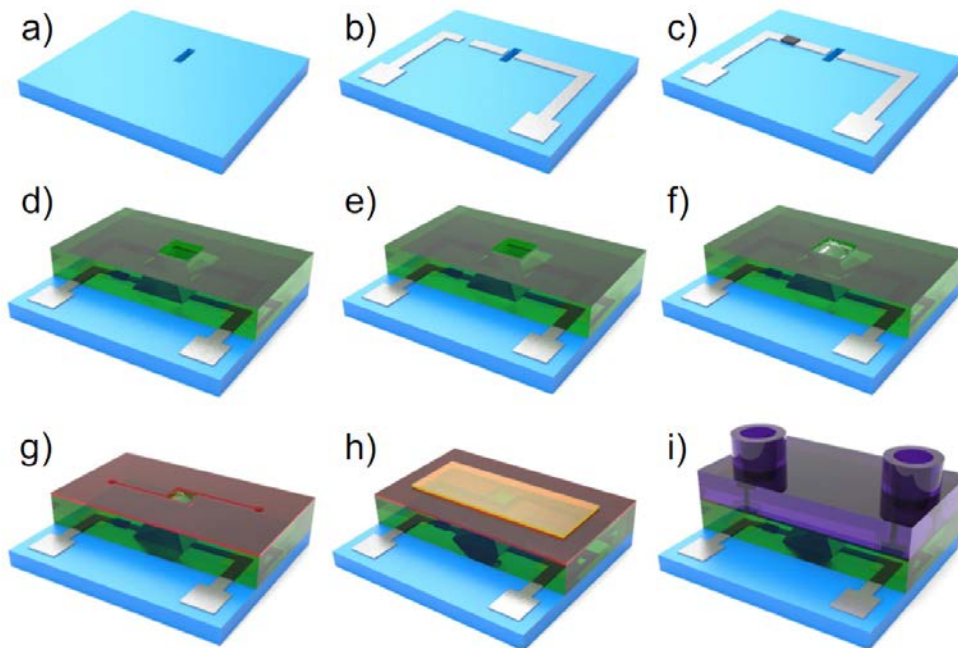
Figure 7.18.   Step by step AM method for microfluidic manufacturing

Table 7.1 summarises each of the 9 process stages represented in Figure 7.18.

Table 7.1.   Step by step AM method for microfluidic manufacturing

Stage	Process
a)	Fabricate substrate with cooling trench for UV LED
b)	Print traces and pads for electrodes, resistors and LED
c)	Position SMD resistor and thermally cure ICA
d)	Embed resistor and build LED cavity
e)	Deposit wet ICA on LED interconnects
f)	Place LED in cavity onto wet epoxy interconnects
g)	Build channel and mixing chamber using SL process
h)	Wash and seal channel using tape
i)	Continue SL process to fabricate entry and exit ports

The base substrate is first fabricated in a layer-by-layer fashion using DLP Stereolithography with an upward projection orientation. A hole was included through the base over which the LED will be inserted. Conductive tracks and component interconnects were then deposited onto the substrate surface using an isotropic conductive adhesive before the resistor was positioned onto one pair of

interconnects. The substrate was then baked at 80 °C for 3 hours to cure the ICA and consequently secure the resistor before it is embedded in a thick layer of photopolymer as shown in Figure 7.19.
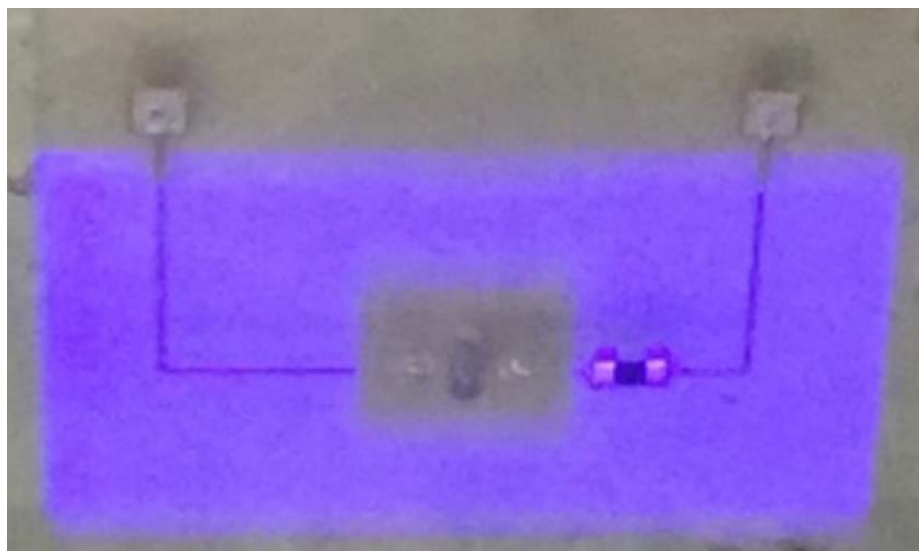
Figure 7.19.   Embedding circuity and resistor within photopolymer substrate

The normal SL build process is continued to produce a cavity to house the UV LED and position a quartz window, through which the reactant will be exposed. Figure 7.20 shows the placement of the UV LED onto the deposited ICA and testing of its function.
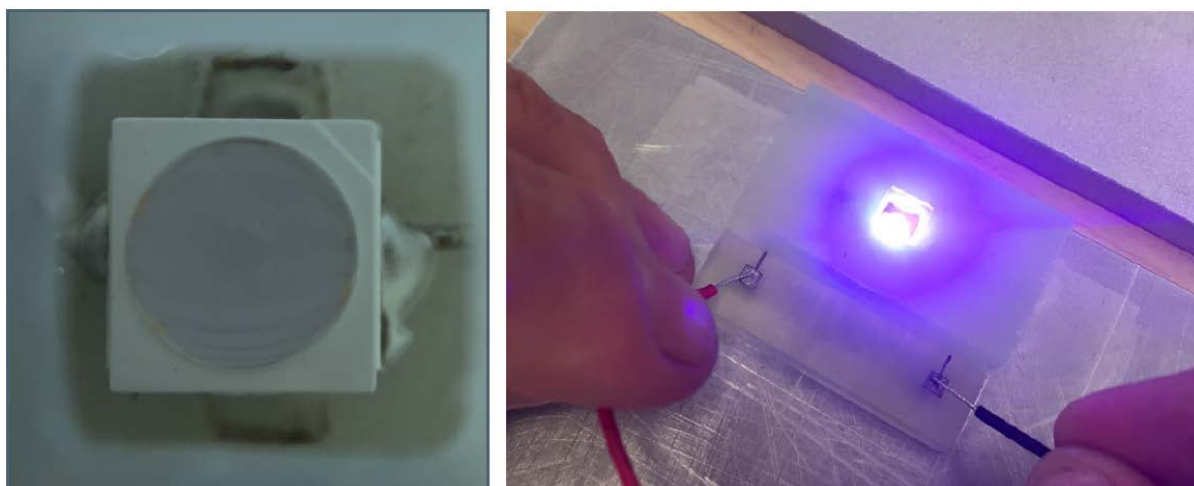
Figure 7.20.   UV LED in its pre-fabricated cavity before and after thermal curing

The quartz window was then positioned and embedded, to create the fluid channel and reaction chamber. The channel and chamber was then cleaned and the chemically inert tape manually positioned to seal the feature as shown in Figure 7.21. This stage prevents more resin from entering and blocking the channel.
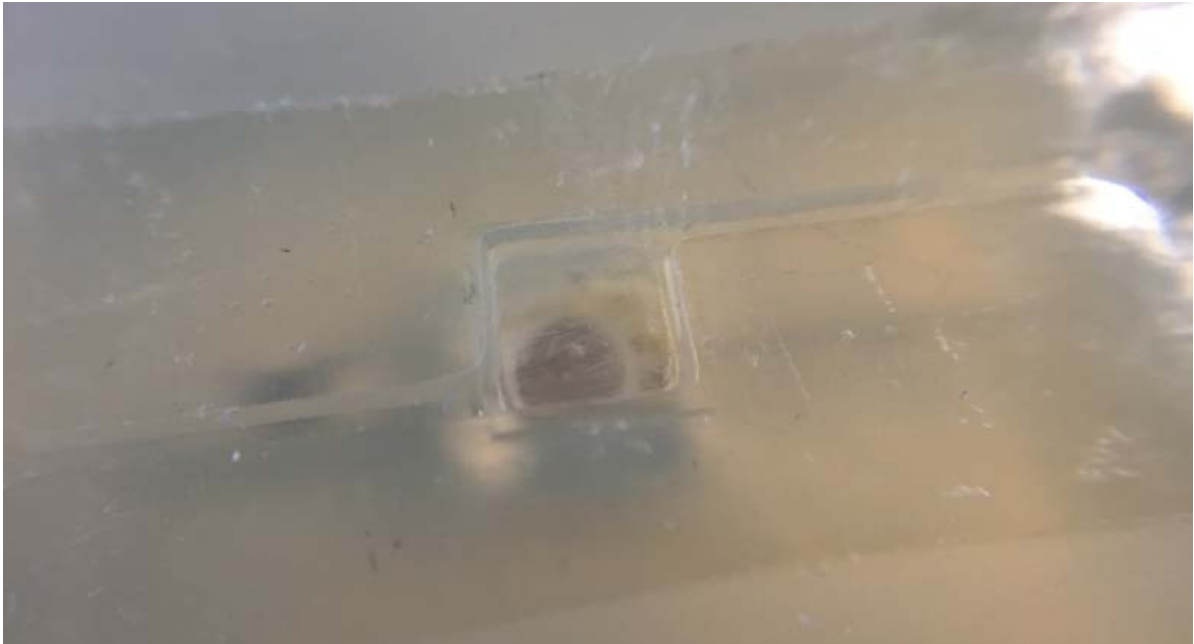
Figure 7.21.   High resolution channel and reaction chamber sealed with tape

The channel was embedded and two entry ports fabricated at either end of the channel during the build process. The ports in Figure 7.22 were tapped and the tape pierced to create a continuous channel from one port to the other. When connected to a power source the UV LED lights up.
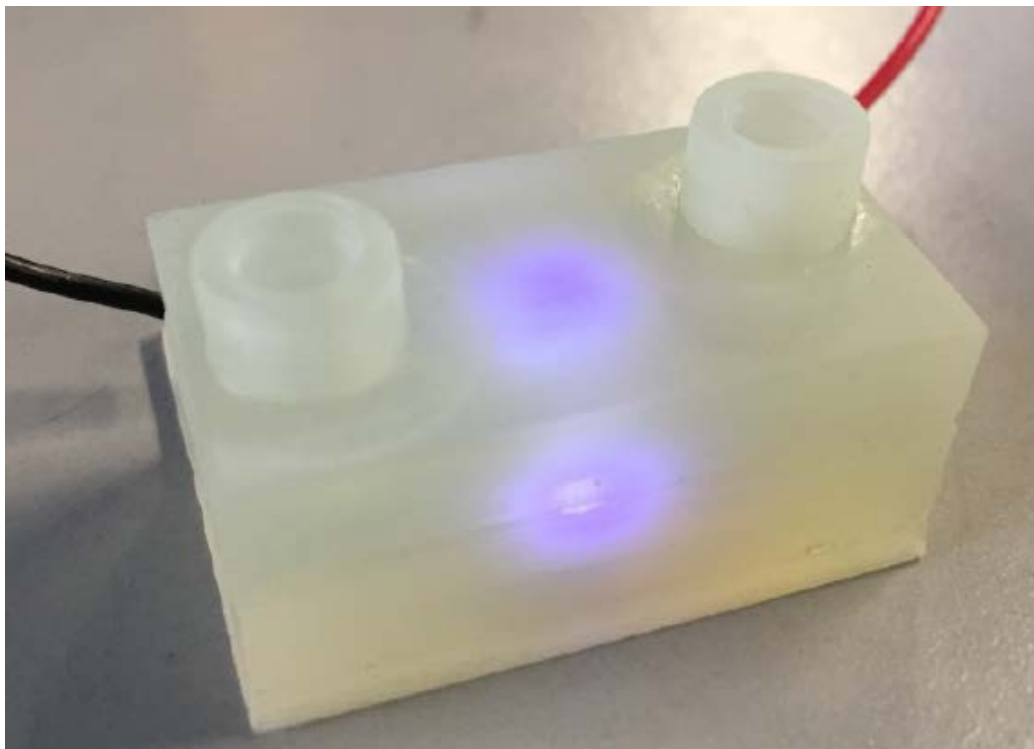
Figure 7.22.   Successfully fabricated AM microfluidic for UV catalysis

Testing of the fluid flow through the device was then conducted to ensure that there are no obstructions and that a reaction to UV light is achieved.

7.5.5 UV Catalysis Test

The capability of this microfluidic device to enable a UV initiated reaction was assessed through the use of a photochromic ink designed to change colour from clear to orange when exposed to sunlight. The ink was injected into the device using a syringe. On close examination, the ink exiting the channel was a pale orange colour as shown in Figure 7.23, proving that the exposure mechanism worked.
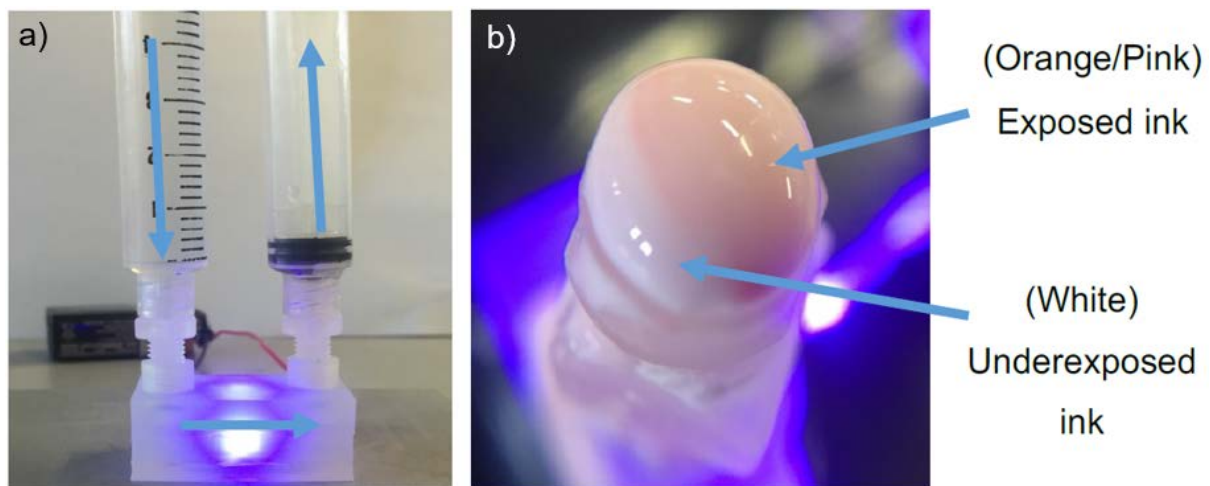
Figure 7.23.   UV catalysis test a) setup and b) resulting exposed ink

The ink did not display a full reaction to the ultraviolet light as it is designed for UV exposure once cured however, the feasibility of this hybrid additive manufacturing technique to create a fully functioning microfluidic device with integrated components has been proven.

This process has the potential to demonstrate much greater functionality with multiple LEDs to tailor the intensity of the light source dependant on the reactant. This could be set, measured and controlled through intensity feedback achieved through the integration of sensor systems and actuators within the embedded electronic systems. In addition complex channel designs can be included providing a number of separate measurement points, greater exposure to the UV light source and the potential to mix multiple reactants.

An LED has previously been added to a microfluidic created by fused filament fabrication. Cavities created for embedding required smoothing before addition of silicone adhesive before positioning of the LED to create a water tight seal [237]. The integrated stereolithography and dispensing process presented here improved on this method as the LED and drive resistor could be directly embedded without the need to smooth the cavity and, the SL resin itself cured to create the water tight cavity with adjacent mixing chamber.

8 Conclusions

The capability to produce three dimensional multilayer electronics has been demonstrated, improving on previous methods that were limited to printing on and in cavities on the substrate surface. This was achieved by:

- Developing and characterising bespoke UV DLP stereolithography apparatus.

- Introducing a photopolymer developing process to optimise the quality of an SL substrate surface.

- Characterising the material dispensing of ICAs for the deposition of conductors on photopolymer substrates.

- Analysing and optimising the compatibility between stereolithography and dispensing processes and their materials.

- Miniaturising the manufacturing process to facilitate the flip-chip packaging of bare die.

The use of a DLP based Stereolithography system has been shown to provide greater functionality than previous SL and DW hybrid manufacturing systems. A bottom up build orientation was proven to produce a flatter substrate than its top down equivalent in addition to demonstrating a faster build time than laser based Stereolithography systems. This system was fitted with a dedicated 405 nm projection source and was coupled with a broad-band resin sensitive to wavelengths of light up to 440 nm with a low photoinitiator concentration, reducing the sensitivity to light and therefore residual stresses demonstrated by the resin. The bottom-up projection orientation facilitated the fabrication of 15 mm x 15 mm substrates with only a 6 μm surface height variation, compared to a value of 70 μm achieved using top-down orientation.

Material dispensing was chosen for integration with Stereolithography due to its potential processing resolution and range of candidate materials. The photopolymer substrate limited the maximum processing temperature to 100 °C and therefore low temperature curing isotropic conductive adhesives were used to print conductors. Two ICAs were chosen for their behavioural properties including viscosity, thixotropic index and maximum particle size which allowed dispensing to occur on a flat surface without the need for channel features to control the material rheology. These materials also facilitated the compatibility of material dispensing with surface mount assembly.

Compatibility of conductive pastes and cured photopolymers were tested through investigation of their electrical properties. The resistivity of both ICAs after three different low temperature curing

regimes was measured resulting in values of ~$3x10^{-4}$ Ωcm, one order of magnitude lower than the material data sheets. In addition, higher temperatures resulted in lower resistivities in both materials however, these values were still higher than that of bulk silver. The dispensing process and its printing parameters were characterised for the fabrication of two different conductive features, tracks and novel z-axis connections. Previous hybrid systems incorporating material dispensing have used surface features to control the deposition however, this experimentation demonstrated that high resolution circuitry could be deposited in high density. Conductive traces with a minimum width of 150 μm and height of 43 μm were achieved using the higher viscosity of the two ICA materials as it demonstrated less slumping and a smoother track profile.

To enable the development of multilayer electronic systems unique z-axis conductive pillars have been presented that were printed by depositing a number of layers on top of one another. The features were printed simultaneously with tracks and component interconnects in one continuous process. The pillars were specifically intended for use in combination with the bespoke substrate fabrication process and subsequent thick layer embedding technique. Pillars with heights of 3.8 mm and 2.04 mm with respective, aspect ratios of 3.81 and 3.68 were achieved, the latter of which is only 550 μm wide, resulting in a minimal electronic footprint and a feature capable of creating an electrical connection through a 2 mm thick layer of substrate. During embedding, these pillars could be pressed into the PDMS layer on the base of the vat, leaving small contacts, <100 μm in height, for connection of subsequent layers of circuitry.

Packaging of electronic circuitry was achieved by overcoming a number of hybrid process limitations, most notably the capability of the SL process to successfully embed surface mount components. Surface levelling of the liquid photopolymer would be obstructed by SMDs however, the unique, thick layer embedding process introduced during this research provides a solution. This enables the packaging of full layers of circuitry and underfilling of components in geometrically complex structures. The chosen resin also demonstrates the reduced appearance of stresses in layers with embedded SMDs as cracks propagating from corners of components are eliminated and warping of the substrate is also reduced to under 10 μm across the entire surface. This measurement is comparable to the surface profile and roughness of the base substrate.

Tensile testing was used to measure the adhesive strength between the substrate surface and thick layers of embedded material, proving that even a layer 2 mm thick and a bonding area of 9 mm x 5 mm requires a force in excess of 1200 N, perpendicular to the layer boundary to fracture the specimen. This force increases by 200 N at 1 mm layer thickness, showing that this reduced layer thickness improves the mechanical properties of the structure. In addition, no negative effect was

measured on the resistivity of conductive material once embedded, proven by the encapsulation of conductive traces within the substrate material and subsequent measurement of track resistance.

In this work the material dispensing process was proven to produce high resolution interconnects at a fine pitch. Flip-chip packaging was conducted by this hybrid additive manufacturing process, using processing capabilities of both SL and DW to produce a planar surface with conductive channels and ICA bumps with a diameter of 150 µm at a pitch of 457 µm. The 80 µm bump height also ensured that the standoff height of the chip is minimised, creating a more reliable array of connections. The interconnects were achieved by timed point deposition with a range of pressures, print gaps, nozzles and pressure actuation times investigated to produce the dimensions above. A bonding force of 0.08 N was used to package a daisy chain bare die before it was embedded and underfilled with a liquid photopolymer, resulting in no change in interconnect contact resistance.

Individual processes were combined to produce the feasibility demonstrators in Figure 8.1, proving this novel hybrid concept and creating embedded electronic systems. A single layer 555 flashing timer circuit with a footprint of 25 mm x 15 mm and 1206 SMDs was produced and embedded within a 2 mm thick layer of photopolymer. A second layer was added to the subsequent device proving the success of the freestanding pillar structures in connecting multiple layers. Finally, the circuit was redesigned reducing its footprint to 9 mm x 9 mm, adding a third layer and halving the component size to 0603 SMDs and consequently, the layer thickness from 2 mm to 1.2 mm.
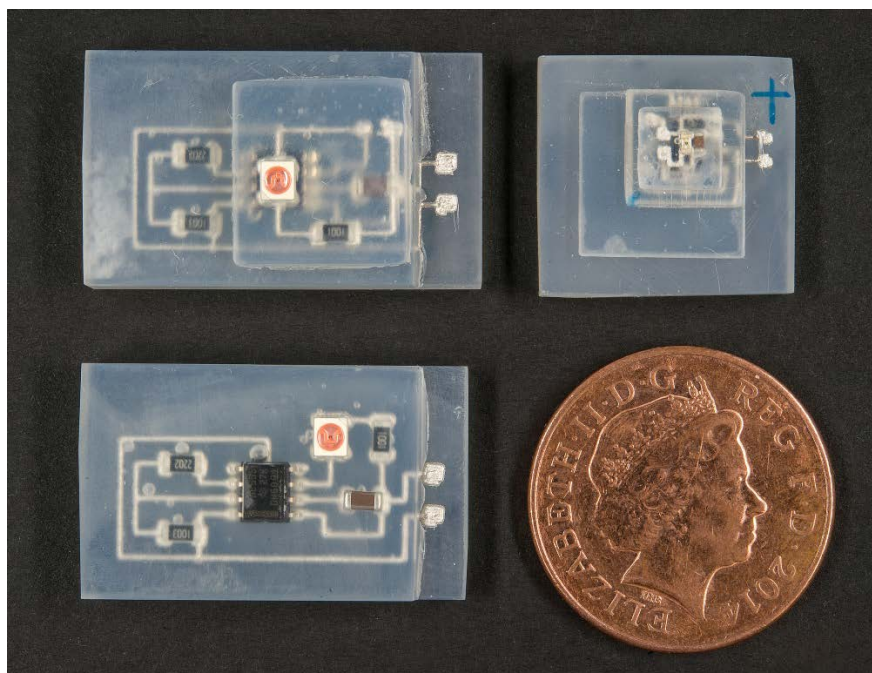
Figure 8.1.   Images of one, two and three layer 555 timer circuit demonstrators

Pyramid shaped demonstrators were fabricated to verify the capability of this process to produce complex geometries with internal electronics. These examples exhibited a constantly changing cross

sectional profile with electronics integrated into the package using cavities in which full layers of circuitry and components including z-axis connections are deposited. These pyramid structures were reduced in size from a base width of 30 mm x 30 mm to 20 mm x 20 mm and finally 15 mm x 15 mm. The reduction in conductor size and increased printing density facilitated this minimisation.

This integrated additive manufacturing technology shows great potential in microfluidic applications. A device designed to conduct UV catalysis of a reactant was built in multiple stages with embedded electronics to power a UV LED also encapsulated within the system. A high resolution 500 μm channel and mixing chamber were built above the light source providing an internal exposure volume for the reactant fed through the system by a syringe. A successful reaction was catalysed through the reactor with an observed change in the colour of a photochromic ink.

This method presents several novel improvements on and additions to previously developed hybrid additive manufacturing systems. Multilayer circuitry can now be fabricated and packaged within highly complex three dimensional structures.

9 Future Recommendations

The feasibility of this process has been demonstrated. However further development of processes and materials would contribute to reducing the size of the electronics and facilitate the use of this hybrid process for a wider range of applications. This can be achieved through changes to the Stereolithography system, specifically the projection source and its compatible materials and by tailoring the properties of isotropic conductive adhesives to this application by developing bespoke formulations. Further testing can also be conducted on a fabricated electronic system including exposure to temperature cycling and comparison to standards for commercial electronics provided by JEDEC. Finally, a system and corresponding software facilitating the automated transfer of samples between integrated AM techniques and processing modules would realise this technology as a fully digitally driven manufacturing chain for the production of bespoke multi-layered electronics.

9.1 Substrate Production

To demonstrate the proof of concept of integrating multiple manufacturing processes the resolution of substrate fabrication by Stereolithography has been limited by time and financial constraints. The resolution of the UV projection source could be improved by either purchasing a more expensive, high definition projection source or, the addition of an array of lenses to reduce the size of the projected image or the projection distance, both of which would result in the reduction of focused pixel size. This change would reduce the minimum feature resolution, making the process more attractive for applications requiring microscale fabrication capability, particularly MEMS.

This research has thus far been limited by the projection wavelength, making the use of low cost, acrylic based, broad-band sensitive photopolymers necessary. The development of a high power, high resolution projection source with a source wavelength of 365 nm would significantly increase the available material choice, allowing epoxy based resins specifically developed for use with 365 nm laser sources to be utilized. These different photopolymers have a broader range of characteristics tailored for different applications ranging from high glass transition temperatures providing greater heat resistance [238], biocompatible materials for contact with the skin in the healthcare industry [239] and, ceramic-like materials demonstrating high detail resolution and stiffness ideal for prototyping and wind tunnel testing [240]. With significantly more investment and resources having been devoted to the development of these materials, fabricated parts are much higher quality than white light alternatives, making their use highly advantageous.

9.2   Material Development

One major limitation of the majority of currently available photopolymer materials is their poor heat resistance, with very few possessing a glass transition temperature greater than 100 °C. A Stereolithography resin sensitive at 365 nm is available that requires post processing to increase its heat resistance, this would allow higher temperature curing regimes to be utilized. An increased curing temperature was proven to reduce the resulting ICA resistivity, making it a favourable processing characteristic for conductive materials. The number of commercially available conductive adhesives suitable for use in this hybrid process would also increase with an improved heat resistance due to the wider availability of materials that cure at temperatures over 100 °C.

The vast majority of research conducted into the development of photopolymers is directed towards polymerisation using 365 nm light sources in laser form. The formulation of these same resins with a photo initiator sensitive at 405 nm would allow the same, high quality materials to be applied to this research using the 405 nm dedicated pico-projection source. The advantages of these materials have already been discussed in section 9.1. This presents an alternative to the development of a 365 nm projection source.

Process resolution can also be improved through the development of conductive materials that can be deposited through smaller nozzles. This would require the reduction in size of filler particles or flakes from micro to nano scale. Difficulties have previously been encountered ensuring prolonged suspension and equal distribution of silver nanoparticles in a solvent, a solution to which has been developed for inks [127] and may be transferable to low temperature curable conductive adhesives. The reduction in conductor dimensions directly impacts the dimensions of compatible SMD's and therefore the circuit footprint and embedding layer thicknesses.

9.3   Reliability Testing

The reliability of electronics can be determined through a number of accelerated life testing procedures, the most common of which is temperature cycling in a HALT chamber. Accelerated life testing is a method by which failure times and mechanisms of electronics can be assessed on a reduced time scale. Test cycles can be designed to simulate an accelerated life through environmental and physical changes to the point where failure occurs, at which point the most vulnerable part of the device can be determined.

Two types of test exist, qualitative testing provides failure information only and has been referred to as HALT and shake and bake tests. Samples are subjected to single, multiple or time varying stresses and are designed to reveal failure modes that will occur during the life of the product. These failures

can consequently be designed out to improve the product. This testing cannot however quantify the reliability of the product during normal use [241].

Quantitative life testing, in contrast to the previous method, comprises of tests designed to quantify life characteristics and can provide probability of failure and product life. Two further acceleration methods are deployed in this branch, usage rate acceleration whereby devices that are not continuously used have their use hastened until failure. The second method is overstress acceleration with stresses above the predicted use being applied and using time to failure data to determine failure time under normal use conditions [241].

There are a number of test conditions and therefore standards, shown in Table 9.1 that can be assigned to these products, the most common of which are established by JEDEC, a global leader in developing open standards for the microelectronic industry. The most suitable in this case is condition 'J' given the 100 °C glass transition temperature of the photopolymer material.

Table 9.1. JEDEC temperature cycling test conditions [242]

Test Condition*	Nominal $T_{s(min)}$(°C)	Nominal $T_{s(max)}$(°C)
A	-55	+85
B	-55	+125
C	-65	+150
G	-40	+125
H	-55	+150
I	-40	+115
J	-0	+100
K	-0	+125
L	-55	+110
M	-40	+150
N	-40	+85
R	-25	+125
T	-40	+100

Each test condition has a specific number of cycles, the full length of which is designed to subject the part to stresses it may otherwise undergo during its effective lifetime. Additively manufactured electronics have never before been subject to accelerated life testing, the expectation is that cured photopolymers would delaminate after a number of cycles however this has not yet been proven.

9.4 Manufacturing Automation

During the conception of this research idea the functionality of an all-in-one electronics printer was compared with a manufacturing line both possessing the same functionality, with the latter chosen for the basis of this system. This approach demonstrated a more suitable solution to electronics fabrication through hybrid AM technology with advantages including the capability to produce more

than one sample simultaneously and, the ability to add increased functionality by adding additional processing modules to the line; this in contrast to adding additional functionality to a single machine where space is already at a premium. To prove this concept, manual transfer between processes was conducted. However, to fully utilize the digitally driven potential of the Additive Manufacturing techniques, automated transfer between processes and processing modules would be necessary. Such a system would require automated alignment, a rotational element to facilitate substrate fabrication through bottom up Stereolithography and conductive track deposition by material dispensing and, bespoke software to interpret specimen design and control the manufacturing process flow.

At present, substrate fabrication and dispensing systems do not communicate. The substrates and conductors are designed and fabricated independently of one another, with the user ensuring that parts are correctly aligned and designs accurately produced. Bespoke software would allow individual designs to be combined aligning the conductor design with a location or origin on the substrate design before the part is fabricated. This pre-defined origin location can then be tracked through the fabrication process ensuring accurate alignment at each stage.

10 References

[1]   R. Sharma, "The Future of 3D Printing and Manufacturing," *Forbes*, 2014. [Online]. Available: http://www.forbes.com/sites/rakeshsharma/2014/01/15/1255/.

[2]   "Obama Administration Announces New Public Private Partners," *www.whitehouse.gov*, 2012. [Online]. Available: http://www.whitehouse.gov/the-press-office/2012/08/16/we-can-t-wait-obama-administration-announces-new-public-private-partners.

[3]   H. Lipson and M. Kurman, *Fabricated: The New World of 3D Printing*, 1st ed. John Wiley & Sons, 2013.

[4]   J. A. Paulsen, M. Renn, K. Christenson, and R. Plourde, "Printing conformal electronics on 3D structures with Aerosol Jet technology," in *IEEE Future of Instrumentation International Workshop (FIIW) Proceedings*, 2012, pp. 1–4.

[5]   E. Macdonald, R. Salas, D. Espalin, M. Perez, E. Aguilera, D. A. N. Muse, and R. B. Wicker, "3D Printing for the Rapid Prototyping of Structural Electronics," *IEEE Access*, vol. 2, pp. 234–242, 2014.

[6]   R. Hopeless, "Build a Laser 3D Printer - Stereolithography at Home," *Instructibles*, 2011. [Online].   Available: http://www.instructables.com/id/Build-a-Laser-3D-Printer-Stereolithography-at-Ho/.

[7]   C. Naramore, "mUVE 1: DIY stereolithography 3D printer on indiegogo," *3D Printer*, 2013. [Online]. Available: http://www.3dprinter.net/muve-1-diy-stereolithography-3d-printer.

[8]   J. M. Pearce, "Building Research Equipment with Free, Open-Source Hardware," *Science (80-.).*, vol. 337, no. 6100, pp. 1303–1304, 2012.

[9]   Y. L. Kong, I. a Tamargo, H. Kim, B. N. Johnson, M. K. Gupta, T.-W. Koh, H.-A. Chin, D. a Steingart, B. P. Rand, and M. C. Mcalpine, "3D Printed Quantum Dot Light-Emitting Diodes," *Nano Lett.*, vol. 14, no. 12, pp. 7017–7023, 2014.

[10]   J. A. Lewis and B. Y. Ahn, "Device fabrication: Three-dimensional printed electronics," *Nature*, vol. 518, no. 7537, pp. 42–43, 2015.

[11]   K. Sun, T. S. Wei, B. Y. Ahn, J. Y. Seo, S. J. Dillon, and J. A. Lewis, "3D printing of interdigitated Li-ion microbattery architectures.," *Adv. Mater.*, vol. 25, no. 33, pp. 4539–4543, 2013.

[12]   H. J. Lewis and A. Ryan, "Printing as an Alternative Manufacturing Process for Printed Circuit Boards." INTECH Open Access Publisher, 2010.

[13]   Epoxy Technology Inc., "EPO-TEK® E4110-PFC," *Technical Data Sheet*. 2012.

[14]   D. Giancoli, "Electric Currents and Resistance," in *Physics for Scientists and Engineers with Modern Physics*, 4th ed., Prentice Hall, 1984, p. 658.

[15]   R. A. Serway, *Principles of physics*. Saunders College Pub., 1998.

[16]   R. R. Schaller, "Moore's law: past, present and future," *Spectrum, IEEE*, vol. 34, no. 6, pp. 52–59, 1997.

[17]   F. Sarvar, N. J. Poole, and P. A. Witting, "PCB glass-fibre laminates: thermal conductivity measurements and their effect on simulation," *J. Electron. Mater.*, vol. 19, no. 12, pp. 1345–1350, 1990.

[18]   C. J. Broaddus, J. R. Jephson, E. M. Scales, C. C. Sissenstein, and J. P. Wiley, "Circuit member for use in multilayered printed circuit board assembly and method of making same," U.S. Patent 4,916,260, 1990.

[19]   J. M. Shaw, J. D. Gelorme, N. C. LaBianca, W. E. Conley, and S. J. Holmes, "Negative

photoresists for optical lithography," *IBM J. Res. Dev.*, vol. 41, no. 1.2, pp. 81–94, 1997.

[20]   M. J. Madou, *Fundamentals of microfabrication*. CRC Press, 2002.

[21]   A. Bandyopadhyay and S. Bose, *Additive Manufacturing*. CRC Press, 2016.

[22]   K. Dietz, "Dry Film Photoresist Thickness Selection Criteria," *The PCB Magazine*, pp. 79–72, Jul-2015.

[23]   R. S. Khandpur, *Printed circuit boards: design, fabrication, assembly and testing*. Tata McGraw-Hill Education, 2005.

[24]   Micro Systems Technologies, "Dyconex Rigid PCBs," 2016. [Online]. Available: http://www.mst.com/dyconex/products/standard_pcb_products/rigid/index.html.

[25]   IPC, "Generic Standard on Printed Circuit Board Design." 2012.

[26]   Fujitsu, "High Density Interconnect PCB Design Rules," 2016. [Online]. Available: http://www.fujitsu.com/uk/products/devices/pcbs/pcb-interconnect/multilayer/hdi/index.html.

[27]   S. Kalpakjian and S. Schmid, *Manufacturing, Engineering and Technology*, 6th ed. Pearson Education, 2006.

[28]   "Directive 2002/95/EC of the European Parliament and of the Council on the restriction of the use of certain hazardous substances in electrical and electronic equipment," *Off. J. Eur. Union*, pp. L37/19–23, 2002.

[29]   B. R. Freitag, "Method and apparatus for stencil printing printed circuit boards," U.S. Patent 5,553,538, 1996.

[30]   T. Nanzai, "Apparatus and system for screen printing of solder paste onto printed circuit boards," U.S. Patent 5,287,806, 1994.

[31]   R. Kay, M. Desmulliez, S. Stoyanov, C. Bailey, R. Durairaj, N. Ekere, M. Hendriksen, F. Frimpong, B. Smith, D. Price, A. Roberts, M. Whitmore, P. Ongley, and J. Gourlay, "Low Temperature Flip-Chip Packaging Based on Stencil Printing Technology," in *Proceedings of the IMAPS Micro Tech Conference, Oct.1-2, 2003, Stratford-upon-Avon, UK, 2003*, 2003, p. -.

[32]   R. W. Kay, S. Stoyanov, G. P. Glinski, C. Bailey, and M. P. Y. Desmulliez, "Ultra-fine pitch stencil printing for a low cost and low temperature flip-chip assembly process," *IEEE Trans. Components Packag. Technol.*, vol. 30, no. 1, pp. 129–136, 2007.

[33]   R. W. Kay, "Novel micro-engineered stencils for filp-chip bonding and wafer level packaging (PhD Thesis)," Heriot-Watt University, 2008.

[34]   A. C. Arias, J. D. MacKenzie, I. McCulloch, J. Rivnay, and A. Salleo, "Materials and applications for large area electronics: solution-based approaches," *Chem. Rev.*, vol. 110, no. 1, pp. 3–24, 2010.

[35]   J. M. Rabaey, A. P. Chandrakasan, and B. Nikolic, *Digital integrated circuits*, 2nd ed. Englewood Cliffs: Prentice Hall, 2002.

[36]   W. Greig, *Integrated circuit packaging, assembly and interconnections*. Springer Science & Business Media, 2007.

[37]   M. I. Montrose, *EMC and the printed circuit board: design, theory, and layout made simple*. John Wiley & Sons, 2004.

[38]   Tummala, *Fundamentals of Microsystems Packaging*. McGraw-Hill, 2001.

[39]   K. Gilleo, "Chip Scale or Flip Scale - the Wrong Question?," *Circuits Assem.*, vol. 9, pp. 30–35, 1998.

[40]   K. Gilleo and D. Blumel, "The great underfill race," in *Proceedings of SPIE The International*

Society for Optical Engineering, 1998, pp. 701–706.

[41] K. Gilleo and D. Blumel, "New Generation Underfills Power the 2nd Flip Chip Revolution," in *Pan Pacific Microelectronics Symposium*, 1998, p. 147.

[42] American Society for Materials and Testing, *Annual Book of ASTM Standards*, vol. 10.04. 2013.

[43] E. M. Sachs, M. J. Cima, P. Williams, D. Brancazio, and J. Cornie, "Three dimensional printing: rapid tooling and prototypes directly from a CAD file," *J. Eng. Ind.*, vol. 114, no. 4, pp. 481–488, 1992.

[44] I. Gibson, D. W. Rosen, and B. Stucker, *Additive Manufacturing Technologies*. Springer, 2010.

[45] N. Hopkinson, R. Hague, and P. Dickens, *Rapid manufacturing: an industrial revolution for the digital age*. John Wiley & Sons, 2006.

[46] J. O'Donnell, F. Ahmadkhanlou, H.-S. Yoon, and G. Washington, "All-printed smart structures: a viable option?," in *SPIE Smart Structures and Materials Nondestructive Evaluation and Health Monitoring*, 2014, p. 905729.

[47] B. Geving, A. Kataria, C. Moore, I. Ebert-Uphoff, T. Kurfess, and D. W. Rosen, "Conceptual design of a generalised stereolithography machine," in *Japan-USA Symposium on Flexible Automation, Ann Arbor, MI*, 2000, pp. 1159–1166.

[48] CustomPartNet, "Stereolithography," 2009. [Online]. Available: http://www.custompartnet.com/wu/stereolithography.

[49] A. S. Limaye and D. W. Rosen, "Process planning method for mask projection micro-stereolithography," *Rapid Prototyp. J.*, vol. 13, no. 2, pp. 76–84, 2007.

[50] A. Bertsch, S. Zissi, J. Y. Jezequel, S. Corbel, and J. C. Andre, "Microstereophotolithography using a liquid crystal display as dynamic mask-generator," *Microsyst. Technol.*, vol. 3, no. 2, pp. 42–47, 1997.

[51] C. Chatwin, M. Farsari, S. Huang, M. Heywood, P. Birch, R. Young, and J. Richardson, "UV Microstereolithography System that uses Spatial Light Modulator Technology," *Appl. Opt.*, vol. 37, no. 32, pp. 7514–7522, Nov. 1998.

[52] M. Farsari, S. Huang, P. Birch, F. Claret-Tournier, R. Young, D. Budgett, C. Bradfield, and C. Chatwin, "Microfabrication by use of a spatial light modulator in the ultraviolet: experimental results," *Opt. Lett.*, vol. 24, no. 8, pp. 549–50, Apr. 1999.

[53] C. R. Chatwin, M. Farsari, S. Huang, M. I. Heywood, R. C. D. Young, P. M. Birch, F. Claret-Tournier, and J. D. Richardson, "Characterisation of Epoxy Resins for Microstereolithographic Rapid Prototyping," *Int. J. Adv. Manuf. Technol.*, vol. 15, no. 4, pp. 281–286, Apr. 1999.

[54] M. Farsari, F. Claret-Tournier, S. Huang, C. R. Chatwin, D. M. Budgett, P. M. Birch, R. C. D. Young, and J. D. Richardson, "Novel high-accuracy microstereolithography method employing an adaptive electro-optic mask," *J. Mater. Process. Technol.*, vol. 107, no. 1–3, pp. 167–172, 2000.

[55] S. Monneret, V. Loubère, S. Corbel, D. De Chimie, and B. P. N. Cedex, "Microstereolithography using a dynamic mask generator and a non-coherent visible light source," vol. 3680, no. April, pp. 553–561, 1999.

[56] S. Monneret, C. Provin, and H. Le Gall, "Micro-scale rapid prototyping by stereolithography," *ETFA 2001 8th Int. Conf. Emerg. Technol. Fact. Autom. Proc.*, vol. 2, pp. 299–304, 2001.

[57] A. Bertsch, H. Lorenz, and P. Renaud, "3D microfabrication by combining microstereolithography and thick resist UV lithography," *Sensors Actuators A Phys.*, vol. 73, no. 1–2, pp. 14–23, Mar. 1999.

[58] L. Beluze, a Bertsch, and P. Renaud, "Microstereolithography: a new process to build

complex 3D objects," *Des. Test, Microfabr. Mems Moems, Pts 1 2*, vol. 3680, no. April, pp. 808–817, 1999.

[59] A. Bertsch, P. Bernhard, C. Vogt, and P. Renaud, "Rapid prototyping of small size objects," *Rapid Prototyp. J.*, vol. 6, no. 4, pp. 259–266, 2000.

[60] G. Hadipoespito, Y. Yang, and H. Choi, "Digital micromirror device based microstereolithography for micro structures of transparent photopolymer and nanocomposites," in *Proceedings of the 14th …*, 2003, no. Ic, pp. 13–24.

[61] A. Neumeister, R. Himmelhuber, T. Temme, and U. Stute, "Generation of Micro Mechanical Devices Using Stereo Lithography," in *Proceedings of the Solid Freeform Fabrication Symposium, The University of Texas at Austin, Austin, TX*, 2006, pp. 12–24.

[62] G. Oda, T. Miyoshi, Y. Takaya, T. Ha, and K. Kimura, "Microfabrication of Overhanging Shape using LCD Microstereolithography," in *Fifth International Symposium on Laser Precision Microfabrication*, 2004, vol. 5662, pp. 649–654.

[63] M. R. Douglass, "Lifetime Estimates and Unique Failure Mechanisms," in *36th IEEE Annual International Reliability Physics Symposium*, 1998, pp. 9–16.

[64] M. P. Lee, G. J. T. Cooper, T. Hinkley, G. M. Gibson, M. J. Padgett, and L. Cronin, "Development of a 3D printer using scanning projection stereolithography.," *Sci. Rep.*, vol. 5, p. 9875, 2015.

[65] Y. M. Ha, J. W. Choi, and S. H. Lee, "Mass production of 3-D microstructures using projection microstereolithography," *J. Mech. Sci. Technol.*, vol. 22, no. 3, pp. 514–521, May 2008.

[66] D. T. Pham and C. Ji, "A study of recoating in stereolithography," *Proc. Inst. Mech. Eng. Part C J. Mech. Eng. Sci.*, vol. 217, no. 1, pp. 105–117, Jan. 2003.

[67] C. Zhou, Y. Chen, Z. Yang, and B. Khoshnevis, "Digital material fabrication using mask-image-projection-based stereolithography," *Rapid Prototyp. J.*, vol. 19, no. 3, pp. 153–165, 2013.

[68] F. P. W. Melchels, J. Feijen, and D. W. Grijpma, "A review on stereolithography and its applications in biomedical engineering.," *Biomaterials*, vol. 31, no. 24, pp. 6121–30, Aug. 2010.

[69] H. F. Gruber, "Photoinitiators for free radical polymerization," *Prog. Polym. Sci.*, vol. 17, no. 6, pp. 953–1044, 1992.

[70] C. Decker, "Photoinitiated crosslinking polymerisation," *Prog. Polym. Sci.*, vol. 21, no. 4, pp. 593–650, 1996.

[71] P. F. Jacobs, *Rapid Prototyping & Manufacturing: Fundamentals of Stereolithography*. New York: Society of Manufacturing Engineers, 1992.

[72] I. Gibson, D. W. Rosen, and B. Stucker, *Additive Manufacturing Technologies: Rapid Prototyping to Direct Digital Manufacture*. Springer Science & Business Media, 2010.

[73] K. H. Dusel, J. Eschl, and B. Wiedemann, "Improvement of part accuracy - investigations into the basics of photopolymerization," in *Proceedings of the fifth european conference on rapid prototyping and manufacturing*, 1995.

[74] P. F. Jacobs, *Stereolithography and other RP&M Technolgies: From Rapid Prototyping to Rapid Tooling*. Society of Manufacturing Engineers, 1996.

[75] J. Colton and B. Blair, "Experimental study of post-build cure of stereolithography polymers for injection molds," *Rapid Prototyp. J.*, vol. 5, no. 2, pp. 72–81, 1999.

[76] J. Eschl, T. Blumenstock, and P. Eyerer, "Comparison of the curing process of epoxy and acrylate resins for stereolithography by means of experimental investigations and FEM-simulation," in *The 10th Solid Freeform Fabrication Symposium, Austin, Texas, USA*, 1999, pp.

453–460.

[77] L. Lu, J. Y. H. Fuh, A. Y. C. Nee, E. T. Kang, T. Miyazawa, and C. M. Cheah, "Origin of Shrinkage, Distortion and Fracture of Photopolymerized Material," *Mater. Res. Bull.*, vol. 30, no. 12, pp. 1561–1569, 1995.

[78] D. Karalekas and A. Aggelopoulos, "Study of shrinkage strains in a stereolithography cured acrylic photopolymer resin," *J. Mater. Process. Technol.*, vol. 136, no. 1, pp. 146–150, 2003.

[79] G. C. A. M. Janssen, M. M. Abdalla, F. Van Keulen, B. R. Pujada, and B. Van Venrooy, "Celebrating the 100th anniversary of the Stoney equation for film stress: Developments from polycrystalline steel strips to single crystal silicon wafers," *Thin Solid Films*, vol. 517, no. 6, pp. 1858–1867, 2009.

[80] D. Karalekas and D. Rapti, "Investigation of the processing dependence of SL solidification residual stresses," *Rapid Prototyp. J.*, vol. 8, no. 4, pp. 243–247, 2002.

[81] J. Y. H. Fuh, L. Lu, C. C. Tan, Z. X. Shen, and S. Chew, "Processing and characterising photo-sensitive polymer in the rapid prototyping process," *J. Mater. Process. Technol.*, vol. 89, pp. 211–217, 1999.

[82] J. Y. H. L. Fuh, L. Lu, C. C. Tan, Z. X. Shen, and S. Chew, "Curing characteristics of acrylic photopolymer used in stereolithography process," *Rapid Prototyp. J.*, vol. 5, no. 1, pp. 27–34, 1999.

[83] A. J. Lopes, E. MacDonald, and R. B. Wicker, "Integrating stereolithography and direct print technologies for 3D structural electronics fabrication," *Rapid Prototyp. J.*, vol. 18, no. 2, pp. 129–143, 2012.

[84] DSM Somos, "ProtoTherm 12120 ™ Resin Specification." .

[85] A. Lopes, M. Navarrete, F. Medina, J. Palmer, E. Macdonald, and R. Wicker, "Expanding Rapid Prototyping for Electronic Systems Integration of Arbitrary Form," in *Proceedings of the 17th Annual Solid Freeform Fabrication Symposium, University of Texas at Austin*, 2006, pp. 644–655.

[86] M. N. Cooke, J. P. Fisher, D. Dean, C. Rimnac, and A. G. Mikos, "Use of stereolithography to manufacture critical-sized 3D biodegradable scaffolds for bone ingrowth," *J. Biomed. Mater. Res. Part B Appl. Biomater.*, vol. 64, no. 2, pp. 65–69, 2003.

[87] J. W. Choi, H. C. Kim, and R. Wicker, "Multi-material stereolithography," *J. Mater. Process. Technol.*, vol. 211, no. 3, pp. 318–328, Mar. 2011.

[88] J. W. Choi, E. MacDonald, and R. Wicker, "Multi-material microstereolithography," *Int. J. Adv. Manuf. Technol.*, vol. 49, no. 5–8, pp. 543–551, 2010.

[89] J. Stampfl, S. Baudis, C. Heller, R. Liska, A. Neumeister, R. Kling, A. Ostendorf, and M. Spitzbart, "Photopolymers with tunable mechanical properties processed by laser-based high-resolution stereolithography," *J. Micromechanics Microengineering*, vol. 18, no. 12, p. 125014, 2008.

[90] T. Chartier, C. Duterte, N. Delhote, D. Baillargeat, S. Verdeyme, C. Delage, and C. Chaput, "Fabrication of Millimeter Wave Components Via Ceramic Stereo- and Microstereolithography Processes," *J. Am. Ceram. Soc.*, vol. 91, no. 8, pp. 2469–2474, Jun. 2008.

[91] F. Doreau, C. Chaput, and T. Chartier, "Stereolithography for manufacturing ceramic parts," *Adv. Eng. Mater.*, vol. 2, no. 8, pp. 493–496, 2000.

[92] J. Deckers, J. Vleugels, and J. P. Kruth, "Additive manufacturing of ceramics: A review," *J. Ceram. Sci. Technol.*, vol. 5, no. 4, pp. 245–260, 2014.

[93]   K. Renap and J. P. Kruth, "Recoating issues in stereolithography," *Rapid Prototyp. J.*, vol. 1, no. 3, pp. 4–16, 1995.

[94]   J. Palmer, J. Summers, D. W. Davis, P. L. Gallegos, B. D. Chavez, P. Yang, F. Medina, and R. B. Wicker, "Realizing 3-D interconnected direct write electronics within smart stereolithography structures," in *Proceeding of 2005 ASME International Mechanical Engineering Congress and Exposition, Orlando, Florida USA*, 2005, pp. 287–293.

[95]   A. Inamdar, M. Magana, F. Medina, Y. Grajeda, and R. Wicker, "Development of an automated multiple material stereolithography machine," in *Proceedings of 17th Annual Solid Freeform Fabrication Symposium, Austin, TX*, 2006, pp. 624–635.

[96]   J. H. Sandoval, L. Ochoa, A. Hernandez, O. Lozoya, K. F. Soto, L. E. Murr, and R. B. Wicker, "Nanotailoring stereolithography resins for unique applications using carbon nanotubes," in *Proceedings of the 16th Solid Freeform Fabrication Symposium, University of Texas at Austin*, 2005, pp. 513–524.

[97]   M. Bengtsson and T. Laurell, "Ultrasonic agitation in microchannels," *Anal. Bioanal. Chem.*, vol. 378, no. 7, pp. 1716–1721, 2004.

[98]   L. H. Thompson and L. K. Doraiswamy, "Sonochemistry: science and engineering," *Ind. Eng. Chem. Res.*, vol. 38, no. 4, pp. 1215–1249, 1999.

[99]   3D Systems Corporation, "'Lotus F1 Team Uses 3D Systems' Solutions to Race by Competition'," 2013. [Online]. Available: http://www.3dsystems.com/sites/www.3dsystems.com/files/3ds-lotus-f1-2013_0.pdf.

[100]   R. Wicker, F. Medina, and C. Elkins, "Multiple material micro-fabrication: extending stereolithography to tissue engineering and other novel applications," in *Proceedings of 15th Annual Solid Freeform Fabrication Symposium, Austin, TX*, 2004, pp. 754–764.

[101]   R. B. Wicker, F. Medina, and C. Elkins, "Multi-Material Stereolithography," U.S. Patent No. 7,556,490, 2009.

[102]   A. Ovsianikov and B. N. Chichkov, "Three-dimensional microfabrication by two-photon polymerization technique," in *Computer-aided tissue engineering*, Humana Press, 2012, pp. 311–317.

[103]   S.-H. Park, D.-Y. Yang, and K.-S. Lee, "Two-photon stereolithography for realizing ultraprecise three-dimensional nano/microdevices," *Laser Photonics Rev.*, vol. 3, no. 1–2, pp. 1–11, Feb. 2009.

[104]   A. Bertsch, P. Bernhard, and P. Renaud, "Microstereolithography: Concepts and Applications," in *Proceedings of 8th IEEE International Conference on Emerging Technologies and Factory Automation*, 2001, vol. 2, pp. 289–298.

[105]   J. R. Tumbleston, D. Shirvanyants, N. Ermoshkin, R. Janusziewicz, A. R. Johnson, D. Kelly, K. Chen, R. Pinschmidt, J. P. Rolland, A. Ermoshkin, E. T. Samulski, and J. M. Desimone, "Continuous liquid interface production of 3D objects," *Science (80-.).*, vol. 347, no. 6228, pp. 1349–1352, 2015.

[106]   D. Dendukuri, D. C. Pregibon, J. Collins, T. A. Hatton, and P. S. Doyle, "Continuous-flow lithography for high-throughput microparticle synthesis," *Nat. Mater.*, vol. 5, no. 5, pp. 365–369, 2006.

[107]   T. C. Merkel, R. Pinnau, R. Prabhakar, and B. D. Freeman, *Materials science of membranes for gas and vapor separation*. John Wiley & Sons, 2006.

[108]   J. A. Lewis and G. M. Gratson, "Direct writing in three dimensions," *Mater. Today*, vol. 7, no. 7, pp. 32–39, 2004.

[109]   A. J. Lopes, R. Wicker, J. Palmer, C. Robinson, and B. Stucker, "Integration of Direct-Write

(DW) and Ultrasonic Consolidation (UC) Technologies to Create Advanced Structures with Embedded Electrical Circuitry .," in *Proceeding of the 17th Annual Solid Freeform Fabrication Symposium, University of Texas at Austin, Austin, TX*, 2006, pp. 60–69.

[110] D. Tobjörk, H. Aarnio, P. Pulkkinen, R. Bollström, A. Määttänen, P. Ihalainen, T. Mäkelä, J. Peltonen, M. Toivakka, H. Tenhu, and R. Österbacka, "IR-sintering of ink-jet printed metal-nanoparticles on paper," *Thin Solid Films*, vol. 520, no. 7, pp. 2949–2955, 2012.

[111] S. B. Fuller, E. J. Wilhelm, and J. M. Jacobson, "Ink-jet printed nanoparticle microelectromechanical systems," *J. Microelectromechanical Syst.*, vol. 11, no. 1, pp. 54–60, 2002.

[112] A. Mette, P. L. Richter, M. Horteis, and S. W. Glunz, "Metal aerosol jet printing for solar cell metallization," *Prog. Photovoltaics Res. Appl.*, vol. 15, no. 7, pp. 621–627, 2007.

[113] P. Kopola, B. Zimmermann, A. Filipovic, H. F. Schleiermacher, J. Greulich, S. Rousu, J. Hast, R. Myllylä, and U. Würfel, "Aerosol jet printed grid for ITO-free inverted organic solar cells," *Sol. Energy Mater. Sol. Cells*, vol. 107, pp. 252–258, 2012.

[114] M. Renn, B. King, M. O'Reilly, J. Leal, and S. Pangrle, "Aerosol Jet Printing of High Density, 3-D Interconnects for Multi-Chip Packaging," in *Additional Papaers and Presentations: Device Packaging Conference*, 2010, pp. 2131–2152.

[115] M. Hedges and A. B. Marin, "3D Aerosol Jet ® Printing - Adding Electronics Functionality to RP/RM," in *Proceedings from Direct Digital Manufacturing Conference*, 2012, pp. 14–15.

[116] M. O'Reilly and J. Leal, "Jetting Your Way to Fine-pitch 3D Interconnects," *Chip Scale Rev.*, vol. 14, no. 5, pp. 18–21, 2010.

[117] K. Obata, "Hybrid Micro-stereo-lithography by Means of Aerosol Jet Printing Technology," *J. Laser Micro Nanoeng.*, vol. 9, no. 3, p. 242, 2014.

[118] J. A. Lewis, "Direct Ink Writing of 3D Functional Materials," *Adv. Funct. Mater.*, vol. 16, no. 17, pp. 2193–2204, Nov. 2006.

[119] B. Niese, T. Stichel, P. Amend, U. Urmoneit, S. Roth, and M. Schmidt, "Manufacturing of Conductive Circuits for Embedding Stereolithography by Means of Conductive Adhesive and Laser Sintering," *Phys. Procedia*, vol. 56, pp. 336–344, 2014.

[120] nScrypt Inc, "nScrypt Smart Pump 100 Specification." .

[121] F. Medina, A. Lopes, A. Inamdar, R. Hennessey, J. Palmer, D. Davis, P. Gallegos, and R. Wicker, "Hybrid manufacturing: integrating direct write and stereolithography," in *Proceedings of the 2005 Solid Freeform Fabrication*, 2005, pp. 39–49.

[122] F. Medina, A. J. Lopes, A. V. Inamdar, R. Hennessey, J. A. Palmer, B. D. Chavez, and R. B. Wicker, "Integrating multiple rapid manufacturing technologies for developing advanced customized functional devices," in *Proceedings of Rapid Prototyping & Manufacturing Conference Proceedings*, 2005, pp. 10–12.

[123] D. Lu, Q. K. Tong, and C. P. Wong, "Conductivity mechanisms of isotropic conductive adhesives (ICA's)," *IEEE Trans. Electron. Packag. Manuf.*, vol. 22, no. 3, pp. 223–227, 1999.

[124] J. C. Jagt, "Reliability of Electrically Conductive Adhesive Joints for Surface Mount Applications: A Summary of the State of the Art," *IEEE Trans. Components, Packag. Manuf. Technol. Part A*, vol. 21, no. 2, pp. 215–225, 1998.

[125] B. K. Park, D. Kim, S. Jeong, J. Moon, and J. S. Kim, "Direct writing of copper conductive patterns by ink-jet printing," *Thin Solid Films*, vol. 515, no. 19, pp. 7706–7711, 2007.

[126] S. Bhat and U. Maitra, "Facially amphiphilic thiol capped gold and silver nanoparticles," *J. Chem. Sci.*, vol. 120, no. 6, pp. 507–513, 2008.

[127] B. Yeop and J. a Lewis, "Amphiphilic silver particles for conductive inks with controlled wetting behavior," *Mater. Chem. Phys.*, vol. 148, no. 3, pp. 686–691, 2014.

[128] D. Borghino, "Voxel8 Paves the Way for 3D-Printed Electronics," *Gizmag*, 2015.

[129] M. Navarrete, A. Lopes, J. Acuna, R. Estrada, E. Macdonald, J. Palmer, and R. Wicker, "Integrated layered manufacturing of a novel wireless motion sensor system with GPS," in *Proceedings from the 18th Annual Solid Freeform Fabrication Symposium*, 2007, pp. 575–585.

[130] A. J. Lopes, I. H. Lee, E. MacDonald, R. Quintana, and R. Wicker, "Laser Curing of Silver-Based Conductive Inks for In Situ 3D Structural Electronics Fabrication in Stereolithography," *J. Mater. Process. Technol.*, vol. 214, no. 9, pp. 1935–1945, Sep. 2014.

[131] J. Chung, N. R. Bieri, S. Ko, C. P. Grigoropoulos, and D. Poulikakos, "In-tandem deposition and sintering of printed gold nanoparticle inks induced by continuous Gaussian laser irradiation," *Appl. Phys. A*, vol. 79, no. 4–6, pp. 1259–1261, 2004.

[132] P. Buffat and J.-P. Borel, "Size effect on the melting temperature of gold particles," *Phys. Rev. A*, vol. 13, no. 6, p. 2287, 1976.

[133] J. R. Greer and R. a. Street, "Thermal cure effects on electrical performance of nanoparticle silver inks," *Acta Mater.*, vol. 55, no. 18, pp. 6345–6349, 2007.

[134] N. R. Bieri, J. Chung, S. E. Haferl, D. Poulikakos, and C. P. Grigoropoulos, "Microstructuring by printing and laser curing of nanoparticle solutions," *Appl. Phys. Lett.*, vol. 82, no. 20, pp. 3529–3531, 2003.

[135] K. Maekawa, K. Yamasaki, T. Niizeki, M. Mita, Y. Matsuba, N. Terada, and H. Saito, "Influence of wavelength on laser sintering characteristics of Ag nanoparticles," in *Proceedings of IEEE Electronic Components and Technology Conference*, 2009, pp. 1579–1584.

[136] M. K. Kim, J. Y. Hwang, H. Kang, K. Kang, S. H. Lee, and S. J. Moon, "Laser sintering of the printed silver ink," in *Proceedings of 2009 IEEE International Symposium on Assembly and Manufacturing, Suwon, Korea.*, 2009, pp. 155–158.

[137] L. Fu, S. Shang, E. Fearon, W. Perrie, S. P. Edwardson, G. Dearden, and K. G. Watkins, "A thermal investigation on conductive silver ink tracks cured on flexible substrates by repeating irradiations of ND:YAG laser at the wavelength of 532nm," in *ICALEO Congress Proceedings*, 2012, pp. 1304–1310.

[138] S. Shang, D. Wellburn, E. Fearon, S. Yan, S. P. Edwardson, G. Dearden, and K. G. Watkins, "Laser assisted direct write process with novel beam profiles," *Opt. Lasers Eng.*, vol. 51, no. 5, pp. 527–532, 2013.

[139] M. L. Allen, M. Aronniemi, T. Mattila, A. Alastalo, K. Ojanperä, M. Suhonen, and H. Seppä, "Electrical sintering of nanoparticle structures.," *Nanotechnology*, vol. 19, no. 17, p. 175201, 2008.

[140] D. A. Roberson, R. B. Wicker, and E. MacDonald, "Ohmic curing of printed silver conductive traces," *J. Electron. Mater.*, vol. 41, no. 9, pp. 2553–2566, 2012.

[141] D. a. Roberson, R. B. Wicker, and E. MacDonald, "Ohmic Curing of Three-Dimensional Printed Silver Interconnects for Structural Electronics," *J. Electron. Packag.*, vol. 137, no. 3, p. 031004, 2015.

[142] D. B. Chrisey, "The power of direct writing," *Science (80-.).*, vol. 289, no. 5481, pp. 879–881, 2000.

[143] B. Y. Ahn, E. B. Duoss, M. J. Motala, X. Guo, S.-I. Park, Y. Xiong, J. Yoon, R. G. Nuzzo, J. a Rogers, and J. a Lewis, "Omnidirectional printing of flexible, stretchable, and spanning silver microelectrodes.," *Science (80-.).*, vol. 323, no. 5921, pp. 1590–1593, Mar. 2009.

[144] J. Lewis, "Innovation Micro Batteries," *Bloomberg Businessweek*, p. 34, Jul-2013.

[145] J. J. Adams, E. B. Duoss, T. F. Malkowski, M. J. Motala, B. Y. Ahn, R. G. Nuzzo, J. T. Bernhard, and J. a Lewis, "Conformal Printing of Electrically Small Antennas on Three-Dimensional Surfaces," *Adv. Mater.*, vol. 23, no. 11, pp. 1335–1340, Mar. 2011.

[146] C. Aymonier, U. Schlotterbeck, L. Antonietti, P. Zacharias, R. Thomann, J. C. Tiller, and S. Mecking, "Hybrids of silver nanoparticles with amphiphilic hyperbranched macromolecules exhibiting antimicrobial properties.," *Chem. Commun.*, vol. 24, pp. 3018–3019, 2002.

[147] K. B. Perez and C. B. Williams, "Design considerations for hybridizing additive manufacturing and direct write technologies," in *ASME International Design Engineering Technical Conferences and Computers and Information in Engineering Conference*, 2014, p. V004T06A005.

[148] Y.-H. Chang, K. Wang, C. Wu, Y. Chen, C. Zhang, and B. Wang, "A facile method for integrating direct-write devices into three-dimensional printed parts," *Smart Mater. Struct.*, vol. 24, no. 6, p. 065008, 2015.

[149] D. Espalin, D. W. Muse, E. MacDonald, and R. B. Wicker, "3D Printing multifunctionality: Structures with electronics," *Int. J. Adv. Manuf. Technol.*, vol. 72, no. 5–8, pp. 963–978, Mar. 2014.

[150] C. E. Folgar, L. N. Folgar, D. Cormier, and R. Hill, "Multifunctional material direct printing for laser sintering systems," *Proc. 16th Solid Free. Fabr. Symp. Univ. Texas Austin*, pp. 282–296, 2013.

[151] D. Periard, E. Malone, and H. Lipson, "Printing embedded circuits," in *Proceedings of the 18th Solid Freeform Fabrication Symposium, Austin, TX.*, 2007, pp. 6–8.

[152] H.-C. Kim, J.-W. Choi, and R. Wicker, "Scheduling and process planning for multiple material stereolithography," *Rapid Prototyp. J.*, vol. 16, no. 4, pp. 232–240, 2010.

[153] A. Kataria and D. W. Rosen, "Building around inserts: methods for fabricating complex devices in stereolithography," *Rapid Prototyp. J.*, vol. 7, no. 5, pp. 253–262, 2001.

[154] J. A. Palmer, P. Yang, D. W. Davis, B. D. Chavez, P. L. Gallegos, R. B. Wicker, and F. Medina, "Rapid prototyping of high density circuitry," in *Rapid Prototyping & Manufacturing Conference Proceedings*, 2004, pp. 10–13.

[155] R. B. Wicker and E. W. MacDonald, "Multi-material, multi-technology stereolithography: This feature article covers a decade of research into tackling one of the major challenges of the stereolithography technique, which is including multiple materials in one construct," *Virtual Phys. Prototyp.*, vol. 7, no. 3, pp. 181–194, Sep. 2012.

[156] S. H. Jang, S. T. Oh, I. H. Lee, H. C. Kim, and H. Y. Cho, "3-dimensional circuit device fabrication process using stereolithography and direct writing," *Int. J. Precis. Eng. Manuf.*, vol. 16, no. 7, pp. 1361–1367, 2015.

[157] B. Geving and I. Ebert-Uphoff, "Enhancement of Stereo-Lithography Technology to Support Building Around Inserts," in *Proceedings of ASME Design Engineering Technical Conference*, 2000, vol. 7, pp. 1399–1408.

[158] P. Amend, O. Hentschel, C. Scheitler, M. Baum, J. Heberle, S. Roth, and M. Schmidt, "Fast and Flexible Generation of Conductive Circuits," *J. Laser Micro Nanoeng.*, vol. 8, no. 3, p. 276, 2013.

[159] G. Esser, B. Jahrsdorfer, and U. Urmoneit, "Laser assisted fabrication of electronic circuits using the ADDIMID process," in *Photonics West - Lasers and Applications in Science and Engineering Conference Proceedings*, 2001, pp. 375–384.

[160] K. Ikuta and K. Hirowatari, "Real three dimensional micro fabrication using stereo lithography

and metal molding," in *Proceedings of IEEE International Workshop on Micro Electro Mechanical Systems*, 1993, pp. 42–47.

[161] K. Ikuta, T. Ogata, M. Tsubio, and S. Kojima, "Development of mass productive micro stereo lithography (Mass-IH process)," in *Proceedings of Ninth IEEE International Workshop on Micro Electro Mechanical Systems*, 1996, pp. 301–306.

[162] A. Piqué, S. A. Mathews, B. Pratap, R. C. Y. Auyeung, B. J. Karns, and S. Lakeou, "Embedding electronic circuits by laser direct-write," *Microelectron. Eng.*, vol. 83, no. 11, pp. 2527–2533, Nov. 2006.

[163] J. G. Cham, B. L. Pruitt, M. R. Cutkosky, M. Binnard, L. E. Weiss, and G. Neplotnik, "Layered manufacturing with embedded components: process planning considerations," in *ASME Design Engineering Technical Conference*, 1999, pp. 12–15.

[164] C. Mavroidis and K. J. De Laurentis, "Rapid fabrication of a non-assembly robotic hand with embedded components," *Assem. Autom.*, vol. 24, no. 4, pp. 394–405, 2004.

[165] E. De Nava, M. Navarrete, A. Lopes, M. Alawneh, M. Contreras, D. Muse, S. Castillo, E. Macdonald, and R. Wicker, "Three-dimensional off-axis component placement and routing for electronics integration using solid freeform fabrication," in *Proceedings from the 19th Annual Solid Freeform Fabrication Symposium, The University of Texas at Austin, Austin, TX*, 2008, pp. 4–6.

[166] Eccosorb, "Dielectric Materials Chart — Eccostock," *Technical Reports AFML-TR-72-39 and 74-250*. .

[167] Delta Controls Corporation, "Dielectric Constants of Various Materials." p. 3, 1997.

[168] Avago Technologies, "PCB Layout Guidelines for Designing with Avago SFP+ Transceivers." 2005.

[169] H. S. Nalwa, *Handbook of low and high dielectric constant materials and their applications*. Academic Press, 1999.

[170] 3D Systems Corporation, "Product Data Sheet - 3D Systems Accura 60." 2015.

[171] Farnell, "FR4 Data Sheet." 2016.

[172] M. Hatzenbichler, "Additive manufacturing of photopolymers using the Texas Instruments DLP lightcrafter," in *SPIE MOEMS-MEMS*, 2013, p. 86180A.

[173] International Light Technologies, "UV LED Datasheet," 2016. [Online]. Available: http://www.intl-lighttech.com/sites/default/files/pdf/datasheet/UV-LED-SL-Datasheet-web.pdf.

[174] Motion Control Products Ltd., "Precision Hybrid Stepper Linear Actuators." p. 22, 2011.

[175] E. Hecht, *Optics: pearson new international edition*. Pearson Higher Education, 2013.

[176] Edmund Optics, "Edmund Optics Data Sheet: 15.0mm Diameter x 15.0mm Focal Length, 405nm V-Coat, PCX Lens." 2014.

[177] M. R. Bouschlicher and F. A. Rueggeberg, "Effect of ramped light intensity on polymerization force and conversion in a photoactivated composite," *J. Esthet. Restor. Dent.*, vol. 12, no. 6, pp. 328–339, 2000.

[178] "Illumination," *Leyden Science*. [Online]. Available: http://www.leydenscience.org/physics/electmag/illum.htm.

[179] R. S. Quimby, "Gaussian Beam Optics," in *Photonics and Lasers: An Introduction*, John Wiley & Sons, 2006, pp. 307–325.

[180] S. Kulkarni, *Nanotechnology - Principles and Processes*. Capital Publishing House, 2009.

[181] Thorlabs, "Protected Silver Coating, 45° AOI," 2016. [Online]. Available: https://www.thorlabs.com/NewGroupPage9_PF.cfm?ObjectGroup_ID=903.

[182] Spot-A Materials, "Spot-A Materials LV Resin," 2016. [Online]. Available: http://spotamaterials.com/product/spot-lv-1kg/.

[183] mUVE 3D, "Spectral Analysis of ViewSonic PJD7820HD Projector," *Spectral Workbench*, 2014. [Online]. Available: http://spectralworkbench.org/spectrums/29967.

[184] J. Wen, "T-Topping Study Report," 2015.

[185] MakerJuice Labs, "MakerJuice Labs 'Substance G+' Resin Datasheet." .

[186] A. Kataria, "Standardization and Process Planning for Building Around Inserts in Stereolithography Apparatus," 2000.

[187] International Organisation for Standardization, "ISO 25178-2:2012 Geometrical Product Specifications (GPS) – Surface texture: Aerial, Part 1: Terms, definitions and surface texture parameters." pp. 1–47, 2012.

[188] J. Clayden, N. Greeves, and S. Warren, *Organic Chemistry*. Oxford University Press, 2012.

[189] K. Alfonsi, J. Colberg, P. J. Dunn, T. Fevig, S. Jennings, T. A. Johnson, H. P. Kleine, C. Knight, M. A. Nagy, D. A. Perry, and M. Stefaniak, "Green chemistry tools to influence a medicinal chemistry and research chemistry based organisation," *Green Chem.*, vol. 10, no. 1, pp. 31–36, 2008.

[190] S. Caron, *Practical Synthetic Organic Chemistry*. John Wiley & Sons, 2011.

[191] A. Valavanidis and T. Vlachogianni, *Green Chemistry and Green Engineering from Theory to Practice for the Protection of the Environment and Sustainable Development*. 2012.

[192] J. S. Choi, H. W. Kang, I. H. Lee, T. J. Ko, and D. W. Cho, "Development of micro-stereolithography technology using a UV lamp and optical fiber," *Int. J. Adv. Manuf. Technol.*, vol. 41, no. 3–4, pp. 281–286, 2009.

[193] R. Leyden, T. Almouist, M. Lewis, and H. Nguyen, "Stereolithography method and apparatus," U.S. Patent No. 5,143,663, 1992.

[194] J. W. Lee, P. X. Lan, B. Kim, G. Lim, and D. W. Cho, "3D scaffold fabrication with PPF/DEF using micro-stereolithography," *Microelectron. Eng.*, vol. 84, no. 5, pp. 1702–1705, 2007.

[195] Fargo 3D Printing, "Using D-Limonene to Dissolve 3D Printing Support Structures," 2014. [Online]. Available: http://www.fargo3dprinting.com/using-d-limonene-dissolve-3d-printing-support-structures/.

[196] R. W. Eklund, "Developer solvent for photopolymer printing plates and method," U.S. Patent No. 6,248,502, 2001.

[197] J. Sun, "D-Limonene : Safety and Clinical Applications," *Altern. Med. Rev.*, vol. 12, no. 3, pp. 259–264, 2007.

[198] Cambridge Polymer Group, "Swelling Measurements of Crosslinked Polymers." [Online]. Available: http://www.campoly.com/files/3013/5216/6056/005.pdf.

[199] S. Costello, N. Strusevich, M. K. Patel, C. Bailey, D. Flynn, R. W. Kay, D. Price, M. Bennet, A. C. Jones, R. Habeshaw, C. Demore, S. Cochran, and M. P. Y. Desmulliez, "Characterisation of ion transportation during electroplating of high aspect ratio microvias using megasonic agitation," in *18th IEEE European Microelectronics & Packaging Conference*, 2011, pp. 1–7.

[200] L. A. Crum, "Comments on the evolving field of sonochemistry by a cavitation physicist," *Ultrason. Sonochem.*, vol. 2, no. 2, pp. S147–S152, 1995.

[201] K. S. Suslick, *The yearbook of science and the future*. Chicago: Encyclopedia Britannica, 1994.

[202] T. J. Mason and J. P. Lorimer, *Applied sonochemistry: The uses of power ultrasound in chemistry and processing*. 2002.

[203] M. D. Luque De Castro and J. L. Luque Garcia, *Acceleration and automation of solid sample treatment*. Elsevier, 2002.

[204] M. D. Luque De Castro and F. Priego Capote, *Analytical Applications of Ultrasound*. Elsevier, 2007.

[205] D. P. Naidu, R. Rajan, R. Kumar, K. S. Gandhi, V. H. Arakeri, and S. Chandrasekaran, "Modelling of a batch sonochemical reactor," *Chem. Eng. Sci.*, vol. 49, no. 6, pp. 877–888, 1994.

[206] B. S. Everitt, *The Cambridge Dictionary of Statistics*, 2nd ed. Cambridge University Press, 2002.

[207] A. J. Capel, "Design and additive manufacture for flow chemistry," Loughborough University, 2015.

[208] A. J. Capel, S. Edmondson, S. D. R. Christie, R. D. Goodridge, R. J. Bibb, and M. Thurstans, "Design and additive manufacture for flow chemistry.," *Lab Chip*, vol. 13, pp. 4583–90, 2013.

[209] P. M. Dentinger, W. M. Clift, and S. H. Goods, "Removal of SU-8 photoresist for thick film applications," *Microelectron. Eng.*, vol. 61–62, pp. 993–1000, 2002.

[210] C.-H. Lin, G.-B. Lee, B.-W. Chang, and G.-L. Chang, "A new fabrication process for ultra-thick microfluidic microstructures utilizing SU-8 photoresist," *J. Micromechanics Microengineering*, vol. 12, no. 5, pp. 590–597, 2002.

[211] C. M. Cheah, J. Y. H. Fuh, a. Y. C. Nee, L. Lu, Y. S. Choo, and T. Miyazawa, "Characteristics of photopolymeric material used in rapid prototypes Part II. Mechanical properties at post-cured state," *J. Mater. Process. Technol.*, vol. 67, no. 1–3, pp. 46–49, 1997.

[212] S. Corbel, F. Evenou, F. Baros, N. Martinet, M. Donner, and M. C. Carré, "Microstructured reactors designed by stereolithography and characterized by fluorescent probes," *Int. J. Photoenergy*, vol. 2008, 2008.

[213] B. P. Carr, "Introduction to Thick Film Fine Line Printing Screens," *Microelectron. Int.*, vol. 11, no. 1, pp. 4–7, 1994.

[214] M. M. Cross, "Relation between viscoelasticity and shear-thinning behaviour in liquids," *Rheol. Acta*, vol. 18, no. 5, pp. 609–614, 1979.

[215] J. E. Smay, J. Cesarano, and J. A. Lewis, "Colloidal inks for directed assembly of 3-D periodic structures," *Langmuir*, vol. 18, no. 14, pp. 5429–5437, 2002.

[216] D. Giancoli, *Physics*. Prentice Hall, 1995.

[217] Epoxy Technology Inc., "EPO-TEK® EJ2189," *Technical Data Sheet*. 2014.

[218] C. M. Cheah, a. Y. C. Nee, J. Y. H. Fuh, L. Lu, Y. S. Choo, and T. Miyazawa, "Characteristics of photopolymeric material used in rapid prototypes Part I. Mechanical properties in the green state," *J. Mater. Process. Technol.*, vol. 67, pp. 41–45, 1997.

[219] N. T. Nguyen and S. T. Wereley, *Fundamentals and applications of microfluidics*, 2nd ed. Artech House, 2002.

[220] G. M. Whitesides, "The origins and the future of microfluidics," *Nature*, vol. 442, no. 7101, pp. 368–73, 2006.

[221] B. Bhattacharyya, J. Munda, and M. Malapati, "Advancement in electrochemical micro-machining," *Int. J. Mach. Tools Manuf.*, vol. 44, no. 15, pp. 1577–1589, 2004.

[222] D. J. Beebe, G. a Mensing, and G. M. Walker, "Physics and applications of microfluidics in biology," *Annu. Rev. Biomed. Eng.*, vol. 4, no. 1, pp. 261–286, 2002.

[223] H. Becker and L. E. Locascio, "Polymer microfluidic devices," *Talanta*, vol. 56, no. 2, pp. 267–

287, 2002.

[224] J. W. Choi, S. Kim, R. Trichur, H. J. Cho, A. Puntambekar, R. L. Cole, J. R. Simkins, S. Murugesan, K. Kim, J. B. J. Lee, and G. Beaucage, "A plastic micro injection molding technique using replaceable mold-disks for disposable microfluidic systems and biochips," in *Proceedings of the Micro Total Analysis Systems Symposium*, 2001, pp. 411–412.

[225] M. Focke, D. Kosse, C. Müller, H. Reinecke, R. Zengerle, and F. von Stetten, "Lab-on-a-Foil: microfluidics on thin and flexible films.," *Lab Chip*, vol. 10, no. 11, pp. 1365–1386, 2010.

[226] D. J. Beebe, J. S. Moore, Q. Yu, R. H. Liu, M. L. Kraft, B. H. Jo, and C. Devadoss, "Microfluidic tectonics: a comprehensive construction platform for microfluidic systems," *Proc. Natl. Acad. Sci.*, vol. 97, no. 25, pp. 13488–13493, 2000.

[227] P. Kim, K. W. Kwon, M. C. Park, S. H. Lee, and S. M. Kim, "Soft lithography for microfluidics: a review," *Biochip J.*, vol. 2, pp. 1–11, 2008.

[228] A. Bonyar, H. Santha, M. Varga, B. Ring, A. Vitez, and G. Harsanyi, "Characterization of rapid PDMS casting technique utilizing molding forms fabricated by 3D rapid prototyping technology (RPT)," *Int. J. Mater. Form.*, vol. 7, no. 2, pp. 189–196, 2014.

[229] J. L. Erkal, A. Selimovic, B. C. Gross, S. Y. Lockwood, E. L. Walton, S. McNamara, R. S. Martin, and D. M. Spence, "3D printed microfluidic devices with integrated versatile and reusable electrodes.," *Lab Chip*, vol. 14, no. 12, pp. 2023–2032, 2014.

[230] P. Cooley, D. Wallace, and B. Antohe, "Applicatons of ink-jet printing technology to BioMEMS and microfluidic systems," *J. Assoc. Lab. Autom.*, vol. 7, no. 5, pp. 33–39, 2002.

[231] A. K. Au, W. Lee, and A. Folch, "Mail-order microfluidics: evaluation of stereolithography for the production of microfluidic devices.," *Lab Chip*, vol. 14, no. 7, pp. 1294–1301, 2014.

[232] C. W. Ziemian and P. M. Crawn III, "Computer aided decision support for fused deposition modeling," *Rapid Prototyp. J.*, vol. 7, no. 3, pp. 138–147, 2001.

[233] L. Novakova-Marcincinova and I. Kuric, "Basic and advanced materials for fused deposition modeling rapid prototyping technology," *Manuf. Ind. Eng.*, vol. 11, no. 1, pp. 24–27, 2012.

[234] W. Zhong, F. Li, Z. Zhang, L. Song, and Z. Li, "Short fiber reinforced composites for fused deposition modeling," *Mater. Sci. Eng. A*, vol. 301, no. 2, pp. 125–130, 2001.

[235] J. M. Lee, M. Zhang, and W. Y. Yeong, "Characterization and evaluation of 3D printed microfluidic chip for cell processing," *Microfluid. Nanofluidics*, vol. 20, no. 1, pp. 1–15, 2016.

[236] N. Bhattacharjee, A. Urrios, S. Kang, and A. Folch, "The upcoming 3D-printing revolution in microfluidics," *Lab Chip*, vol. 16, no. 10, pp. 1720–1742, 2016.

[237] S. Tsuda, H. Jaffery, D. Doran, M. Hezwani, P. J. Robbins, M. Yoshida, and L. Cronin, "Customizable 3D Printed 'Plug and Play' Millifluidic Devices for Programmable Fluidics," *Public Libr. Sci. ONE*, vol. 10, no. 11, p. e0141640, 2015.

[238] Royal DSM, "Product Data Sheet - Somos ProtoTherm 12120." 2012.

[239] Royal DSM, "Product Data Sheet - Somos BioClear." 2012.

[240] Royal DSM, "Product Data Sheet - Somos NanoTool ™." 2012.

[241] Reliasoft Corporation, "Accelerated Life Testing Reference." 2014.

[242] JEDEC Solid State Technology Association and Jedec, "Temperature Cycling," *JesD22-A10D4*, no. May 2005, p. 11, 2009.